USE OF MULTICELLULAR HUMAN LIVER MODELS TO INVESTIGATE CLEARANCE OF THERAPEUTIC ANTIBODIES

By

BETHANY HOPE JAMES

A thesis submitted to the University of Birmingham for the degree of DOCTOR OF PHILOSPHY

Centre of Liver and Gastrointestinal Research
Institute of Immunology and Immunotherapy
School of Medical and Dental Sciences
University of Birmingham
March 2024

UNIVERSITY OF
BIRMINGHAM

University of Birmingham Research Archive

e-theses repository

This unpublished thesis/dissertation is copyright of the author and/or third parties. The intellectual property rights of the author or third parties in respect of this work are as defined by The Copyright Designs and Patents Act 1988 or as modified by any successor legislation.

Any use made of information contained in this thesis/dissertation must be in accordance with that legislation and must be properly acknowledged. Further distribution or reproduction in any format is prohibited without the permission of the copyright holder.

Abstract

Background and Aims: Therapeutic antibodies make up the majority share of the drug industry, estimated to be worth $495 billion by 2030. Often, inadequate understanding of the tissue distribution and pharmacokinetics has resulted in many biotherapeutics being unable to attain clinical success. The liver plays a crucial role in the internalisation and catabolism of these antibodies due to their vast vasculature system and high expression of scavenger and Fc-receptors. Liver sinusoidal endothelial cells (LSEC) express many of these receptors and are known to contribute in the clearance of immune complexes. The liver is often susceptible to injury and disease, possibly leading to changes in key receptors involved in antibody clearance. Therefore, we wanted to explore the role of LSEC in health and disease and assess how they impact upon non-specific clearance of therapeutic antibodies.

Method: LSEC were isolated from diseased and normal human liver tissue to ascertain changes in receptor expression by qPCR, western blotting, and immunohistochemistry. A novel recycling assay was adapted to quantify the binding and clearance of 11 therapeutic antibodies at 4- and 8-hours by ELISA, flow cytometry and confocal microscopy. Pharmaceutical inhibitors were utilised to interrogate the internalisation mechanism of both healthy and cirrhotic LSEC and colocalisation with lysosomal markers were also performed to establish the end fate of these therapeutics.

Results and Conclusions: Our results confirm that LSEC express an extensive portfolio of receptors able to bind biotherapeutics, and the distribution of these receptors are significantly altered in disease. We have also demonstrated that LSEC not only internalise antibodies, but they can also partition these for lysosomal degradation. The rate at which this happens differs between healthy and diseased cells. Most importantly, we describe how cirrhotic LSEC favour internalisation via a receptor-mediated clathrin-dependent pathway, whereas healthy cells favour a clathrin-independent pinocytic mechanism. Therefore, we conclude cirrhosis alters pharmacokinetics and that the role of LSEC (both in health and disease) should be considered during antibody development.

Acknowledgements

I would first like to express my gratitude to my supervisors, Patricia Lalor, and Chris Weston. For their invaluable guidance throughout and for the many Friday morning coffees.

I'm thankful to GSK and the BBSRC for funding this research. My GSK supervisory team and Joseph Mabbit (GSK) for his patience and insight through the many failed SPR experiments.

I'm grateful for the past and present members of the Lalor lab and the rest of the CLGR who made every day in lab enjoyable. Thankful for Lozan Sheriff, whose guidance throughout my MSc enabled me to gain this PhD. Particular thanks go to Ellie Northall, for making weekend labs fun and whose Western Blots inspire me daily.

To the NHS staff, particularly Jen and Janine. To all the donors who made this work possible.

To my family, friends, partner, and PlayStation: thank you for your patience, presence, and support throughout this whole process.

Table of Contents

Abstract ..... *ii*

Acknowledgements ..... *iii*

Table of Contents ..... *iv*

List of Figures ..... *vii*

List of Tables ..... *x*

Abbreviations ..... *xi*

Chapter One: Introduction *1*

1.1 A Brief History of Therapeutic Antibodies **1**

1.2 Therapeutic Antibody Structure and Formats **5**

1.3 Recycling or clearance of therapeutic antibodies **8**

1.4 Biophysical properties of therapeutic antibodies **10**

1.5 Liver: Anatomy, Architecture and Catabolic Function **18**

1.6 Hepatic Reticuloendothelial System **23**

1.6.1 Kupffer Cells 23

1.6.2 Liver Endothelial Sinusoidal Cells 25

1.7 Deciphering Non-Specific Clearance: LSEC vs Kupffer Cells- Size Matters **27**

1.8 The Liver in Disease **30**

1.8.1 Phenotypic and Functional Changes in Liver Disease 33

1.9 Impact of Liver Disease on Therapeutic Antibody Clearance: Clearance Dynamics and Clinical Implications. **36**

1.10 Scope of this work **38**

Chapter Two: Materials and Methods *40*

2.1 Materials **40**

2.2 Liver Tissue Samples **41**

2.3 Histological assessment of liver tissue **42**

2.4 Isolation and maintenance of cell cultures **43**

2.4.1 Isolation of LSEC 43

2.4.2 Culture of LSEC 46

2.4.3 Use of siRNA for transient gene knock down in LSEC 46

2.5 Phenotype characterisation of cirrhotic and healthy livers **47**

2.5.1 Immunohistochemistry and quantification of receptors 47

2.5.2 Immunofluorescence staining of liver tissue 50

2.5.3 Assessment of gene expression of liver tissue and LSEC 50

2.5.4 Assessment of protein expression of liver tissue and LSEC 54

2.5.5 Immunocytochemistry on LSEC 57

2.6 Fluorescent labelling of monoclonal/bispecific antibodies **58**

2.7 Human Endothelial Recycling Assay (HERA) to quantify antibody uptake and processing 59
2.7.1 Quantification of mAb/bsAb uptake through Enzyme-linked immunosorbent assay 60
2.7.2 Quantification of mAb/bsAb uptake through Meso-Scale Discovery(MSD) 61
2.7.3 Use of Flow Cytometry to quantify antibody binding from HERA 62
2.7.4 Fixed cell imaging after HERA 64
2.7.5 Live cell imaging and co-localisation from HERA 65

2.8 Receptor binding elucidation and kinetics 68
2.8.1 Proteome Profiler 68
2.8.2 Antibody binding to FcRs, FcRn CD206 and CD209 by Surface Plasmon Resonance (SPR) ... 69
2.8.3 Assessment of antibody: receptor interactions using Chemical crosslinking 69
2.8.4 *In silico* assessment of antibody Fab: receptor interactions using ClusPro and PDBSUM 70

2.9 Statistical analysis 70

Chapter Three: Characterising hepatic expression of antibody binding receptors in health and disease 71

3.1 Characterisation of the clinical parameters and architecture within liver 71

3.2 FcRn: In health and disease 80
3.2.1 FcRn expression in tissue is unaffected by cirrhosis. 83
3.2.2 FcRn expression in LSEC is unaffected by cirrhosis. 85

3.3 Expression of mannose receptor (CD206) In health and disease 86
3.3.1 Expression of CD206 in whole tissue 89
3.3.2 CD206: expression by LSEC 92

3.4 LSIGN/CLEC4M expression in health and disease 93
3.4.1 LSIGN expression in whole liver tissue 95
3.4.2 LSIGN protein expression was absent in LSEC lysates despite detectable levels of *CLEC4M* mRNA 97

3.5 FcγR expression in healthy and diseased liver 99
3.5.1 CD32b protein expression but not mRNA expression is reduced in cirrhosis 102
3.5.2 CD32b mRNA expression on LSEC is significantly lost in cirrhosis 106

3.6 Expression of receptors through isolation and passaging of LSEC 108
3.6.1 Expression of receptors through isolation and passaging 108
3.6.2 IOX2 can restore expression of CD32b. 113

3.7 Discussion 114

3.8 Summary 125

Chapter Four: The binding and processing of therapeutic antibody 126

4.1 The trials and tribulations of the HERA assay 127
4.1.1 An ELISA approach to quantifying the HERA assay 128
4.1.2 A Meso-Scale Discovery (MSD) approach to quantifying the HERA assay 131

4.2 Alternative approach to measuring therapeutic antibody's interaction with LSEC 134
4.2.1 Validation of methods. 135
4.2.2 Interpretation of findings using antibody uptake assays 143

4.3 LSEC can internalise and traffic IgG-based therapeutic antibodies. 145
4.3.1 Chimeric antibodies 145
4.3.2 Humanised antibodies. 149
4.3.3 Fully Human antibodies. 156

4.3.4 Bispecific antibodies. ... 161
4.3.5 Origin of antibody affects its internalisation and processing rate. ... 165

4.4 LSEC can divert therapeutic antibody for lysosomal degradation. ... **171**
4.4.1 Discussion ... 180

4.5 Summary ... **184**

Chapter Five: Mechanism elucidation for Internalisation of antibody by LSEC. ... ***186***

5.1 Each receptor can bind to the Fab region of antibodies ... **186**

5.2. Direct approaches to determine receptors responsible for antibody internalisation **188**
5.2.1 Impact of CD206 siRNA on antibody traffic ... 188
5.2.2 Impact of LSIGN (*CLEC4M*) siRNA on antibody traffic ... 193
5.2.3 The impact of CD32b on antibody traffic ... 196
5.2.4 Interactions between FcRn and our antibodies ... 206

5. 3 Discussion: Receptor mediated clearance by LSEC ... **207**

5.4 Indirect approaches which could explain LSEC antibody uptake ... **211**
5.4.1 Cirrhotic LSEC have a delayed signal transduction response. ... 212
5.4.2 Dextran Sulfate suggested a receptor mediated mechanism of antibody internalisation . 214
5.4.3 Sucrose significantly affected cirrhotic LSECs ability to internalise mAbs ... 216
5.4.4 Cirrhotic LSEC need microtubules to internalise therapeutic antibodies ... 220
5.4.5 PI3K played a more important role in cirrhotic LSEC internalisation ... 222
5.4.6 Cdc42 plays a vital role in Antibody E internalisation ... 224

5.5 Indirect Approaches: Discussion ... **228**

Chapter Six: Conclusion and Considerations ... ***234***

6.1 Clinical implications ... **236**

6.2 Limitations and future research ... **237**

6.3 Concluding statements ... **240**

References ... ***242***

Supplementary Methods and Figures ... ***287***

List of Figures

Figure 1.1: Global antibody market share by source 4
Figure 1.2: mAb and mAbdAb Structure 7
Figure 1.3: An overview of the non-specific clearance mechanism of therapeutic antibodies 9
Figure 1.4: The Liver Anatomy 20
Figure 1.5: Scavenging capacities of the RES 23
Figure 1.6: Mortality rates of major diseases 31
Figure 1.7: Stage progression of liver injury 32
Figure 1.8: Brief pathogenesis of fibrosis 34
Figure 2.1: Key stages in the LSEC isolation protocol 45
Figure 2.2: % coverage of IHC workflow 49
Figure 2.3: Outline of the Hera Assay 60
Figure 2.4: Flow cytometry gating strategy 64
Figure 2.5: Exemplar images of workflow for vesicle count and colocalisation 67
Figure 3.1: Healthy liver stained with hematoxylin and eosin 75
Figure 3.2: ARLD liver stained with hematoxylin and eosin 77
Figure 3.3: MASLD liver stained with hematoxylin and eosin 79
Figure 3.4: Schematic of FcRn binging to IgG 81
Figure 3.5: FcRn expression pattern within human liver 84
Figure 3.6: FcRn and B2M expression profile in whole liver 85
Figure 3.7: FcRn and B2M expression profile in LSEC 86
Figure 3.8: Structure of CD206 88
Figure 3.9: CD206 expression in liver tissue 90
Figure 3.10: IHC CD206 on liver 91
Figure 3.11: CD206 expression in LSEC 93
Figure 3.12: Structure of LSIGN 95
Figure 3.13: LSIGN expression liver tissue 96
Figure 3.14: LSIGN expression in endothelial cells 98
Figure 3.15: Structure of FcγRs 100
Figure 3.16: IHC staining of CD32b within human liver 104
Figure 3.17: CD32b expression pattern within human liver 105
Figure 3.18: CD32b expression in LSEC 107
Figure 3.19: Changed in gene expression through isolation 111
Figure 3.20: Tracking of mRNA receptor expression through passaging 112
Figure 3.21: Effect of incubation of LSEC with the hypoxia-mimic IOX2 for 48-hours on gene expression of CD32a and CD32b 114
Figure 4.1: Hera assay determined by a human IgG ELISA 129
Figure 4.2: Hera assay determined by a Rituximab ELISA 130
Figure 4.3: MSD determination of HERA assay 132
Figure 4.4: Validation of flow-based method in LSEC with anti-CD20 136
Figure 4.5: Flow based evaluation of passaging in LSEC ability to bind anti-CD20 137
Figure 4.6: Confocal images of anti-CD20 internalisation into healthy LSEC 138
Figure 4.7: Confocal images of anti-CD20 internalisation into cirrhotic LSEC 140
Figure 4.8: Corrected Total Cell Fluorescence quantification of anti-CD20 internalisation 142
Figure 4.9: Flow cytometric analysis of Antibody A in healthy and cirrhotic LSEC. 146

Figure 4.10: Flow cytometric analysis of anti-CD20 and anti-CD20 LAGA in healthy and cirrhotic LSEC 148
Figure 4.11: Immunofluorescence of internalised anti-CD20 LAGA at 4-hours 149
Figure 4.12: Flow cytometric analysis of Antibody B in healthy and cirrhotic LSEC 150
Figure 4.13: Representative image of Antibody B internalised into healthy LSEC at 4-hours 150
Figure 4.14: Flow cytometric analysis of Antibody C in healthy and cirrhotic LSEC 151
Figure 4.15: Representative image of Antibody C internalised into healthy LSEC at 4- and 8-hours 152
Figure 4.16: Flow cytometric analysis of Antibody D in healthy and cirrhotic LSEC 153
Figure 4.17: Representative image of Antibody D internalised into healthy LSEC at 4- and 8-hours 154
Figure 4.18: Corrected Total Cell Fluorescence quantification of Antibody D internalisation 155
Figure 4.19: Flow cytometric analysis of Antibody E in healthy and cirrhotic LSEC 156
Figure 4.20: Representative image of Antibody E internalised into healthy LSEC at 4- and 8-hours 157
Figure 4.21: Corrected Total Cell Fluorescence quantification of Antibody E internalisation 158
Figure 4.22: Flow cytometric analysis of Antibody F in healthy and cirrhotic LSEC 159
Figure 4.23: Flow cytometric analysis of Antibody G in healthy and cirrhotic LSEC 160
Figure 4.24: Flow cytometric analysis of Antibody H in healthy and cirrhotic LSEC 161
Figure 4.25: Flow cytometric analysis of Antibody I in healthy and cirrhotic LSEC 162
Figure 4.26: Representative image of Antibody I internalised into healthy LSEC at 4- and 8-hours 163
Figure 4.27: Corrected Total Cell Fluorescence quantification of Antibody I internalisation 164
Figure 4.28: Summary of % Process of MFI 165
Figure 4.29: MFI comparison for CD20 targeting antibodies 166
Figure 4.30: Representative images of CD20 colocalising with lysosomal marker LAMP1 171
Figure 4.31: LSEC capacity for lysosomal degradation 172
Figure 4.32: Colocalisation of Antibody D, E, and I with lysosomes in LSEC 174
Figure 4.33: Antibody D localisation within the lysosomes 175
Figure 4.34: Antibody E localisation within the lysosomes 176
Figure 4.35: Antibody I localisation within the lysosomes 178
Figure 5.1: Fab fragments docking to CD206 186
Figure 5.2: Flow cytometry analysis of MRC1 KD LSEC. 188
Figure 5.3: : Flow cytometry analysis for MRC1 KD healthy LSEC 189
Figure 5.4: SPR sensograms for CD206 190
Figure 5.5: Confocal analysis of MRC1 KD on cirrhotic LSEC 191
Figure 5.6: Flow cytometry analysis for LSEC with reduced CLEC4M expression 192
Figure 5.7: Confocal analysis of CLEC4M KD on cirrhotic LSEC 194
Figure 5.8: Fc block effects on internalisation in cells 197
Figure 5.9: Confocal analysis of impact of Fc-block on anti-CD20 internalisation 198
Figure 5.10: IOX2 effects on internalisation of Antibody C 199
Figure 5.11: IOX2 effects on internalisation of Antibody F 200
Figure 5.12: IOX2 effects on internalisation of Antibody A and H 200
Figure 5.13: Fixed microscopy quantification of antibody D fluorescence following IOX treatment 201
Figure 5.14: : CD32b crosslinked to bsAbs H and I 202

Figure 5.15: Interactions between CD32b and the mAb portion of antibody H 204
Figure 5.16: Human phospho-immunoreceptor profile following Antibody I treatment 213
Figure 5.17: Dextran sulfate effects on therapeutic internalisation 214
Figure 5.18: 2-Hour incubation of antibodies following sucrose treatment 216
Figure 5.19: Representative images of sucrose treated LSEC internalising antibodies 217
Figure 5.20: Quantification of AF647 positive vesicles post sucrose treatment 218
Figure 5.21: : 2-Hour incubation with antibody post nocodazole treatment 219
Figure 5.22: Time course quantification of internalised antibody post nocodazole treatment 220
Figure 5.23: Representative images of nocodazole treated LSEC internalising antibodies 221
Figure 5.24: PI3K inhibition effects on therapeutic internalisation 222
Figure 5.25: Cdc42 inhibition on cirrhotic LSEC at 4-hours 223
Figure 5.26: FcRn blocker effect on antibody internalisation 225
Figure 5.27: Co-localisation of lysosomes and antibody under FcRn block 227
Figure S.1: THP-1 antibody uptake 288
Figure S.2: Coculture treated with therapeutic antibodies 289
Figure S.3: : Comparison of mono- vs co-cultures in LSEC uptake of antibody 290
Figure S.4: Validation of MRC1 Knockdown. 291
Figure S.5: SPR sensograms for CD206 binding kinetics with antibodies 291
Figure S.6: mRNA expression validation of CLEC4M knockdown 292
Figure S.7: SPR sensograms for LSIGN binding kinetics with antibodies 292
Figure S.10: Liver tissue injections of Antibody D 294

List of Tables

Table1.1: Fc-disabled mAbs currently on the market/late-stage development	15
Table 1.2: Outline of thesis aims	39
Table 2.1: TaqMan used in qPCR	40
Table 2.2: Antibodies used.	40
Table 2.3: H&E inhouse staining protocol	43
Table 2.4: Thermocycler reaction protocol	53
Table 2.5: Overview of RefFinder software analysis for best housekeeper	54
Table 2.6: SDS-PAGE gel casting ratios	56
Table 2.7: Internalisation inhibitors	66
Table 3.1: Demographics and clinical characteristics of liver tissue donors	72
Table 3.2: Summary of chapter 3 results	124
Table 4.1: Therapeutic antibody characteristics	127
Table 4.2: Summary of Chapter 4 results	184
Table 5.1: ClusPro analysis of Antibody C and anti-CD20 fab fragments to receptors.	187
Table 5.2: SPR analysis of binding kinetics for CD32aH, CD32aR and CD32b	196
Table 5.3: SPR analysis of FcRn interaction with antibodies at a pH of 6.	205
Table 5. 4: Summary of finding throughout chapter for each antibody.	232
Table 6.1: Conclusions made from each aim set out by this thesis	234

Abbreviations

ADCC	Antibody-Dependent Cell-mediated Cytotoxicity
AF488	Alexafluor 488
AF647	Alexafluor 647
ALP	Alkaline Phosphatase
ALT	Aminotransferase
ARLD	Alcoholic-Related Liver Disease
ASGPR	Asiaglycoprotein Receptor
AST	Aspartate Aminotransferase
B2M	Beta-2-Microglobulin
BEC	Biliary Epithelial Cells
BME	β-mercaptoethanol
BMI	Body Mass Index
BSA	Bovine Serum Albumin
bsAbs	Bispecific Antibody
CD206	Mannose Receptor
CD32b	Fc Gamma Receptor 2b
CDC	Complement-Dependent Cytotoxicity
cDNA	Complementary Deoxyribonucleic Acid
CDR	Complementary Determining Region
CysR	Cysteine-rich Domain
CTCF	Corrected Total Cell Fluorescence
CTLD	C-type Lectin Domains
dAbs	Domain Antibodies
DAMPS	Damage-associated molecular patterns
DAPI	4′,6-diamidino-2-phenylindole
DTSSP	3,3′-Dithiobis(sulfosuccinimidylpropionate)
ELISA	Enzyme Linked Immunosorbent Assay
FAB	Fragment antigen-binding
FBS	Fetal Bovine Serum
FcR	Fc Receptors
FcRn	Neonatal Fc Receptor
FFPE	Formalin-Fixed Paraffin-Embedded
FOV	Field of View
GlcNAc	N-acetylglucosamine
H&E	Hematoxylin and Eosin
HAMA	Human anti-mouse antibody
HBSS	Hanks Balanced Salt Solution
HCC	Hepatocellular Carcinoma
HERA	Human Endothelial Recycling Assay
HRP	Horse Radish Peroxidase
HSC	Hepatic Stellate Cells
IDA	Industrial Denatured Alcohol
IF	Immunofluorescence
IgG	Immunoglobulin G
IMC	Isotype Matched Control
KCs	Kupffer Cells
LPS	Lipopolysaccharide
LSEC	Liver Sinusoidal Endothelial Cells
mAbs	Monoclonal Antibody
MASLD	Metabolic Dysfunction-associated Steatotic Liver Disease

MELD	Model for End Stage Liver Disease
MSD	Meso-Scale Discovery
ON	Overnight
PAMPS	Pathogen-associated molecular patterns
PBS	Phosphate Buffered Saline
PD	Pharmacodynamics
PFA	Paraformaldehyde
pI	Point Isoelectric
PK	Pharmacokinetics
PMA	Phorbol-12-myristate-13-acetate
PSG	Penicillin-Streptomycin Glutamin
RBC	Red Blood Cells
RES	Reticuloendothelial System
RNA	Ribonucleic Acid
RTC	Rat Tail Collagen
scFv	Single chain variable fragments
SDS-PAGE	Sodium dodecyl-sulfate polyacrylamide gel electrophoresis
SRSF4	Serine/arginine-rich splicing factor 4
TBS	Tris-buffered Saline
TEMED	N,N,N',N'-Tetramethyl ethylenediamine
WT	Wild Type

Chapter One: Introduction

In this thesis, I have examined the role of the liver sinusoidal endothelial cells (LSEC) in the uptake of antibody-based biological therapeutics. This has important implications for antibody pharmacokinetics and the design of new therapeutics. Thus, I begin with a consideration of antibody structure and clearance before moving on to discuss the functions of key cells in the human liver as we explore how and if liver injury/disease affects this antibody uptake. Previously, I have published a review on this topic that may provide additional context.[211] To note, this research took place during the COVID-19 pandemic, therefore for a considerable amount of time access to liver tissue was hindered. As a result, some of the later experiments described in this thesis are limited in the number of biological replicates.

1.1 A Brief History of Therapeutic Antibodies

Therapeutic antibodies are biopharmaceuticals with a unique structural formation that can recognise and target specific cells, proteins, or genes. Monoclonal antibodies (mAbs) are a rapidly expanding class of drugs due to their high specificity, affinity, long *in vivo* half-life, and potent therapeutic effects. Functioning akin to endogenous antibodies, upon recognition of a specific epitope, this elicits either an antibody cell mediated cytotoxic (ADCC) and/or a complement dependent cytotoxic (CDC) effector response. They can also opsonise target cells, activating Fc receptors upon phagocytes actuating their internalisation and degradation; this process is called antibody dependent cellular phagocytosis (ADCP). mAbs have emerged as the predominant therapeutic modality for a diverse spectrum of conditions, spanning from inflammation to autoimmune diseases. Notably, their profound impact is evident in cancer treatment, with an emphasis on personalised medicine and government backed R&D spending, the global mAbs market is predicted to reach over $495 billion at a compound annual growth rate of 11% by 2030.[1] Alongside this, regulatory approval rates have seen an unprecedent surge. In 2013 only three antibodies were approved by the FDA[2] conversely, as of 2022, 175 are

currently in regulatory review or have been approved and it's estimated that 1200 therapeutics are currently undergoing trials in clinical studies.[3]

The first inadvertent use of antibodies as treatment, was in Von Behring and Kitasato's (1890) work within the infectious disease, diphtheria.[4,5] Here, they demonstrated that employing serum from infected animals could treat and prevent subsequent infection in others.[4,5] Building on this, Paul Ehrlich introduced the 'side chain' theory in 1891. He proposed that target cells produce structures he called 'side chains' or nutrient receptors, and that in response to damage or infection these 'side chains' were released into the blood to act against pathogens. He thus coined the term antibody[6,7,8] which paved the way for further study and description of antibody generation and function.

The field was revolutionised in 1975 by the development of the hybridoma technique by Köhler and Milstein, a method that allowed the large-scale production of mAbs with a predefined specificity.[9] Here they fused a myeloma cell line, P3-X63-Ag8 with spleen cells from a mouse immunized with red blood cells (RBC) of a sheep. Following a 2-week incubation in hypoxanthine aminopterin thymidine media to add selection pressure, they generated hybridoma cells that displayed the immortality of myeloma cells whilst possessing the ability to secrete antibodies specific to sheep RBC.[10] Although revolutionary, this technique often uses murine splenocytes and thus the resultant murine immunoglobulin can cause adverse effects within humans. This is termed the HAMA response, after the 'human anti-mouse' antibodies produced by the body's immune system response to the foreign mouse-derived mAbs. It can present with mild (rash) to severe (kidney failure) side effects. In 1986, the first murine therapeutic mAb, an anti-CD3 antibody (muromonab; mouse IgG2A format) was approved by the FDA for use in acute transplant rejection.[11] This has since (2010) been withdrawn from the market, due to numerous adverse events (particularly cytokine release syndrome) and better tolerated alternatives are now available.[12,13]

With the progression of recombinant DNA technology, Morrison *et al.,* (1984) developed the first mouse-human antibody molecule.[14] This was achieved by taking the variable region genes of a mouse antibody-producing myeloma cell line with a known binding specificity, and ligating this to a human immunoglobulin constant region.[14] These chimeric antibodies display a reduced immunogenicity *in vivo* given the absence of murine constant regions and typically around 67% humanisation.[15] The first chimeric mAb approved by the FDA was produced in 1994, and was a Fab based format which acted as an antagonist to glycoprotein IIb/IIIa receptor, which in turn inhibited platelet aggregation.[16] Three years later in 1997, the first full length IgG chimeric antibody, an anti-CD20 known as rituximab was approved. This is used in diseases such as non-Hodgkin's lymphoma, rheumatoid arthritis and in some kidney transplant recipients to incite ADCC and CDC functions as well as induce apoptosis of CD20 expressing B cells.[17]

With aspirations to reduce *in vivo* immunogenicity further, Jones *et al.,* (1986)[18] engrafted the complementary determining region (CDR) from the mouse antibody B1-8 (ligand to hapten NP-cap) to the corresponding CDRs of a human antibody, thus developing the first humanised mAb.[18] For a mAb to receive the '-zumab' nomenclature, the human germinality of the variable heavy and light chains are required to be >85%.[19] In 1997, the first humanised mAb was FDA approved. This was Daclizumab which binds to CD25, a subunit of the IL-2 receptor of T-cells. This reduced T cell responses and in turn recruits natural killer cells[20], it was developed for the use in adults with relapsing multiple sclerosis. However, as of March 2018, this therapeutic was taken off the market due to cases of autoimmune encephalitis and immune dysregulation in patients with multiple sclerosis.[21]

At present, developments in antibody engineering have resulted in the generation of fully human antibodies with antigen specificity being selected either by *in vitro* screening or via transgenic mice. Phage display was first demonstrated in 1985,[22] in brief, this technique uses a bacteriophage (a virus that can infect bacteria) to display polypeptides on its surface. This can then be screened against large libraries of proteins to identify

targets. Nine years later, Gregory P. Winters utilised this technique to screen for antibodies, whereby single chain variable fragments (scFv) were displayed on a phage (fd-tet phage).[23] This revolutionised the monoclonal antibody development space, providing a robust method for high throughput antigen screening now considered the gold standard in drug discovery. Adalimumab, the first fully human mAb derived by phage display, was approved by the FDA in 2002. This anti-TNF inhibitor is used in numerous diseases and is currently one of the best-selling drug-based therapeutic in the world, making $20 billion in 2018.[2,24]

Transgenic animals have supported another advancement for antibody engineering. Here, the endogenous repertoire of IgG within an animal is replaced with human immunoglobulin genes inserted within the genome. This allows the animal to synthesise fully human antibodies once immunised. Transgenic animals were introduced in 1994 and propelled forward following the development of two transgenic murine lines, namely the Xeno-mouse and HuMabMouse.[2,25,26] This method is advantageous as it needs no affinity maturation step and full-length IgG antibodies are made, however, if the antigen being used to immunise is particularly toxic or cross-reactive then phage display is the preferred technique. To date human and humanised mAbs dominant the therapeutic antibody space, accounting for respectively 51 and 35% of all mAbs currently in clinical use (see Figure 1.1).[2]

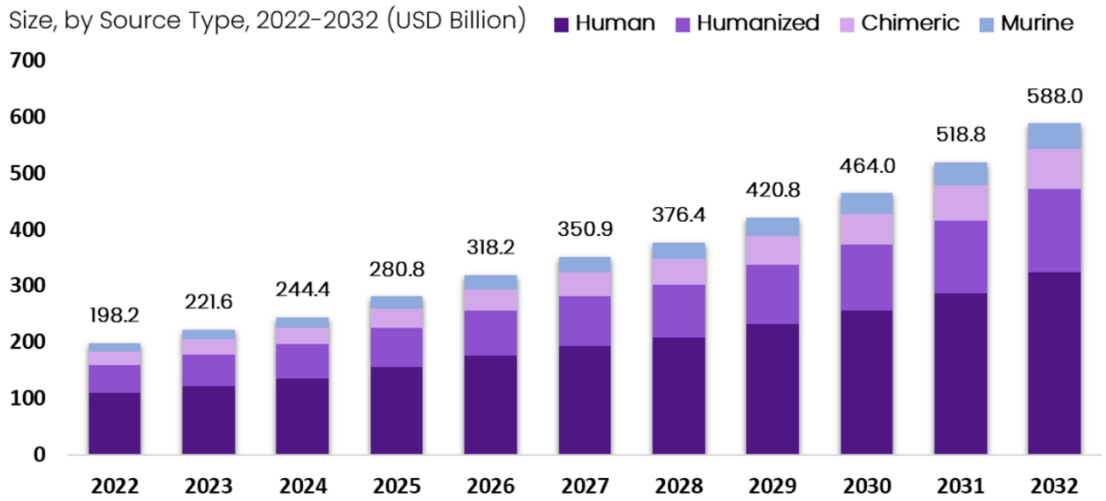


Figure 1. 1: Global antibody market share by source. This graph shows the global market share of monoclonal antibodies, and their share per origin of antibody. Numbers on top of bars shows amount in USD billion worth. Image sourced from US Market.[222]

Although advances in increasing the human proportion of antibodies have led to greater success, further antibody engineering has been developed to improve clinical efficacy. These are outlined in Section 1.4. Despite this, over half of global spending on antibody therapies are wasted on 'poor' therapeutics.[215] Off-target rapid clearance, poor pharmacokinetics and toxic side-effects are the main factors responsible for this waste in time and money. With such a vast amount of money wasted each year, has led us to question if the models used in the strict in-house testing of these biotherapeutics are fit for purpose. Before we examine this, we need to understand the structure of these therapeutics.

1.2 Therapeutic Antibody Structure and Formats

The covalent structure of Immunoglobulin G1 (IgG1) was first mapped out in 1969 by Edelman.[27] By 1977, with the use of electron density maps and x-ray diffraction, the full 3D structure of human immunoglobulin was elucidated.[28] mAbs adopt the same structure as endogenous immunoglobulin, in that they possess four polypeptide chains, two light and two heavy, with a Fab fragment and an Fc region. This forms a complex

quaternary Y-shaped structure (Figure 1.2). The Fab fragment is composed of one constant region and one variable domain which makes up the antigen binding site. Antibody antigen binding portions can be engineered such that they recognise two different epitopes, either on the same or different antigens to engage two targets. These so called 'bispecific antibodies' (bsAbs) have unique functional properties and represent a fast-growing share of the therapeutics market.[216]

The Fc region is the tail end of the antibody and binds to proteins and receptors of the immune system such as the complement system and surface receptors known as Fc receptors (FcRs). Here too, options exist to generate altered structural formats or Fab fragments which lack Fc portions. Removal of Fc with proteolytic enzymes or generation of fragments in cell expression systems results in small antibody fragments.[217] This alters clearance, can minimize detrimental immune effects, and improves penetration of tissue.[217] Whatever the final structure, the IgG class of immunoglobulins is the most abundant form used therapeutically and is split into four subclasses, IgG1-4. These subclasses differ in their constant regions, namely the 7-chain sequence and disulphide bond patterns, but overall share the same basic structure. Most on-market mAb therapeutics are IgG1 based.[29]

For the research described in this thesis, both monoclonal (mAbs) and bispecific (bsAbs) antibody classes were used (Table 4.1). mAbs are designed to bind a single target and typically possess identical antigen binding sites. Disease is typically not driven by a single factor and bsAbs provide a novel approach through improvements of the antibody framework which allow for the engagement of two molecular targets for improved affinity or to facilitate binding of independent proximal targets. BsAbs were first proposed by Nisonoff *et al.,* in 1960.[218] Early bsAbs were developed through the fusion of hybridomas each expressing one of the antibodies, into a quadroma. This was inefficient due to low homogenous batches, and the resultant antibodies also exhibited the same xenogenicity as described previously with murine-derived antibodies.[30-34]

Nowadays, a mixture of genetic engineering and chemical conjugation is the prominent method for forming bsAbs.

In recent years, the most noticeable and promising bsAb, particularly for anti-cancer treatment, is a bispecific T-cell engager named BiTE™. This genetically engineered therapeutic consists of 2 scFv connected by a short linker. The antibody recognises both a T cell and tumour target via ability to bind to CD3 and a tumour-specific epitope concurrently, thereby redirecting cytotoxic T cells towards the tumour.[35] This format has a short half-life of around 2 hours due to both its small size and lack of Fc for FcRn-dependent recycling, so therefore needs to be continuously infused.[36] Amgen has sought to rectify this by the addition of a Fc domain onto the CD3 scFv, which has extended the half-life up to 7 days.[37] Where more favourable pharmacokinetics are of importance, full length IgG formats are of use since the increased size and complexity improves stability. In this thesis, I have studied antibodies made with the bsAbs scaffold approach, also known as the mAbdAb (see Figure 1.2).

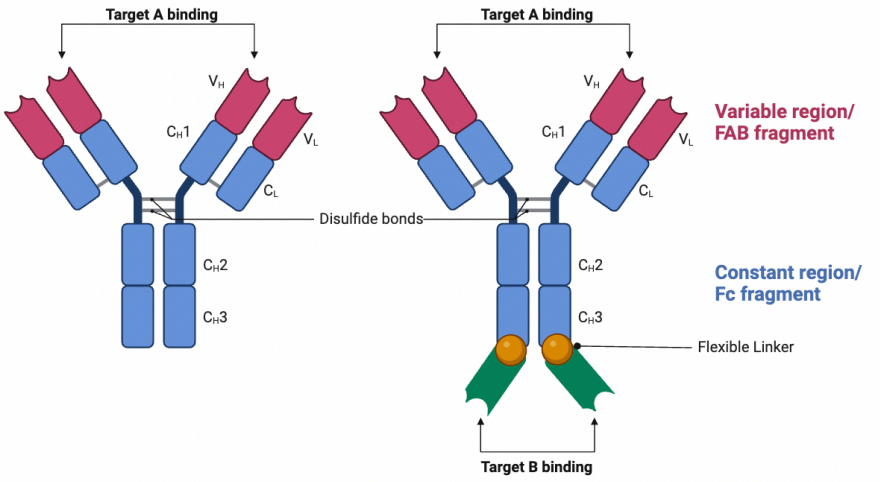


Figure 1. 2: mAb and mAbdAb structure. Left shows the standard structure of an IgG monoclonal antibody targeted at a single epitope (red regions), right shows the structure of a mAbdAb where a flexible linker (orange) allows the addition of a domain antibody (green) that can bind a second epitope. C= constant region; H= heavy chain; L= light chain; V= Variable region. Image made on Biorender.

mAbdAbs consist of a full IgG scaffold coupled at the C-terminus heavy chain with a domain antibody (dAbs) via a flexible linker.[38] dAbs are composed of a 110 amino-acid long peptide chain of approximately 15kDa, in comparison to the standard IgG which is typically around 150kDa. This strategy provides a novel mechanism to bivalently bind and act either discreetly on two independent epitopes or biparatopically.

Despite the advancements made in antibody engineering, there is still an incomplete understanding for the complexity of the *in vivo* mechanisms involved in mAb pharmaco-kinetics (PK) and dynamics (PD). The challenge to design a clinically applicable therapeutic that can circumvent the natural body's immune clearance system whilst also balancing the need to not accumulate causing toxicity is an area to still be improved upon. The following section investigates how the body clears and recycles IgG-based therapies.

1.3 Recycling or clearance of therapeutic antibodies

Renal filtration is often the route for elimination for therapeutics from the bloodstream. The average kidney glomeruli pore size is ~8nm, and since mAbs typically have a larger complex size of 10nm, this means renal filtration alone is not a viable means for clearance.[39] It is generally accepted that there are instead two main mechanisms for clearance: 1) target mediated clearance and 2) non-specific clearance (off-target). Target mediated clearance refers to the cellular binding and internalisation of target antigen complexed with the mAb and the subsequent proteolytic intracellular clearance of the complex.[41] Non-specific clearance can occur via 3 possible pathways: 1) activation of C1q and clearance via the classical complement pathway 2) fluid phase pinocytic uptake and 3) receptor mediated endocytosis.[40,41] The latter two pathways lead into either lysosomal degradation or return to the extracellular space via the neonatal Fc receptor

(FcRn)-dependent recycling pathway.[42] See Figure 1.3 for overview of pathways of interest.

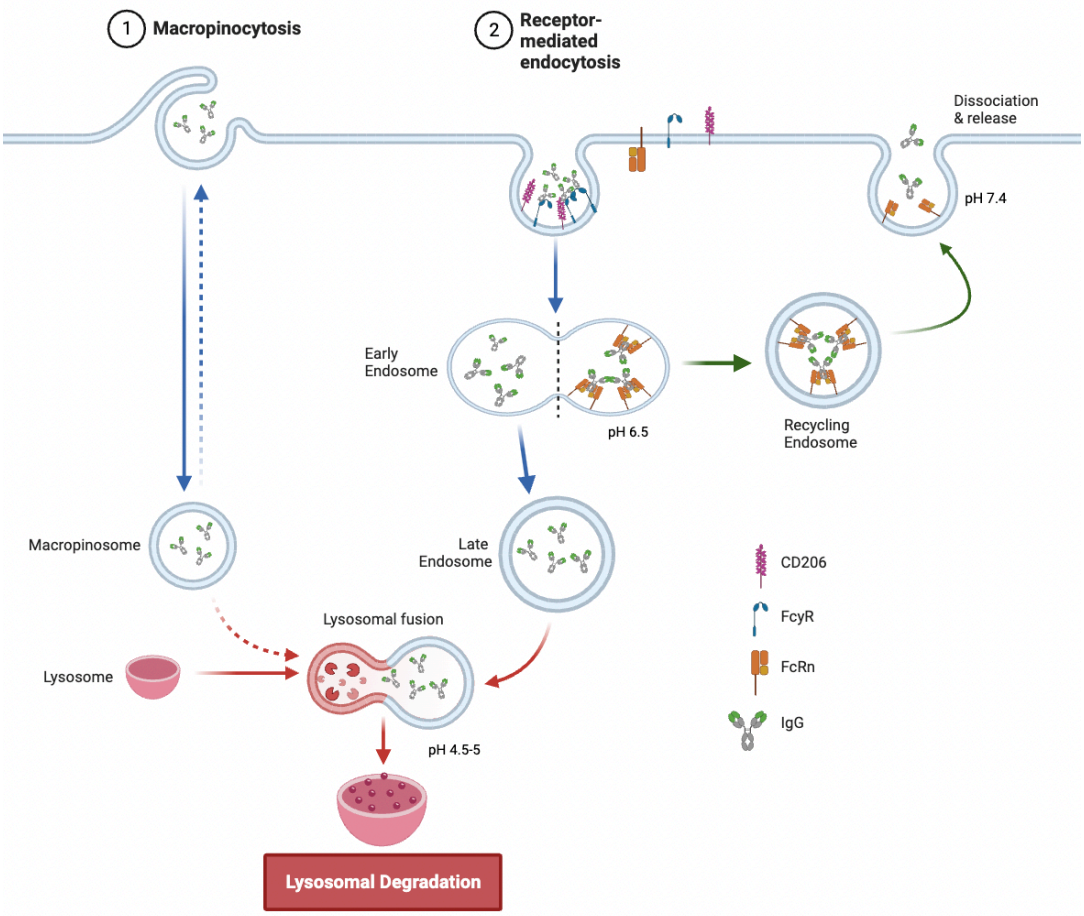


Figure 1. 3: An overview of the non-specific clearance mechanism of therapeutic antibodies. 1. Shows the macropinocytosis route, a fluid mediate intake where the antibodies are taken into a macropinosome where it can either be recycled or progress on to adjoin the lysosome for degradation. Pathway 2 shows the receptor mediated internalisation process. Here, Mannose receptors (CD206) or Fc gamma receptors (FcγR) are bound to immunoglobulin G (IgG) and internalised into an early endosome. In a *p*H dependent reaction, IgG is either bound by the neonatal Fc receptor (FcRn) or not. Those that interact with FcRn are rescued and undergo the recycling process where the endosome returns to the surface and are released from the FcRn following an increase in *p*H and return to the circulation. IgG that failed to bind to FcRn are re-routed to the lysosome where the fate of the IgG is lysosomal degradation. Image made in BioRender.

The antibody clearance processes are described in greater detail in Chapters 4 and 5, but for the purposes of this thesis, the non-specific pathway, and in particular the receptor-mediated mechanism of clearance, is our focus. Here it is understood that IgG format mAbs bind to Fc gamma receptors (FcγR) expressed on cell surface membranes; often at

a 1:1 ratio at the CH2-CH3 interface of the IgG Fc domain.[43-45] However other receptors may also be involved, and this shall be discussed later. Following internalisation of the receptor: mAb complex into an endosomal compartment the IgG is released from the complex and may come into proximity with the FcRn. FcRn is a heterodimeric receptor, first described by Brambell,[46] comprising of a glycosylated transmembrane MHC class I like heavy chain, associated noncovalently with beta-2-microglobulin (β_2m).[47] This receptor is key for the process of recycling IgG back into the extracellular space and is highly *p*H dependent. mAbs may also encounter FcRn via pinocytic means. Binding efficacy is only achieved at *p*H <6.5. A binding ratio of 2:1 (FcRn: IgG) involving multiple histidine residues at the CH2-CH3 domain allows this receptor to function as a saviour of IgG from lysosomal degradation.[43,45,48] Recycling endosomes are diverted back to the surface membrane, whereby a near neutral blood *p*H of 7.4 causes the dissociation of antibody from FcRn and thus recycling of IgG back into the circulation.[49,50] Therefore, the tendency of antibodies towards recycling rather than disposal is of upmost importance in early-stage drug discovery. Non-specific clearance and poor antibody stability are often the cause of failure in drug discovery programmes with clinical success accountable to many different factors. These complexities are discussed in the following section.

1.4 Biophysical properties of therapeutic antibodies

The clinical success of therapeutic antibodies is determined by the early understanding of its PK/PD properties and how this translates to efficacy within the complex physiological setting of humans. Usually, following intravenous administration, a mAbs serum PK profile is biphasic: a quick distribution phase and a slowed elimination phase.[51] This is characterised by a long half-life and limited tissue distribution properties for many antibodies. Thus, it is important to fine tune the PK of a therapeutic agent as not only does this lead to improved safety and efficacy, but it also permits better dosing/ frequency of dosing; helping improve both patient compliance and comfort. Therefore, when designing optimal reagents, considerations on the design of the physiochemical

attributes of antibodies such as molecular weight and size, charge and hydrophobicity patches, overall stability and post translational modifications all have a role to play.

Size and molecular weight

Firstly, as discussed in Section 1.3, monoclonal and bispecific antibodies are larger complexes at approx. 150kDa (10nm) that circumvent the obvious route of expulsion from the body via renal filtration.[39] Thus, movement from the vasculature network into the interstitial space occurs via diffusion across endothelia or via convection transport driven by a hydrostatic pressure gradient within the blood vessels.[52,53] Therefore, the tissues with the most exposure to these therapeutics are typically highly vascularised with an abundance of fenestrated endothelia such as the liver and/or spleen.[39]

Charge and hydrophobicity

Solvent exposed residues are indicators for PK, forming globalised or localised charge and hydrophobic patches within an antibody. These characteristics determine and enable the interaction with various extracellular matrices. This has been demonstrated in experimental studies using heparin as a substitute for the expression of negatively charged glycocalyx on endothelial cells.[54,55] Chromatography was utilised to investigate the retention time of 130 IgG antibodies. A correlation was found between heparin retention and isoelectric point (pI) in that the higher the charge on the molecule, the longer the retention.[54,55] This method was suggested as an *in vitro* tool to assess the affinity of non-specific binding of therapeutics to endothelial cells.

In mice, Igawa *et al.* showed that of 4 humanised IgG4 antibodies (each with different variable regions, but same constant regions), those with a higher pI displayed quicker elimination and a reduced half-life.[56] This was determined to be a non-FcRn dependent mechanism, most likely via fluid phase pinocytosis. This was then further explored by the same group, who used a modification of a humanised anti-IL-6 receptor (anti-IL-6R) IgG1 antibody. Here several substitutions to the heavy and light chain variable region led to a reduction from the parent antibody's pI (9.3) to 6.9 and 5.5 for variant antibodies. Following IV administration in cynomolgus monkeys, variant mAb (pI 6.9) showed a 2-

fold reduction in clearance in comparison to the parent anti-IL6R mAb . The variant mAb (pI 5.5) demonstrated a further clearance reduction of 3.1-fold in comparison to the original antibody.[56] Li *et al.,* observed similar in rats.[57] An antibody variant with a pI of 8.61 displayed rapid clearance (140mL/day/kg) in comparison to that of an antibody with a pI of 6.10 (5.8mL/kg/day). Although both displayed similar binding affinity to FcRn, they differed in tissue distribution; with the liver and spleen being the major site for catabolism of the high pI variant.[57] These studies led to understanding that electrostatic interactions between negatively charged cell surface membranes and the predominately net positive charge of an antibody influenced both its tissue deposition and blood concentrations. A positive shift in pI results in increased tissue retention, possible catabolism and increased blood clearance; and the opposite can be said for a net decrease. Here, each study is evidence for the modification of the variable region to reduce the overall pI as an answer to poor PK, however, practically this cannot be achieved. Often, the manipulation needed to shift the pI more favourably would lead to a loss of target binding through the loss of essential residues or improper conformation.[58] Boswell *et al.,* states there is only a measurable difference in PK and distribution, if the pI is shifted ~1 unit.[59] However, research whereby a single Tyr30Glu substitution (acidic residue addition) neutralised a large charge cluster on a bsAb, distinctly led to improved PK and reduced clearance in cynomolgus monkeys.[60]

Considerations beyond just isoelectric point have been demonstrated in clinical studies with antibodies in humans. Briakinumab and Ustekinumab, both human IgG1 therapeutics, targeted at the p40 subunit of IL-12 and IL-23 are characterised by their vastly different half-lives; 9 and 23 days respectively. They have identical constant IgG1 domains and only differ in a few amino acids that play no role in FcRn binding. Their pIs are similar at 9.6 and 9.3 however, Briakinumab has a large positively charged patch on the Fv domain in comparison to Ustekinumab. Both exhibit a similar association with FcRn at *p*H 6, however differed on the dissociation time. Briakinumab was unable to dissociate from FcRn at a higher *p*H in comparison to Ustekinumab.[61] Through further investigation this was deemed to be due to electrostatic interactions. Microscopy studies

demonstrated that despite both being associated with FcRn, Briakinumab was differentially partitioned at the sorting endosome stage towards the lysosomal compartment at ~20 minutes post interaction.[61] Gan *et al.,* describes a process where FcRn is transferred from late endosomes to lysosomes and undergoes degradation.[62] Which may be the mechanism underlying dissociation behaviour of different antibodies.

Grevys *et al.,*[50] replicated the Briakinumab and Ustekinumab study and found that in $FcRn^-$ knockout mice, Briakinumab still exhibited a 7-hour shorter half-life than Ustekinumab, thereby suggesting that FcRn interactions couldn't solely explain the differential behaviour.[50] Indeed it was found that Briakinumab also demonstrated increased uptake and accumulation in HMEC-1 (an endothelial-like immortalised cell line) over an 8-hour period. To expand on this, through substitutions of positive amino acids with uncharged alanine, 5 residues were changed in the heavy chain of Briakinumab resulting in a 2-fold reduction in cellular uptake. More drastically, substitution of 3 positively charged residues in the light chain resulted in further reduction of uptake to that seen for Ustekinumab.[50] Thus both charge and receptor interactions are key to antibody behaviour in complex models.

Native antibody backbone also impacts on eventual distribution *in vivo*. A study[58] comparing the actions of two differential isotype backbones of humanised IgG1 and IgG4 both targeted at the same epitope in mice, showed that the IgG4 had greater distribution to the liver over 168 hours (2-6-fold increase at 6 hours to a 12-fold increase at 168 hours). Both presented higher distribution in liver in comparison to the kidneys.[58] Balancing the charge in the complementary determining region (CDR) of both formats with no shift in pI and no loss of target binding, led to a 7-fold reduction in elimination for the IgG4 derivative. IgG1 saw a more subtle reduction of 1.4-fold improvement.[58]

Charge and hydrophobic indicators often go hand in hand. Hydrophobicity leads to faster antibody clearance.[63,64] Some mAbs extrinsically exhibit high levels of hydrophobicity in their complete tertiary structure; whereas some expose hydrophobic side chains during

partial unfolding in physiological conditions.[65] This is demonstrated during the development of a humanised anti-amyloid beta antibody. Early PK investigations in cynomolgus monkeys found rapid clearance of the reagent. This was later linked to off-target binding of antibody to fibrinogen in the host, leading to the conversion of fibrin; vastly increasing its hydrophobicity.[66] It was found that this rapid elimination was not mirrored in humans and therefore the antibody progressed through trials. Moreover, the fully human mAb, MEDI1912, targeting nerve growth factor was found to exhibit poor PK and underwent reversible hydrophobicity induced self-association in rat and cynomolgus monkeys. Introduction of a 3 amino acid mutation disrupting the hydrophobic interface led to increased serum longevity with no loss of function.[37,67] Thus charge and hydrophobicity are both important facets to the biochemical properties that affect PK. Although there is limited research into this area, there appears to be a current consensus that the higher the pI the more likely an antibody is to undergo rapid clearance. Knowledge of the exact reasoning behind this observation and how the isotype backbone affects this is yet to be elucidated. Developing better *in silico* and model-based drug selection tools will help this endeavour and reduce non-specific clearance.

Post translational modifications

Structural modification of antibodies also impacts on function and clearance *in vivo*. Modifications can be either purposely engineered or a result of non-proteolysis-based transformation within a physiological system. Such modifications include glycosylation, deamidation and isomerization. Fc engineering is an example of purposeful intervention and manipulation. FcRn rescue is one of the key factors to a therapeutics half-life. Triple substitutions within the CH2/CH3 Fc region (M252Y/S254T/T256E; YTE) have generated clinical success exemplified by Motavizumab-YTE.[68] This humanized IgG1 anti-RSV mAb has shown a decrease in clearance of >71% and a 2- to 4-fold increase in half life in healthy volunteers in comparison to the unmodified parent antibody.[68] The YTE mutations optimise the binding interface displayed for FcRn, increasing the binding affinity at a *p*H beyond 6 and as a result its escape from degradation. Another mode of

Fc engineering to escape the fate of non-specific clearance or Fc-effector function is by disabling an antibodies' Fc region. A mAbs Fc is known to interact with Fc Gamma Receptors (FcγRs) to support uptake into a cell. As far as my research extends there are currently 3 Fc-disabled mAbs on the market or in late-stage development,[69] see Table 1.1.

Table 1. 1: Fc-disabled mAbs currently on the market/late-stage development

Name (Company)	Target	Mutation	EU approval?
Atezolizumab (AstraZeneca)	PD-L1	N298A	Yes
ALP502 (Roche)	PD-L1	Not known	Phase 3 Trials
Durvalumab (AstraZeneca)	PD-L1	L234F/L235E/P331S	Yes

As an example of an Fc-disabled mAb strategy currently under development, LAGA antibodies have an IgG1 heavy chain constant region engineered with either both or singular mutations of L235A and G237A.[70] An anti-CD20 LAGA will be used in this research.

Glycoengineering is the addition of sugar molecules to specific sites on an antibody structure. The purpose of such glycosylation is to increase stability by impeding access of proteases, but in turn affects an antibodies functionality and immunogenicity. IgG1 contains one N-linked glycan at Asn297 on both heavy chains within the Fc region.[71] These sites are often utilised for glycosylation, which impacts Fc conformation leading to changes in target binding affinity.[72,73] Glycosylation may also be resultant of different cell culture conditions.[74] Glycosylated proteins are known to undergo one of two clearance pathways. Firstly, Asiaglycoprotein (ASGPR) receptors are integral membrane proteins highly expressed on liver hepatocytes. They recognise and bind terminal galactose and N-acetylglucosamine (GlcNAc) of glycoproteins and remove these from circulation via endocytosis, thus reducing an antibody's half-life.[39,75] It has been shown that the

addition of sialic acid masks this terminal galactose thus preventing clearance.[76] This is evidenced in deliberately desialylated erythropoietin which has a half-life of approx. 10 minutes in contrast to untouched sialylated erythropoietin exhibiting a half-life of >5hours.[77] In a mAb context, Pertuzumab, a humanised IgG1 anti-HER2 from which a sialic acid can be removed using sialidase A, exhibited different properties in its deglycosylated form. It was determined that the binding affinity of the antibody towards HER2 antigen and FcRn was equal for both proteins and there was no impact of the desialylation process *in vitro*. In mice however, sialic acid (-) Pertuzumab exhibited rapid clearance in comparison to fully glycosylated Pertuzumab.[78] This rate of clearance was decreased by the co-injection of asialofetuin, a competitor for ASGPR.[78] This study concluded that the increased elimination was due to hepatic clearance and that consideration for the sialyation on proteins is an important practise for better drug development and PK considerations.

The second pathway of clearance for glycoproteins is via the mannose receptor (CD206). This receptor is described in more detail in Chapter 3, and can recognise terminal GlcNAc, mannose and fucose of N-glycans. It is continuously recycling from the membrane to endosomal compartments, via clathrin-dependent means, as it functions to bind both extracellular and endogenous proteins.[79] In contrast to the mechanism above, the impact of CD206 on an antibody's half-life is debated. High mannose glycans often contain five to nine mannose residues. Three notable studies in mice, cynomolgus monkeys and humans found there to be no relation between possession of high mannose residues and faster clearance.[80-82] Of the three, Chen *et al.,* suggested the loss of specific high mannose species was by the *in vivo* trimming of glycans (Man6-Man9 converting to Man5) rather than clearance by CD206.[82] This research was only focused on IgG2; however an earlier study using Omalizumab, an IgG1 isotype humanised mAb, also found its clearance rates unaffected by Fc glycan structure.[83] Alternatively, three studies in mice and cynomolgus monkeys, determined the opposite, that Man5 glycans cleared significantly faster than mAbs that lacked mannosylated terminals.[84-86] In humans, Goetze *et al.,* found evidence for IgG containing high mannose glycans, in

oppose to other glycan forms, were the cause for rapid serum clearance.[87] This study also confirmed the conversion of Man6-Man9 to Man5 in humans (also seen in mice).[85] While Yu *et al.,* and Chen *et al.,* state there is no difference in clearance rates between Man5 through to Man9, Goetze *et al.* agreed with other previous studies[84,86] that Man5 glycosylated antibodies exhibit the fastest clearance rates through experimentation with IgG1 and IgG2 isotypes. Overall, with an unclear outcome and contrasting narrative within the literature, the influence of CD206 on PK is yet to be fully understood and may be an antibody specific factor.

Deamidation is another protein modification for which a consensus has not yet been reached. Deamidation of a protein can impact on its PK and immunogenicity, but also impacts on sensitivity to proteases. It is considered to contribute to one of the main degradation pathways of antibodies and is controlled for heavily in the development and storage stages of antibody development. Most commonly, deamidation is a chemical reaction whereby a neutrally charged asparagine residue is converted to a negatively charge aspartate or isoaspartate residue. Liu *et al.,* showed that this had no outright effect on PK and suggested that the deamidation process of IgG1 and IgG2 are similar *in vivo.*[88] Years later, Yan *et al.,* explored the risk of deamidation particularly of asparagine residues within the complementary determining region (CDR). This was tested in both neutral and acidic buffers and deamidation altered IgGs structural conformation and flexibility, as well as accessibility for solvents.[89] With this knowledge and the evolving landscape of how subtle changes in charge can affect PK, suggests a more in-depth look at this process may be worthwhile as these subtle changed in storage may modify their uptake and processing.

Summary

This section has provided a brief overview of the biophysical factors that can affect PK, and in particular a focus on those that lead to off-target clearance. Here it was determined that tissue deposition was skewed towards organs that possessed high vascularity with a discontinuous line of highly fenestrated endothelium. Both CD206 and

ASGPR were also implicated. Coincidently, the liver possesses all these factors and is well established as the detoxifying organ within the body and often pointed to as being responsible for the catabolism of antibodies. In the following section we will explore how the structure of the liver affords it the opportunity to interact and clear antibody as well as discuss the possible cells responsible in this off-target clearance.

1.5 Liver: Anatomy, Architecture and Catabolic Function

Located in the upper right quadrant of the abdominal cavity, the liver is the largest solid organ. Accounting for between 2 to 3% of total average body weight, the liver is responsible for performing over 500 differing functions ranging from bile production, detoxification, plasma protein synthesis and glycogen storage.[90,91] Anatomically the liver is split into two lobes; with the falciform ligament dividing the left and right side. The liver in its entirety is encapsulated in a fibrous tissue known as the Glisson's capsule, named after the British anatomist Francis Glisson, and held in place by various ligaments. At rest, the liver receives 25% of total cardiac output and is unique in the fact that it is the only organ that possesses dual afferent blood supplies.[92] The first being the hepatic artery, which delivers oxygen-rich blood directly from the aorta and contributes between 23-30% of the total blood supply within the liver. Secondly, the portal vein which supplies the remaining 70-77%, delivers nutrient-rich venous blood from the spleen, pancreas and gastrointestinal (GI) tract.[90] The blood is mixed in low pressurised capillary-like vascular channels, known as sinusoids, and is directed towards a central vein; whereby the blood is drained from the liver by the inferior vena cava.

Each liver lobe consists of thousands of microscopic units of cells called lobules, which are arranged into polygonal or hexagonal structures when cross sectioned (Figure 1.4). Described in 1906 by Mall[92], lobules are the functional units of the liver centred around the central vein, with the hepatic artery, portal vein and bile duct located around the peripheral 'corners', in structures termed the portal triad.[92] There are usually six portal

triads per one lobule in a healthy liver. Hepatocytes are the predominant ’parenchymal’ liver cells accounting for 65% of the total liver mass. These cells carry out most of the liver’s function regarding detoxification of both exogenous and endogenous substances, protein synthesis, bile formation and secretion. To fulfil these functions hepatocytes run in proximity with the sinusoids, separated only by a subendothelial space known as the Space of Disse. As a major function of these cells is the production and secretion of bile, small ducts known as canaliculi form between adjacent hepatocytes allowing drainage into the bile ducts. Other non-parenchymal cells located in the liver lobule include hepatic sinusoidal endothelial cells (LSEC), Kupffer cells (KC), stellate cells, biliary epithelial cells, and intrahepatic immune cells.

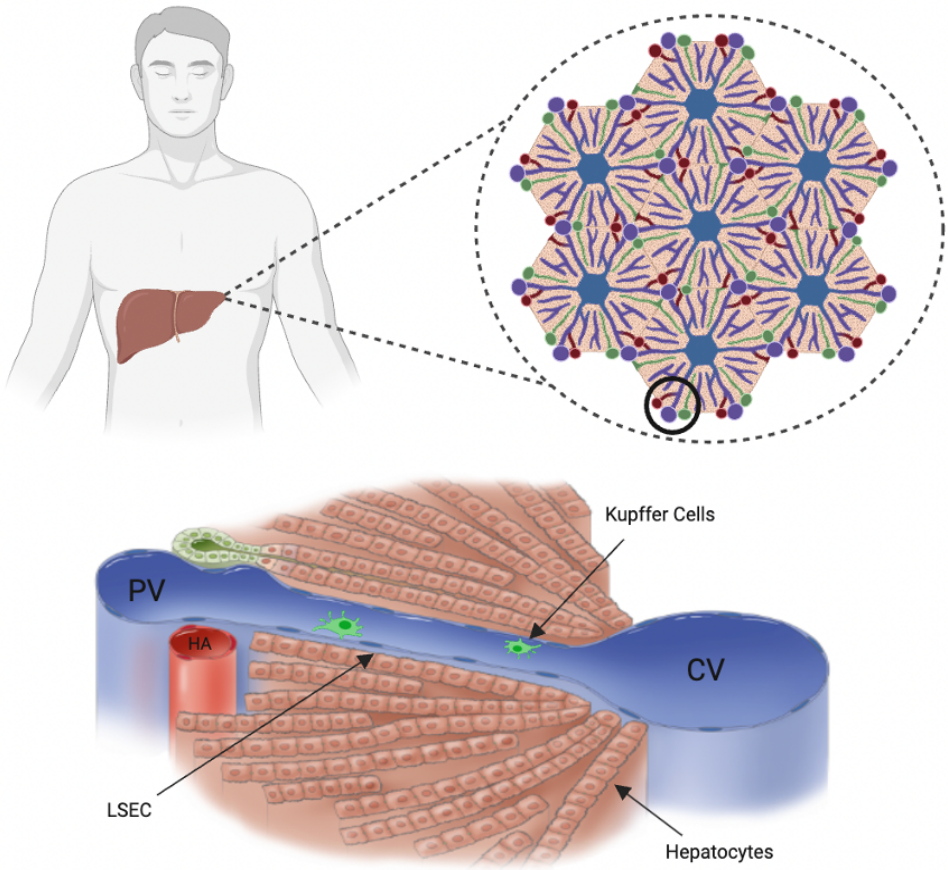


Figure 1. 4: The liver anatomy. Top left shows the placement of the liver within the abdominal cavity. Top right shows a cross section of lobules. Hexagon account for one lobule with the central vein in the middle (blue). The portal triad is circled whereby the purple denotes the portal vein, red vessel is the hepatic artery and green signifies the bile ducts. Bottom image shows a close-up of the cellular structure. Hepatocytes can be seen radiating out from the sinusoids, with liver sinusoidal endothelial cells (LSEC) surrounding. Kupffer cells (green) are also present within the sinusoid. PV= portal vein; HA= hepatic artery; CV= central vein. Figure made on BioRender.

A liver lobule can be divided into three metabolic zones based upon the availability of oxygen imposed by the blood supply. Zone 1 (periportal) encompasses the highly oxygenated region closest to the portal tract, whereas zone 3 (pericentral) encapsulates the area surrounding the central vein, with reduced amount of oxygen in comparison. Zone 2, the transition zone, refers to the space in between.[93] As the environment between the different three zones differ, so does the phenotype of the cells present in those areas.[93,94]

The liver holds a vast network of vasculature comprising of millions of sinusoids, these ensure close contact between parenchymal cells and the blood supply. These capillaries cover a total area equivalent to that of a tennis court at ~210m^2.[95] Blood flow varies in each sinusoid in response to distance from zone 1 and as a consequence of resident cells in the lumen and structural variations, thus blood flow changes speed, and can even occasionally stop or reverse.[96,97] This allows ample opportunity for hepatic cells to survey and interact with therapeutic antibodies within the circulatory system. In 1981, Henderson *et al.,*[98] using radioactively labelled IgG1 and IgG2a, found on a weight basis, antibody catabolism was most prevalent within the liver in rats.[98] Following on in 2000, using chimeric IgG1 antibodies *in vivo* with varying glycosylation patterns, the liver was found to have the highest catabolic activity for antibodies with a terminal mannose or galactose residue.[99] As discussed above, ASGPR and CD206 are highly expressed in the liver, both of which are known to result in the clearance of both of these glycoproteins. In mice, three studies using humanised IgG1 mAbs explicated the liver and spleen as major sources of catabolism.[100-102] All three studies also included the derivatives of each antibody with reduced FcRn affinity. Here, those with the absence of FcRn protection saw significant degradation in the liver in comparison to other tissues.[100-102]

The liver isn't responsible solely for the catabolism of standard full length IgG antibodies. Ferl *et al.,* designed a 105kDa scFv-Fc antibody fragment, utilising an intact IgG1 Fc bound to two scFv dimers.[103] This was intended for use in combination immunotherapy, whereby an anti-tumour antibody is conjugated to a radionuclide allowing discreet radiation to be delivered to the tumour site. To assess the levels of off-target catabolism, ^{111}In- and ^{125}I-labels were conjugated to these fragments and assessed in mice with and without tumour. Liver, again, was pivotal to IgG catabolism. Interestingly, it was found that mice with larger tumour burdens saw less degradation within the liver.[103] It was estimated that the liver was responsible for ~50% of antibody elimination when tumour burden was ~0.1g. This this reduced to 35% when tumour burden exceeded 0.3g, suggesting a change in PK or elimination in diseased conditions.[103] In contrast, to the studies above involving full length IgG, in experiments with antibodies bearing decreased

FcRn affinity, there was no significant difference in clearance. This led the authors to conclude that liver clearance was not heavily FcRn dependent.[103]

Similarly, the biodistribution of bsAb is also skewed towards the liver. Using intravital microscopy in mice, Datta-Mannan *et al.,*[104] showed following a single IV administration of either mAb or bsAb, both were distributed within the liver in less than 20 minutes. Punctate staining was visualised on the liver endothelial cells at 11-minutes post infusion for mAb and 19-minutes for the bsAbs.[104] Initially, fluorescent intensity was higher for mAbs, however after 24-hours, comparable intensity levels were reported with bsAbs.[104] Co-staining with F4/80 and imaging in Lys-EGFP mice ruled out contribution of Kupffer cells (liver-resident macrophages) and neutrophils, leaving the author to conclude the liver endothelia to be responsible for enhanced degradation of these antibodies.[104] It is worthy to note, no direct lysosomal indicators nor markers beyond CD206 were performed for the endothelia in this study.

In summary, this section aimed to give an overview of the healthy liver's architecture with an emphasis on the vast vascular network that supplies this organ. With varying flow rates throughout each acinar zone, and close proximity of all cells to the circulation, there is extensive opportunity for cells to interact with blood-borne therapeutics. This has been confirmed experimentally in many studies, with the liver often exhibiting high levels of distribution and catabolism. This is not exclusive to full length IgGs. With evidence supporting the liver's pivotal role in the off-target clearance of mAbs and bsAbs, the next section will investigate the hepatic cellular constituents that make up the reticuloendothelial system possibly responsible for this clearance process.

1.6 Hepatic Reticuloendothelial System

The hepatic reticuloendothelial system (RES) refers to a specialised network of cells, namely the Kupffer cells (KCs) and liver sinusoidal endothelial cells (LSEC), that collectively survey the vasculature and phagocytose and clear particles, cellular debris and other substrates. RES was coined in 1924 by Aschoff, defining this system as a group of cells able to incorporate vital dyes from the circulatory system.[105] Knowledge has since improved regarding these cells and today LSEC are described as endothelial cells with a high scavenging capacity, equipped to clear macromolecules and colloids <100nm in size.[106] Kupffer cells on the other hand are specialised macrophages, resident to the liver that are capable of phagocytosing particles and debris larger than 100nm (Figure 1.5).[106] The RES is described as the most powerful scavenging system within the entire body.[132]

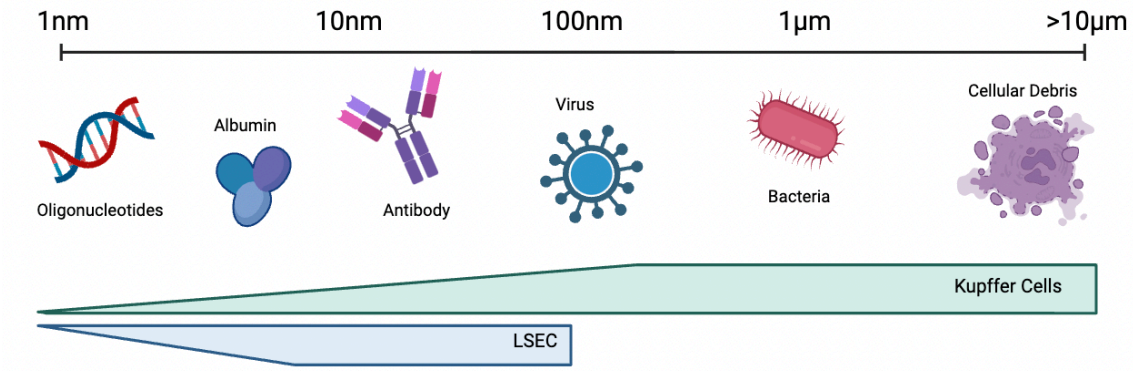


Figure 1. 5: Scavenging capacities of the RES. This depicts the capacity of the reticuloendothelial system (RES), namely the liver endothelial sinusoidal cells (LSEC) and Kupffer cell's ability to internalise components of varying size. LSEC are capable up to 100nm, whereas Kupffer cells phagocytose larger complexes. Adapted from Bhandari[97] on BioRender.

1.6.1 Kupffer Cells

Karl Wilhelm von Kupffer first observed star-like cells present within the lumen of the sinusoids.[107] In 1976, Browicz defined these cells as macrophages, establishing them as the phagocytes of the liver.[108] Originating as fetal macrophages in the yolk sac, upon entry into the blood stream, they migrate to the liver. Here these cells mature into Kupffer cells (KCs) with a high proliferative capacity and the ability to self-renew.[109]

Despite being the most abundant population of macrophages within the body,[110] they are a challenging cell to study. Due to lack of a validated phenotypic identifier that distinguishes these cells from other newly infiltrating blood-derived hepatic macrophages, particularly in humans. Through a compilation of sc/snRNA-seq data,[111-115] Guilliams and Scott formulated a core gene signature for KCs across 7 species, with genes coding for CD5L, $VSIG_4$, CD163, $FOLR_2$, MARCO (mice) and SLC40A1 being characteristic.[116] Surface receptors often used for identification include CD68, CD11b, CD14, CD16 and recently the suggestion for $CD32^{mid}$ has also be included.[117] Both CD16 and CD32 are members of the FcγR family and are ligands for IgG uptake, thus this family will be described in more detail in Chapter 3. In mice, KCs may also be identified as $CD11b^{int}$, $F4/80^{hi}$, $CLEC4F^{+}$.[458]

Kupffer cells also play a role in the immune surveillance against gut-derived toxins and pathogens such as the endotoxin, lipopolysaccharides (LPS). In order to do this, KCs express a vast range of Toll like receptors (TLR1-9) which recognise pathogen-associated molecular patterns (PAMPs), and the host endogenous damage-associated molecular pattern molecules (DAMPs).[118-120] Alongside these, they also express scavenger receptors (SR) such as SR-A and CD36, both play a role in lipid metabolism and pathogen uptake; with the latter functioning to internalise apoptotic cells.[121-123] As mentioned KCs express FcγRs that bind to IgG, and KCs are also antigen presenting cells able to induce T-cell mediated responses. Galactose binding receptors are also present on KCs. One known as the macrophage galactose lectin, was detailed in 1988.[124] In rats, it was shown to confer strong binding affinity for GalNAc terminated glycans.[125] In mice, this galactose lectin alongside the Ashwell-Morell receptor (an ASGPR) on Kupffer cells mediated the clearance of desialylated platelets within the liver.[126]

Interestingly, the expression of CD206 by KC's appear divisive in literature. With the rise in scRNA seq and spatial transcriptomics, the idea of two populations of KCs has become popular, particularly in a rodent context.[113,116,127,128] It has been suggested that these two populations are split based on their expression levels of CD206 and ESAM.[127,128] With

cells termed KC1 lacking expression of CD206. In another publication, Martens *et al.,* concur and describe human KCs completely lacking expression of CD206.[129] This directly contrasts such databases as the human protein atlas[130] where two KC clusters were described with both showing increased expression of *MRC1*, the gene encoding for CD206. Guilliams *et al.,* addresses this suggesting that as KC2 and LSEC have extensive crossover for their expression profiles, confusion in regard to marker expression may relate to presence of doublets during analyses.[113] Further to this Hume *et al.,* suggested contamination of LSEC with KCs during the digestion stage may account for the emergence of the two populations.[131] Taking everything into account, more research needs to be conducted in order to fully determine the distinction of these cells from circulatory macrophages/monocytes and there is yet to be a consensus on the homogeneity or heterogeneity of this cell type within the liver. Nevertheless, KC have both the endocytic machinery and surface receptor profile to internalize some antibodies.

1.6.2 Liver Endothelial Sinusoidal Cells

The liver is unique due to its dual afferent blood supply mixing within the sinusoids. Not only does oxygenated blood arrive from the hepatic artery but also the nutrient dense blood from the portal vein. This blood also bathes the liver in bacteria, toxins and viruses gathered from the gut. These vessels are lined by vast numbers of liver sinusoidal endothelial cells (LSEC). Often as the first point of contact with blood contents, LSEC are equipped with a vast array of scavenger receptors and are considered to have the highest endocytic capacity of any human cell type.[133] This allows for the mass elimination of macromolecules from the circulatory system.

LSEC were first described in 1970 when Ed Wisse distinguished them from Kupffer cells in rat, via electron microscopy.[134] Accounting for 70% of all sinusoidal based cells within a lobule, LSEC are highly specialised, with functions facilitated by their morphology. LSEC are characterised by the absence of a basal membrane and are highly fenestrated (diameter ranging from 50-300nm); approximately between 2 and 20% of an LSEC

surface is covered by fenestrations.[135] Due to these fenestrations and their permissible nature, LSEC are in affect an ultrafiltration system acting as the interface between the lumen of the sinusoids and hepatocytes.[136] LSEC play a pivotal role in the modulation of cholesterol metabolism through their regulation of bidirectional lipid exchange.[137] Although Wisse, described an abundance of endocytic vesicles,[134] LSEC's capacity as scavenger cells was not revealed until 1982. Here, it was described that LSEC could endocytose hyaluronan.[138] Since then these cells have been implicated in the clearance of a multitude of proteins, glycans, tissue waste products, immune complexes and lipoproteins to name a few.[139] These processes are achieved through either receptor mediated mechanisms or via pinocytosis.[140,141]

In humans, LSEC express heterogeneous phenotypes, that vary across acinar zones: for example, zone 1 cells are $CD36^{hi}$, $CD32^{-}$, $CD14^{-}$, LYVE-1^{-}; whereas those in zones 2 and 3 are LYVE-1^{+}, $CD32^{hi}$, $CD14^{+}$, $CD54^{+}$, $CD36^{Mid\text{-}Low}$.[142] Several scavenger receptors are expressed by LSEC. Stabilin 1 and Stabilin 2 are noteworthy to mention. It was shown that inhibition of the latter led to an 80% reduction in hyaluronan uptake by LSEC.[143] These receptors are involved in the resultant degradation of oxidised low-density lipoproteins, protein waste products and extracellular matrix molecules.[139,143,144] Similar to KCs, expression of $CD36^{+}$ is also seen within LSEC. Another scavenger receptor, the C-type lectin, LSIGN (Liver specific ICAM-3 grabbing non-integrin; CLEC4M; CD209L) is a type 2 transmembrane glycoprotein.[145] This is highly expressed on LSEC and known to bind to hepatitis C and Human immunodeficiency virus[146,147] During the SARS-CoV-2 pandemic, this receptor was of great interest. Here it was described that LSIGN has a strong binding affinity to high mannose glycans; but lacked affinity to more complex glycans.[145,148]

Less controversial than KCs, LSEC are known to express CD206, which plays a very important role. In CD206 knock out vs wild type (WT) mice, it was shown this receptor was responsible for the removal of circulating lysosomal enzymes. Both experimental groups exhibited equivalent liver uptake of formaldehyde treated albumin, however

intracellular catabolism of this protein was reduced by 50% in CD206$^{-/-}$ mice. This suggested that although CD206 was not wholly responsible for the internalisation of albumin, it was responsible for the recruitment of these enzymes to degrade endocytosed material.[94] During the process of tissue turnover, LSEC are dependent on CD206 to remove many of these by-products which cause significant damage if they accumulate. This includes denatured collagen fragments, plasminogen activators and neutrophil derived myeloperoxidase to name a few.[139,149-151] Another main waste-clearing receptor expressed on LSEC is CD32b (FcγRIIb). As with KCs, this receptor is known to internalise immune complexes for degradation. Expression of CD32b is prominent in humans and rats and is often regarded as a selection biomarker for these cells.[152] Approximately 75% of all CD32b within the body is expressed on the LSEC; here the isoform of CD32b majorly expressed was found to be CD32b2 (typically found on macrophages).[155]

1.7 Deciphering Non-Specific Clearance: LSEC vs Kupffer Cells- Size Matters

Ascertained throughout this introduction that the leading cause of an antibody having a poor PK is off-target interactions and clearance kinetics. Design of these therapeutics obviously has a big impact on extent of clearance and specificity as considered in Section 1.4. It has also been established that the liver is the major organ responsible for this early elimination from the body. An unmet research question however is understanding the cell type responsible for this non-specific clearance. This is crucial for optimizing drug design and dosing to enhance overall efficacy and safety for patients. Considering their location within the sinusoids and extensive array of scavenging receptors, LSEC and KCs emerge as the most probable cell types responsible.

Shown in Figure 1.5, uptake by either cell is dependent on the size of the components. Often mAbs/bsAb are targeted as soluble ligands and thus form immune complexes in the periphery. It is a known concept that the size of these complexes determines its fate.[156-158] Skogh *et al.,* formed immune complexes of varying sizes through the

conjugation of anti-DNP IgG and dinitrophenylated albumin.[159] Smaller complexes was determined to be cleared by LSEC, whereas large complexes were cleared by KCs.[159] Worthy of note, IgG in circulation have a penchant to aggregate, particularly if they are more basic.[55] With this, Bogers *et al.,* administered monomeric IgG and aggregated IgG into a rat.[160] Using a technique whereby splenic and liver macrophages could be depleted completely by clodronate in a liposome,[161] they investigated how WT vs KC depleted rats distributed and eliminated these complexes.[160] Monomeric IgG (1:1 antibody to antigen; 1 Fc in complex) was cleared similarly by each experimental group. Aggregated IgG, however, showed a delayed elimination response which became accelerated on day 5 upon replenishment of KCs back to 50% of the original population. Localisation of monomeric and aggregated IgG were both absent from hepatocytes in both groups; but in WT mice immunofluorescent staining of the IgG was present on both LSEC and KCs. In the KC depleted group, staining was only present on LSEC. Complex staining was not present on LSEC proximal to the portal or central vein area.[160] LSEC were shown to possess the capacity to degrade aggregated IgG, just to a slower extent than in models with their KC population intact. Inhibition of the FcγR on LSEC by the pre-treatment of IgG on the KC depleted rats completely eradicated the ability to clear aggregated IgG;[160] suggesting LSEC action clearance through their FcγR receptors.

In a similar study, utilizing an IgG isotype biparatopic antibody to the soluble ligand, IL-6, KCs were the predominant cell type responsible for clearance in mice.[162] Ensuring each complex contained at least >3 bsAb molecules, co-localisation was seen with F4-80, a mouse macrophage marker, via intravital microscopy. Further experimentation with FcεR1γ$^{-/-}$ mice (a commonly conserved gamma chain), showed significantly reduced internalisation and co-localisation of complex with macrophage. Leading the authors to conclude FcγR on KCs were responsible for the clearance of immune complex.[162] To be critical of this paper, no co-localisation staining, or analysis was performed on LSEC to compare the two cell types. Interestingly, this publication also included intravital microscopy of administered mAbs, whereby little to no staining was seen co-localised with F4-80.[162]

This work is somewhat contrasted by the research published by Datta-Mannan in 2016, who used IgG fusion bsAb (e.g. IgG-scFv) intravenously administered into cynomolgus monkeys.[163] Here one group was pre-treated with clodronate liposomes to achieve a clearance of 95% of macrophages and the other group remained untreated. Very little change was observed with each bsAbs PK profile, indicating KCs had very little effect on peripheral clearance. Through immunofluorescent imaging, each bsAb was seen to co-localise with the endothelial marker CD31 in comparison to that of the KC marker, CD68.[163] Complex size here was unknown and focus was aimed more at elucidating off-target clearance rather than Antibody-Antigen clearance. In later work by the same authors and referred to in Section 1.5, intravital microscopy in mice showed punctate staining was visible on the endothelium within 20 minutes for both mAbs and bsAbs, with no co-localisation with F4-80.[104] This suggests a key role for LSEC in antibody clearance. Moreover, Ganesan *et al.,* proposed that CD32b on LSEC was responsible for the clearance of small immune complexes. In mice, 90% of CD32b is expressed on LSEC with the remaining 10% on KC.[164] In CD32b knock out mice, a striking reduction in clearance of small immune complexes was observed. It was suggested here that the small fraction of 10% of total liver CD32b being on KC could not be the major contributor to significantly reduced clearance seen in these genetically modified mice.[164] A similar comment was echoed by Johansson *et al.,* that although on a 1:1 basis, Kupffer cells are more efficient at clearing these complexes, the sheer number of LSEC outweigh that of KC so in turn may exhibit equal total capacity.[165]

To summarise, there is considerable evidence to show both KC and LSEC have a role in the clearance of therapeutic antibodies. A considerably amount of research has focused on the clearance of immune complexes and how size determines which cell type. Immune complexes often comprise antigen and antibody so in this respect, the clearance is considered more target mediated clearance. To explore more the off-target mechanism, this research thesis will be focused on LSEC. This is justified by the likelihood not all antibodies form complexes in serum before target engagement, and the fact that

the majority of the mAbs and bsAbs used in this research are not targeted at soluble ligands or directed against LSEC antigens. In addition, size exclusion chromatography confirmed these therapeutics had not aggregated during storage (data not shown). Binding determination with THP-1s polarised to characterise macrophages in both anti- and pro-inflammatory phenotypes showed little to no binding at 4- and 8-hours (Supplementary Figure S1).

Shown throughout, the LSEC's role has been discussed within the setting of animal models only. Although a useful tool, this does not recapitulate the complex histoarchitecture and physiological conditions seen within the human liver. This unmet area of exploration is further extended if we consider how the liver is often susceptible to injury and how this disruption in healthy liver architecture may skew clearance profiles further. The following section introduces the common forms of liver disease and explores how the change in liver landscape may be an important factor to consider in pre-clinical screening of antibody-based therapeutics.

1.8 The Liver in Disease

Globally, liver disease is the 11th most common cause of death.[166] In the UK alone, it claims more than 27 deaths a day.[167] Since 1970, it is the only major disease to see a rise in mortality rate, with a four-fold increase (see Figure 1.6).[167,168] 50% of liver disease related deaths are in patients aged 45-64[169]; on average, men are more likely to die than women (62% to 38%).[170]

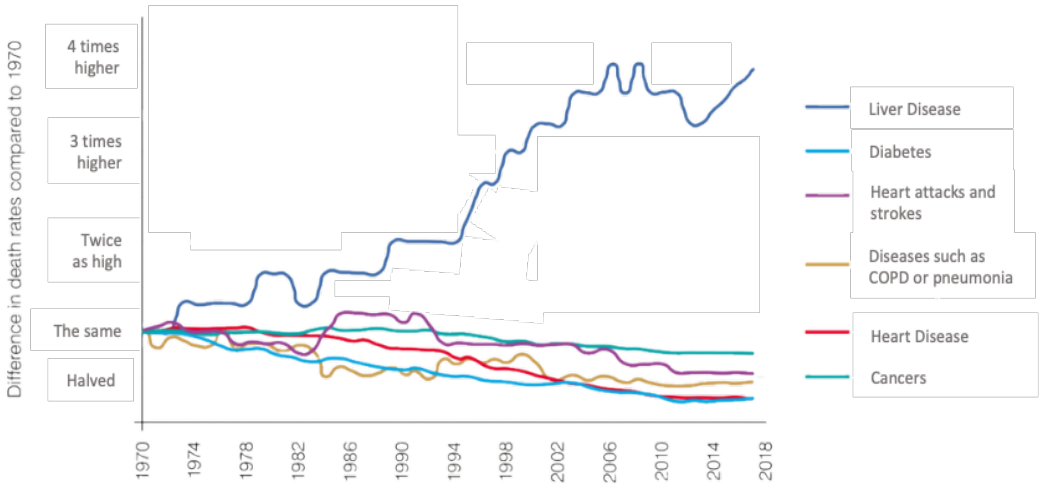


Figure 1. 6: Mortality rates of major diseases. A graph depicting the increase of mortality rates of liver disease in comparison to other major diseases since 1970 in the UK. This data has been normalised and figure taken from the British Liver Trust.[167]

Liver disease is an umbrella term encompassing a spectrum of aetiologies. Liver damage progresses commonly through four stages (see Figure 1.7). Often, early stages of inflammation and steatosis (fat accumulation) within the liver is reversible. This is most likely caused by preventable environmental factors such as alcohol, obesity, and viral hepatitis; and in some cases, can easily be treated with early intervention by lifestyle changes. However, this stage is asymptomatic and thus with continuous insult this damage will progress onto fibrosis in patients unaware of their condition.[171] Liver fibrosis is characterised by the deposition of extracellular matrix. This deposition forms scars and leads to a reduction or loss of function of cells affected in this area.[172] Again, although mostly asymptomatic in its early stages, with intervention this is a reversible dynamic process. The following stage of progression is cirrhosis. Cirrhosis is late-stage fibrosis whereby the scarring has reached such a level of burden that the liver architecture is disrupted, and function is compromised. This leads to a loss of characteristic functions, hemodynamic instability, and portal hypertension.[173] If liver disease is advanced through to cirrhosis than there is an exponential risk of developing liver cancer/hepatocellular carcinoma (HCC) such that in approximately 90% of those with HCC, cirrhosis is present.[174]

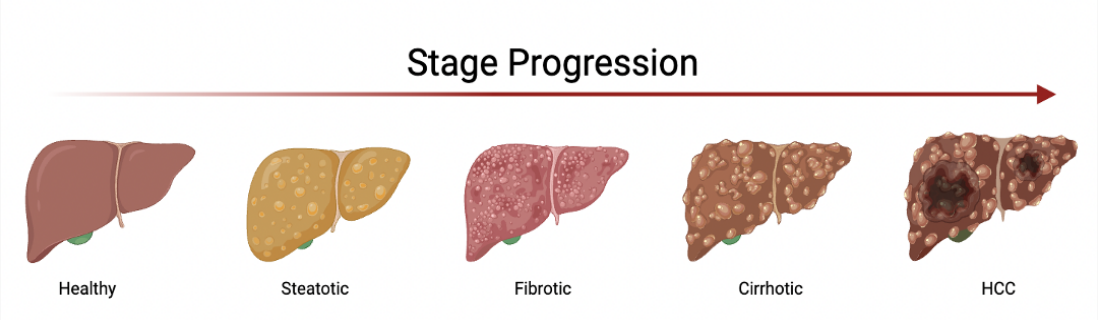


Figure 1. 7: Stage progression of liver injury. Starting at healthy and moving to steatotic defined by its fat accumulation. Next is fibrosis, characterised by the deposition of scarring. This point is a dynamic reversible process. If the pathological insult is not removed, then fibrotic tissue becomes cirrhotic leading to dysfunction and irreversible changes to the liver's architecture. Often cirrhosis can progress to hepatocellular carcinoma (HCC), a primary liver cancer. Figure made on BioRender.

The pathological spectra described above can result from any form of chronic liver disease. In our research, the focus is on two aetiologies that arguably are the most preventable and the most common: alcoholic related liver disease (ARLD) and metabolic dysfunction-associated steatotic liver disease (MASLD). To note, MASLD nomenclature changed from non-alcohol related fatty liver disease (NAFLD) in 2023,[175] this encompassed the more severe form of non-alcoholic steatohepatitis (NASH), now known as metabolic-associated steatohepatitis (MASH). For ease of comparison between alcohol related vs non-alcohol related comparisons, MASLD will include data from MASH explants. Whereby, comparisons that are drawn between healthy vs cirrhotic, the cirrhotic group will include MASLD and ARLD. ARLD is characterised by the excessive and prolonged consumption of alcohol. Continued intake can result in cirrhosis. Approximately 24% of people in the UK are reported to drink over the recommended guideline of 14 units per week.[176] In those who develop ARLD, once cirrhosis develops the only treatment is liver transplantation. In the Birmingham liver transplantation centre a 6-month period of proven abstinence needs to be met before consideration, however 1 in 4 individuals are dead within 60 days of diagnosis with the serve form of ARLD (alcoholic hepatitis) this criterion is often missed.[177,178] MASLD is the leading cause of chronic liver disease worldwide, with an overall prevalence estimated to be 32.4% in adults.[179,180] However, this number may be grossly underrepresented with suggestions that 4 in 5 people within the UK with MASH are undiagnosed.[181,182] Characterised by

accumulation of fat within the liver, risks factors of this disease include obesity and in turn high fat diets and sedentary lifestyles, type 2 diabetes and metabolic dysfunction.[183] Here too disease progresses to cirrhosis and MASLD remains one of the most significant drivers of transplantation as no preventive therapeutic is currently available.

1.8.1 Phenotypic and Functional Changes in Liver Disease

The effects of cirrhosis in terms of observation in histology are explored more in Chapter 3. However, it is important to understand how the accumulation of scar tissue and increased inflammatory stimuli change the microenvironment within the liver leading to loss of function and disruption of histoarchitecture, particularly with LSEC.

A brief overview for the progression of fibrosis may be found in Figure 1.8. In brief, in the preliminary stages of liver injury, LSEC undergo a process called capillarisation.[187,188] Here they lose their characteristic fenestrations and gain a basement membrane. This hinders their capacity to act as a permissive barrier and in turn their transmigratory function.[188] Membrane formation prevents the metabolic exchange leading to hepatocyte hypoxemia and their loss of microvilli.[188] Both hepatocytes and LSEC then release stress signals and pro-inflammatory cytokines such as transforming growth factor beta 1 (TGFß-1), which activates quiescent stellate cells within the Space of Disse to transdifferentiate into myofibroblasts. These cells produce extracellular matrix proteins (ECM) to aid in healing.[189] If harmful stimulus is chronic, the regenerative capacity of the liver is exceeded and myofibroblasts become the drivers of scar deposition that characterise fibrosis.[189]

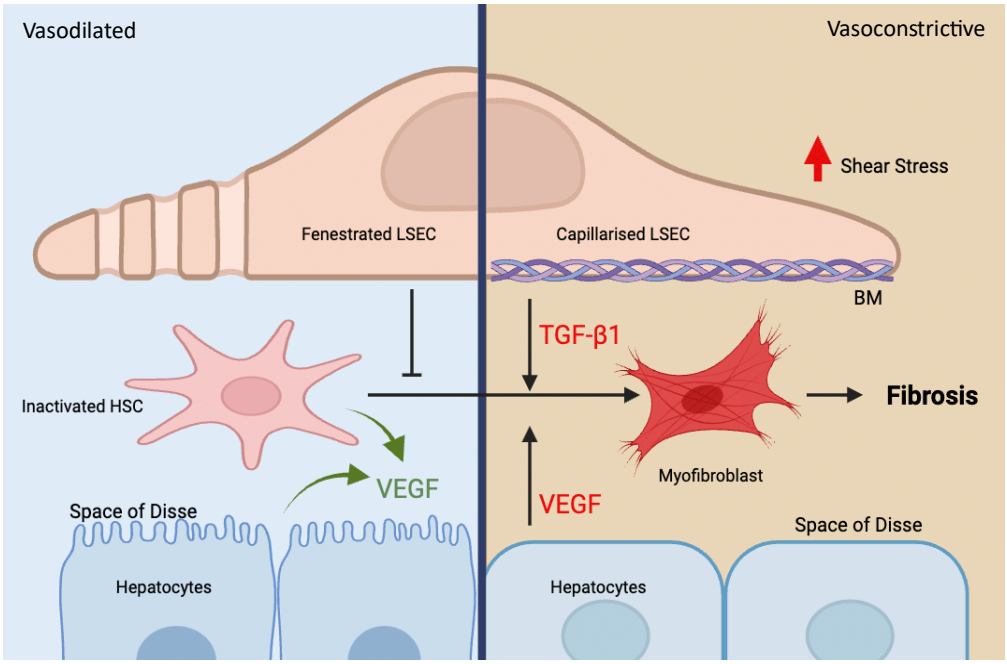


Figure 1. 8: Brief pathogenesis of fibrosis. Left shows cells in a healthy state whereby, liver sinusoidal endothelial cells (LSEC) are fenestrated and lack a basement membrane. Hepatic stellate cells are quiescent, and hepatocytes maintain their regular morphology. On the right shows the early progression of fibrosis. Here LSEC lose their fenestrations and gain a basement membrane. This leads to the production of TGF*ß*-1 that activate HSC to transdifferentiated into myofibroblast. With the loss of metabolic interchange from the blood supply, hypoxia-inducible factor (HIF) expression is elevated leading to the increased production of vascular endothelial growth factor (VEGF). This further perpetuates activation of HSCs. Myofibroblasts release extracellular matrix proteins (ECM) leading to the deposition of scars. This characterises the scarring seen in fibrosis. Created on BioRender with adaptions from Poisson *et al.*,[223]

Scar deposition skews the liver architecture and often leads to the occlusion/ loss of sinusoids.[219] This in turn leads to a reduction in blood flow and results in the most common side effect of cirrhosis, portal hypertension.[184,185] LSEC dysfunction in liver injury further exacerbates this restrictive blood flow by deregulating vascular tone and adopting a vasoconstrictive phenotype.[184] With this, LSEC lose the capacity to produce and respond to vasodilators such as nitric oxide, cyclooxygenase, and prostaglandin I[221,222]; and instead increase the production of vasoconstrictors such as endothelin-1 and angiotensin II. Another consequence of LSECs gain in basement membrane leading to hypoxia, is the overexpression of the transcription factor, hypoxia-inducible factor (HIF).

This stimulates vascular endothelial growth factor (VEGF) production promoting angiogenesis.

With architectural changes and exposure to an increasing pro-inflammatory environment, the LSEC phenotype changes and they show both a gain and loss of receptors.[220] For instance in both cirrhosis and HCC, it was noted serum levels of hyaluronan became elevated.[190] This was in direct response to the loss of expression in the scavenger receptor, Stabilin 2 on LSEC.[97,191] These elevated levels increased the viscosity of the blood resulting in further increases in blood pressure.[192] The loss of Stabilin 2 also reduced the capacity of LSEC to clear ECM.[97,191]

Liver injury induced by CCL4 is a well-established animal model to study cirrhosis.[193] Using this method and single cell transcriptomics, Su *et al.,* showed mice with cirrhosis had increased expression of CD34 (associated with capillarisation) and an associated downregulation of CD32b in zone 3 (pericentral zone).[194] Overall there was a noted loss in total LSEC abundance in diseased mice. LSEC constituted an 89% share of total endothelial cells within a healthy mouse liver and a reduced total of 73% in cirrhotic livers. Muro *et al.,* concurred with observations in the loss of CD32b in cirrhotic rat and human livers. [195,196] Sequential losses in expression of this receptor were also noted during tumour progression in HCC patients.[191] In another study using CCL4 injured rats, the expression density of Fc receptors alongside LSECs ability to uptake circulated immune complexes was reported to be reduced.[197]

In contrast to the downregulation of CD32b and other scavenger receptors in disease, CD206 exhibits an overexpression in an inflammatory environment. The proinflammatory cytokine, IL-1, is known to upregulate both the expression and endocytic capacity of CD206.[198] Whereas, the anti-inflammatory cytokine, IL-10, is described as the opposite, reducing CD206's activity.[199] Soluble mannose receptor concentration are significantly heightened in individuals with liver cirrhosis and ARLD.[200] Here levels are used to predict disease severity with a correlation drawn between

concentration increase and portal hypertension, gut permeability and mortality from liver injury.[201-203]

Glmp$^{gt/gt}$ mice lack the expression of the glycosylated lysosomal membrane protein and in turn spontaneously develop chronic liver injury. This model has been well characterised, and the process is a slow progression of collagen accumulation until it replicates periportal liver fibrosis.[204] Using this model to track fibrosis progression, Antwi and colleagues described a lack of fluorescent signal of CD206 around the site of inflammation in comparison to that of the Stabilin receptors. This contrasts some of the research stated above, where stabilin was thought to be reduced and CD206 increased. They further described, using electron microscopy, that in fibrosis, LSEC did not lose their fenestrations but in fact the diameter of these increased to >400nm.[205] In agreement though, CD32b was significantly lost in *Glmp*$^{gt/gt}$ mice at both protein and mRNA level within whole liver lysates. It was noted, this loss was expressed throughout even on those LSEC that had their fenestrations intact.[205]

KCs are also affected in cirrhosis. It is understood that with the inflammatory response, there is an influx of monocytic-derived infiltrating macrophages that dilute ratios of KCs. Bringing different cell types and expression profiles into the environment.[116,206,207] For instance, in HCC, KCs are known to express their own unique transcriptional profile that promotes angiogenesis within a tumour. This is a result of their increased expression of VEGF and matric metalloproteases.[208]

1.9 Impact of Liver Disease on Therapeutic Antibody Clearance: Clearance Dynamics and Clinical Implications.

The expression landscape of the liver is ever changing, especially in the context of disease progression. Section 1.8.1 describes how receptor expression changes in fibrosis and how the ability to internalise immune complexes is diminished in CCL4 rats.[197] It has

been shown how a loss of a single receptor can significantly shift the entire transcriptome of an LSEC in mice, leading to the downregulation of important genes.[209] For example, a knockout of stabilin 1 led to 82 significantly altered genes, 96 genes with stabilin 2 and a total of 238 genes in a double receptor knock out mouse.[206] These expression changes evident in liver injury have significant impact on receptors present on the surface of the cell. This further evidence changes in cirrhosis could impact how these LSEC interact with biotherapeutics in comparison to healthy cells.

Notably in microenvironments such as tumours in HCC, target (tumour antigens) concentrations will be greater in comparison to that in healthy individuals. This could result in higher order immune complexes being formed with target: mAbs/bsAbs, thus altering their PK[162] in a way that wouldn't be seen in the *in vitro* screening currently being used. As mentioned previously, size of complexes alters how the liver internalises and clears antibodies, therefore antibody exposure in cirrhotic tissue may be affected by this. Furthermore, in some antibody-based therapies pre-existing liver disease is considered exclusion criteria. For instance, in rheumatoid arthritis patients with pre-existing liver disease, are unable to take tocilizumab (anti-IL-6 receptor) and anakinra (anti-IL-1R antagonist) due to increased hepatotoxicity risks.[210]

Liver disease is currently highly prevalent, often it remains undiagnosed and undetected until clinical presentations are evident. This could mean millions more have some form of undisclosed liver injury. In a recent study by the British Liver Trust, it was reported that 73% of individuals with a liver condition felt stigmatised, with this a further 29% felt that this prevented them from seeking medical care sooner.[91] With such a vast population affected, it is a major omission to not investigate how the changing nature of the liver, in particular with LSEC, may affect the pharmacokinetics of such therapeutics.[211]

1.10 Scope of this work

The biggest challenge in the development of new antibody-based therapies is the need to exert target mediated action whilst also bypassing the natural defences of the human immune system. The intricate balance between target mediated clearance and toxic accumulation is determined by an antibody's PK. Highlighted throughout, is that the main cause of poor PK is non-specific clearance. The liver has been pinpointed as the major catabolic organ responsible for this process. The liver is susceptible to injury and disease, with this there is an everchanging landscape of phenotypes and receptor expression. Studies, thus far, to characterise a therapeutic's PK are within healthy individuals and/or animal vectors so do not recapitulate the true environment of the chronically diseased individuals these antibodies are often developed to treat. Therefore, our thesis **hypothesises that LSEC play an over-looked role in the non-specific clearance of therapeutic antibodies, and this has further implications with liver injury/disease**. We question if current pre-clinical models appropriately recapitulate the complex physiological systems these biotherapeutics are exposed too *in vivo*.

To investigate this hypothesis, we utilized a panel of 9 mAbs and 2 bsAb and endeavoured to answer the 4 following aims, see Table 1.2.

Table 1. 2: Outline of thesis aims

Aims	Methods used
1. **To assess expression of key receptors thought to be involved in the scavenging of antibodies within healthy and diseased tissue and cells**	• Western blotting • qPCR • Immunohistochemistry
2. **Quantify LSEC's ability to bind and uptake mAbs/bsAbs**	Expose therapeutic antibody to both mono- and cocultured cells. Quantified by: • ELISA/MSD • Flow cytometry • Immunofluorescence
3. **Elucidate the mechanisms by which LSEC internalize antibody**	• Receptor knockdowns • Receptor overexpression • Pharmacological inhibitors
4. **To track the fate of internalized therapeutics within the cell**	• Confocal microscopy to quantify co-localization with compartmental markers

Chapter Two: Materials and Methods

2.1 Materials

Table 2. 1: TaqMan used in qPCR

TaqMan Assay	Target	Assay ID	Lot number
	AP3M	Hs00931835	2140559
	B2M	Hs00187842_m1	2015681
	CLEC4M	Hs03805885_g1	2036173
	FCGR2A	Hs01013401_g1	1902704
	FCGR2B	Hs01634996_s1	2035622
	FCGRT	Hs09108967_m1	1512359
	MRC1	Hs07288635_g1	2022180
	PECAM1	Hs01065279_m1	4331182
	SRSF4	Hs00194538_m1	1944656
	STAB2	Hs01000844_m1	1883639

Table 2. 2: Antibodies used

Antibodies for IHC, Western blot & IF	Target	Host/Format	Use (conc)	Cat no.
	CD32b	Goat IgG	WB (1µg/mL)	Ab77093
	CD32b	Rabbit pIgG	IF (3µg/mL)	Ab151497
	CD32b	Rabbit IgG	IHC (4µg/mL)	Ab45143
	CD206	Rabbit pIgG	IHC/IF/WB (1µg/mL)	Ab64693
	CLEC4M	Rabbit IgG	IHC (1µg/mL)	HPA042661
	FcRn	Rabbit pIgG	IHC/WB (0.4 µg/mL)	NBP1-89128
	FcRn recombinant	/	WB +ve (0.4µg/mL)	8639-FC
	Lysotracker	/	50nM	L7525
	LAMP1	Rabbit	3µg/mL	MA5-29385
	LIVE/DEAD Near IR	/	FC (1µL:1mL)	L34992
	Mouse IgG IMC	Mouse IgG	Matched*	X0931
	Rabbit IgG IMC	Rabbit IgG	Matched*	Ab34417

Goat IgG IMC	Goat IgG	Matched*	02-6202
Human IgG IMC	Human IgG	Matched*	02-7102
Anti-Human IgG Secondary (Alexafluor 647)	Goat anti-Human IgG (H+L)	IF/FC (3µg/mL)	A21445
Anti-Human IgG Secondary (Alexafluor 488)	Goat anti-Human IgG (H+L)	IF/FC (3µg/mL)	A11013
Anti-Rabbit IgG Secondary (Alexafluor 488)	Goat anti-Rabbit IgG	IF (3µg/mL)	A11034
Anti-Mouse IgG Secondary (Alexafluor 488)	Goat anti-Mouse IgG (H+L)	IF/FC (3µg/mL)	A11001
Anti-Rabbit IgG HRP	Goat anti-Rabbit IgG (H+L)	WB (0.2µg/mL)	172-1019
Anti-Mouse IgG HRP	Goat anti-mouse IgG (H+L)	WB (0.2µg/mL)	172-1011
Anti-Goat IgG HRP	Rabbit anti-Goat IgG (H+L)	WB (0.2µg/mL)	172-1034

pIgG= polyclonal. (H+L)= heavy and light chain. IMC= Isotype matched control. Matched* means matched to concentration used with primary antibody. IHC= immunohistochemistry; IF= immunofluorescence; WB= Western blot; +'ve = control; FC= Flow cytometry

2.2 Liver Tissue Samples

Human liver samples were obtained from explanted organs collected during transplantation surgery at the Queen Elizabeth Hospital (Birmingham, UK). Informed written consent was gained from patients and our studies were approved by the local research ethics committee guidelines (Local Research Ethics Committee: reference numbers 06/Q2702/61 Immune Regulation; 18-WA-0214 Liver Inflammation and 19-WA-0129 Liver Fibrosis). Samples were collected from patients with the following

aetiologies: Alcohol related Liver Disease (ARLD) and Metabolic dysfunction-associated fatty liver disease (MAFLD). In addition, donor liver tissue that was deemed unfit for transplant and healthy margins from resected liver formed the 'non-diseased' cohort used throughout this research. Often this tissue exhibits signs of significant steatosis, both micro and macro vesicular forms.

2.3 Histological assessment of liver tissue

Haematoxylin and Eosin (H&E) staining of human liver tissue was performed to visualise liver morphology and assess the extent of steatosis and fibrosis of the different diseased and healthy cohorts. Staining was performed on 5µm formalin fixed paraffin embedded (FFPE) tissue sections in accordance with the inhouse staining procedure summarized in Table 2.3. Following the sequential reagent exposures detailed, sections were mounted using DPX mounting media (Leica, Germany) with 24x40mm coverslips (Cell Path, UK). Following a 24-hour drying period, 20x brightfield images were collected using a Zeiss Axio Scan Z.1 (Zeiss, Germany) microscope and the accompanying software, Zen Blue (Zeiss, Germany).

Table 2. 3: H&E inhouse staining protocol

H&E Protocol	Reagent	Time (Repeats)
	Xylene	2 minutes (3x)
	Alcohol	2 minutes (3x)
	Water	2 minutes (2x)
	Harris Haematoxylin	4 minutes
	Acid Alcohol	30 seconds
	Water	2 minutes
	Scott's Tap Water	30 seconds
	Water	2 minutes
	Eosin	1 minute
	Water	2 minutes (2x)
	Alcohol	2 minutes (4x)
	Xylene	2 minutes (3x)
	Mount with DPX	

2.4 Isolation and maintenance of cell cultures

2.4.1 Isolation of LSEC

The Centre for Liver and Gastrointestinal Research follows a standardised protocol for LSEC isolation adapted from Joplin *et al.,* 1989.[212] Liver slices received from the Queen Elizabeth Hospital (Birmingham, UK) were initially placed into a sterile petri dish (Corning Inc, USA) and finely diced (see Figure 2.1) using scalpels (Swann-Morton, UK). The diced tissue was then transferred to a 200mL beakers, and 20mL of sterile phosphate-buffered saline (PBS; Sigma, USA) was added. Enzymatic digestion was performed by the addition of 5mL collagenase type 1A (10mg/mL; from *Clostridium Histolyticum*; Sigma Aldrich, USA) and incubated with continuous agitation in an orbital shaker (Stuart scientific, UK) at 37°C, 125RPM for ≤45 minutes. Incubation time was varied dependent on the extent of fibrosis in the tissue.

Following this, the digest was filtered through fine mesh into a fresh sterile beaker and washed several times using PBS. The buffer volume was adjusted to 200mL before being aliquoted into eight universal tubes and centrifuged (Hettich, Germany; 196 RAD) at 870xg (accelerator 9; decelerator 9) for 5 minutes. The supernatant was then discarded, and two pellets were combined into one and was distributed into 4 universal tubes. Cells were resuspended in PBS to the volume of 25mL and centrifuged at 870xg for 5 minutes. This step was repeated, combining two pellets at a time until only one universal tube remained. Here, the pellet was resuspended in 25mL of PBS.

A Percoll (Sigma, USA) density gradient was prepared with two solutions at 33% and 77% v/v in PBS using the following dilutions:

- Stock percoll: 99mL percoll + 11mL 10x PBS (ThermoFisher, USA)
- 33% percoll: 33mL of stock + 67mL 1x PBS
- 77% percoll: 77mL of stock + 23mL 1x PBS

3mL of 33% Percoll was placed into eight 15mL conical bottom tubes (Corning Inc, USA) followed by the careful layering of 3mL of 77% Percoll underneath. The cell suspension was then layered on top of each gradient, with a total of 3mL/tube. The tubes were then centrifuged at 870xg for 25 minutes, with a brake setting of 2. The top layer of cell debris was discarded, and the band of non-parenchymal cells at the interface of the Percoll gradient (approx. at the 3mL mark; see Figure 2.1) was divided between four different universal tubes. These were resuspended in 25mL of PBS, mixed thoroughly, and centrifuged at 870xg for 5 minutes (with the brake reset at 9). The supernatant was aspirated, and two pellets were continually combined into one universal tube and resuspended to 25mL and centrifuged as before. The final cell pellets were combined into a 15mL conical bottom tube and washed as previously described. Cells were resuspended in 500µl PBS containing 50µl of mouse anti-human HEA 125 antibody (anti-CD326/EPCAM, 2.5µL/mL; Progen, Germany). The mixture was incubated at 37°C for 30 minutes with intermittent agitation. The suspension was then adjusted to 14mL and washed as before (870xg, 5min). The supernatant was discarded, and 500µl of ice-cold PBS and 10µL of cold goat anti-mouse IgG Dynabeads (ThermoFisher, USA) were added

and incubated at 4°C for 30 minutes with constant agitation. Subsequently, 6mL of ice-cold PBS was added, and the tube was placed in a magnet (ThermoFisher, USA) to positively select the $EPCAM^+$ population. The supernatant containing endothelial cells was transferred into another 15mL conical bottom tube and returned to the magnet for 2 minutes to remove any residual beads. After collection of the supernatant, the volume was topped up to 14mL with PBS; before being centrifuged at 870xg for 5 minutes.

The supernatant was discarded, and 500µl of ice-cold PBS and 10µl of anti-human CD31 coated magnetic beads (ThermoFisher, USA) were added and incubated for 30 minutes at 4°C with continual agitation. 5mL of ice-cold PBS was thoroughly mixed into the suspension and the tube was placed into the magnet. The supernatant was discarded, and the process was repeated once more. The $CD31^+$ population was then resuspended in 5mL of complete LSEC media and transferred into a $25cm^2$ rat tail collagen type I (RTC; Sigma, USA)-coated Corning flask (Corning Inc, USA). The flask was incubated in a humified atmosphere of 5% CO_2 and 37°C until the cells formed confluent monolayers.

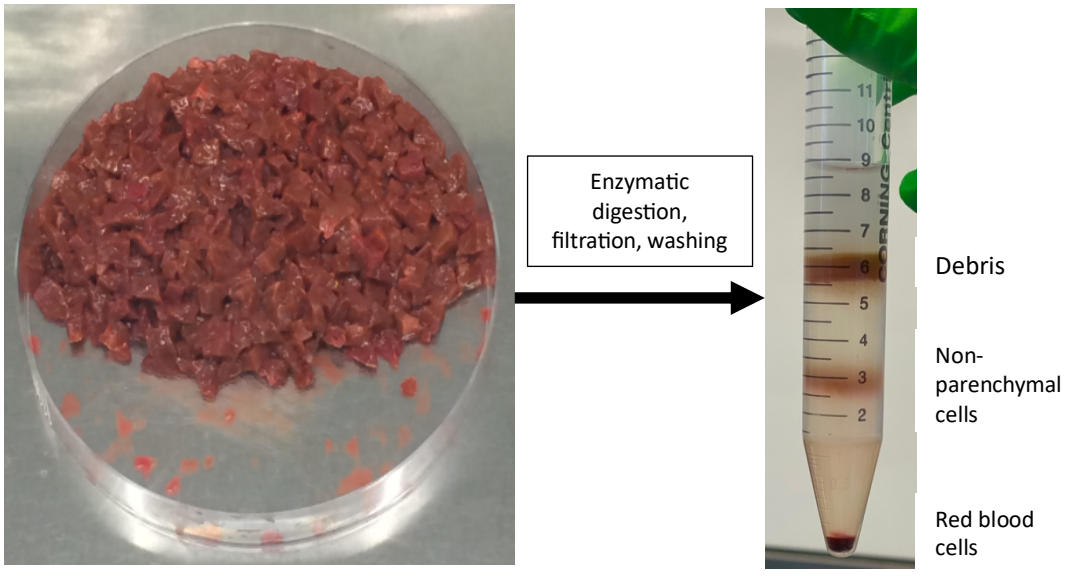


Figure 2. 1: Key stages in the LSEC isolation protocol. Left image shows chopped liver tissue ready for digestion. Right image shows the cell suspension after gradient centrifugation. The top band contains debris, the middle band is the desired non-parenchymal cells, and the bottom pellet contains red blood cells.

2.4.2 Culture of LSEC

Liver sinusoidal cells were cultivated as monolayer cultures in complete LSEC media (unless stated otherwise) within 75cm^2 Corning flasks (Corning Inc, USA) pre-coated with RTC (Sigma, USA). Complete LSEC media was composed of Human Endothelial serum free media (ThermoFisher, UK) supplemented with 100 units/mL penicillin/streptomycin/L-glutamine (PSG; ThermoFisher, USA), 10% heat-inactivated human serum ('Off the clot'; TCS Biosciences, UK), 10ng/mL of Vascular Endothelial Growth Factor (VEGF; Peprotech, USA) and 10ng/mL Hepatocyte Growth Factor (HGF; Peprotech, USA). Cultures were maintained in a humified atmosphere of 5% CO_2 at 37°C. Monitoring of cells occurred every 2-3 days, and when ~80% confluency was achieved, cells were either passaged or utilised in experiments.

For passaging, spent media was discarded, and cells underwent two consecutive washes with 10mL of pre-warmed PBS. Following these washes, 3mL of TrypLE Express enzyme (ThermoFisher, USA) was used to enzymatically cleave peptide bonds on the C-terminal residues of lysine and arginine, facilitating cell detachment from the collagen coating. Cells were incubated for <3 minutes at 5% CO_2 and 37°C in the TrypLE solution. Microscopic assessment confirmed the degree of cell detachment. When sufficient dissociation was achieved, 5mL of media was added to inactivate the TrypLE. The cell-containing solution was then aspirated into a 15mL conical bottom tube and centrifuged at 870xg for 5 minutes. The resulting pellet was resuspended in 1mL of media, and a cell count, and viability assessment were conducted using a haemocytometer (Hirschmann Laborgerate & co, Germany) and trypan blue (0.4%) solution (Sigma-Aldrich, USA) in a 1:1 ratio with the cell suspension. Cells were then either employed in experiments or transferred to a newly labelled RTC coated flask along with 9mL of fresh pre-warmed LSEC media.

2.4.3 Use of siRNA for transient gene knock down in LSEC

Gene knockdowns were used to explore how loss of key receptors affected the uptake and processing of biotherapeutics. LSEC were seeded at 2x10^5 per well in a RTC coated 6-well plate (Corning Inc, USA) and incubated overnight. The following day, a duplex mix

was made up of 1.25µl of 20µM siRNA (Horizon Discovery, UK) and 167.5µl Opti-MEM I Reduced serum medium (ThermoFisher, USA) per treatment well (this concentration was obtained through using a titration of siRNA (50, 20, 10 and 5µM) and determining 20µM as the most effective); and a Lipofectamine mix containing (per well), 3µl of RNAiMAX Lipofectamine (ThermoFisher, USA) and 27µl Opti-MEM. These solutions were incubated separately for 10 minutes at RT and then mixed (3µl Lipofectamine mix and 170µl duplex mix/ well) and further incubated for 10 minutes. Lipofectamine is used to entrap the negatively charged nucleic acid molecules allowing them to overcome the electrostatic repulsion of the cell membrane. Meanwhile, cells were rinsed with PBS twice before the addition of the duplex/Lipofectamine mix and incubated for 4 hours at 37°C. Fresh prewarmed LSEC basal media (prepared with 10% (v/v) heat-inactivated human serum but without the addition of growth factors) was added after removal of the siRNA containing supernatant. No antibiotics were added to the media at this point to avoid increased uptake due to altered membrane permeability. This could result in increased antibiotic exposure causing toxicity and reduction of knockdown efficacy. Cells were then incubated for 48 hours until use.

2.5 Phenotype characterisation of cirrhotic and healthy livers

2.5.1 Immunohistochemistry and quantification of receptors

Immunohistochemistry (IHC) was used to visualise and quantify scavenger receptor expression within healthy and diseased tissue. Staining was performed on 5µm cut FFPE sections of human liver tissue from varied aetiologies such as ARLD, MAFLD and healthy donor. The sections were dewaxed through 3x immersions of xylene (PFM, UK) and 3x industrial denatured alcohol (IDA; PFM, UK) submersions (3 minutes each) followed by two 2-minute exchanges in water (3x) to rehydrate the tissue (as per Table 2.3). Heat-induced antigen retrieval was used to increase antibody-epitope binding via unmasking in low pH citrate-based solution or high pH Tris-based solution (both Vector Labs, USA). These stock solutions of antigen retrieval buffer are diluted 1:100 in 1L of water and preheated in a microwave for 10 minutes. Following the final rehydration step, the slides were added to the pre-warmed unmasking solution and further heated in the microwave

for 30 minutes. Sections were cooled for 10 minutes under cold running tap water, before being washed in PBS with 0.1% Tween-20 (PBST; Sigma-Aldrich, USA) for 5 minutes on a rocking platform (Stuart scientific, UK; 15 rev/min) (2x).

A hydrophobic wax ring was drawn around the tissue before sections were placed into a humified chamber. Here, 150µL of Dako REAL peroxidase-blocking solution (Agilent technologies, USA) was added and incubated at room temperature on a rocking platform (Stuart scientific, UK; 15 rev/min) for 15 minutes. To reduce non-specific staining and high background, two blocking steps were performed consisting of 2x casein solution (in dH2O; Vector Labs, USA) followed by 2.5% serum of the secondary antibody's host species, as included in the ImmPress peroxidase (HRP) polymer kits (Vector Labs, USA). These were incubated for 30 minutes on a rocking platform (Stuart scientific, UK; 15 rev/min) at RT. Primary antibodies were prepared at dilutions shown in Table 2.2 and incubated either for 1 hour at RT on a rocker or overnight (ON) at 4°C. Isotype matched control (IMC) concentrations were matched to those of the primary antibody. Slides were washed twice for 5 minutes each, before being incubated at RT for 30 minutes with the appropriate secondary antibody provided in the ImmPress peroxidase (HRP) polymer kits (Vector Labs, USA). Following this, sections were washed in three exchanges of PBST for a duration of 5 minutes each. The immunoreaction was detected using the ImmPact DAB substrate peroxidase kit (Vector, USA) made up per manufacturer's instructions. This was placed on the slides for ≤5 minutes prior to 3x 5-minute wash steps in PBS. Nuclei counterstaining was performed by 30 second submersion in filtered Meyers haematoxylin (PFM medical, USA) before being 'blued' off in hot tap water for 5 minutes. The sections were then dehydrated and cleared once again through a reverse of the initial steps mentioned above; IDA 3x 3 minutes then xylene 3x 3 minutes. Sections were mounted using a coverslip and DPX fixative (Leica, Germany) and left to dry overnight.

Representative images were obtained using brightfield 20x magnification on the Zeiss AxioScan Z1 (Zeiss, Germany); images were processed using the accompanying software, Zen Blue (Zeiss, Germany). Quantification was performed on 5 randomly selected fields

of view (FOV) per section analysed on the same digital zoom %. Images were curated into a .TIFF (Tagged image file) and FIJI image analysis software was employed as shown in Figure 2.2 to quantify % coverage of the each FOV. To do this, the colour deconvolution (version 1.7) plugin developed by Ruifrok and Johnston[214] (selection H DAB) allowed for the separation of up to 3 stains. Here the DAB channel (colour 2) was selected, and a threshold was applied independently on each image to select the areas of positive staining. Next the platform permitted quantitation of this area as a % of FOV using " Set measurements> select area fraction> analyse > measure" workflow. For each tissue, 5 FOV were averaged giving a representative stained area per section and which was plotted on GraphPad Prism.



Figure 2. 2: % coverage of IHC workflow. Healthy and cirrhotic liver tissue was stained for receptors of interest using immunohistochemistry. Top left image shows example of FcRn stained tissue. The top right image shows threshold applied to quantify % coverage following the colour deconvolution 1.7 plugin (below) used to separate H DAB staining.

2.5.2 Immunofluorescence staining of liver tissue

Immunofluorescence staining (IF) was performed on 5µm FFPE sections of human liver tissue. The same protocol was applied here for the clearing, dehydration, unmasking and subsequential washing steps as described in Section 2.4.1. To reduce non-specific binding, a blocking step using 2x casein (Vector, USA) and 10% serum from the host species of the secondary antibody was applied for 30 minutes at RT on a rocking platform (Stuart scientific, UK; 15 rev/min). Primary antibody was diluted to the appropriate concentration as highlighted in table 2.2 and incubated on the sections for either: 1 hour at RT or ON at 4°C. Following this, sections were washed in 3x exchanges of PBST for 5 minutes each; before being incubated with the appropriate fluorescent secondary antibody for 1 hour at RT, protected from light. Once again, sections were washed and nuclei were counterstained with 4',6-diamidino-2-phenylindole (DAPI) (ThermoFisher, USA) for 5 minutes. Sections then went through 2x exchanges of PBS washes (5 minutes each) before being mounted using Shandon Immu-Mount (ThermoScientific, UK). Sections were left overnight to dry before being imaged on the Zeiss AxioScan Z1 (Zeiss, Germany) with the appropriate lasers. Zen Blue (Zeiss, Germany) was utilised to capture images which were converted to TIFFs and analysed as above.

2.5.3 Assessment of gene expression of liver tissue and LSEC

2.5.3.1 RNA Extraction

Ribonucleic acid (RNA) was first extracted from either LSEC or liver tissue using the Qiagen RNeasy (Qiagen, Netherlands) micro or mini kit respectively depending on the likely yield:

- RNeasy Micro Kit: Human cells (<$5x10^5$) or human tissue (<5mg)
- RNeasy Mini Kit: Human cells (~$1x10^7$) or human tissue (~30mg)

Solutions were prepared prior to starting the protocol:

- RLT buffer: 10µl of 2-Mercaptoethanol (BME; Bio-Rad, USA) per 1mL of RLT buffer to reduce activity of RNases
- RPE buffer: 44mL of 100% ethanol added to 11mL of RPE buffer

- DNase1: 10µl of DNAse1 added to 70µl buffer RDD

For **tissue**: ~20mg of frozen liver tissue was cut and transferred into a gentleMACS M-tube (Miltenyi, Germany) for disruption using the GentleMACS Dissociator (Miltenyi, Germany) using programme 'RNA01_01' alongside 600µl of RLT buffer. The sample was then removed and placed in a 1.5mL Eppendorf (Eppendorf, Germany) where it was centrifuged at 10,000xg for 3 minutes.

For **cells**: frozen pellets of cells were thawed and lysed in 350µl of RLT buffer; alternatively seeded cells were lysed in the wells. This solution was then disrupted by aspiration via a 20-gauge needle (0.9mm diameter; Terumo, Japan) at least 4 times.

Equal volume of 70% ethanol (made up with RNAse free H2O; VWR, USA) was then added to the sample and mixed. Both the sample and any precipitate were transferred onto the RNeasy MinElute spin column placed within a 2mL collection tube. This was centrifuged at >8000xg for 30 seconds prior to discarding any flow through. To wash the spin column, 350µl of buffer RW1 was added and spun at >8000xg for 30 seconds. Next, to remove any residual DNA, 80µl of DNase 1 solution was added directly onto the silica-gel membrane of the column and left to incubate at RT for 15 minutes. This was followed by a repeated buffer RW1 step to wash the column once more. Discarding the flow through again, 500µl of buffer RPE was then added and centrifuged at >8000xg for 30 seconds.

Next for samples processed using the Qiagen mini kit: Another 500µl of RPE buffer was added and centrifuged at >8000xg for 2 minutes. The column was then transferred to a new 2mL collection tube and centrifuged at full speed for 1 minute to allow the column to dry. Following this, 30µl of RNase-free water was added directly to the membrane and spun for 1 minute at >8000xg to elute the RNA.

Next for samples processed using the Qiagen micro kit: 500µl of 80% ethanol was added to the column following the RPE buffer step and was centrifuged at >8000xg for 2 minutes. The spin columns were then placed into a new 2mL collection tube and spun at full speed for 5 minutes to dry the membrane. Here, the column was moved to a new 1.5mL collection tube and 14µl of RNase-free water was added directly to the membrane. This was then spun at full speed for 1 minute to elute the RNA.

The concentration (ng/µL) of the RNA eluted was determined using a Nanophotometer (Implen, Geneflow, UK), which also provided the purity information through the 260/280nm and 260/230nm ratios. A ratio 1.8-2.0 for 260/280nm and between 2.0-2.2 for 260/230 was deemed acceptable and taken through to cDNA synthesis. The samples were stored at -80°C until needed.

2.5.3.2 cDNA synthesis

Complementary deoxyribonucleic acid (cDNA) was synthesised using the iScript cDNA synthesis kit (Bio-Rad, USA). Each 20µl reaction was made up of 4µl of 5x iScript reaction mix (containing a mix of oligo(DT) and random hexamer primers), 1µl of iScript reverse transcriptase and enough RNA template to equate to 1µg/20µl and topped off with nuclease-free water (Qiagen, Netherlands) to reach the desired final volume, 20µl. A no template control (NTC; everything excluding an RNA template) and no enzyme control (NEC; everything excluding reverse transcriptase) was also prepared each time. Once mixed, the samples were placed in the SensoQuest Thermocycler (SensoQuest, Geneflow, UK) with the reaction protocol as stated in Table 2.4.

Table 2. 4: Thermocycler reaction protocol.

Reaction	Process	Temperature	Time
Protocol	Priming	25°C	5 minutes
	Reverse Transcription	46°C	20 minutes
	RT inactivation	95°C	1 minute
	Hold	4°C	Infinite

2.5.3.3 RT-qPCR

mRNA expression was quantified through RT-qPCR; and was performed in 384 multiwell plates (Roche, Switzerland). A total reaction volume of 10µl/well consisted of 5µl of TaqMan Universal Master Mix II (no UNG; ThermoFisher, USA), 0.5µl of TaqMan assay (see Table 2.1; ThermoFisher, USA) and 4.5µl of cDNA diluted in nuclease-free water (Qiagen, Netherlands). The desired concentration per reaction of cDNA was 25ng/well. Each sample and gene of interest were assessed in triplicate.

The most appropriate housekeeping gene was chosen via a screen of different possible genes on different aetiologies of liver tissue and cells using RefFinder software[450] and the raw CT values. This software integrates the 4 top computational programmes (geNorm[451], Normfinder[452], Bestkeeper[453], and the comparative ΔCt method[454]) and gives an overall ranking as seen in Table 2.5. Serine/arginine-rich splicing factor 4 (SRSF4) was chosen as the housekeeping gene as it was consistently ranked the second most stable, whereas first place gene varied from programme to programme.

Table 2. 5: Overview of RefFinder software analysis for best housekeeper

Program	1	2	3	4	5
Delta CT	GAPDH	SRSF4	ACTB	18S	B2M
Bestkeeper	B2M	SRSF4	GAPDH	ACTB	18S
Normfinder	GAPDH	SRSF4	ACTB	18S	B2M
GeNorm	ACTB/GAPDH	SRSF4	18S	B2M	

The plate was sealed with an optical adhesive film and centrifuged at 200xg for 3 minutes to remove bubbles and ensuring samples were mixed. RT-qPCR was performed using the Roche LightCycler 480 (Roche, Switzerland) with the following temperature cycles: 95°C (15 seconds); 60°C (1-minute) and 72°C (1 second) for 40 cycles. mRNA expression relative to the housekeeping gene was assessed using the 'E-analysis' device software provided on the light cycler (version 1.5.0.39; Roche, Switzerland). CT cut off was 35.

2.5.4 Assessment of protein expression of liver tissue and LSEC

Extraction of protein from liver tissue: Frozen liver tissue (>50mg) was lysed in pre-chilled 1x RIPA buffer (20µl/mg; Millipore, USA) supplemented with complete ULTRA proteinase inhibitor cocktail (Sigma, USA) and PhosSTOP (Sigma, USA) tablets and placed in gentleMACS M-tubes (Miltenyi, Germany). This was then homogenized using the gentleMACS Dissociator (Miltenyi, Germany) on program 'protein 01_01'. Next, the suspension was microcentrifuged (Sigma 1-14K, Germany) at 13,000xg at 4°C for 10 minutes, followed by transferring the supernatant into a fresh prechilled Eppendorf before discarding the pellet.

Extraction of protein from LSEC: Seeded LSEC were incubated on ice for 15 minutes with 250µl of 1x RIPA buffer (Millipore, Germany). Cells were then scrapped using 1.8cm bladed cell scrapers (Corning Inc, USA) and transferred into 0.5mL Eppendorf tubes. Following centrifugation at 13,000xg for 10 minutes, supernatant was aspirated into a fresh 0.5 mL Eppendorf and the pellet discarded.

Protein concentration was then determined using Pierce™ Rapid Gold BCA Protein Assay Kit (ThermoFisher Scientific, USA) with bovine serum albumin (BSA; Bio-Rad, USA) as a standard and read at 480nm on a Synergy HT plate reader (Biotek, USA) per manufacturer's instructions. Once concentration was determined, the lysates were diluted to a 2mg/mL stock and stored at -80°C until needed.

Sodium dodecyl sulfate polyacrylamide gel electrophoresis (SDS-PAGE) was first employed to allow the separation of proteins. SDS is an anionic detergent that disrupts non-covalent bonds within proteins and masks the intrinsic charge to that which it is bound. This results in the mobility of proteins through the gel being size dependent only, allowing for molecular weight determination. TGX Stain-Free™ FastCast™ Acrylamide 10% gels (Bio-Rad, USA) were prepared for 1.5mm glass plates (Bio-Rad, USA) at the stated ratios (Table 2.6). The oxidising agent ammonium persulfate (APS) was added to the gel prior to the addition of N,N,N',N'-Tetramethyl ethylenediamine (TEMED; National Diagnostics, USA, to catalyse the formation of free radicals from APS causing the polymerisation of acrylamide. The stacking gel was left to polymerise for 30 minutes once a 10- or 15- well comb (Bio-Rad, USA) was inserted.

Meanwhile, lysates were diluted to 20µg/20µl including 1:1 of SDS-PAGE loading buffer for ease of visualisation in 0.5mL Eppendorf tubes. The loading buffer consisted of 950µl Laemmli sample buffer (Bio-Rad, USA) with 50ul BME (Bio-Rad, USA). The samples were boiled for 5 minutes at 100°C. The gels were placed in the electrode assembly unit within the Protean Tetra vertical buffer tank (both Bio-Rad, USA) and filled to the rim with 1X running buffer (10x Running buffer containing 0.25M Tris, 1.92M Glycine and 1% SDS diluted in dH2O; Geneflow, UK). The combs were removed from the set gels, and 20µg/ lane of sample was loaded alongside a 5µl PageRuler plus pre-stained protein ladder (ThermoFisher, UK) for reference. The gels were run at 200V, 400mA for 45 minutes. Being stain free gels, these contain a proprietary trihalo compound within the polyacrylamide gel; this covalently binds to tryptophan residues and upon activation, fluoresces said proteins allowing them to be detected at concentrations as low as >10ng.

These gels were activated on the ChemiDoc MP imaging system (Bio-Rad, USA) selecting the Protein Gels > Stain Free Gel setting.

Table 2.6: SDS-PAGE gel casting ratios

Gel casting ratios		**Resolver**	**Stacker**
	Resolver A	4mL x n	-
	Resolver B	4mL x n	-
	Stacker A	-	1.5mL x n
	Stacker B	-	1.5mL x n
	TEMED	4µl x n	3µl x n
	10% APS	40µl x n	15µl x n

Following gel electrophoresis, the western blotting technique was used to transfer the separated proteins onto a nitrocellulose membrane and visualised by using antibodies, resulting in the identification and abundance determination of a protein of interest. Semi-dry transfer was performed using the Turbo-blot (Bio-Rad, USA). Gels and pre-cut nitrocellulose membrane (Bio-Rad, USA) were pre-equilibrated in transfer buffer (Bio-Rad, USA) for 5 minutes; this step removes any contaminating electrophoresis buffer salts as well as preventing dry out of the membranes. To prepare 1L of 1x transfer buffer (Bio-Rad, USA): 200mL of nanopure water, 200mL of reagent grade 85% ethanol were added to 5x transfer buffer. The gel was laid horizontally on top of the nitrocellulose and was sandwiched between two buffer-soaked ion reservoir stacks before being positioned between two electrode plates: the lid being a cathode and the base an anode. Using the TGX Turbo midi selection on the turbo blot, electroblotting occurred at 2.5A, <25V for 3 minutes pulling the negatively charged proteins from the SDS gel towards the anode and thus onto the nitrocellulose membrane. Successful transfer was confirmed via the Chemidoc (Bio-Rad, USA) before blots were blocked to prevent non-specific binding in non-fat 5% milk (diluted with TBS + 0.1% tween (TBST; Premier food groups, UK) ON at 4°C.

The following day, the spent blocking solution was removed and fresh 5% milk was added containing the primary antibody at the desired concentration as stated in Table 2.2. This incubation step occurred for either 1 hour at RT or ON at 4°C . Subsequential washing steps of TBST were performed 3x for 10 minutes each before the addition of the species-specific secondary IgG-Horse Radish Peroxidase (HRP) conjugate (BioRad, USA) diluted in fresh 5% milk. Incubation occurred for 1 hour at RT on a rocking platform (Stuart scientific, UK; 15 rev/min). The blot was washed as before and incubated for 5 minutes at RT with the clarity ECL substrate kit (prepared per manufacturer's instructions; Bio-Rad, USA). This protocol utilizes the emission of light as a product of a chemical reaction between the HRP enzyme and HRP substrate luminol which emits a light at 428nm; this was captured on the ChemiDoc (Bio-Rad, USA) using the chemiluminescent pre-programmed setting. The signal obtained corresponds to the amount of protein bound meaning densitometry was performed to quantify the abundance of each protein comparatively in each aetiology. This was measured using Image Lab software produced by Bio-Rad (USA). To note the gels used in this methodology utilize Bio-Rad's stain free technologies therefore a need for a housekeeping protein as a loading control is negated. Instead, each blot data is normalised to total protein loaded in each line.

2.5.5 Immunocytochemistry on LSEC

Using fluorescently labelled antibodies, both direct and indirect approaches, allow for receptor visualisation in context of the cell; allowing assessment of localisation, distribution, and intensity to be attained via immunocytochemistry (ICC).

This protocol was performed on cells grown in either µSlide VI 0.4 ibitreat 6 channel IBIDI (Ibidi, Germany) or 96 well blacked out/clear flat bottom polystyrene plates (Corning Inc/ USA). Beforehand, both were manually coated using 1/100 RTC (Diluted in PBS); 100µl of RTC was pipetted in each well/channel and incubated for 5 minutes at 37°C before being removed, rinsed with sterile PBS and left to dry. LSEC were seeded at a density of $7x10^4$/ channel (Ibidi) or $6x10^4$/well (96 well plate) in a final volume of 100µl per well/ channel before being left in a humified atmosphere of 5% CO_2 and 37°C until confluent.

Once confluency was achieved, cells were fixed using 4% paraformaldehyde (PFA; Sigma-Aldrich, USA) for 10 minutes at RT. PFA was removed and cells were rinsed with 1x PBS. The nonionic detergent Triton X-100 (Sigma, USA) diluted in 1X PBS to 0.1% was utilized to solubilize the bio-membrane creating pores allowing access for intracellular staining. This was incubated on fixed cells for 5 minutes at RT before being washed off with PBST 3x for 5 minutes each. To avoid unwanted background and non-specific staining, cells were blocked in 1% BSA in PBST for 30 minutes at RT on a rocking platform. This solution was then replaced with fresh blocking solution, this time containing the primary antibody diluted to the desired concentration (Table 2.2). Subsequent washing steps with PBST were performed, before the addition of the secondary antibody in 1% BSA and PBST for 1hr at RT. From this point onwards the cells were protected from light. Unbound secondary antibody was decanted, and cells were washed 3x with PBST for 5 minutes. Counterstaining was implemented using 0.5ug/mL of DAPI in 1x PBS and incubated for 5 minutes at RT. This was aspirated off, followed by 3x washes in PBS before being stored at 4°C submerged in PBS until imaged. Images were taken on the LSM780 confocal (Zeiss, Germany).

2.6 Fluorescent labelling of monoclonal/bispecific antibodies

The visualisation of the GSK provided mAbs/bsAbs internalisation and eventual deposition into different organelles, was enabled through antibody labelling. Here the conjugation of fluorophore 647 via the Alexafluor antibody labelling kit (ThermoFisher, USA) was performed per manufacturers instructions. In brief, 10µL of 1M sodium bicarbonate was added to 100µL of GSK antibody (1mg/mL). This was transferred into the provided vial containing the reactive dye. This was intermittently rotated and incubated in the dark for 1-hour. Following this, a purification step was performed with placing the reaction volume onto a resin bed within a spin column and centrifuged at 1100xg for 3-minutes. The labelled antibody is then collected and degrees of labelling(DOL; mole dye per mole protein) was obtained through assessment on the nano-spectrometer. Here it was determined that DOL was close equivalent for each antibody.

2.7 Human Endothelial Recycling Assay (HERA) to quantify antibody uptake and processing

Utilizing an already described protocol by Grevys *et al.,*[455,50] we adapted the human endothelial recycling assay (HERA) to assess the processing of biotherapeutics by primary isolated LSEC. This was done in either a 2D monoculture or 3D co-culture format. The assay is outlined in the schematic below (Figure 2.3) but in brief, LSEC were seeded at $5x10^4$/well in a RTC coated 24 well plate (Corning Inc, USA) and cultured for 24 hours in complete LSEC media (total volume of 1.5mL/well). Cells were washed 3x with Hank's balanced salt solution (HBSS; ThermoFisher, UK) before being starved for 1 hour in HBSS at 5% CO_2 and 37°C. Next, 500ng/mL and 50ng/mL of monoclonal (mAb)/bispecific (bsAbs) antibody (see table 4.1 provided by GSK) was diluted in 1mL HBSS/well (pH 7.4) and incubated for 4 hours on LSEC in a humified atmosphere of 5% CO_2 and 37°C. Each individual plate contained 4x non-treated control wells (2 for each time point) and all mAbs/bsAbs were used in duplicate.

Following the first incubation, depending on the output desired (see following sections) cells were either lysed (1x RIPA buffer (Millipore, USA)), fixed (4% PFA; Sigma, USA) or dissociated from the well (TrypLE express), to be used in flow cytometry. Supernatants from each well were collected and snap frozen to be stored at -80°C until needed. Remaining wells had the media decanted and fresh LSEC media or pre-warmed HBSS with no additions added and a further incubation of >4 hours took place. To note, depending on the end point, the fresh media either contained human serum or not. At the 8-hour timepoint, the supernatants were taken, and cells were once again either lysed, fixed or dissociated. Of note, this is a generic overview and with each output there may be a variation in protocol which will be described in the following sections.

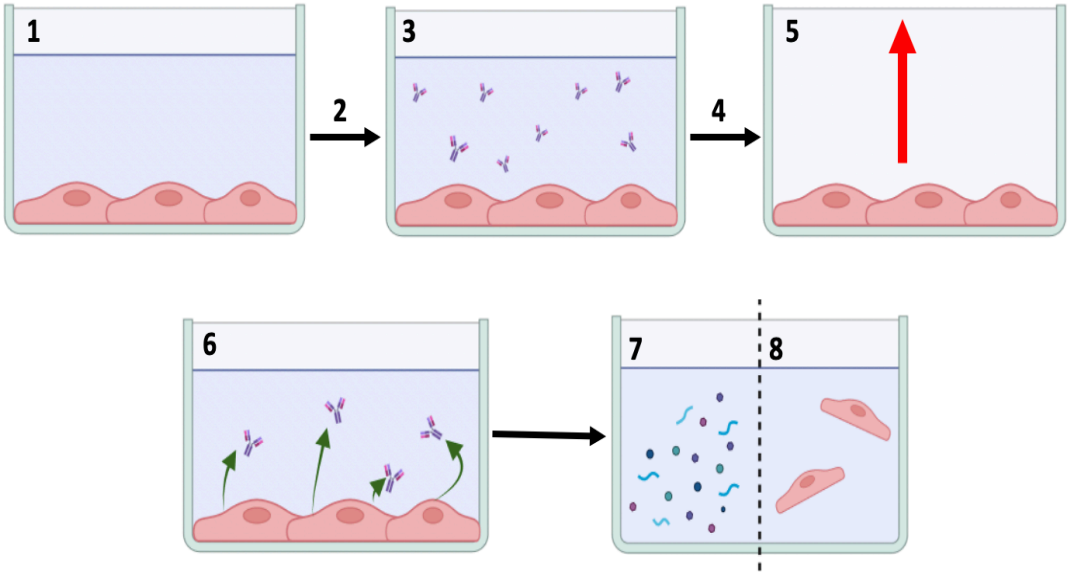


Figure 2. 3: Outline of the Hera assay: 1. LSEC were seeded into 24-well plates to achieve ~80% confluency. 2. Cells were washed, and serum starved for 1-hour. 3. Antibodies were diluted to 50ng/mL and 500ng/mL and incubated on cells for 4-hours. 4. Here LSEC were dissociated from wells and media removed to analyse later. 5. Fresh media was replaced onto the remaining cells. 6. Following 8-hours/overnight of incubation media was removed and cells were dissociated for multiple different outputs: 7-MSD or ELISA and 8- Flow cytometry/ microscopy.

2.7.1 Quantification of mAb/bsAb uptake through Enzyme-linked immunosorbent assay

Here we wanted to measure the amount of antibody within treated LSEC lysates at -4 and 8-hours post exposure to establish how much mAb/bsAb had been internalised, and if there was a loss in concentration, the therapeutic would have been considered 'processed' as either degraded or recycled. To establish the definition of 'processed,' the supernatants were also quantified to establish what was recycled back into the media at the 8-hour timepoint. To obtain the samples used in this method, the exact method as described in section 2.7 was followed with no variations. Here pre-warmed HBSS was used at the 4-to-8-hour time point, to prevent either the phenol red or IgG within the human serum of the LSEC media skewing the results. To enable quantification, a sandwich ELISA was utilized. As all the initial mAbs provided by GSK were of an IgG format, an IgG specific ELISA was initially chosen (reference). In addition, a more specific Kribiolisa^{TM} Rituxuman ELISA (Eagle Biosciences, USA) for samples that had been treated

with the anti-CD20 mAb (GSK inhouse biosimilar, UK). Each protocol was performed per manufacturer's instructions.

2.7.2 Quantification of mAb/bsAb uptake through Meso-Scale Discovery(MSD)

Meso-scale discovery is a sandwich immunoassay, similar to an ELISA. However rather than using detection via colorimetric reaction, it uses electrochemiluminescence (ECL) resulting in increased sensitivity. To obtain the samples quantified by this method, the exact protocol as described in section 2.5 was followed with no variations; pre-warmed HBSS was used for each step. The MSD Human/NHP IgG kit, was in part provided by GSK. Prior to starting the assay, the following reagent preparations were undertaken:

- MSD Blocker A: 1.25g of Blocker A powder was diluted in 20mL of diH2O and stirred until complete resuspension. Then 5mL of 5x MSD phosphate buffer was added.
- Calibrator dilutions: 7-point calibration curve was utilised with a 4-fold serial dilution and a zero blank. Each calibrator provided in the kit was diluted with Diluent 100 (MSD, USA).
- Sample dilutions: samples were diluted in Diluent 100 at a dilution factor of 1, 10, 100 and 1000. Each sample and dilution factor were run in duplicate.
- Detection antibody- 60µl of 50x SULFO-TAG Anti-Hu/NHP IgG Antibody was added to 2940µl of Diluent 100.
- Read buffer- a 2X working solution was prepared by combining 10mL of Read Buffer T (4x) to 10mL of diH2O.
- PBST- this was made up at 0.05% Tween-20

MSD plates provided were pre-coated with capture antibodies and exposed to proprietary stabilizing treatment to ensure integrity of said antibodies. This plate was then blocked using 150µl of the prepared Blocker A solution for 30 minutes with constant agitation at RT. Subsequent, wash steps using 150µl PBST 0.05% were performed 3x before incubation with 25µl of sample or calibrator per well commenced at RT for 2

hours. A repeat of the 3x wash steps was then followed by the addition of 150µl of 2x Read Buffer T to each well. The plate was then read immediately in the MSD instrument. Data was generated by MSD's own software DISCOVERY WORKBENCH using a 4-parameter logistic curve fitting model (sigmoidal dose-response) with a $1/y^2$ weighting function.

2.7.3 Use of Flow Cytometry to quantify antibody binding from HERA

Flow cytometry is a technique that allows for the characterisation of a population of cells within a sample suspended in liquid. Here sheath fluid running in a laminar flow, accelerates the cell solution to the centre; in a process known as hydrodynamic focusing. This results in a single file of cells passing through the laser at any one time. Each cell is then analysed for both visible light scatter and fluorescent parameters detected by a photomultiplier (PMT). The signal is amplified and converted into a voltage pulse and then a digital value using an analog-to-digital converter. In this research, flow cytometry was used to assess the extent of interaction between biotherapeutic and isolated LSEC. This technique was performed on both mono-layered single cell cultures and HepG2-LSEC co cultures.

2.7.3.1 Flow cytometry on 2D monolayer single cell cultures

LSEC were seeded at $5x10^4$ /well in a RTC coated 24-well plate and left to achieve +80% confluency in a humidified environment of 5% CO_2 and 37°C. mAbs/BsAbs were diluted to 50ng/mL and 500ng/mL in complete LSEC media and pre-warmed. Cells were washed 3x with PBS before being incubated with the antibodies for 4- or 8-hours in a 5% CO_2 and 37°C incubator. For controls, 8 wells were left untreated. At their elected time points, cells were washed twice with PBS before dissociation with 300µl of TrypLE Express enzyme (ThermoFisher, USA) for 3 minutes at 37°C. 700µl of complete LSEC media was added to each well and duplicates were combined and pipetted into polystyrene round bottom 12x 75 mm BD Falcon tubes (BD Biosciences, USA). Cells were pelleted at 300xg in a pre-chilled 4°C centrifuge (Hettich, Germany; RAD/mm 85). The following incubation steps were all carried out on ice and in the dark. FACS buffer was prepared using Ca^{2+} /

Mg^{2+} free PBS (ThermoFisher, USA); 1mM EDTA (Sigma, USA) to prevent cell to cell adhesion; 0.1% sodium azide (Sigma, USA) to reduce photo-bleaching and antibody shedding and 5% FBS (Fisher Scientific, USA) to reduce heterophilic antibody interference. The pellet was resuspended in FACs buffer and 'washed' via repeated resuspension and centrifugation (300xg) steps 2x. Cells were then resuspended with 1mL of FACs buffer containing 1µl of LIVE/DEAD fixable near IR viability stain and incubated for 30 minutes. The wash steps were repeated, followed by the resuspension and fixation of cells in 4% PFA for 20 minutes. Cells were washed and then permeabilized in 0.1% Triton for 5 minutes. Following subsequent wash steps, secondary antibody, 2µg/mL goat anti-human Alexafluor 488 or 647 (ThermoFisher, USA, diluted in FACS buffer), was added and incubated for 30 minutes. Cells were then repeatedly washed with FACS buffer (3x) before analysis on the BD LSR Fortessa 4 (BD Bioscience, USA).

2.7.3.2 Flow cytometry analysis

I initially used a Cyan ADP (Beckman Coulter, USA) for preliminary experiments with anti-CD20 treatment of LSEC. Results were analysed using the Summit Software (Beckman Coulter, USA), and only % fluorescence was assessed. I later progressed to using the BD LSR Fortessa 4 (BD Biosciences, USA) instrument with DIVA software. This was utilised for all GSK assets and a typical gating strategy can be see below in Figure 2.4. Data was analysed using FlowJo (BD Biosciences, USA). Median fluorescence intensity (MFI) and % of population positive for mAbs/bsAbs staining were measured at 4- and 8-hours. Both the individual values as well as the % Processed are reported. To obtain the value for % processed, the following equation was used:

$$\left(\frac{4hr\ MFI - 8hr\ MFI}{4hr\ MFI}\right) X\ 100 = \%Processed$$

A positive % processed value refers to mAb/bsAb that has either been degraded or recycled demonstrating a loss in MFI over time; this is captured under the umbrella term

'processed.' A negative % Processed value highlights a retention or further gain of therapeutic labelling with LSEC.

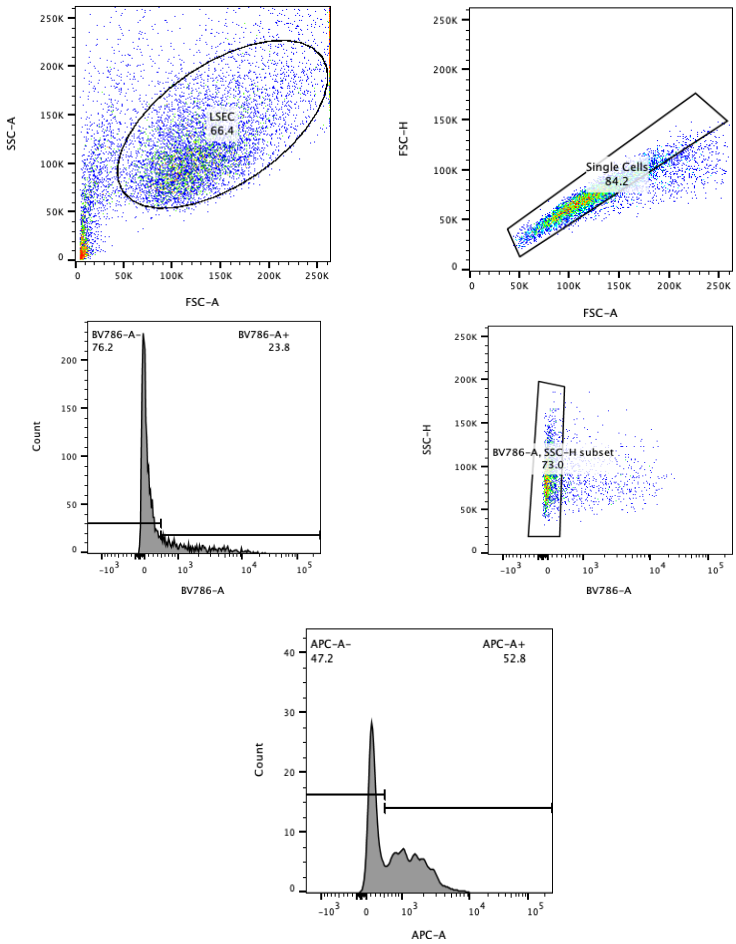


Figure 2. 4: Flow cytometry gating strategy. LSEC were selected based on size and granularity assessed by forward and side scatter (top left). Doublet exclusion was performed by plotting height against area for forward scatter (top right). The middle panel shows the selection of viable cells by LIVE/DEAD fixable, BV786 negative cells were classed as viable and proceeded to be assessed for MFI as shown in the bottom histogram.

2.7.4 Fixed cell imaging after HERA

Immunofluorescent imaging was utilized to gain contextual information about the localisation of biotherapeutics within the cells. LSEC were seeded at a density of $7x10^4$/ channel in µSlide VI 0.4 ibitreat 6 channel IBIDI (Ibidi, Germany). With a final volume of 100µl per channel, IBIDIs were left in a humified atmosphere of 5% CO_2 and 37°C until 80% confluent. mAbs/BsAbs were diluted to 50ng/mL or 500ng/mL in pre-warmed LSEC

media and dispensed into the appropriate channels for 4- or 8-hours. At the desired time points, channels were rinsed through 3x with sterile PBS before cells underwent fixation with 4% PFA for 10 minutes in 37°C. The staining protocol was performed as described in 2.4.5, with an indirect technique of using a goat anti-human Alexafluor 488 secondary to detect the biotherapeutics being employed. As mentioned, images were taken on the LSM780 confocal (Zeiss, Germany) at 40x magnification and H_2O immersion before being converted to .TIFF files through the accompanying Zen software.

To quantify the amount of fluorescent signal within the cell, correct total cell fluorescence (CTCF) was calculated. The method allows for background subtraction alongside considering the area of a cell. This was calculated as: CTCF= Integrated Density – (Area of selected cell x Mean fluorescence of background readings). To obtain the background readings, a region outside of the cell with no fluorescence is selected and read after each positive reading. All analysis was carried out on the Fiji (ImageJ) software.

2.7.5 Live cell imaging and co-localisation from HERA

Live imaging provides a more insightful look into the dynamic changes within the cells' processes. This would allow me to assess antibody accumulation in cells throughout my 8-hour incubation. This method utilized the conjugated therapeutics described in section 2.6. LSEC were seeded into either μSlide VI 0.4 ibitreat 6 channel IBIDI (Ibidi, Germany) or 96 well blacked out/clear flat bottom polystyrene plates (Corning Inc, USA), exactly as described in section 2.4.5.

Live cell imaging with Alexafluor 647 conjugated mAbs/bsAb**:** LSEC were incubated with 500ng/mL of chosen mAb/bsAb conjugate with 50nM of Lysotracker blue DND-22 (ThermoFisher, USA) in 5% CO_2 and 37°C. Cells were taken to image on the 2^{nd}, 8^{th} and 22^{nd} hour using a LSM780 confocal with Zen Black accompanying software (Zeiss, Germany).

2.7.5.1 Cellular trafficking inhibition in live cell imaging

It was important to understand the subcellular localization and receptor dependency of therapeutic antibodies in LSEC. Elucidation of trafficking within the cell was observed by direct (receptor knockdown) and indirect (chemical inhibition) means. Indirect methodologies utilized the blockade of certain proteins and systems within and on the surface of the cell to explore if this led to altered internalisation and processing of biotherapeutics. Table 2.7 below shows each method employed, its time course/concentration and its effect/target. LSEC were treated with these inhibitors for the allotted time course before undergoing incubation with the Alexafluor 647 conjugated mAbs/bsAbs as described in 2.7.5. Imaging or assessment of antibody location was then quantified as described in Section 2.7.5.2. Concentrations chosen were based upon either suppliers recommendation or previously published literature which is referenced within the results chapters when used.

Table 2. 7: Internalisation inhibitors

Inhibition of cellular process	Material	Concentration	Incubation Time	Effect	Cat no. (supplier)
	Dextran Sulfate	100µg/mL	15 Minutes	Blocks receptor mediated uptake	42867 (Sigma)
	Fc Blocker	2.5µg/mL	30 Minutes (during)	Block FcR binding	564219 (BD Biosciences)
	FcRn B2M blocker	5- and 25µg/mL	2 Hours	Inhibition of FcRn binding	71283 (BPS Bioscience)
	IOX2	100nM	48 Hours	Upregulation of CD32b	SML0652 (Sigma)
	ML141	15 µM	24 Hours	Inhibition of Cdc42	22764-1 (Tocris Bioscience)
	Nocodazole	0.2µg/mL	1 Hour	Inhibits microtubules polymerisation	M1404 (Sigma)
	Sucrose	0.4M	2 Hours	Blocks formation of clathrin coated pits	50-38-9 (Sigma)
	Wortmannin	1µM	30 Minutes	Inhibition of PI3K	681675 (Merck)

2.7.5.2 Quantification of live cell imaging

Once images were converted to .TIFFs files via the Zen Blue software (Zeiss, Germany), they were analysed using Fiji (ImageJ) software. Quantification of Alexafluor 647 positive vesicles, lysosome quantity and the colocalization of antibody with lysosomes at each time point was performed. Both co-incidence (Manders Overlap Coefficient) and correlation (Pearson's correlation coefficient) were used as measurements for colocalization. To do this, the "Just another co-localisation" plug-in (JACoP) compilation tool was used as published by Bolte and Cordelière.[256] The Macro used for quantification can be found below alongside examples for the vesicle counting and co-localisation.

The workflow for analysing an image within Image J progressed as below :

```
rename("vesicles count");
run("Split Channels");
setAutoThreshold("Default dark");
//run("Threshold...");
selectImage("vesicles count (red)");
run("Despeckle");
setAutoThreshold("Default dark");
//run("Threshold...");
run("Analyze Particles...", "display summarize");
selectImage("vesicles count (blue)");
run("Analyze Particles...", "display summarize");
run("JACoP ");
selectImage("vesicles count (red)");
selectImage("vesicles count (green)");
selectImage("vesicles count (red)");
selectImage("vesicles count (blue)");
run("JACoP ", "imga=[vesicles count (red)] imgb=[vesicles count (blue)]
thra=97 thrb=102 pearson mm costesthr");
```

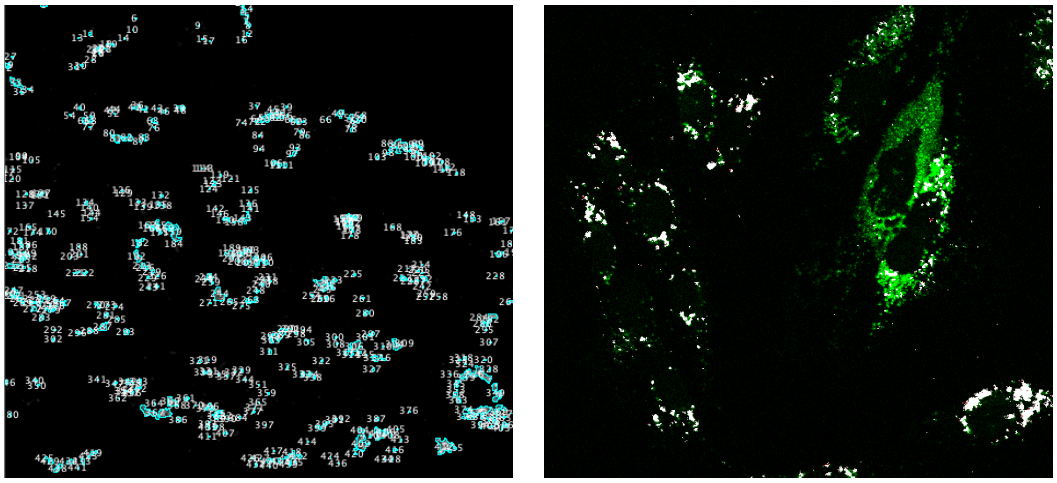


Figure 2. 5: Exemplar images of workflow for vesicle count and colocalisation. Workflow per analysis in ImageJ. Left shows an example of vesicle count of a particular conjugated antibody. Right panel shows the Costes threshold obtained via the JACop plugin, white show co-localisation and green shows the absence of overlap between antibody and lysosomal compartment.

2.8 Receptor binding elucidation and kinetics

2.8.1 Proteome Profiler

A membrane-based antibody array was used to further our understanding of the possible downstream processes initiated by the mAb/bsAb interaction with the cell surface membrane. Using the Proteome Profiler Human Phospho-Kinase Array kit (Biotechne, USA), changes to the phosphorylation level of 37 kinases were detected. LSEC were seeded in RTC coated 12 well plates overnight at $1x10^5$ cells/well in LSEC media (1mL/well). The following day, cells were incubated with 500ng/mL of therapeutics diluted in buffer provided by manufacturers for 15- or 45-minutes at 37°C before being lysed on ice for 10 minutes (lysis buffer provided in kit). Next steps followed manufacturer's instructions, but in brief, lysates were incubated on nitrocellulose membranes that were coated with different capture antibodies. Captured protein from the lysates were then detected with biotinylated detection antibodies and finally, were visualised using chemiluminescent detection on the ChemiDoc (Bio-Rad, USA). The signal produced was considered proportional to the degree of phosphorylation of the

analyte and was analysed using Biotechne's Quick Spot image analysis software, which adjusts for control background.

2.8.2 Antibody binding to FcRs, FcRn CD206 and CD209 by Surface Plasmon Resonance (SPR)

All SPR binding experiments were carried out on the Biacore 8K+ (Cytiva Healthcare, Sweden) at 25°C. HBS-EP+ (GE Healthcare, USA) was used as a running buffer. CD209 (5-20ug/mL; RnD Systems, USA) and CD206 (20-40ug/mL; Acrobiosystems, USA) were immobilised onto CM3 series 3 sensor chips per manufacturer's instructions (Cytiva Healthcare, Sweden). Biotinylated FcRn (Acrobiosystems, USA; 0.2mg/mL) and FcyR (0.5ug/mL; GSK provided) were immobilised onto series S Cap chips (Cytiva Healthcare, USA). mAbs were perfused over bound recombinant receptor at concentrations serially diluted 2-fold starting from 1000nM at a rate of 30ul/min for 120 seconds. Running buffer alone was used to double reference the binding curve. 10mM glycine pH 2.0 was used to regenerate the antibody to receptor interaction. Each antigen was run at *p*H 7. Capture times are as follows: association: 120 seconds; dissociation: 300 seconds; Flow rate: 30ul/min. Binding affinity was evaluated, and K_D ranked using Biacore insight evaluation software V3.

2.8.3 Assessment of antibody: receptor interactions using Chemical crosslinking

3,3′-Dithiobis(sulfosuccinimidylpropionate) (DTSSP) is a water-soluble crosslinker that houses an amine reactive sulfo-NHS-ester at both ends held by an 8-carbon spacer arm. Antibodies contain several primary amines which can form stable amide bonds in replacement of the NHS to DTSSP. As DTSSP is not lipid soluble, this allows capture of antibodies to the cellular surface proteins. LSEC were seeded in RTC coated 6 well plates ON at $3x10^5$ in LSEC media (1mL/well). On the day of the experiment, DTSSP was dissolved fresh in water at a stock concentration of 25mM; this can only be used on the day of experimentation due to its unstable nature. Cells were rinsed 3x with PBS before being incubated with antibodies for 2 hours at either 37°C or 4°C. DTSSP was then added

at a final concentration of 2mM, and all plates were incubated on ice for a further 2 hours. The reaction was quenched using 1M Tris (pH 7.5) for 15 minutes. The spent solution was removed and 200µl of complete RIPA buffer was incubated for 10 minutes at 4°C on a rocking platform. Cells were scraped using 1.8cm bladed cell scrapers, pooled in duplicate per condition and stored at -80°C until analysis. Samples were assayed using western blots and in some cases amide bonds were cleaved through the reducing agent, BME. Blots for each sample were run under both reducing and non-reduced samples to assess the difference in band size for an identified protein. See western blot protocol, Section 2.5.4

2.8.4 *In silico* assessment of antibody Fab: receptor interactions using ClusPro and PDBSUM

To investigate the binding interaction between Fab regions of GSK antibodies and receptors, ClusPro software was utilised. Protein structures of receptors and antibodies were obtained from the protein data bank and in some cases edited on Pymol to remove ligands. This was then saved as a .PBD file and fed into the ClusPro 2.0 Protein-Protein docking software, selecting the use of antibody mode within the advanced settings menu. This software utilises a 3-point algorithm PIPER, whereby a receptor is rotated around the antibody 70,000 times to obtain binding interactions of each residue cluster. Following this, clusters are bottle necked depending on the number of members per cluster and the lowest energy required to bind (considering repulsion and attraction of Van der Waals and electrostatic forces). This then ranks the top 30 docked models. The top ranked models were then taken and illustrated in Pymol. These docked models were also ran through the PDBsum software, that provides infographics of bonds present between each protein chain.

2.9 Statistical analysis

Graphical presentation and significance were calculated through GraphPad Prism software. Distribution was ascertained for all data set prior to performing the appropriate statistical test. See individual figures for listed analysis.

Chapter Three: Characterising hepatic expression of antibody binding receptors in health and disease

This chapter aims to introduce the sample cohort used throughout this thesis. It provides context for the clinical parameters in our healthy and diseased populations and highlights differences in hepatic tissue architecture between each aetiology. More importantly, this chapter aims to provide a more in-depth introduction to the four receptors of interest: FcRn, CD206, LSIGN and CD32b; and explore how their expression changes with liver disease and in culture. This provides context for any discrepancies we see in antibody internalisation and degradation between cirrhotic and healthy LSEC in later chapters. The initial section of this chapter (Section 3.1) will deviate from the conventional layout the rest of this thesis will follow. It will read as a mixture of results and discussion to allow immediate context to be given to the clinical parameters and histology seen. The continuing sections will follow the standard layout of results followed by discussion.

3.1 Characterisation of the clinical parameters and architecture within liver

Samples from a total of 147 patients were utilised throughout this thesis. Clinical data was collated from the NHS patient electronic database and is presented in Table 3.1. Of note biochemical data for donors was limited because of the way in which this tissue is accessed (typically from deceased patients with non-hepatology related medical conditions). The values for healthy and cirrhotic volunteers were averaged (range presented) and compared to the UK's reference ranges.[225] The average age of both healthy and cirrhotic tissue donors was similar at 53 and 55 years respectively, however, the cirrhotic cohort exhibited a larger age range of 69 years (aged: 18-87) in comparison to a 38-year range for non-diseased donors (aged: 31-69).

Table 3. 1: Demographics and clinical characteristics of liver tissue donors

Clinical characteristics of liver tissue donors.	Parameter	Normal Ranges (UK)	Healthy controls (n=10/53*)	Cirrhotic livers (n=88)	Resected liver (n=6)
	Age (mean and range)		53 (31-69)	55 (18-87)	76 (60-87)
	BMI	18-24.5	26.2 (22-30)	28.7 (20-45)	25.4 (21-28)
	ALT (U/L)	0-55	56 (12-301)	647(14-2443) (17/88 values)	178 (82-301)
	AST (U/L)	5-34	33 (19-38)	1202 (17-1151)	NA
	ALP (U/L)	30-130	77 (51-111)	141 (8-121)	88.5 (63-113)
	Bilirubin (mmol/L)	<21	9 (4-17)	95 (5-451)	34(14-62)
	Albumin (g/L)	35-50	30 (21-42)	32(17-44)	35 (28-42)
	INR	0.8-1.2	1 (0.85-1.15)	1.8 (1.0-18)	1.3(1-1.6)
	WBC (x10^9/L)	3.6-11	12.3 (7.8-19.3)	11 (2.4-89)	10.8 (3-19.3)
	Platelets (x10^9/L)	150-450	213 (67-399)	96, with l (46-614)	186 (95-292)
	Hb (g/L male)	130-180	121.5 (95-148)	97 (64-173)	103 (77-139)
	MELD score			16.6 (7-27) (56/88 values)	

Explanted tissue samples were obtained from patients with liver cirrhosis (ARLD and MASLD) or those undergoing anatomical resection for malignancy. Donor livers deemed unsuitable for transplantation were used as controls (NOTE: due to nature of these samples clinical data was not available for all donor livers). Clinical parameters were obtained from University Hospitals Birmingham electronic patient records. Age is rounded to the nearest year. Data is listed as mean (interquartile range). ALT, alanine aminotransferase; AST aspartate aminotransferase; ALP, alkaline phosphatase; INR, international normalised ratio; MELD, Model for End-Stage Liver Disease. Key: Vastly over normal range, just over normal range, within range, Black below normal range.10/53* refers to the amount of clinical data able to be obtain from this group.

On average, each cohort exhibited similar body mass index (BMI), placing them in the overweight category according to the government guidelines.[256] The cirrhotic volunteers exhibited a larger range of BMI from 20-45, with those above 30 considered obese[256]; this is reflective of our inclusion of MAFLD samples with this liver disease driven by lifestyle factors such as obesity. Liver function tests are used to measure the integrity of hepatocytes and cholestasis (the slowing or stoppage of bile flow); one or two liver enzyme abnormalities are indicative of liver disease.[256] Although never set, often

elevated alanine aminotransferase (ALT) and aspartate aminotransferase (AST) levels are present alongside a slight increase in alkaline phosphatase (ALP).[256] As seen in Table 3.1, the cirrhotic cohort on average exhibited significantly raised AST, ALT, and ALP levels in comparison to the healthy control group.

ALT is predominately found in the liver and is localised within the cellular cytoplasm of hepatocytes, whereas AST is expressed in various tissues and is both cytosolic and present in the mitochondria.[258] Both aminotransferases are enzymes that catalyses the transfer of an α-amino group from alanine or aspartate to an α-keto group of ketoglutarates producing acids that play important roles in the citric acid cycle.[259,260] Clearance of both enzymes in the liver is regulated by the LSEC.[261] In cirrhosis, the integrity of hepatocytes is lost leading to the leakage of AST and ALT into the blood stream, with this increase in serum concentration and the capillarisation/ loss of function in LSEC in disease, these concentrations are unable to be cleared.[261,262] ALP is a marker for cholestasis, this enzyme is responsible for the transport of metabolites through cell membranes.[257] Localised on the bile duct epithelial within the liver, in disease the accumulation of bile salts leads to the release of membrane-bound ALP; leading to elevated serum values.[263]

Bilirubin is also an important parameter to investigate in the early biochemistry screening for liver function. Bilirubin presents as yellowish pigment produced in the catabolism of haemoglobin by the RES. Hepatocytes are responsible for the conjugation of bilirubin to glucuronic acid allowing it to be excreted via the bile.[262] In healthy patients as seen in our cohort, bilirubin presence is minimal due to the high clearance rates.[457] In individuals with liver cirrhosis, hepatocytes have reduced capacity to either uptake or conjugate bilirubin leading to its accumulation within the liver.[265] As evidenced in the stark difference in our healthy vs cirrhotic donors, whereby our cirrhotic cohort displayed on average 86mmol/L of bilirubin in comparison. The ranges were also vastly different with healthy controls showing a range of 4-17mmol/L compared to the cirrhotic groups: 5-451mmol/L. Thrombocytopenia is one of many clinical presentations of chronic liver

disease and caused be the reduced production of thrombopoietin[266,267] and increased consumption of platelets by the splenic and hepatic macrophages.[266,267] Thus, as expected we noted a reduced platelet count in our cirrhotic cohort, with a count about half that seen in healthy individuals (Table 3.1)

The final parameter worthy of note is the MELD (Model for End-Stage Liver Disease) score. This score predicts 3-month survival and is used to aid in the prioritisation of patients for transplantation.[268] It considers 3 reproducible and readily available biochemical variables: serum bilirubin, creatinine and the international normalised ratio of prothrombin time (clotting time).[267] In keeping with the fact that our cirrhotic samples came from patients who had been transplanted, it is unsurprising that these had MELD scores of around 16 indicating very poor liver function.

Although clinical observations are an important part of diagnosis, liver disease cannot be determined by these alone. Often biopsies are performed and immunohistochemical analysis are used for confirmation. For instance, in a retrospective study, a total of 37 biopsies from individuals with normal ALT values were assessed histologically. Here, individuals with potential for living donor liver transplantation (n=16) and patients with unexplained hepatomegaly (n=21) were examined. In total, 12 cases presented fibrosis and 6 more with cirrhosis.[269] This has left some clinicians to speculate that some of the population recruited to determine the normalised reference ranges may have been on the spectrum of disease.[257]

Therefore, as well as comparing the demographic parameters for our patients, I also used H+E staining to assess the morphological appearance of their liver samples. Examples of healthy donor tissue can be seen in Figure 3.1. Panel A is a wide view of a section of tissue showing characteristic normal lobular architecture and cellular appearance. Panel B is an example of the zonation of the liver extending from the portal triad (zone 1) through to the central vein (zone 3). Blood flows though the sinusoids from zone 1 to 3 past the hepatocytes (indicated by orange arrows). Panel C highlights the highly

vascularised nature of the liver, with blue arrows illustrating examples of the vast network of sinusoids.

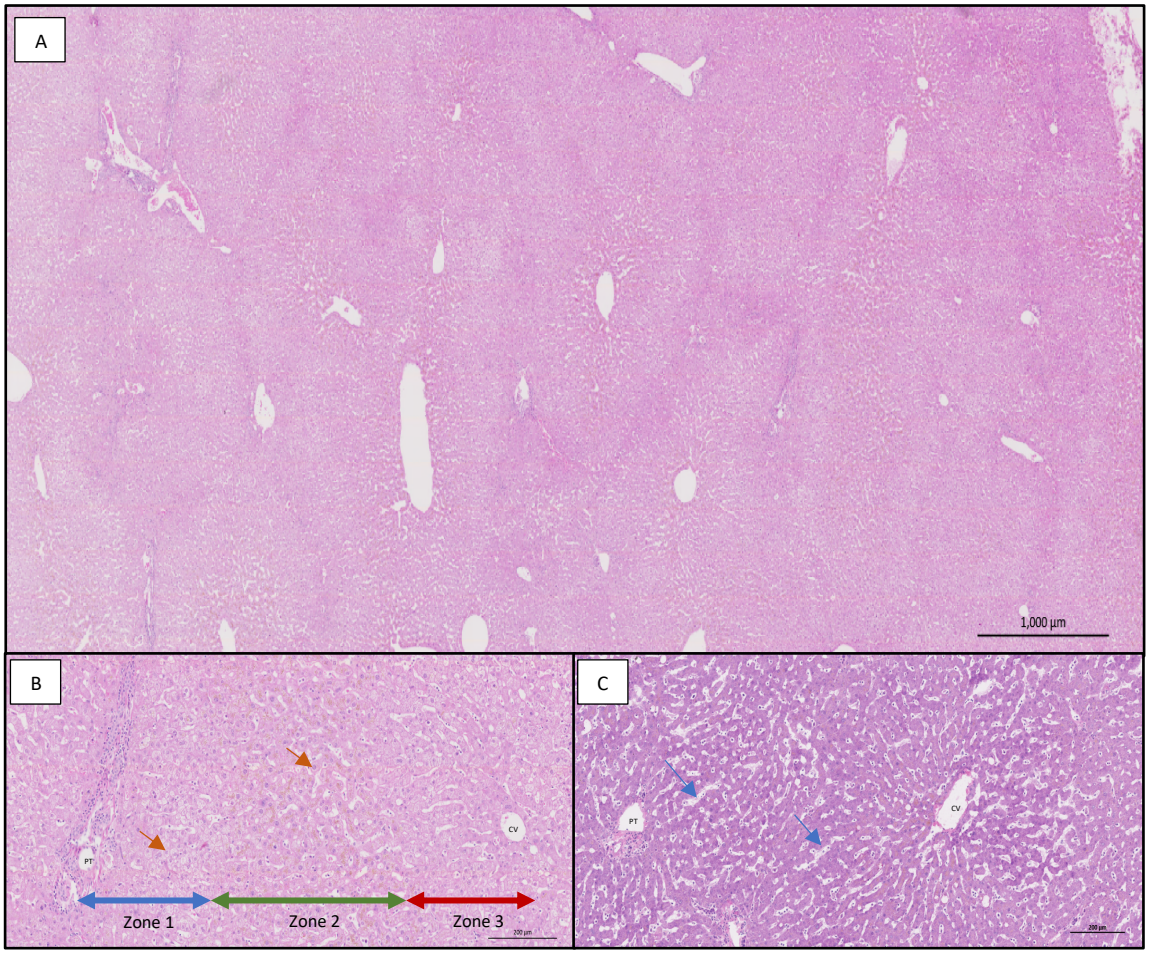


Figure 3. 1: Healthy liver stained with hematoxylin and eosin. Representative images showing formalin fixed paraffin embedded human liver tissue from healthy controls. Sections were stained for hematoxylin and eosin (H&E) and images captured using Zeiss AxioScan Z.1 (20x). Panel A shows a widefield view of healthy liver tissue. Panel B illustrates the zonation of the liver leading from zone 1 of the portal triad (PT) through to zone 3 with the presence of the central vein (CV). Orange arrows indicate hepatocytes. Panel C shows the extensive vascular nature of healthy liver with blue arrows highlighting the sinusoids. Scale bars run as 1000µm, 200µm and 200µm respectively.

Determining the diagnosis of MASLD or ARLD is complex and often requires knowledge of the lifestyle factors of an individual. For instance, a diagnosis of ARLD can be made if an individual's alcohol intake is in excess of 20-40g/day for men and 20g/day for women.[270] ARLD progression spectrum ranges through: alcoholic steatosis (fat accumulation), alcoholic steatohepatitis/fibrosis and alcoholic cirrhosis.[271]

In terms of histology, cirrhosis is defined by the development of regenerative nodules encircled by fibrous bands.[271] Figure 3.2 illustrates a classic example of cirrhotic ARLD. Here as exampled in panel A and C, the space of Disse becomes encumbered with scar tissue, highlighted by the dotted black line in panel C. This scar comprises of complex structures of ECM such as fibril forming interstitial collagen type I and III, fibronectin, basement membrane collagen type IV and glycosaminoglycans to name a few.[272] First evidenced in fibrosis, excess ECM is removed by enzymes such as matrix metalloproteinases (MMP).[273] This is a balanced process hence the potential for reversal of damage at this stage. If injury continues however, this progresses into cirrhosis; here fibrogenesis outweighs fibrolysis.[271] As mentioned in section 1.8.1, the activation of hepatic stellate cells to transdifferentiate into myofibroblasts is the major contributing factor to ECM deposition. The release of cytokines, namely the growth factor TGF-B1 from activated KCs and capillarised LSEC lead this charge.[189] LSEC is also thought to contribute to the release of ECM. Within a disease setting, single cell RNA sequencing and lineage tracing has shown LSEC to adopt a partial endothelial mesenchymal transition like phenotype.[274] This adaption results in LSEC contributing considerably to the release of ECM and can only be found within the sinusoids, not within portal scars.[274]

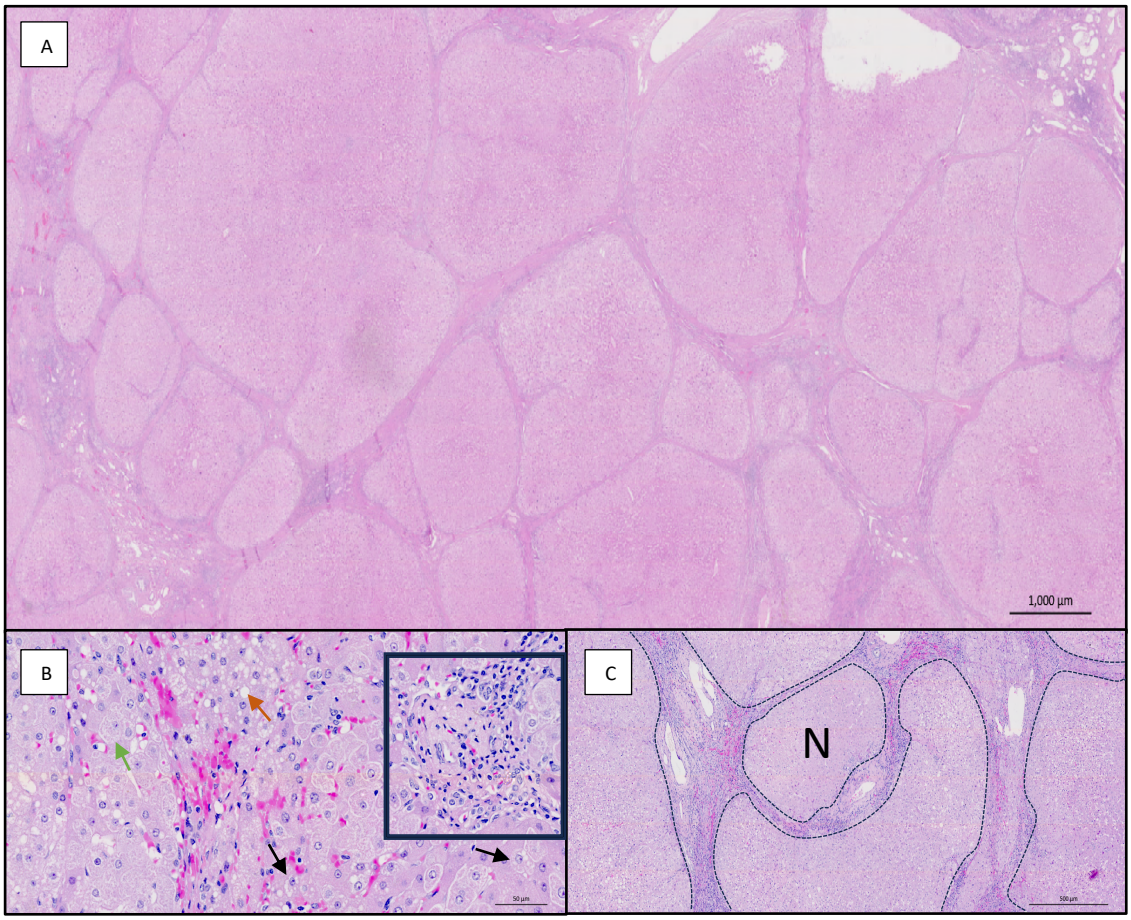


Figure 3.2: ARLD liver stained with hematoxylin and eosin. Representative images showing formalin fixed paraffin embedded human liver tissue from ARLD explants. Sections were stained for hematoxylin and eosin (H&E) and images captured using Zeiss AxioScan Z.1 (20x). Panel A shows a widefield view of ARLD tissue. Panel B illustrates a zoomed in view of immune cell infiltration (black box). Macrovesicular (orange arrow) and microvesicular (black arrows) are also present. Hepatocyte ballooning shown by the green arrow is a common histological feature of ARLD. Panel C shows the vascularised fibrotic septum network (within the dash black lines) forming nodules (N)- a classical feature of ARLD. Scale bars are 1000µm, 50µm and 500µm respectively.

Another common disruption of the liver architecture seen in ARLD is regenerative nodule formation. This is caused by vascularised fibrosis septa that branch the portal tracts and central veins together[271]; this leads to the islanding of hepatocytes known as a nodule (indicated by 'N' in panel C). Bridging starts in zone 3 and extends through to zone 1 in a pericellular pattern.[275] This network of septa allows for communication between the vessels and furthers the vascular distortion seen in diseased liver. This disruption leads to blood shunting, meaning improper exchange between LSEC and the parenchyma.[276] On a cellular level, panel B shows the infiltration of immune cell aggregates (within the black box). Neutrophilic lobular inflammation is a classic hallmark of ARLD, alongside the

recruitment of natural killer T cells, mucosal-associated invariant T cells[277] and circulating monocytic cells.[278] Portal inflammation is often more exaggerated in ARLD than MASLD.[275]

The ARLD tissue also exhibits steatosis with both macrovesicular and microvesicular steatosis present in the exemplar case. Panel B (black arrows) indicates microvesicular steatosis, these small fat droplets accumulate within the hepatocytes and push the nucleus to the edge of the cell. These can often be actively metabolised however with continuous injury can form macrovesicular steatosis (indicated by the orange arrow). Large droplets of fat are more resistant to lipases[279] and thus have longer staying power. In ARLD, steatosis begins at zone 3 and progresses through to zone 1.[275] Ballooning hepatocyte degeneration, another histological feature of ARLD was also observed and is highlighted by the less concentrated eosin stain within the cytoplasm.[280] This can be identified in panel B by the green arrow.

MASLD has a very similar histological appearance to ARLD, but is driven by metabolic syndrome, insulin resistance, hypertension and hyperlipemia with the absence of alcohol intake.[281] Figure 3.3 shows an example of MASLD tissue. In comparison to the ARLD tissue (Figure 3.2), there was considerably more macrovesicular steatosis in the MASLD tissue and far less bridging fibrosis and less nodule formation. Similarly, to ARLD, steatosis and inflammation begin within zone 3 and progresses towards zone 1 as injury continues.[282] Zone 3 is thought to be more susceptible to damage due to its already hypoxic nature.[257]

Localisation within the periportal region by immune cells is preferred as it allows optimised surveillance of the gut derived nutrient rich blood. This becomes exaggerated with inflammation and similar infiltrate is seen as within ARLD. However, it is suggested the displacement of KCs with infiltrating monocytes is a considerable contributor to inflammation and fibrosis within MASLD.[283,284] These infiltrating monocytes are the first immune cell present at the early onset of disease.[284,285]

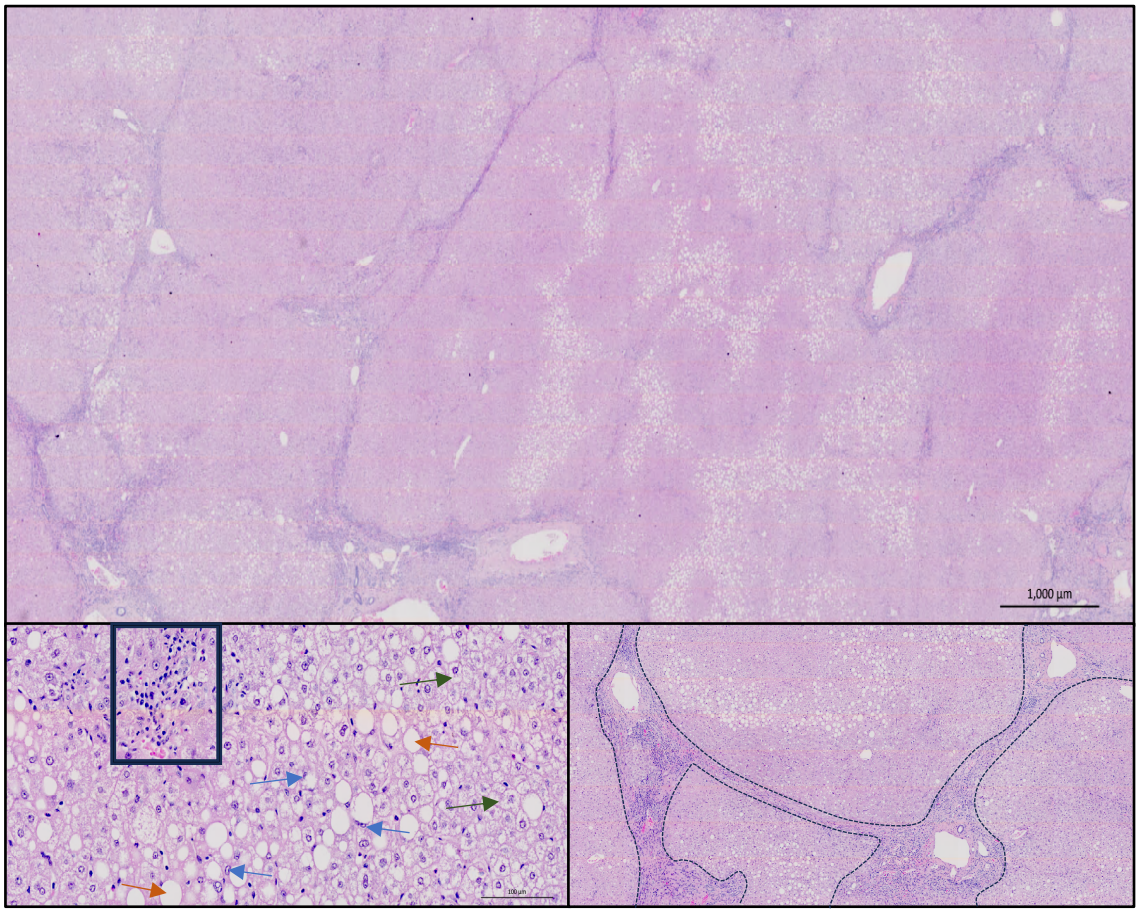


Figure 3.3: MASLD liver stained with hematoxylin and eosin. Representative images showing formalin fixed paraffin embedded human liver tissue from MASLD explants. Sections were stained for haematoxylin and eosin (H&E) and images captured using Zeiss AxioScan Z.1 (20x). Panel A shows a widefield view of MASLD tissue. Panel B illustrates a zoomed in view of immune cell infiltration (black box). Macrovesicular steatosis (orange arrow) and examples of peripherally pushed nucleus (blue arrows) by fat accumulation indicated. Hepatocyte ballooning shown by the green arrow is a common histological feature of MASLD. Panel C shows the fibrotic bridging seen in MASLD (within the dash black lines). Scale bars are 1000µm, 100µm, and 500µm respectively.

Summary

We want to understand the impact of chronic disease on the ability of the liver to clear and recycle therapeutic antibody. Thus, it was important to ensure the liver samples we used are representative of the diseases of interest. Our demographic data and histological assessment confirmed that our non-diseased cohort had broadly normal serological parameters but slightly elevated BMI. This was in keeping with the observed histological appearance of the liver. In contrast our cirrhotic specimens had elevated MELD scores and blood biochemistry indicative of inflammatory liver injury and cholestasis. Histological evaluation also showed extensive scarring and distortion of

regular hepato-architecture. In the following sections we will introduce each receptor of interest and explore how expression pattern changes in healthy and disease.

3.2 FcRn: In health and disease

In 1892, Ehrlich described the phenomena for the transfer of passive immunity between mother and fetus.[286] 60 years later, Brambell *et al.,* concluded that only γ-globulins, namely immunoglobulins, were able to be transferred between the two.[287] Here, it was found the Fc region of immunoglobulin was solely responsible for this transfer mechanism.[288] Brambell also documented the extended half-life of IgG in comparison to other proteins within the plasma. With high concentrated IV administrations, rapid elimination was observed suggesting a saturated rescue response. This led him to hypothesize that a single receptor was responsible for both the transference of IgG and its rescue from catabolism.[289,290] Coined the neonatal receptor (FcRn), it was shown in rabbit and rat intestine to bind with avidity to IgG in acidic conditions and to release IgG at *p*H 7.4.[291]

In 1989, FcRn was purified from rat enterocytes[292], and the crystal structure of FcRn was revealed within a resolution of 2.2Å.[292] The *FCGRT* gene (14kb) located on chromosome 19q13[294] encodes a 40 kDa MHC class I-like α heavy chain that is non-covalently bound to a 12kDa light chain, found to be β2-microglobulin (B2M).[292] The heavy chain consists of 3 extracellular domains, α1, α2 and α3, anchored by a 44 amino acid long cytoplasmic tail.[295,296] Early studies using B2M deficient mice demonstrated rapid catabolism of circulating IgG and the impedance of IgG transfer through maternal milk.[297,298] In B2M deficient FO-1 cells (a melanoma cell line), the FcRn α heavy chain was unable to reach the cell surface and was retained as a homodimer within the endoplasmic reticulum.[299] A significant reduction in affinity of FcRn for IgG was also observed.[299] In humans, the development of familial hypercatabolic hypoproteinaemia is caused by a mutation in the *B2M* gene. This is characterised by a mass reduction of endogenous IgG.[300,301] These studies evidence B2M as being an integral protein aiding FcRn in its function to recycle IgG and transfer passive immunity to an individual's offspring.

FcRn shares a structural homology with MHC class I molecules and it was once thought that the groove formed between α1 and α2 functioned as an antigen presenter.[302,303] This, however, was not the case and the combination of α3 and B2M instead functioned to bind IgG. Illustrated in Figure 3.4, at *p*H 6.0, 3 histidine residues (H310, H435 and H436) located within the CH2-CH3 hinge region of IgG become protonated. This allows for salt bridges to form with the acidic Trp133, Glu117, Asp137, and Glu132 residues on the FcRn heavy chain.[304] IgG may also bind to the N-terminus of B2M via Ile1.[304] Vaughn *et al.,* demonstrated that residues Ile253 on the Fc region of IgG and Trp133 on FcRn formed a hydrophobic binding interface.[304] Mutating Ile253 or any of the 3 histidine residues mentioned above led to the complete inhibition of FcRn binding at *p*H 6.0.[305-307] As *p*H increases, protonation is lost explaining the *p*H dependent nature of this interaction.[308]

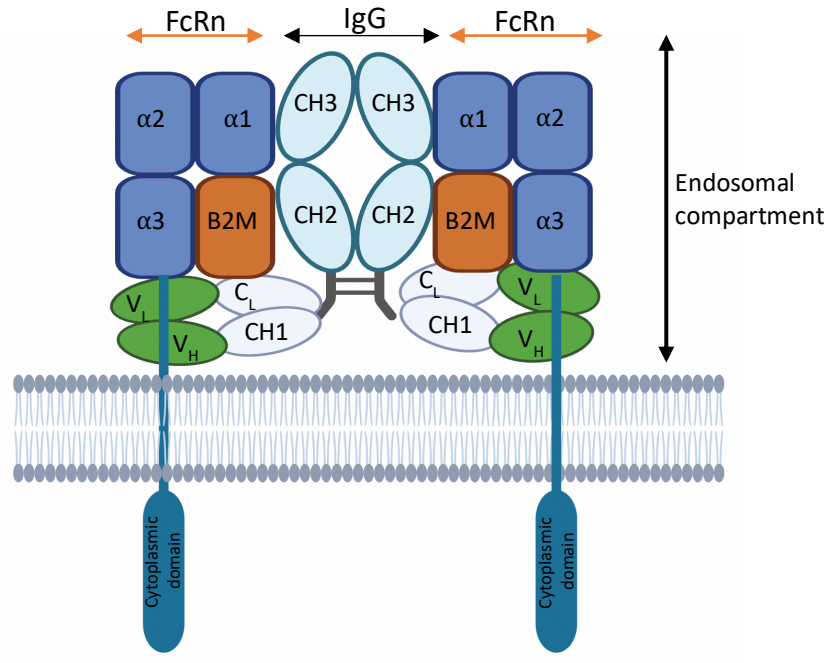


Figure 3.4: Schematic of FcRn binding to IgG. At *p*H 6.0, histidine residues within the CH2-CH3 hinge region of IgG become protonated. This allows the formation of salt bridges with acidic residues with the *α* heavy chain of the FcRn (*α*1,2,3) and the N terminus of Beta2-microglobulin (B2M). The Fab region of the IgG molecules consists of the VL,CL,VH, and CH1. This interaction often occurs within the endosomal compartment following internalisation at a 2:1 ratio. FcRn is anchored via a cytoplasmic domain. Key: VL= variable light chain; CL= constant light chain; VH= variable heavy chain and CH1= constant heavy chain domain 1. Image made using BioRender.

More recent evidence suggests involvement of the Fab arms in FcRn binding. As discussed in the introduction, Ustekinumab and Briakinumab share the same Fc region but differ greatly in extent of half-lives due to a charge cluster within the Fab region.[61] Other notable studies including mAbs which have the same Fc portion but varying Fab arms, showed significant differences in both the binding and dissociation of FcRn at *p*H 6.0 and 7.4 respectively.[309]

IgG has two binding domains within the Fc region meaning the binding ratio of IgG to FcRn is 2:1.[310] However FcRn also recycles albumin in a *p*H dependent manner.[311] The stoichiometry here was found to be 1:1[312], with albumin recycling being the more efficient process. Hence in humans, 1 IgG molecule to 6 albumin proteins are rescued by FcRn.[313] Hepatocytes synthesise albumin and were the first cell type found to express FcRn beyond the neonatal period within rats.[314] FcRn was expressed intracellularly localised within the late or recycling endosomes and not associated with lysosomal compartments.[315] However a small proportion is found on the cellular surface.[315] Hepatocytes have demonstrated the ability to recycle recombinant factor VIII- Fc fusion proteins from degradation.[316] However, hepatocytes that don't express FcRn have shown to have no effect on the concentration of endogenous IgG.[317] So their role in IgG recycling is thought to be minimal.

FcRn is also known to be expressed on LSEC and Kupffer cells.[318-320] In two individual biodistribution studies in which *WT* and $FcRn^{-/-}$ mice were administered labelled antibodies, the liver was found to be the major site of catabolism of IgG in the absence of FcRn.[321,322] Therefore in WT situations FcRn has a role in the recycling and dictate half-life of IgG based antibodies within the liver. Thus, we assessed the expression of FcRn at both mRNA and protein level between healthy and cirrhotic tissue. This will allow us to make assumptions as to whether the differences in mAb/bsAb processing that will be discussed in Chapter 4 are due to differences in the availability/concentrations of FcRn in different settings.

3.2.1 FcRn expression in tissue is unaffected by cirrhosis.

For initial assessment of FcRn expression distribution within healthy and diseased liver, immunohistochemical staining was performed. Figure 3.5 shows representative images with the top panel showing a section of healthy liver stained with FcRn antibody (brown). Expression can be seen exclusively on or within the sinusoids. Black arrows indicate examples of LSEC staining, but other staining more suggestive of Kupffer cell localization is also evident. The middle panel is from ARLD tissue and here more concentrated staining can be found within and on the sinusoid itself. However, diffuse staining is also observed around the periphery of hepatocytes (highlighted by green arrows). Isotype control staining was negative (Inset panel B). The bottom panel is a representative image of MASLD tissue. Staining here is again localised to the sinusoids but to a lesser extent than the previous two panels. Here no parenchymal staining is observed. % coverage was used as a quantifiable measure to compare the extent of FcRn immunoreactivity in increased numbers of samples for each tissue type. Figure 3.6 panel A shows that no significant difference was seen when comparing immunoreactivity in MASLD (n=8) or ARLD (n=9) to healthy tissue (n=10) although there was considerable interpatient variation. There appeared to be a trend for lower expression in MASLD livers, and this was confirmed by Western blotting. Figure 3.6B shows that total protein expression in healthy and ARLD tissue was similar. However, expression in MASLD was significantly reduced vs ARLD. At mRNA level (Figure 3.6C/D), no significant difference was found between any tissue types for *FCGRT* (FcRn) (P=0.8927) or *B2M* (P=0.9582). B2M mRNA was more abundant in each tissue type than FCGRT. Examples of the CT values and Target/Ref plotted can be found in Table S.1 and S.2.

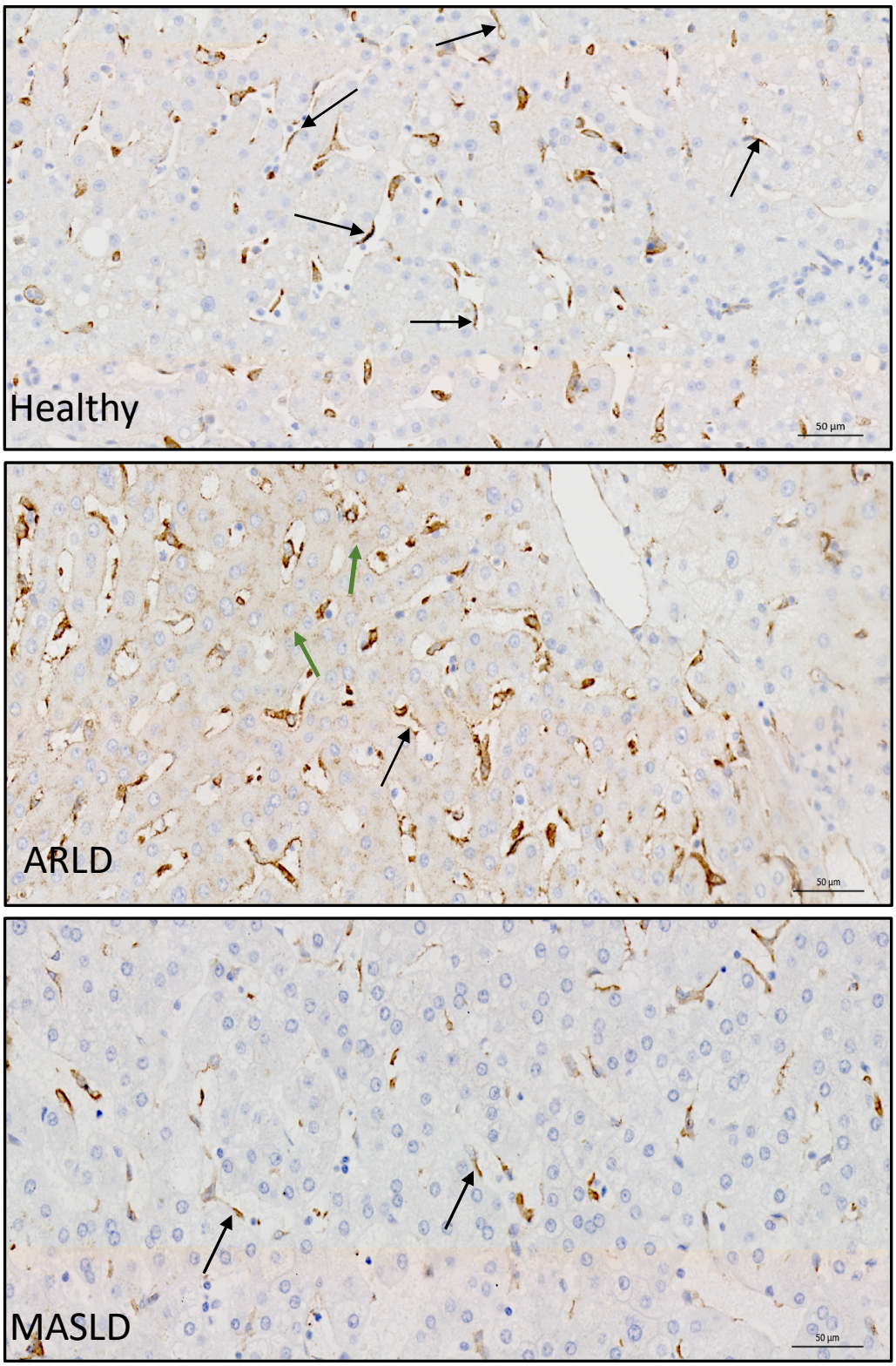


Figure 3.5: FcRn expression pattern within human liver. Representative images showing formalin fixed paraffin embedded human liver tissue from healthy, ARLD and MASLD donors. Sections were stained for neonatal Fc receptor (FcRn) using a rabbit FCGRT polyclonal IgG following citrate-based antigen retrieval. Non-specific staining was blocked using peroxidase blocker and 1x casein. Staining was identified using ImmPress anti-rabbit HRP secondary kit and DAB. Nuclei were counterstained using Mayers hematoxylin. Following alcohol and xylene exchanges slides were mounted using DPX. Images were taken on the Zeiss AxioScan Z.1 at a magnification of 20x. Black arrows indicate FcRn expression on LSEC, Green arrows indicate hepatocyte staining. IMC= isotype matched control. Scale bar 50µm.

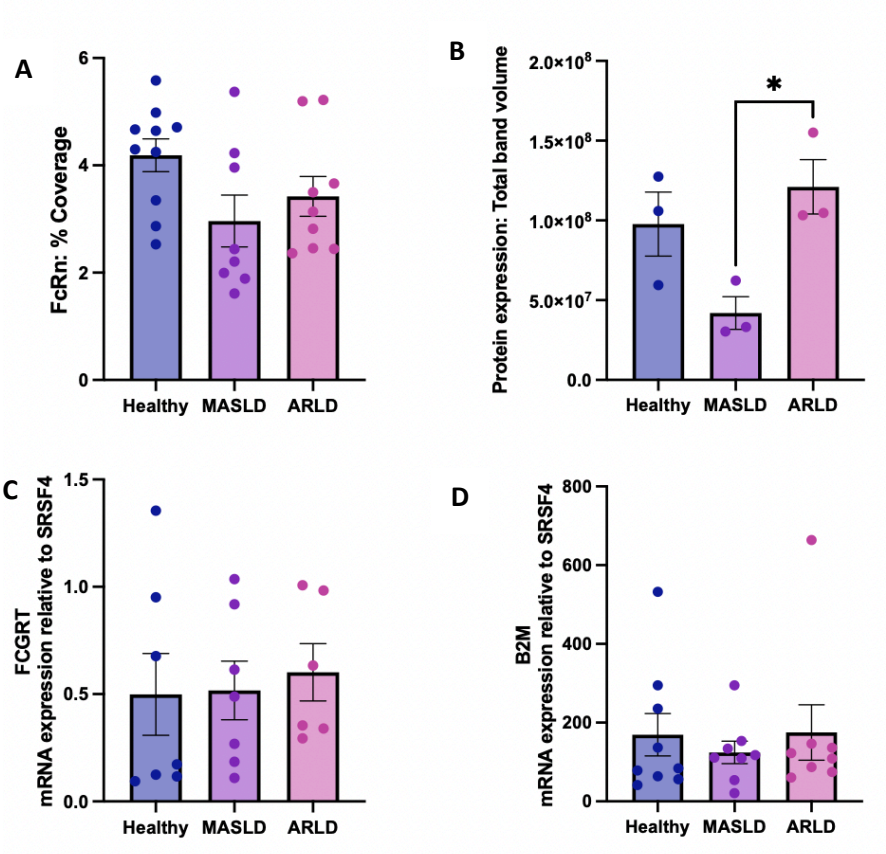


Figure 3.6: FcRn and B2M expression profile in whole liver tissue. A) shows the quantification of FcRn coverage over tissue marked as % coverage. IHC staining of FcRn was performed and sections were scanned via the AxioScan Z1 at 20x magnification. For each section 5 fields of view were randomly selected and analysed on the same digital zoom %. Fiji software was employed to quantify % coverage. Each blot represents a single liver section with a total of 5 field of view averaged per point. Healthy n=10, MASLD n=8, ARLD= 9. Protein expression was gained through the densitometry analysis of western blots of liver lysates in image lab software. B) shows a summary of protein expression of FcRn (n=3 for each). Significance was seen between MASLD and ARLD (P=0.0345). qPCR was undertaken on human liver tissue to quantify mRNA expression relative to the housekeeper, SRSF4.) shows a summary of *FCGRT* expression, the gene for FcRn. Healthy n=7, MASLD n= 7, ARLD n= 6 (P= 0.8927) B) mRNA expression of *B2M* relative to *SRSF4*. Healthy n= 9, MASLD n=8, ARLD n=8 (P=0.9582). Error bars indicate ±SEM. Depending on the normality values, either one way ANOVA or Kruskal-Wallis tests were performed to calculate statistical significance.

3.2.2 FcRn expression in LSEC is unaffected by cirrhosis.

After seeing the expression of FcRn in context of disease in whole liver tissue, we next wanted to assess expression in LSEC. Cells were isolated from slices of human tissue and cultured until confluent (see Section 2.4.1); RNA and protein were extracted from cell

lysates. Figure 3.7 panels A and B shows that there was no difference between healthy and diseased cells for either FcRn or B2M (P=0.9954 and P=0.5028 respectively), furthermore, there was once again significant inter-individual variation. Comparing Figure 3.6 and 3.7 B2M showed a similar expression profile between whole liver and isolated cells, but expression was higher relative to the housekeeping gene *SRSF4* in LSEC. At protein level, ARLD cells expressed the most FcRn, but this did not reach significance (Figure 3.7C).

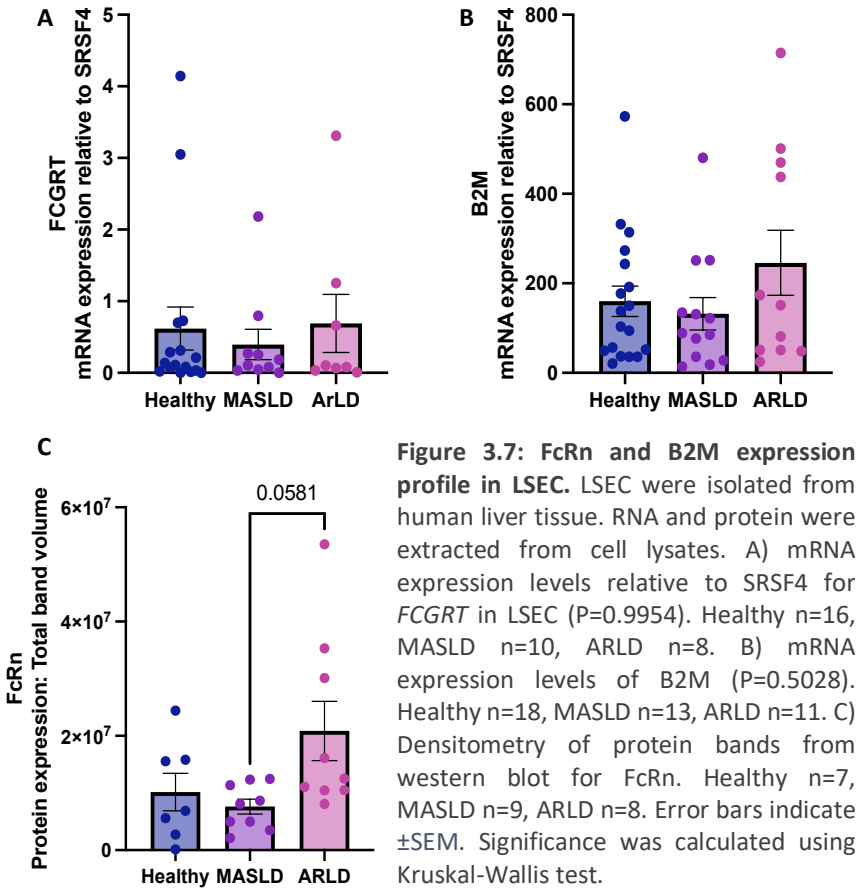


Figure 3.7: FcRn and B2M expression profile in LSEC. LSEC were isolated from human liver tissue. RNA and protein were extracted from cell lysates. A) mRNA expression levels relative to SRSF4 for *FCGRT* in LSEC (P=0.9954). Healthy n=16, MASLD n=10, ARLD n=8. B) mRNA expression levels of B2M (P=0.5028). Healthy n=18, MASLD n=13, ARLD n=11. C) Densitometry of protein bands from western blot for FcRn. Healthy n=7, MASLD n=9, ARLD n=8. Error bars indicate ±SEM. Significance was calculated using Kruskal-Wallis test.

3.3 Expression of mannose receptor (CD206) In health and disease

The next receptor to consider is the Mannose receptor (CD206), which has a potential but yet unclarified role in clearance of certain glycosylated antibodies (Section 1.4).[82-87]

Due to this and its known high expression on LSEC, we wanted to establish its expression pattern in healthy and diseased liver. In 1976, Stahl *et al.,* described a specific receptor responsible for the rapid clearance of lysosomal hydrolases within the liver.[323] Through different inhibition assays, they determined this was due to the binding of the carbohydrate portion of the hydrolase enzyme.[323] This receptor was later determined to be CD206. CD206 has been found to perform a variety of functions from clearance of pathogens[324], to clearance and regulation of glycoproteins and extracellular peroxidases.[325,326] It is also involved in antigen presentation[327], causing many to consider this receptor as the interface of innate and adaptive immunity. CD206 is encoded by the *MRC1* gene on chromosome 10 in humans, it is a 165kDa C-type lectin/ type I membrane glycoprotein. The structure (Figure 3.8) of this receptor enables its multifunctionality. It possesses 3 ecto-binding domains: 1) N-terminal cysteine rich amino-domain that binds sulphated sugars in an Ca^{2+} independent manner[328,329] 2) a fibronectin type II domain which binds the α chain of type I-IV collagen[330] (Ca^{2+} independent) and 3) 8 adjoining C-type lectin domains that bind mannose, L-fucose and N-actylglucosamine.[331] The latter domain is Ca^{2+} dependent and requires two Ca^{2+} ions to bind sugars, with one being present in the binding site and the second binding in the loops of domain 4.[332] C-type lectin domains 4, 5 and 7 play a predominant role in binding and internalisation of ligands.[331]

CD206 is a non-canonical pattern recognition receptor as it lacks a signalling motif, therefore requires association with other co-receptors to transduce a signal cascade.[333-334] The short cytoplasmic C-terminal tail of CD206 has a di-aromatic motif that is responsible for the intracellular trafficking and localisation into the early endosome in a clathrin-mediated mechanism.[335] 30% of CD206 is localised on the surface with the remainder within the cell.[335] Using clathrin-dependent internalisation, CD206 can also be recycled back to the surface. Often with continuous exposure to increasing concentration of ligands, this recycling ability leads to a build-up of these ligands intracellularly.[336] It has been found that the type of sugar bound to CD206 impacts its fate within the cell. Using $CD206^{+}$-CHO cells treated with either mannosylated or

sulphated glycopolymers (M_{32} and S_{32}), it was found that mannosylated glycoproteins were more likely to localise within lysosomes with CD206 being returned to the surface.[337] On the other hand, sulphated glycopolymers caused less recycling of CD206 and an increased localisation within the early endosome.[337] A couple of studies have suggested this is due to the *p*H induced loss of Ca^{2+} leading to a loss of binding to the C-type lectin domains.[337,338] As the cysteine rich domain does not require Ca^{2+} ions, sulphated glycoprotein binding is unaffected. This *p*H change is indicative of the environmental changes within the endosome. Thus, the acidified nature of the endosome leads the loss of binding to the sugars and its return to the surface, fating the glycoprotein for lysosomal degradation. The opposite is true for sulphated sugars.

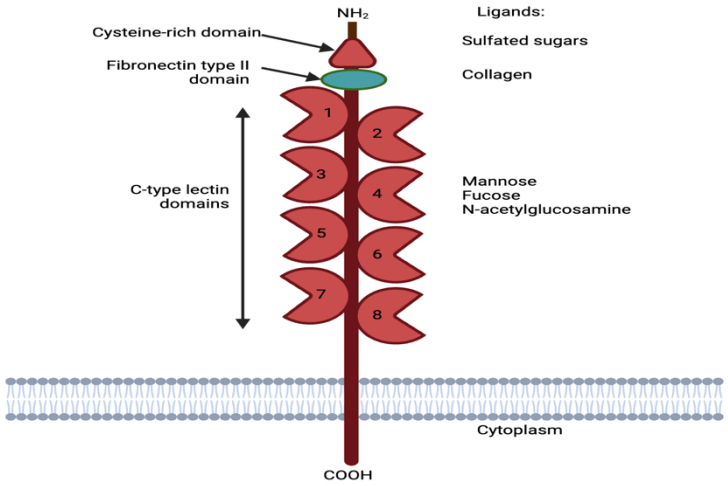


Figure 3.8: Structure of CD206. CD206 is a c-type lectin. It has 3 ectodomains: 1) Cysteine-rich domain that binds sulphated sugars 2) fibronectin type II domain that binds collagen and 3) C-type lectin domains: 8 adjoining carbohydrates that bind to mannose, fucose and N-acetylglucosamine. Image made using BioRender.

CD206 is expressed on a subset of macrophages, dendritic and various endothelial cells.[339] In human LSEC, although the consensus is that CD206 is expressed, it is debated to what extent. Using microarray quantification, *MRC1* was ranked as a top 3 gene marker for LSEC.[340] Whereas in a scRNA-seq dataset, *MRC1* was not found to be a differentially expressed gene.[341] CD206 is thought to function in LSEC in the recruitment of lysosomal enzymes for degradation of internalised material[94], clear tissue turnover

byproducts[139,149-151] and can also help in antigen presentation to CD8+ T cells.[342] Here, CD206 internalises and delivers antigen to MHC class I molecules internally allowing the promotion of CD8+ T cell tolerance.[343]

Cytokines are known to regulate expression of CD206 on LSEC. The pro-inflammatory cytokine IL-1β is known to increase expression of this receptor in mice and rats[344-345], alongside the addition of LPS.[344] IL-10, the anti-inflammatory cytokine has shown contrasting results. In one study, LSEC cultured with IL-10 or IL-4 with IL-13 resulted in increased expression of CD206.[346] Another study, showed that IL-10 led to a decrease in CD206 expression on LSEC.[347] As a consequence this research found there was reduced antigen uptake by CD206 and thus a downregulation of T cell activation arising from an absence of presentation of antigen by LSEC.[347] Metalloproteases are able to cleave CD206 from cellular surfaces resulting in shedding of a soluble form, sCD206.[348] This soluble form still possesses intact ectodomains meaning binding is still functional.[349] In liver diseases such as ARLD, sCD206 is used as a marker to predict disease severity.[350]
With environmental differences in cytokine expression in disease and healthy liver we next investigated whether expression of CD206 in whole liver and LSEC varied with disease

3.3.1 Expression of CD206 in whole tissue

At mRNA level we saw no significant difference between healthy and diseased livers (Figure 3.9A) with mRNA present in all. Although individual samples varied, there was a trend towards more expression of *MRC1* in healthy liver in comparison to MASLD and ARLD tissue. Similar results were observed for protein expression (Figure 3.9B) by Western blotting. All three cohorts exhibited a large range of band intensities matching interindividual variation in expression. Figure 3.9C shows the quantification of % coverage of IHC stained FFPE tissue. Here, healthy tissue had significantly higher expression than ARLD (P=0.0048). This is also evident in the representative images in Figure 3.10. Here both wide and expanded fields of view show the difference in expression distribution and intensity between ARLD and healthy tissue. CD206 (brown) is localized within and on the sinusoids, again suggesting both luminal LSEC and more

punctate KC staining. No staining was evident within the hepatocytes. In healthy tissue CD206 is homogenously expressed throughout whereas, ARLD tissue shows sporadic patches within the lobules. Staining was also present within the fibrotic scar of ARLD tissue.

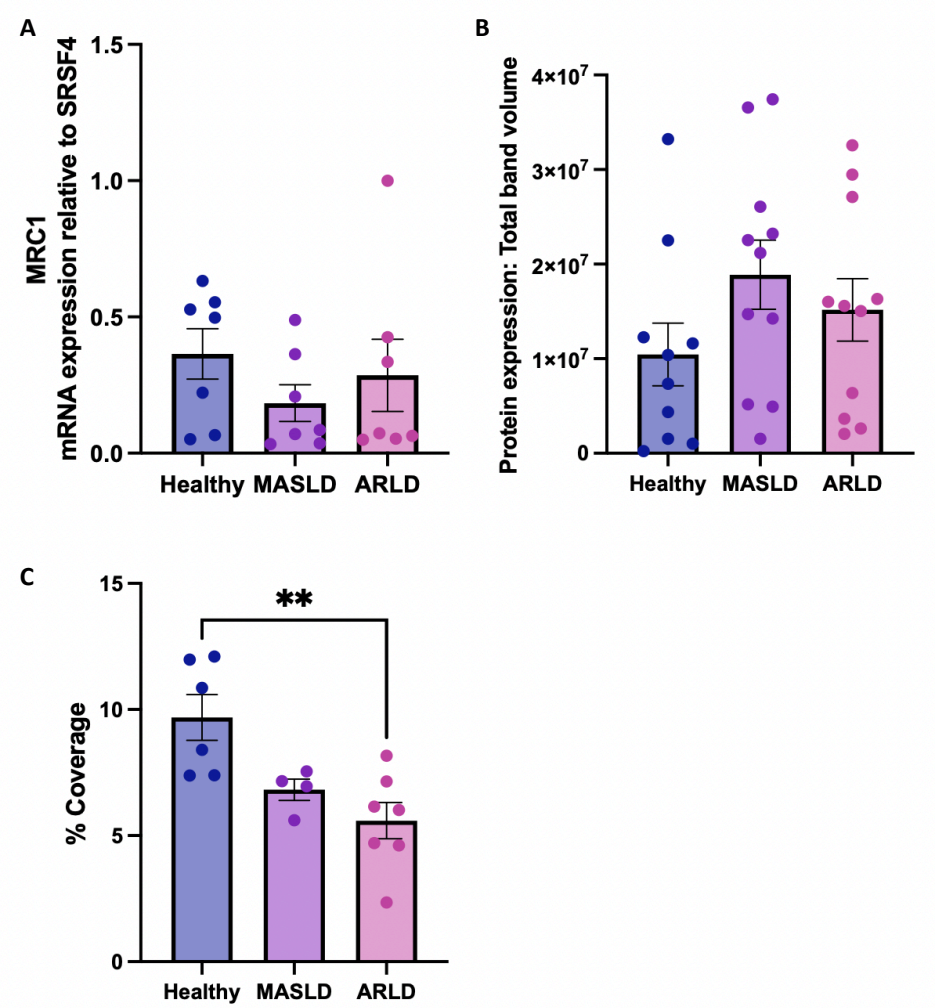


Figure 3.9 CD206 expression in whole liver tissue. Whole liver tissue was used to extract RNA and protein. A) shows the mRNA expression of *MRC1* between the different tissue types (Healthy n=7; MASLD n=7; ARLD=7), expression is relative to the housekeeping gene *SRSF4* B) exhibits the densitometry of total protein band volume ascertained via western blot (healthy n=4; MASLD and ARLD n=5). C) is the quantification of % coverage of CD206 on FFPE tissue. Significance was found between the distribution of CD206 in healthy vs ARLD tissue (P=0.0048; healthy n=6; MASLD n=4 and ARLD n=7). Analysis performed in ImageJ. Significance was calculated using one-way ANOVA. Error bars indicate ±SEM.

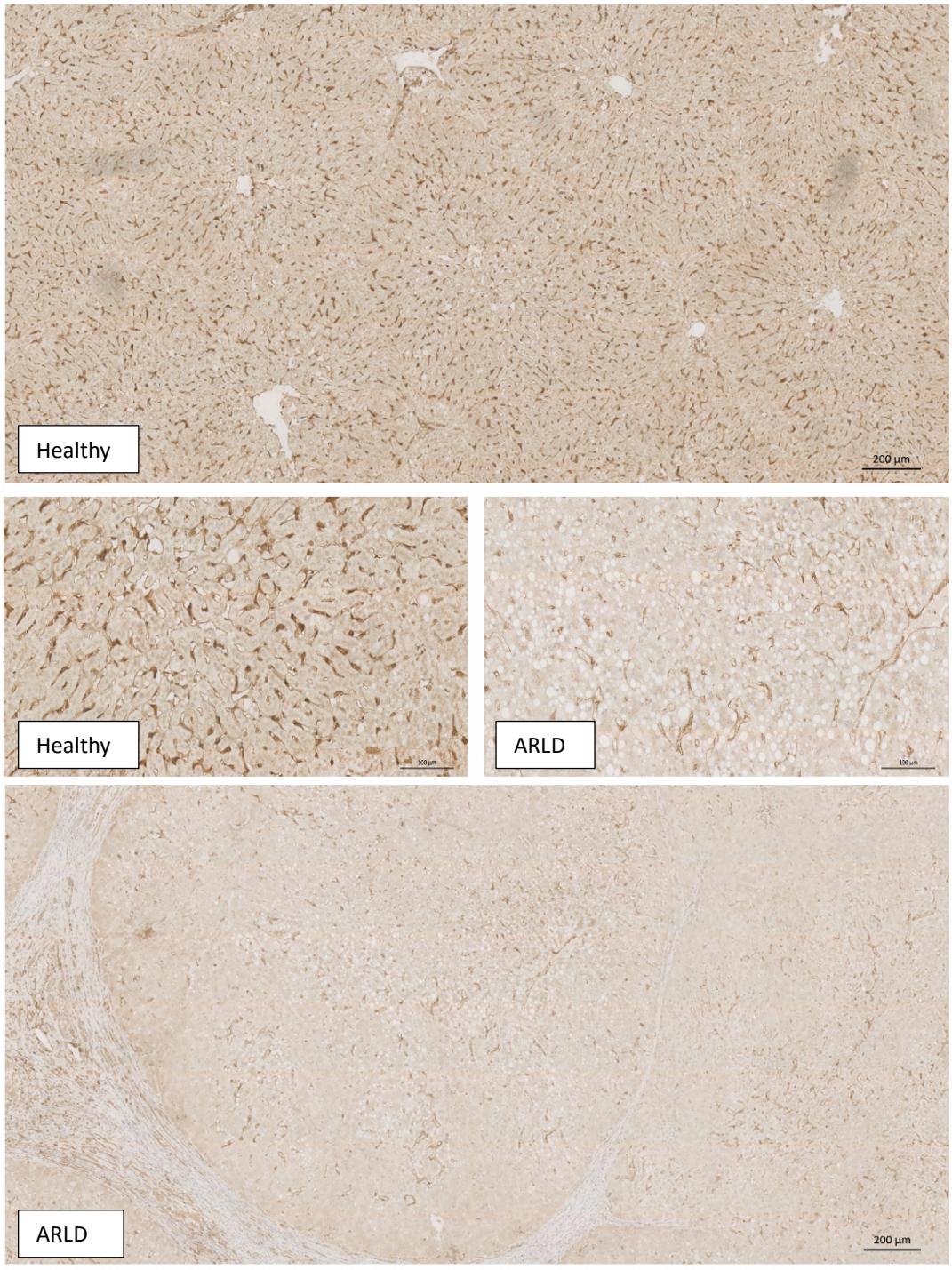


Figure 3.10: IHC of CD206 on liver. This figure shows representative images of FFPE tissue (ARLD and Healthy) stained for CD206. Here brown represents positive CD206 staining. Chromogen staining was with DAB and nuclei counterstained with Mayers hematoxylin. Images taken on AxioScan Z.1 at 20x. Scale bars are 200µm (top and bottom) and 100µm (middle panels).

3.3.2 CD206: expression by LSEC

As seen within the liver tissue, no significant difference was observed in either mRNA or protein expression between healthy, MASLD and ARLD LSEC. The density of protein bands indicated similar expression range between both liver tissue (Figure 3.9B) and LSEC (Figure 3.11B). Worthy of note, the diseased protein level for CD206 isolated LSEC clustered into three distinctive groupings (low, medium, and higher expression).

To gain context for where within the cell CD206 was expressed in isolated LSEC, immunofluorescence was performed on 4% PFA fixed cells. Here, observations of concentrated perinuclear vesicular/punctate staining of CD206 (red) can be seen (blue arrow; figure 3.11C). This staining does not extend to the cellular membrane of the cell. The bottom panel shows the isotype matched control, and whilst there is some background (white arrows) particularly within the nucleus, there was a clear difference between the positive staining and the control. All images were taken on the LSM780 confocal on the same settings (gain, pinhole, magnification 40x water immersion).

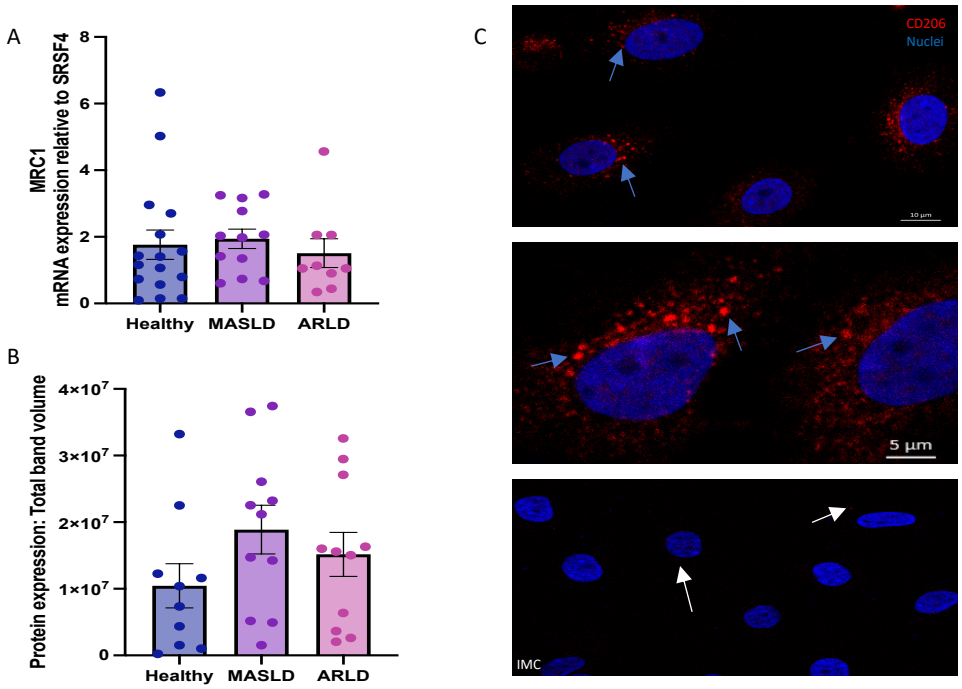


Figure 3.11: CD206 expression in LSEC. LSEC were isolated from healthy and diseased liver (MASLD and ARLD). From cell lysates, mRNA and protein were extracted and ran through either qPCR or western blot protocols. A) shows the mRNA expression of *MRC1* (CD206) in relation to the housekeeping gene *SRSF4*. Healthy n=16, MASLD n=12, ARLD=9. B) presents the band volume following densitometry analysis using Image Lab software. All bands were normalised to the total protein. Healthy n=10, MASLD n=11, ARLD=11. C) shows immunofluorescent staining of CD206 on MASLD LSEC. LSEC were seeded at 70,000 per well in ibidi VI ibitreat chambers and cultured overnight. Following fixation with 4% paraformaldehyde (PFA) for 10minutes at 37 degrees, cells were washed with PBS and then permeabilised using 0.1% Triton X-100 in PBS for 5 minutes at room temperature. Subsequent washing steps are then performed with 0.1% PBS-Tween to ensure cells are still permeabilised. Non-specific staining was blocked using 0.1% BSA diluted in PBST (0.1%) for 30 minutes. Primary anti-mannose receptor (host rabbit) was dilute in blocking buffer at 1ug/mL and incubated for 1 hour. Following wash steps, the secondary goat anti-rabbit IgG Alexa fluor 647 (1ug/mL) was incubated for 1 hr at room temperature. Nuclei was counterstained with DAPI for 5 minutes. Cells were left in PBS at 4 degrees until imaged. Images were taken using the LSM780 confocal at 40x water immersion. Scale bars are 10µm and 5µm. Bottom panel indicates the isotype matched control (IMC). For A and B: statistical analysis was performed through Kruskal-Wallis test with one-way ANOVA. Error bars indicate ±SEM.

3.4 LSIGN/CLEC4M expression in health and disease

Briefly introduced in Section 1.6.2, LSIGN (Liver specific ICAM-3 grabbing non-integrin; CLEC4M; DC-SIGNR/CD209L) is also a C-type lectin. It is a type II transmembrane glycoprotein[145] (Figure 3.12) that is highly expressed on endothelial cells such as LSEC and lymphatic endothelium.[351] It shares homology with the dendritic cell scavenger receptor (DC-SIGN/CD209).[352] Both are encoded within a 105kb region of chromosome 19p13[354], with LSIGN showing a 77% similarity to DC-SIGN at an amino acid level.[352] Its

structure consists of a transmembrane domain, an extracellular domain composed of a variable tandem repeat neck and a C-type carbohydrate recognition domain (CRD).[352] The CRD domain shares a 34% identity with ASGPR[352], the receptor involved in clearing antibodies via binding to their GlcNAc terminals. The cytoplasmic tail of LSIGN contains a di-leucine motif which allows the receptor to internalise in a Ca^{2+} dependent manner.[353] Research into this receptor has mostly centred around its role in LSEC interacting with viruses such as hepatitis C, HIV and SARS-CoV-2.[145-148] In two stand out studies, the authors found LSIGN to bind to the mannose containing glycans on FVIII[354] and von Willebrand factor[355] and this was responsible for their subsequent catabolism. Furthermore, it was found this was a clathrin-dependent internalisation[354] like that seen for CD206. Again, like CD206, LSIGN expression is also regulated by cytokines. Here, the anti-inflammatory cytokine IL-4 was found to upregulate the expression of LSIGN on LSEC.[356]

Admittedly, there is not an abundance of literature on this receptor, nor has any research been conducted on this receptors ability to bind therapeutic antibodies (to my knowledge). However, due to its affinity to bind to high mannose glycans via its CRD, similarity to ASPGR, ability to internalise and its overall high expression on LSEC, I believe this receptor is worth investigating. Thus, we wanted to assess how its expression is affected by cirrhosis.

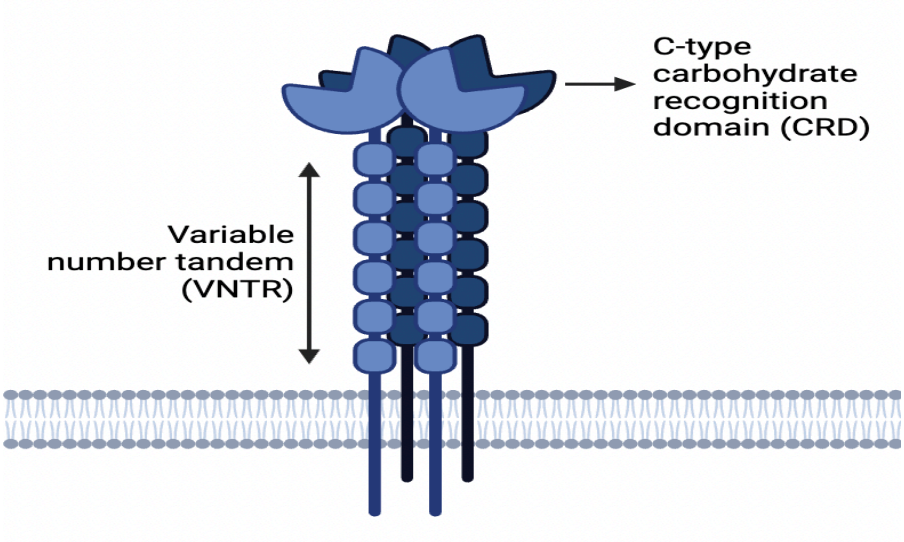


Figure 3.12: Structure of LSIGN. LSIGN is a C-type lectin/type II transmembrane glycoprotein. It has a cytosolic, transmembrane, and extracellular domains. Ectodomain include a variable number tandem repeating neck with a C-type carbohydrate recognition domain (CRD) at the N-terminal. Image made using Bio Render.

3.4.1 LSIGN expression in whole liver tissue

mRNA for LSIGN (*CLEC4M*) was present in whole liver lysates, but we saw no significant difference between healthy, MASLD and ARLD tissue (Figure 3.13A). However, there was a general trend for diseased tissue expressing more LSIGN mRNA. There was a significant difference in protein expression (Figure 3.13B) between healthy and ARLD tissue (P=0.0447). On average there was little expression in healthy tissue, with more in MASLD and the most in ARLD tissue. Our samples from MASLD donors demonstrated a large range of variability with some livers expressing very little LSIGN and some being equivalent to that of ARLD. This pattern was different histologically though, as here healthy tissue showed considerably more staining than cirrhotic tissue (Figure 3.13C). In the representative images (Figure 3.13D) of IHC stained tissue, healthy liver showed more homogenous staining in the sinusoids but with a distinct lobular variation in comparison to the ARLD. In the top panel, staining in normal liver was absent around the periportal area of tissue, but present around the central vein. Expression was determined to be surrounding the sinusoidal lining (black arrows) as well as examples of cellular staining within the vessels (orange arrows). In the ARLD example, the expression

pattern was considerable different. Staining for LSIGN was much more sporadic and lacked the continuous expression along the sinusoids seen with the healthy tissue. More staining appeared to localise upon the cells within the sinusoid (orange arrows) rather than that of the sinusoid lining (black arrows). The staining pattern was consistent within healthy and diseased tissue.

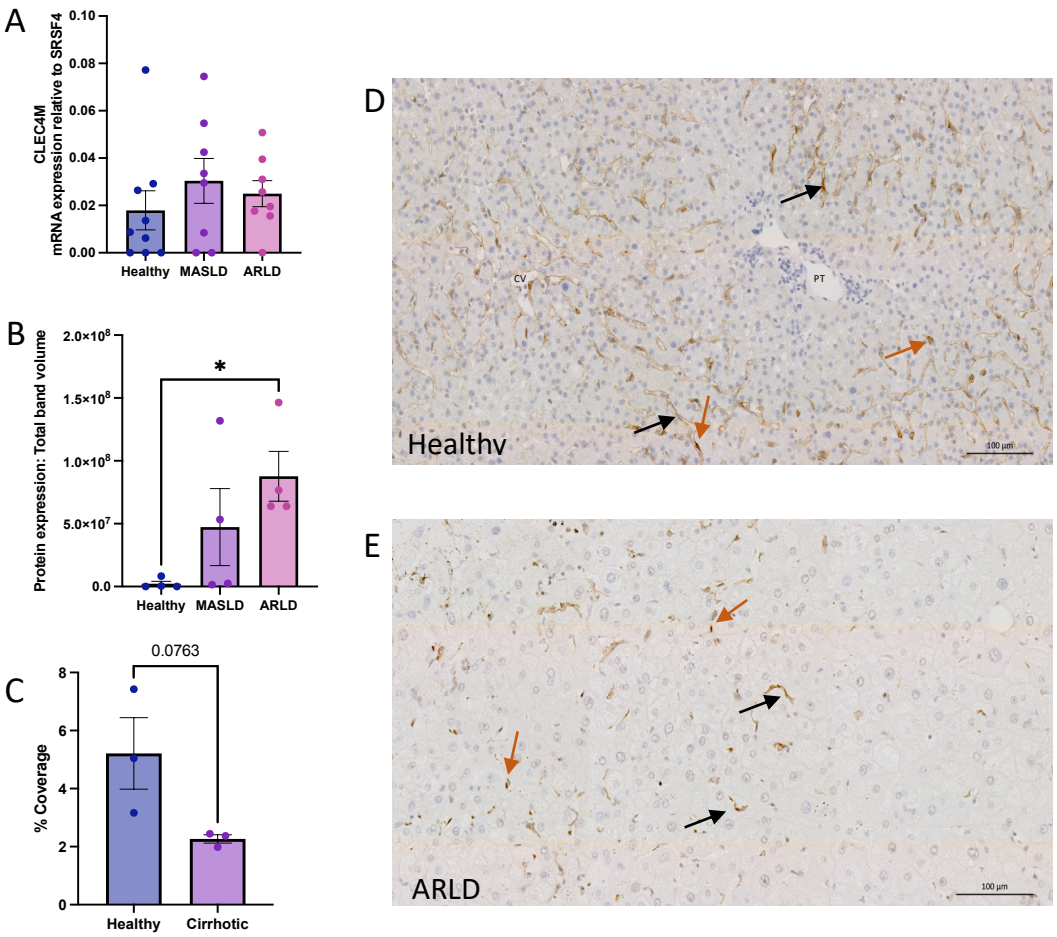


Figure 3.13: LSIGN expression in liver tissue. Whole liver tissue was used to extract RNA and protein. A) shows the mRNA expression of *CLEC4M (*gene for LSIGN) between the different tissue types (Healthy n=9; MASLD n=8; ARLD=8), expression is relative to the housekeeping gene *SRSF4* B) exhibits the densitometry of total protein band volume ascertained via western blot (healthy n=4; MASLD=4 and ARLD n=4). C) is the quantification of % coverage of LSIGN on FFPE tissue. Significance was almost found between the distribution of LSIGN in healthy vs ARLD tissue (P=0.0763); healthy n=3; cirrhotic n=4). Analysis performed in ImageJ D) and E)are representative images of FFPE tissue (ARLD and Healthy). Here brown represents positive LSIGN staining. Chromogen staining with DAB and nuclei counterstained with Mayers hematoxylin. Images taken on AxioScan Z.1 at 20x. Scale bars are 100µm. Significance was calculated using one-way ANOVA or Kruskal-Wallis where appropriate depending on normality scores. Unpaired T test was used for C. Error bars indicate ±SEM. Black arrows represent – sinusoidal staining, orange arrows represent cellular staining within the sinusoids. PT= portal triad and CV= central vein.

3.4.2 LSIGN protein expression was absent in LSEC lysates despite detectable levels of *CLEC4M* mRNA

LSEC were isolated from whole tissue and cultured until confluent. Here lysates were taken for mRNA and protein expression analysis. We saw no positive bands on protein analysis by Western blotting, so this is not shown. Regarding mRNA expression, no significant differences were noted between aetiologies, however both ARLD and healthy LSEC showed more expression of *CLEC4M* than MASLD (Figure 3.14A). This is supported by data from others. Figure 3.14B is taken from the human protein atlas[357-359], which is based on the single cell RNA sequencing from MacParland *et al.,* laboratory.[360] The left side shows the UMAP plot that allows visualisation of all cell clusters present within the liver. Here, C-5 (black arrow) contains the endothelial cells of interest. The tissue specific bar chart to the right, shows RNA expression for each cell type cluster. Fibroblasts and endothelial cells constitute majority of *CLEC4M* expression within the liver, with the third being KCs. This data set does not include cirrhotic liver comparison so next we turned to the Ramachandran *et al.,*[361] scRNA-seq database. Here 8,020 endothelial cells from healthy (n=4) and cirrhotic (n=3) tissue were analysed (Figure 3.14C). The top left panel here shows the cluster UMAP where LSEC can be identified as 'endothelia (1)' indicated by the black arrow. Below this panel shows the extent of expression of *CLEC4M* within the clusters. LSEC were shown as main expressors of LSIGN within all endothelial clusters found within the liver. This is supported by the violin plots to the left, where only endothelial (1) is extensively plotted. This plot shows the distribution of expression in healthy LSEC (uninjured) in comparison to cirrhotic cells. Cirrhotic LSEC show a broader density at the lower end of the y axis, but non-injured LSEC show a higher maximum value. Overall, however as in my PCR analysis there was no significant difference between injured and healthy cells in this study.

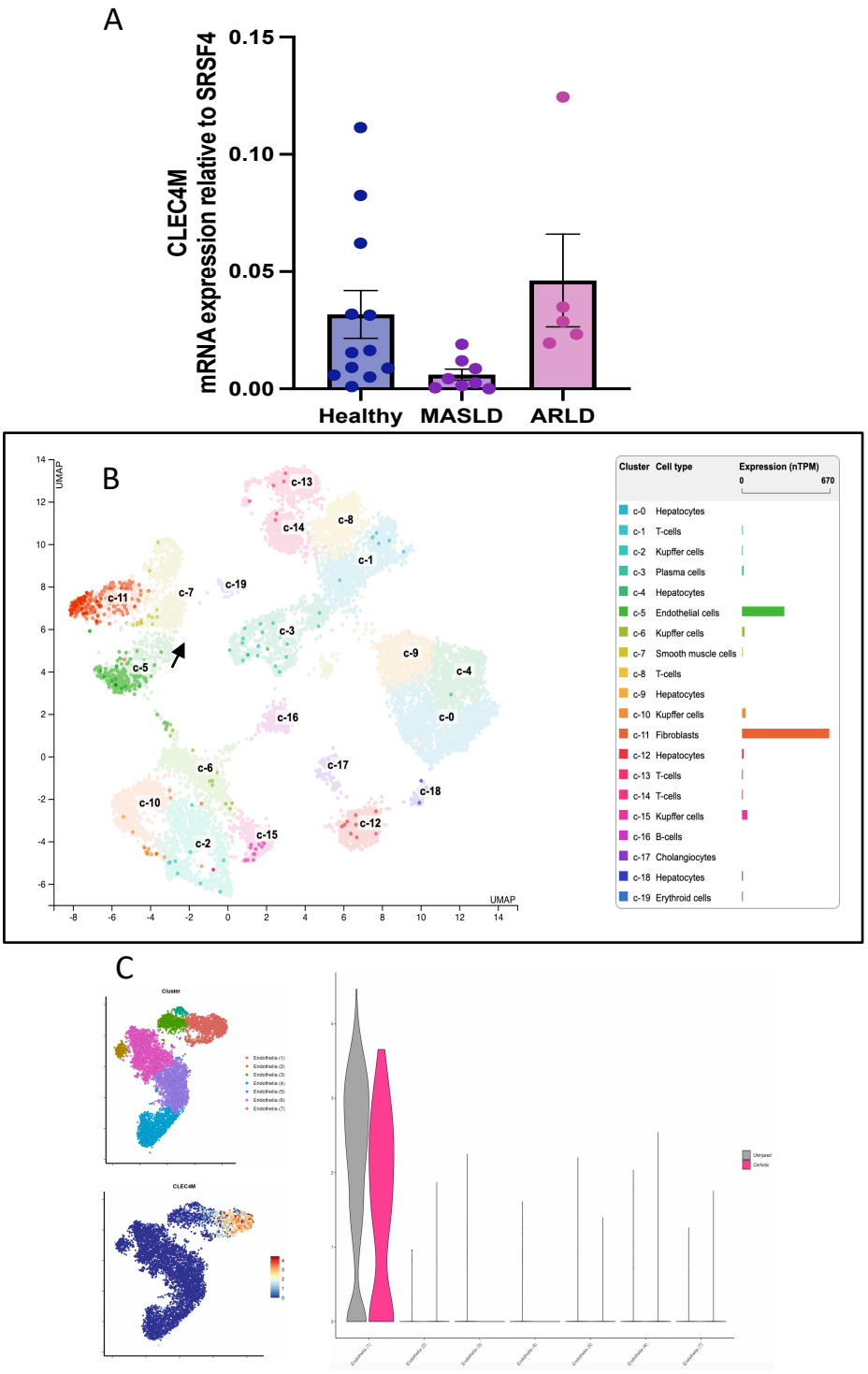


Figure 3.14: LSIGN expression in endothelial cells. A) mRNA expression of *CLEC4M (*gene for LSIGN) between the different aetiologies within isolated LSEC (Healthy n=12; MASLD n=8; ARLD=5), expression is relative to the housekeeping gene *SRSF4*. One-way ANOVA was used to confirm no significance. Error bars indicate ±SEM. B) Exemplar image of scRNA expression obtained from the Protein Liver Atlas.[146] Left UMAP shows the cell type clusters from within the liver, the black arrow indicates C-5 as the endothelial cells. The right bar chart shows the expression of RNA nTPM (normalised transcripts per million). Again, endothelial is coded as C-5. C) scRNA plots obtained from Ramachandran *et al.,*.[114] Top left panel highlights the difference clusters of endothelial found within the liver. Endothelial (1) has been identified as LSEC and is indicated by the black arrow. Below this panel, is the extent of RNA expression within clusters of *CLEC4M.* Here it is abundantly located within the endothelial (1) cluster. To the rights shows violin plots of each endothelial cluster and the extent of comparison of expression of *CLEC4M* between uninjured (healthy) and cirrhotic tissue. Again here, endothelial (1) displays the LSEC population.

3.5 FcγR expression in healthy and diseased liver

As detailed in the introductory chapter, FcγRs are often highlighted through either knock out/down or inhibitory studies as the predominant cause for immune complex clearance within the liver.[160,162,164] FcγRs are a superfamily of cell surface glycoproteins comprising of 3 major classes with multiple isoforms (in humans): FcγRI (CD64), FcγRII (CD32a and CD32b, CD32c) and FcγRIII (CD16a and CD16b). Genetically determined allotypes of CD32a are further subdivided into FcγRIIaR and FcγRIIaH. CD32c arose from a combination of CD32a and CD32b, however is often not expressed in majority of the population due to a stop codon therefore is not included in Figure 3.15. Characterised by their different affinities for human IgG2, these allotypes are determined by an amino acid at position 131.[225,226] FcγRs act as a feedback loop between the humoral and cellular immune response. Cross-linking of these receptors with the Fc portion of an IgG causes an array of effector responses from ADCC, immune complex clearance, antigen presentation and phagocytosis.[227]

Through extensive mapping, the binding site on human IgG for FcγR was revealed on a stretch of amino acids of the N-terminus of the CH2 domain (lower hinge region) at residues 233-239.[228,229] Each receptor is anchored using an α-chain with an extracellular portion comprising of two (CD32 or CD16) or three (CD64) Ig-like domains[230] (see Figure 3.15). CD64 and CD16 also house accessory proteins chains (γ and ζ) alongside the α-chain to aid in signal transduction.[231] Further distinctions are made in the receptor's affinity for IgG. In numerical order, CD64 presents the highest affinity, binding to monomeric IgG1 approximately 100-fold more strongly than either relative receptor[232], with an association of $K_a = 10^8\text{-}10^9 M^{-1}$.[233] CD32 and CD16, both display an association of $K_a \leq 10^7 M^{-1}$ and are suggested to only interact with multimeric immune complexes.[230]

FcγRs are defined as either activatory or inhibitory receptors depending on their signalling motif. Activatory receptors include CD64, CD16 and CD32a and in turn signal down the immune tyrosine activating motif (ITAM). [229] These receptors do not have an intrinsic tyrosine kinase means for signal transduction, so instead rely on the recruitment

of kinases for downstream propagation. For instance, receptor clustering leads to the activation of Lyn and/or Fyn, members of the Src kinase family.[234] These, in turn, phosphorylate the dual conserved tyrosines within the ITAM motif. Acting as docking sites, the tyrosine kinase, Syk, is recruited and phosphorylated; inducing a series of cellular responses, via interactions with proteins like Vav, PLCγ and PI3K. Vav is responsible for the remodelling of the actin skeleton to permit phagocytosis[235]; PLCγ hydrolyses PtdIns(4,5)P2 into the soluble inositol phosphate, IP3 and DAG initiating calcium mobilisation and PKC activation respectively.[236] PI3K converts PtdIns(4,5)P2 into PtdIns(3,4,5)3.[237] Proteins containing pleckstrin homology domains such as Akt and PLCγ can bind to PtdIns(3,4,5)3, resulting in the promotion of proliferation, cell survival and the retainment of signal through activation and phosphorylation.[238,239]

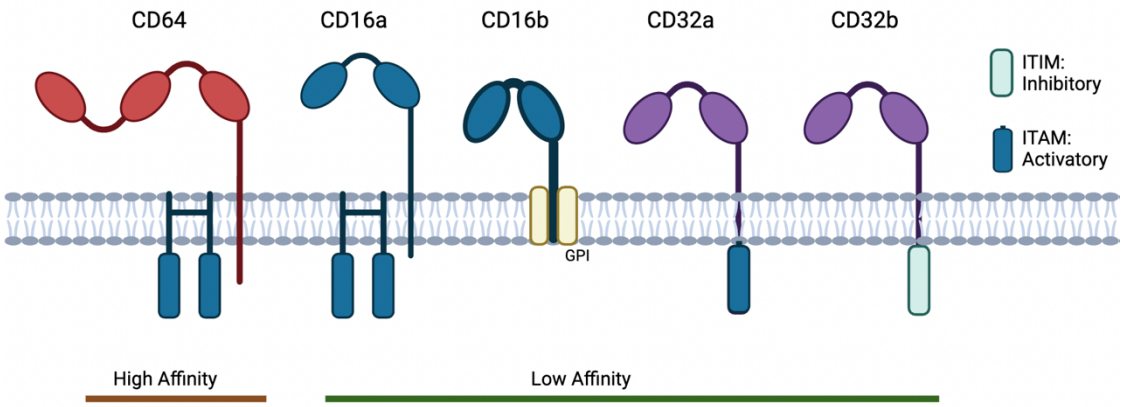


Figure 3.15: Structure of FcγRs. FcγRs are a family of cell surface glycoproteins which recognise the Fc region of IgG. This family comprise of 3 major classes with multiple isoforms (in humans): FcγRI (CD64), FcγRII (CD32a and CD32b) and FcγRIII (CD16a and CD16b). CD64 possesses 3 Ig-like binding domains whereas the rest comprise of only 2. Each receptor is anchored into the membrane via an α-chain, with CD64 and CD16 also associated with a *γ* accessory protein. CD16b is anchored via a glycosylphosphatidylinositol (GPI) anchor. Each receptor is activatory and transduces downstream signalling through immune tyrosine activating motif (ITAM), excluding CD32b which is inhibitory containing the immune tyrosine inhibiting motif (ITIM). The majority of FcγRs are low affinity meaning they only bind to multimeric IgG complexes, however CD64 is high affinity and binds to monomeric IgG. Image made on BioRender.

On the other hand, the singular inhibitory receptor, CD32b, signals via the 13 amino acid sequence, immune tyrosine inhibitory motif (ITIM).[240] Upon coaggregation of CD32a and CD32b receptors with an extracellular ligand, like IgG complexes; the tyrosine in the ITIM motif becomes phosphorylated. This recruits SH2-containing tyrosine phosphatases,

SHP-1 and SHP-2, and the SH2 domain containing inositol phosphatase, SHIP-1.[241] These act to dephosphorylate Syk kinase and converts PtdIns(3,4,5)3 into PtdIns(4,5)P2, inhibiting the downstream activatory cascade of CD32a[242]; meaning prevention of AKT and PLCγ translocation leading to a dampened immune response and reduced phagocytosis.[242] The ITIM motif of CD32b binds more avidly to SHIP-1, however, SHP-1 overexpression in COS-1 (fibroblast like cell) and J774A.1 macrophage cells also exhibited reduced phosphorylation of Syk and reduced efficacy of phagocytosis (reduction of 60%) of IgG complexes.[242-244] Interestingly, it appears SHP-1 attenuates CD32a activatory cascade in the absence of CD32b, meaning inhibition may be independent of the ITIM motif.[242]

In humans, CD32b has been implicated to impair the efficacy of therapeutic antibodies. In mantle cell lymphoma[245], follicular lymphoma[246], diffuse large B cell lymphoma[247,248] and chronic lymphocytic leukaemia[249], high expression of CD32b directly correlates with poor prognosis and reduced response rates to type 1 anti-CD20 (rituximab) treatment.[22,23-27] In comparison to type 2 anti-CD20 therapies, rituximab formed CD20: anti-CD20: CD32b complexes on target B cells leading to faster internalisation and lysosomal degradation.[250] Expanding on this research, with the knowledge of the difference in efficacy between type 1 and type 2 anti-CD20 therapies, Vaughan *et al.,*[251] explored if this interaction had the same impact in other well-known B cell targets. CD19, CD22, CD38 CD40, MHCII, BCR (IgM) mAbs were applied to cell lines and primary chronic lymphocytic leukaemia cells. Despite the majority of mAbs engaging and propagating activation of CD32b to deliver an inhibitory response, this did not affect the rate of internalisation; with the exceptions being CD19 and CD38 antibodies.[251] This suggests that receptor tyrosine phosphorylation may not be the reasoning for the differing internalisation rates.

This theory is supported by Mousavi *et al.,*[252] who found in rats, that CD32b on LSEC was responsible for the receptor-mediated endocytosis of immune complexes independent of ITIM activation. Here, LSEC were treated with an anti-CD32 antibody followed by an

anti-mouse IgG F $(ab')_2$ to promote receptor clustering. Cells were lysed, and CD32b was separated via immunoprecipitation and blotted on SDS-PAGE. In comparison to a control of splenic cells, LSEC observed no bands corresponding to tyrosine phosphorylated CD32b.[252] Instead, this research suggested that CD32b expressed on rat LSEC functioned more as a clathrin-dependent recycling receptor. The role of CD32b was highlighted through inhibition assays. Hence anti-CD16 and anti-rat hyaluronan displayed no reduction in binding of immune complexes to LSEC whereas, an anti-CD32 antibody completely blocked both binding and internalisation. This action was deemed clathrin-dependent as K^+ depletion and hypertonic treatment (known to inhibit the formation of clathrin coated pits[253,254]) led to >72% reduction in uptake of immune complexes and impeded 90% of monomeric IgG internalisation.[252] This pathway will be further explored in Chapter 5. In a pulse-chase study, cells pre-saturated with immune complexes displayed 17% of total unoccupied receptor returned to the cell surface, alternatively cells not pre-incubated with immune complexes saw 35% of receptors recycled to the surface.[252] Compiling this study alongside those mentioned in the introductory chapter and the extent at which LSEC express this receptor, this suggests CD32b is a receptor worthy of note. With this, we looked to see how protein and mRNA expression and biodistribution differed between our healthy and cirrhotic cohort of liver tissue.

3.5.1 CD32b protein expression but not mRNA expression is reduced in cirrhosis

To explore the distribution of CD32b within liver tissue, immunohistochemistry was performed. The top panel of Figure 3.16 is a representative image of healthy liver tissue stained for CD32b (brown). Staining is continuous along the sinusoid, and is in abundance in the pericentral areas, with little staining seen in the periportal end. This is evidenced further in the inner box located in the top right of the image. Here, the portal vein (PV) and central vein (CV) are labelled with the staining localised within zones 2 and 3 of the tissue. The next panel shows ARLD tissue, here staining is much less abundant and mostly confined within the nodules. There is some staining present within the fibrotic scaring. The zoomed in image located in the black box shows CD32b to be

expressed along the sinusoids indicated by the blue arrows. The final image is of MASLD tissue. Higher expression of CD32b is seen here in comparison to ARLD tissue, however, to a lesser extent than healthy tissue. Less staining is also present in the scar and more located within the tissue itself.

After identifying the difference in receptor distribution, we then looked at the difference in expression of mRNA and protein. No sizeable difference was seen in mRNA expression (Figure 3.17A), with MASLD on average expressing more *FCGR2B* than the other two tissue types. Protein expression, however, was considerably different (Figure 3.17C). Healthy liver lysates had considerably more CD32b protein expression identified via band volume with western blot than both MASLD (P=0.0359) and ARLD (P=0.0034). Quantification of % coverage of tissue was performed on FFPE stained tissue, no significant difference was found but on average healthy tissue showed more coverage than the other two (Figure 3.17B). Figure 3.17 D and E are examples of CD32b expression determined using immunofluorescent staining. D shows green CD32b staining around a central vein, and the vast network of sinusoids radiating from this structure in healthy liver. E shows the loss in staining extent and intensity in ARLD in comparison to D.

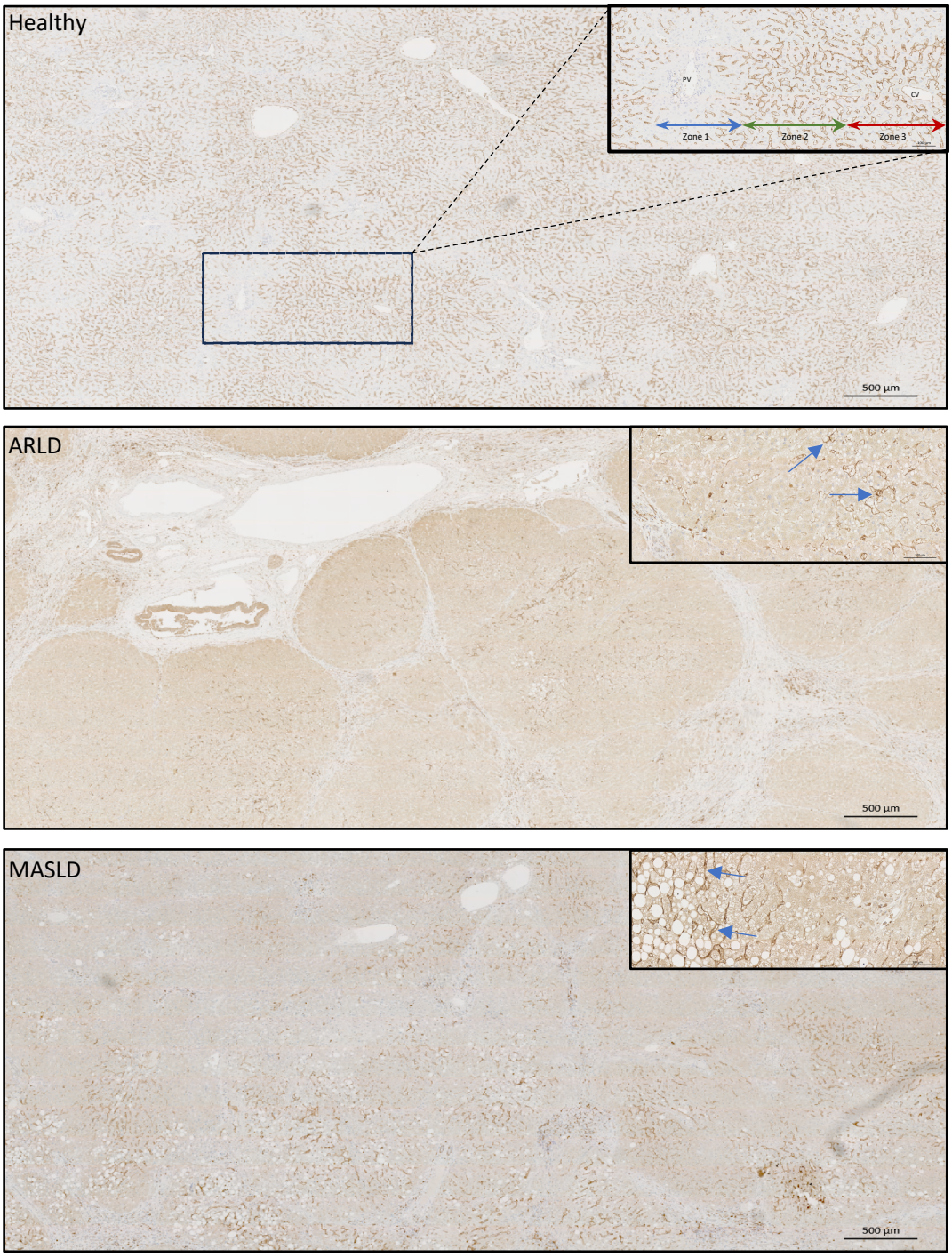


Figure 3.16: IHC staining of CD32b within human liver. Representative images showing formalin fixed paraffin embedded human liver tissue from healthy, ARLD and MASLD donors. Sections were stained for CD32b (brown) using a rabbit polyclonal IgG following citrate-based antigen retrieval. Non-specific staining was blocked using peroxidase blocker, 10% goat serum and 1x casein. Staining was identified used ImmPress anti-rabbit HRP secondary kit and DAB. Nuclei was counterstained using Mayers hematoxylin. Following alcohol and xylene exchanges slides were mounted using DPX. Images were taken on the Zeiss AxioScan Z.1 at a magnification of 20x. Blue arrows indicate CD32b expression on LSEC. PV= portal vein, CV= central vein. Scales bars are 500µm with 100µm on the interior boxes.

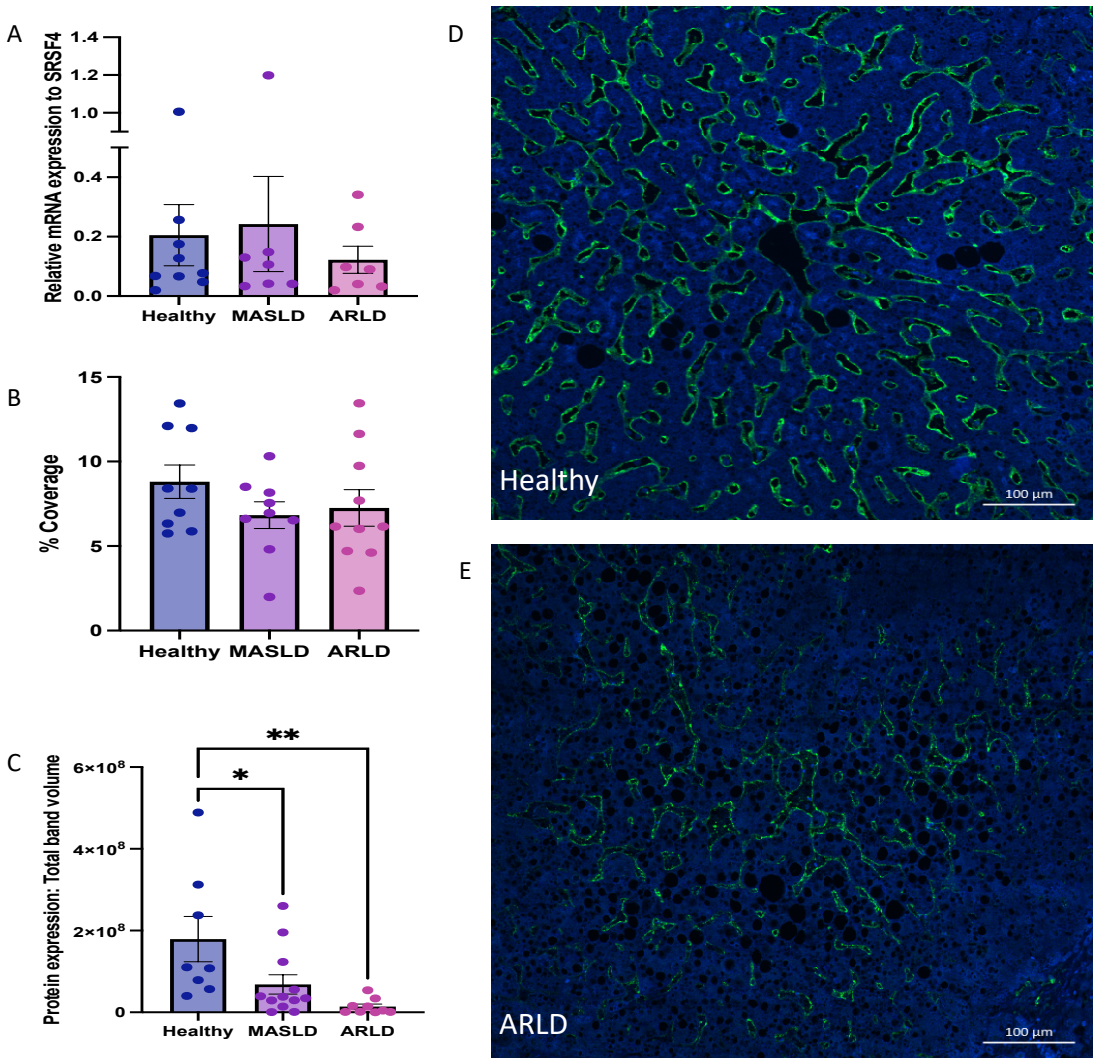


Figure 3.17: CD32b expression pattern within human liver. Whole liver tissue was used to extract RNA and protein. A) mRNA expression of *FCGR2B (*gene for CD32b) between the different tissue types (Healthy n=9; MASLD n=7; ARLD=7), expression is relative to the housekeeping gene *SRSF4* B) Quantification of % coverage of CD32b on FFPE tissue. Healthy n=9; MASLD n=9, ARLD n=10. Analysis performed in ImageJ. C) Densitometry of total protein band volume ascertained via western blot (healthy n=8; MASLD=12 and ARLD n=9). Significance was calculated using one-way ANOVA (P=0.0359) and (P=0.0034) respectively. Error bars indicate ±SEM. D and E both show immunofluorescent images of CD32b (green) in liver tissue. Staining was performed on FFPE sections which went through citrate antigen retrieval and was blocked in 30 minutes at room temperature in 0.1% BSA and PBST. Primary antibody (rabbit polyclonal anti-CD32b) was incubated at 2µg/mL overnight at 4 degrees. The following day, slides were washed and incubated with secondary goat anti-rabbit IgG Alexa fluor 488 for 1 hour at room temperature. Nuclei were counterstained with DAPI. Sections were mounted with fluoro-mount and imaged on the AxioScan Z.1 at 20x.

3.5.2 CD32b mRNA expression on LSEC is significantly lost in cirrhosis

After assessing the difference in expression of CD32b in liver tissue, we wanted to assess expression in isolated LSEC. We were also interested to see how much CD32b differed from CD32a expression. Western blots were performed to quantify CD32b protein expression in LSEC lysates, however no bands were visible using over 20 liver tissue lysates, both diseased and healthy, that were screened (not shown). More success was seen with qPCR. mRNA expression of CD32a was found to be low in healthy cells, and slightly upregulated on diseased cells (Figure 3.18A). CD32b (Figure 3.18B) in contrast exhibited a considerable difference between healthy LSEC and both MASLD ($p=0.0013$) and ARLD ($p=0.0012$). CD32b expression was significantly downregulated in ARLD, with very little expression seen in MASLD. To contextualise the distribution of CD32b within LSEC, immunofluorescent staining was performed on healthy LSEC fixed with 4% PFA. As CD32b has both an intracellular and extracellular domain and can internalise we wanted to see if permeabilising the cells changed the distribution of the fluorescent signal. Panel C is an example of healthy LSEC permeabilised using 0.1% Triton x100 for 5 minutes. Here CD32b (red) was observed intracellularly and presented as diffuse punctate staining throughout the cytoplasm. When cells weren't permeabilised as seen with panel D (CD32b pseudo coloured green), staining was still diffuse however, appeared as a fibrous network throughout the cells. Each cell in the field of view displayed an intense section of staining adjacent to the nucleus (white arrow). This is somewhat observed in permeabilized cells (Panel C) but not to the same extent. Cells were stained and imaged at the same time points with all settings on the confocal remaining the same.

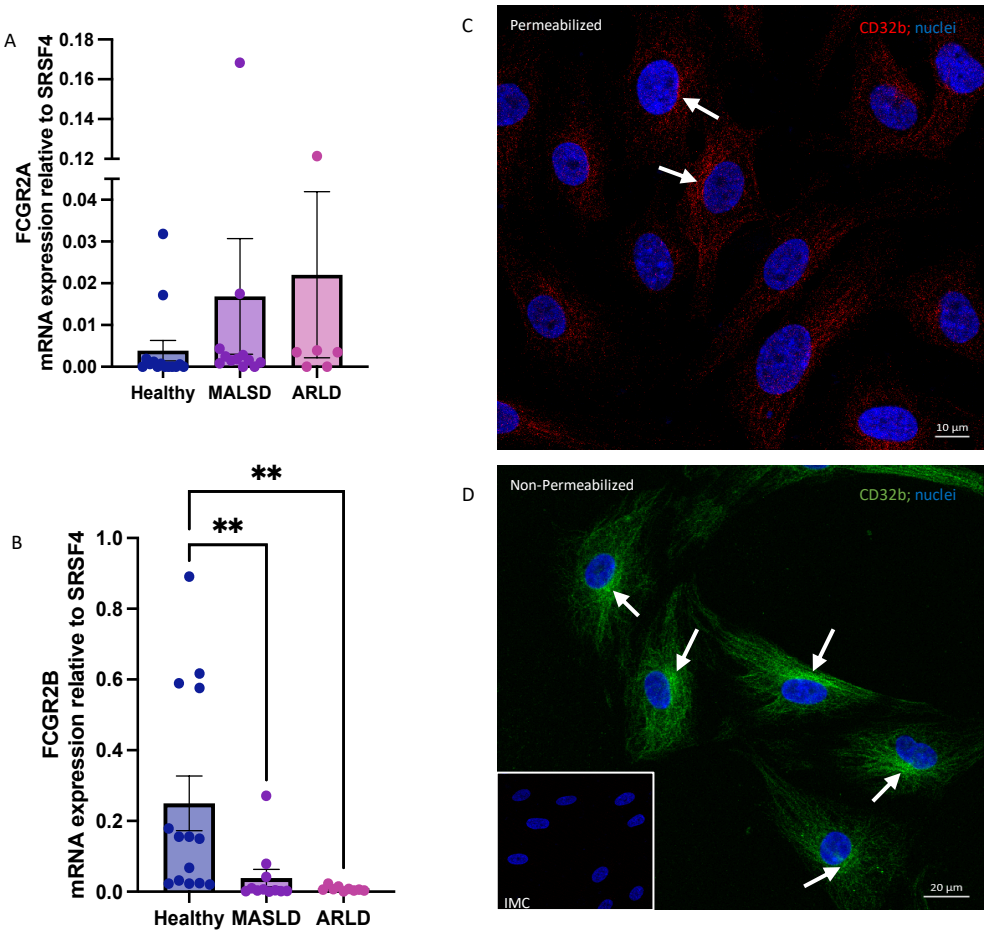


Figure 3.18 CD32b expression in LSEC. LSEC were isolated from healthy and diseased liver (MASLD and ARLD). From cell lysates, RNA was extracted and ran through qPCR. A) shows the mRNA expression of CD32a in relation to the housekeeping gene *SRSF4*. Healthy n=14, MASLD n=12, ARLD=6. B) shows the mRNA expression of CD32b in relation to the housekeeping gene *SRSF4*. Healthy n=14, MASLD n=11, ARLD=9. Significance was calculated through Prism software using Kruskal-Wallis where P=0.0013 and P=0.0012 respectively. Error bars indicate ±SEM. C) shows immunofluorescent staining of CD32b on healthy LSEC. LSEC were seeded at 70,000 per well in ibidi VI ibitreat chambers and cultured overnight. Following fixation with 4% paraformaldehyde for 10minutes at 37 degrees, cells were washed with PBS and then permeabilised using 0.1% triton X-100 in PBS for 5 minutes at room temperature. Subsequent washing steps are then performed with 0.1% PBS-Tween to ensure cells are still permeabilised. Non-specific staining was blocked using 0.1% BSA diluted in PBST (0.1%) for 30minutes. Primary anti-CD32b receptor (host rabbit) was dilute in blocking buffer at 1ug/mL and incubated for 1 hour. Following wash steps, the secondary goat anti-rabbit IgG Alexa fluor 647 (1µg/mL) was incubated for 1 hr at room temperature. Nuclei were counterstained with DAPI for 5 minutes. Cells were left in PBS at 4 degrees until imaged. Images were taken using the LSM780 confocal at 40x water immersion. Scale bar here is 10µm. D) is a repeat of the protocol for C however cells were not treated with Triton or washed in PBST, therefore remained non-permeabilised. Scale bar here is 20µm. White arrows point to concentrated points of the staining.

3.6 Expression of receptors through isolation and passaging of LSEC

Long term culturing and serial passaging of cells is known to affect expression levels of various receptors[362] and to impact morphology.[363] As shall be discussed in section 3.7, there was some examples throughout this chapter where expression of receptors in LSEC were considerably higher than that seen in whole liver. As part of this thesis, we wanted to attempt to elucidate if the off-target internalisation within the liver was receptor mediated and if so by which receptor. Therefore, we needed to ensure that expression within cultured cells used for functional experiments was within an acceptable range to that seen within the liver. Therefore, to do this we took isolated LSEC straight from liver tissue and compared this to LSEC that had been cultured and passaged over time. We also tracked the expression of mRNA for each receptor from fresh up to passage 3 (P3) for a single liver so we could see in real time the difference over each passage. As cells needed to be transported between Birmingham and our industry collaborators to do some functional experiments we also wanted to see if the freeze/thaw process would influence receptor expression.

3.6.1 Expression of receptors through isolation and passaging

To compare fresh vs passaged cells, following immediate isolation, RNA was taken from LSEC and stored. This was then compared to the mRNA expression of LSEC that had undergone passaging and culture. Referring to Figure 3.19, we did note significant changes in expression of CD32a and CD31. CD31 (*PECAM1*) is a classical endothelial marker and is the basis in which we isolate our cells from liver digests. In this case CD31 is well documented to show altered expression (increase) through culture. Starting with FcRn, healthy LSEC saw a steep drop in average mRNA expression through passaging in comparison to diseased cells. This may also be true for MASLD, although we only had an n=1 at the initial timepoint so it's difficult to truly comment. Regarding B2M, on average very little expression appeared to be lost in passaging. On the other hand, CD206 (*MRC1*) presented the opposite of the previous two proteins. Here, expression increased with passage for all three tissue types; with MASLD LSEC showing a considerable upregulation in comparison. Results were mixed with LSIGN, with variability between tissue types but

in general no significant impact of passage. As mentioned, CD32a saw an extensive loss in abundance with passage, particularly in healthy and MASLD isolated cells. There was also a stark difference in expression observed within the 'fresh' group with healthy showing a significantly increased expression compared to both diseased cells. CD32b presented similarly to that seen in Figure 3.18, whereby healthy LSEC saw higher expression comparatively to its disease counterparts. In this case, almost complete ablation of CD32b expression was observed in passaged MASLD and ARLD cells, with expression on healthy LSEC seemingly unaffected by passage.

As it appeared that receptor expression on the diseased cell cohort was the most impacted by the act of culturing, we then wanted to see to what extent this was. Here we took both ARLD and MASLD tissue and isolated LSEC. At the point of seeding, half the cells were taken straight for RNA isolation whilst the remaining went into culture. Following this at each passage point up until P3, some cells were taken for RNA extraction. We also wanted to investigate the effects of the freeze/thaw process on expression. For this, with the MASLD group at P2, a subset of cells was taken and frozen down with 10% DMSO in FBS and stored in liquid nitrogen. At a later date, cells were thawed and cultured. At P3, all cells were taken for RNA extraction. No P1 data is available for the MASLD group as at the time there wasn't sufficient quantity to passage and take for RNA, so data is missing.

Figure 3.20 showcases the tracking of mRNA expression of receptors throughout passaging and the freeze/thaw process. The left-hand side shows the progressive culture of MASLD LSEC. A general observation can be made that over passaging a loss of most receptors is experienced excluding that of *MRC1* (CD206) and FcRn which both show an increase at P2, followed by steep fall to P3. The most exaggerated decrease in expression seen was in CD32b, where expression values went from fresh at 3.18 to 0.00156 by P3 and no expression registered for P3 thawed cells. Comparing P3 fresh vs P3 thawed LSEC (cells that underwent the freeze/thraw process at P2), overall expression was downregulated. In the case of LSIGN, CD32b and CD32a expression was or very close to

0. Again, CD206 was the anomaly displaying an increase in expression during this process.

Moving to the right-hand side of the figure, here ARLD LSEC were tracked from freshly isolated through to P3. Like MASLD, 4 out of 6 receptors showed a loss of expression over passage. This time, FcRn was present in this group and B2M saw an increase in P1. This was then opposed in P2 and returned by P3. CD206 once again was upregulated through passaging, and this steadied out through P1 to P2. CD32b saw a much less drastic decline in expression in ARLD LSEC in comparison, however started out with far less expression in the initially fresh isolated LSEC. For MASLD, CD32a saw the biggest loss in expression by flat lining at P2.

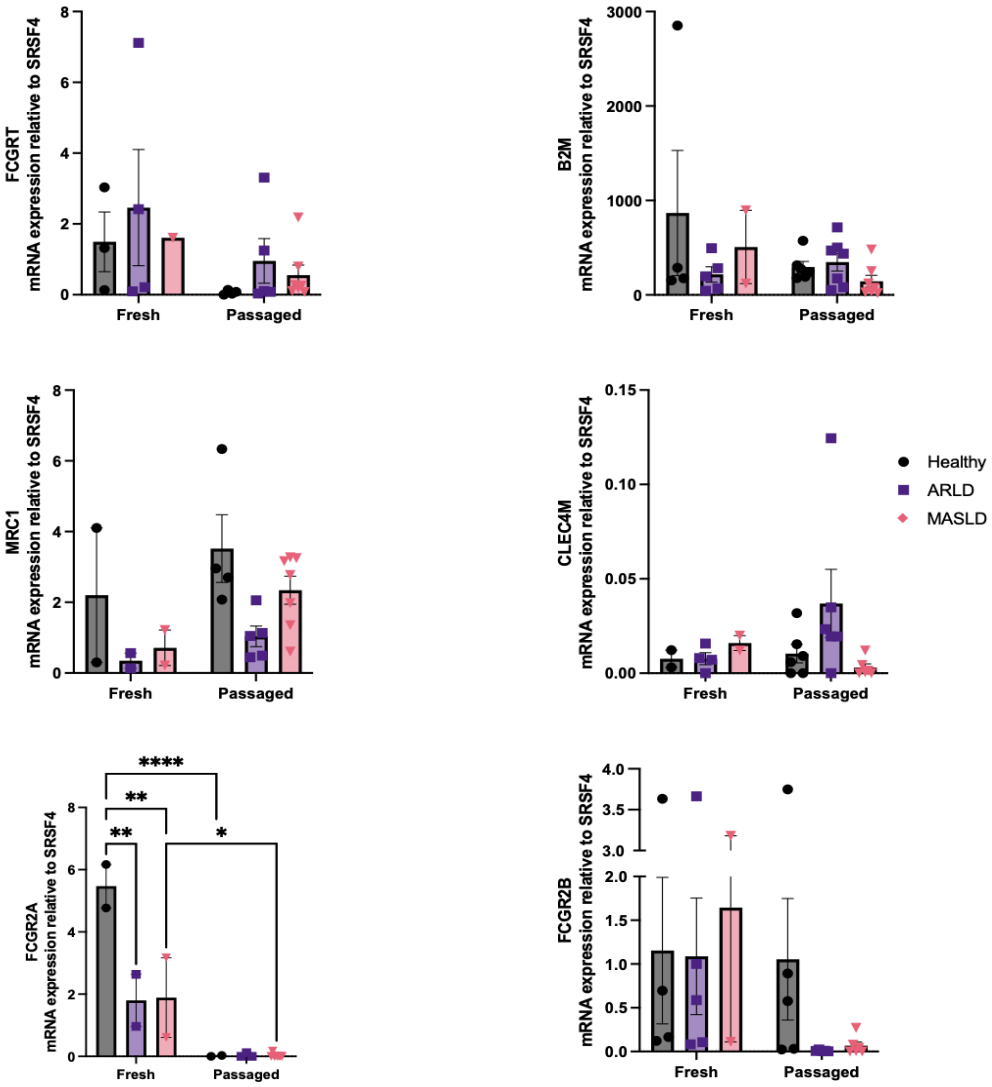


Figure 3.19: Changes in gene expression through isolation. LSEC were isolated from healthy and diseased liver (MASLD and ARLD). Following the isolation process some cells were separated off to be cultured and others had RNA extracted immediately. mRNA expression obtained via qPCR was compared. As shown by key, circles= healthy LSEC, squares= ARLD and inverted triangles= MASLD. N varies for each receptor. Each point represents an individual liver. Significance was calculated using 2-way ANOVA with *= <0.05, **=<0.01 and ***=<0.001.

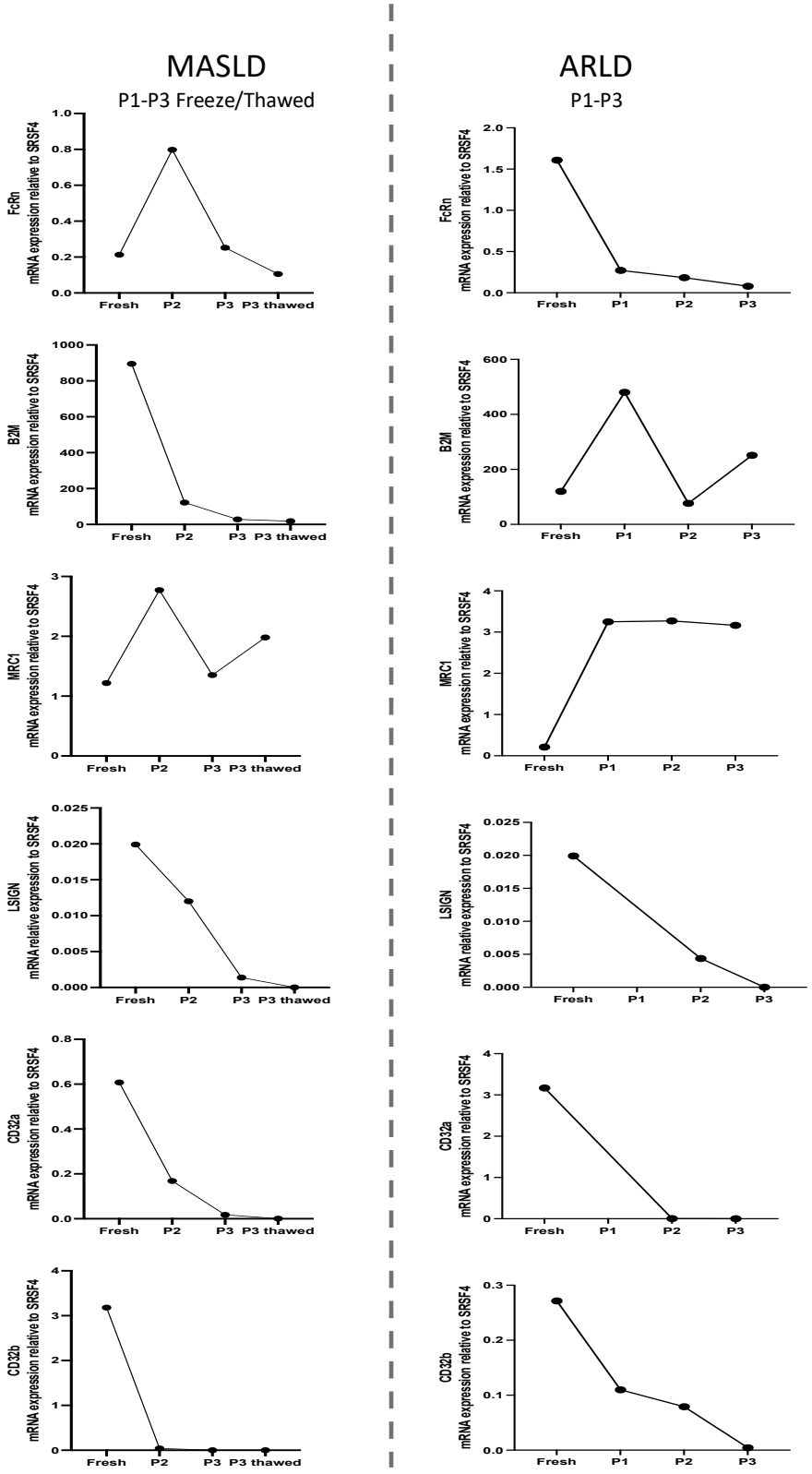


Figure 3.20: Tracking of mRNA receptor expression through passaging. LSEC were isolated from MASLD (n=1) and ARLD (n=1) tissue. Following the isolation process some cells were separated off to be cultured and others had RNA extracted immediately. mRNA expression obtained via qPCR was compared over passaging. P3 thawed cells refers to cells that were frozen and stored in liquid nitrogen before being thawed and cultured.

3.6.2 IOX2 can restore expression of CD32b.

As seen with our IHC of CD32b, this protein is expressed predominantly in the oxygen depleted zones of 2 and 3 within the liver. We also saw throughout section 3.6.1, that this receptor was lost through passaging and culture particularly in ARLD and MASLD cells. This was supported by our inability to visualise protein bands via western blots on over 20 lysates from cultured LSEC. Therefore, we wanted to explore if culturing these cells in an oxygen depleted environment would upregulate or maintain CD32b expression. At this point a hypoxic chamber was not available therefore we turned to on-market inhibitors. IOX2 is a potent inhibitor of the enzyme prolyl hydroxlases-2 that regulates the abundance of hypoxia inducible factor (HIF)[364]; this means it can pseudo induce artificial hypoxic responses with cells. We tried incubating LSEC with varying concentrations of IOX2 for 48 hours and assessed expression of CD32b. ARLD (n=2) isolated cells at P3 were used in this experiment as they showed the largest CD32b expression loss at both mRNA and protein level. Referring to the top panel of Figure 3.21, on average all cells treated with IOX2 exhibited an increase in mRNA expression of CD32b. This was not observed at 600nM IOX which proved to be cytotoxic to the cells. A significant difference was found with 48-hour treatment with 100nM of IOX2 (P=0.0250). Due to the homology between CD32b and CD32a, we wanted to see if this inhibition also influenced CD32a. Here, 600nM exhibited cytotoxicity on the cells as seen before. However no other change of note was detected with expression remaining similar to untreated cells across the dose range. For future functional experiments (see Section 5.2.3), this inhibitor was used at 100nM per this data set.

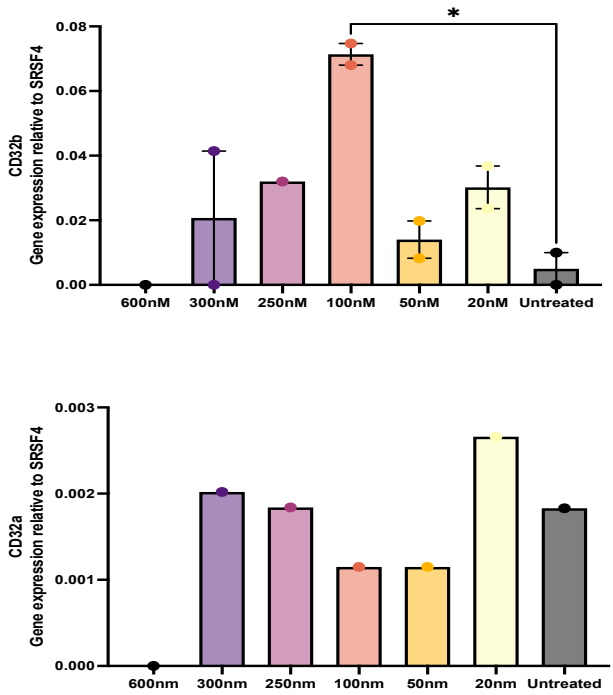


Figure 3.21: Effect of incubation of LSEC with the hypoxia-mimic IOX2 for 48 hours on gene expression of CD32a and CD32b. LSEC were isolated from ARLD tissue. Here cells were treated with IOX2 for 48-hours at varying concentrations to compare to untreated cells. Top panel shows the expression of CD32b mRNA relative to the housekeeping gene *SRSF4* (n=2). Bottom panel shows similar data for CD32a (n=1). Significance was calculated through one way ANOVA (P=0.0250)

3.7 Discussion

The aim of this chapter was to investigate the impact of liver disease on LSEC expression profiles of selected receptors thought to play a role in the removal of antibody within the body. To do this we first investigated the histological changes and clinical parameters seen within our cohort of liver tissue. Both our diseased and healthy donors were of similar age, 55 and 53 respectively. This is important as any significant difference observed in either receptor expression or antibody internalisation later can be appointed to the differences in liver injury in opposed to age associated functional changes. For instance, it is well document that LSEC undergo pseudo-capillarisation with age, observed in human, rat and baboon models.[385-367] With these changes, aged LSEC were found to have a 60-80% reduction in porosity[365], and the liver as a whole exhibited impaired drug metabolism which was found accountable to age-related decrease in both

blood flow and liver mass.[368,369] We also suspect that the change in expression observed through culturing is equivalent to pseudo-capillarisation seen in aging.

We also observed significant increases in liver function enzymes in the cirrhotic cohort. These enzymes such as AST and ALT are released when the integrity of hepatocytes and other cells are lost. This loss in structural integrity is also evidenced throughout the H&E images presented in Section 3.1. Comparing histology between healthy tissue (Figure 3.1) and ARLD (Figure 3.2), ARLD was characterised by the scar deposition within the Space of Disse, formation of regenerative nodules that lack a central vein encircled by fibrotic septa connecting the portal tracts. This clear disruption of vasculature is absent in healthy tissue, where the vast network of sinusoids can be seen running towards the central veins. To note cirrhotic tissue in this thesis is from explanted livers, the progression of said tissue has reached a state of end-stage liver disease. Although not fully replicating the entire spectrum of disease progression, this tissue is still important in demonstrating how the impact of liver disease may affect antibody pharmacokinetics.

With the blood shunting caused by bridging fibrosis, increases in ECM and infiltration of non-resident immune cells, changes within the sinusoidal microenvironment influence the phenotype of LSEC. Thus, we next established the expression levels of key receptors in both whole liver tissue and isolated LSEC from healthy, ARLD and MASLD donors. It was particularly important to look into diseased liver as this relates to the likely demographic of patients in trials (i.e. who may have underlying liver disease when treated for another condition or may be using biologics to manage their own liver injury). We chose the two most common forms of liver disease MASLD and ARLD which are often a result of poor lifestyle factors.

Hepatic expression of FcRn

FcRn is described as the saviour of IgG from catabolism within the body. It was important to establish the expression levels of this receptor as this impacts the pharmacokinetics and clearance of antibody. Our data showed no significant difference in mRNA and

protein expression in both whole liver tissue and LSEC in healthy and disease. Similar was also observed for B2M, the light chain to the functional FcRn complex. This data corresponds with scRNA-seq data obtained from Ramachandran *et al.,* in their published online liver atlas[114], where comparisons between cirrhotic and healthy LSEC saw no discrete differences. This data also showed LSEC to be the highest normalised expressor of *FCGRT* in all the endothelia present within the liver, reinforcing the importance of these cells over macrophages in IgG recycling. To note, this study contained an n=3 cirrhotic livers not distinguished by disease type. Therefore, it is hard to make assumptions about differences between ARLD and MASLD for example.

B2M as expected was expressed to a greater extent in both liver and LSEC than FcRn. This supports its role as the light chain for MHC class I molecules, meaning it is expressed constitutively across any cell that functions to antigen present. In a quantification proteomic study via UPLC-MRM, it was found on average FcRn concentration was 147pmol/g of liver tissue whilst B2M was equal to 1248pmol/g of tissue (i.e. nearly 10x more abundant).[370] This matches the distinctive difference in mRNA expression seen in Figure 3.6 and 3.7.

As mentioned, protein expression for FcRn was significantly different between ARLD and MASLD in whole tissue. LSEC almost achieved significance in this regard, showing the difference in expression between the two diseases may be due to the LSEC. It however is also likely due to the extent of the immune infiltrate seen in ARLD in comparison to MASLD, meaning there are more immune cells present that express FcRn. MASLD is also characterised by the dilution of Kupffer cells for infiltrating monocytes. According to the Human Protein Atlas[359], Kupffer cells are the highest expressors of FcRn within the liver. So, this loss maybe why there is a lower expression between the two aetiologies. Worthy of note and discussed in more depth in the next chapter, the extent of FcRn expression in Kupffer cells in comparison to LSEC may be why some believe it is the LSEC that clear/remove therapeutic antibodies, as Kupffer cells have more FcRn to recycle them back into the circulation.

Immunohistochemistry was an effective way to visualise the distribution of FcRn throughout tissue. Using this we could also gain a quantitative value for the % of this distribution throughout. Although no statistically significant difference was calculated, on average healthy tissue had the highest expression distribution. This was evidenced with the accompanying staining in Figure 3.5. Here, staining was present within and surrounding the sinusoid. The staining inside the sinusoid can most likely be attributed to KCs, however as no co-localisation staining was performed so it can't be stated definitively. The staining observed here, was like that presented in another publication where the researchers wanted to assess FcRn distribution across species and tissues. The authors found strong staining in the Kupffer cells, with mild staining detected in the on the sinusoids.[320] While absent in our healthy tissue, they also found some FcRn expressed on the membrane of the hepatocytes.[320] This was not the case for both MASLD and healthy tissue in our hands but was observed in ARLD samples where vesicular staining was present on the membrane. The presence of FcRn on the hepatocytes in ARLD may explain it having the highest protein expression out of the three aetiologies considered. MASLD matched the expression distribution to healthy but at a lower abundance.

No substantial difference was seen in FcRn through passaging although, overall expression was reduced, particularly evident in the healthy cells. As there was only an n=1 for MASLD in freshly isolated cells it is difficult to say how this is affected in passage. However, as seen in Figure 3.20, P2 saw a raise in expression in comparison to fresh for this tissue type. This returned to equal levels as the freshly isolated cells by P3. Again, this was only determined for one liver sample so is not representative.

As expected with human tissue, the inter-variability is very high thus the data spread for a lot of our cohorts was also vast. Our sample size is reasonably small, but this has also been reported in two other studies within the liver.[370,371] One of these sought to find the cause, so they investigated how age, race and gender affected this varying expression. They found, no significance and thus suggested another factor may be the cause.[370]

Looking through the literature, genomics may provide the answer. Genetic polymorphism within the VNTR located in the promoter of the *FCGRT* gene was correlated to the variable expression of FcRn.[372] In monocytes, it was found VNTR3 was found to increase expression of FcRn in comparison to VNTR2. Therefore, monocytes expressing homozygous VNTR3/VNTR3 presented increased avidity to IVIg.[372] In another study, patients with common variable immunodeficiency who were heterozygous, VNTR2/VNTR3, displayed lower efficacy in IgG replacement than their homozygous counterparts.[373] Another study sought to investigate how this polymorphism affected the pharmacokinetics of the chimeric therapeutic antibody, cetuximab.[374] Patients who expressed VNTR3/VNTR3 saw an overall reduction in clearance and maintained a higher concentration in the peripheral tissues. This was thought to be the result of having higher FcRn expression.[374] In hindsight this would have been an interesting aspect to explore, however was not in the scope of this research at the time. To summarise, FcRn plays a very important role in the pharmacokinetics of therapeutic antibodies. The fact we see no substantial difference in FcRn expression at both mRNA and protein levels between healthy and diseased liver tissue and LSEC suggest that any discrepancies we see in the following chapters is not the cause of one aetiology possessing more receptor for recycling.

Expression of CD206 by LSEC

CD206 was chosen as a potential candidate for off target IgG clearance by LSEC for three reasons. One being it possesses the C-type lectin ecto-domain whose ligands include mannose, L-fucose and N-acetylglucosamine. IgG1 antibodies contain one N-linked glycan at Asn297 on both heavy chains of the Fc region.[71] This is the site for glycosylation; here sugars such as mannose are bound. The role of CD206 in the internalisation of antibodies is still debated, however due to the high expression of LSEC makes this a potential receptor for this function. Additionally, the internalisation of CD206 is known to be clathrin-dependent, a well-established mechanism whereby internalised cargo is delivered from clathrin-coated pits through to early then late endosomes prior to

lysosomal degradation.[376] It has already been established that mannosylated antibodies are more likely to go down the degradation pathway in CD206^{+}-CHO cells.[328] This is on the account that the C-type lectin domain needs calcium to bind. In acidified endosomes, calcium can no longer bind meaning the mannosylated antibody is released from CD206.[329] From here is localises with the lysosome whilst CD206 recycles back to the cell surface membrane.[328] The third and final reason is less regarding CD206 involvement in the internalisation process but more so in the degradation of therapeutic antibodies. In CD206$^{-/-}$ mice, CD206 on LSEC was found to be solely responsible for the uptake of lysosomal enzymes.[313] In these mice models, LSEC were able to internalise albumin, but had a reduction of 50% in ability to catabolise these proteins.[313] This infers CD206 is responsible for obtaining the lysosomal enzymes needed for LSEC to perform degradation within its lysosomes. Therefore, I wanted to investigate as to whether LSEC with *MRC1* knocked down were able to lyse antibody or not. This is discussed in Chapter 5.

Regarding the expression and distribution of CD206, IHC was once again utilised. There were stark differences observed here across tissue type, with healthy livers showing a continuous expression of CD206 uniformly along the LSEC. This has also been corroborated in other labs.[342,379,380] On the other hand, ARLD tissue had much more sporadic staining, with some centralised within the nodules and majority present within the scar. This is reflected in the significance seen in the % coverage quantification in Figure 3.9C between healthy and ARLD tissue. In some regards, this was not what I initially expected, with the evidence that pro-inflammatory cytokines, which would be in abundance in chronic liver injury, upregulated CD206.[344-345] So I suspect the loss in expression along the sinusoids is part due to the capillarisation and change in phenotype LSEC undergo in liver injury and/or due to the cleavage of this receptor from the cell surface by MMP. MMP concentrations are increased with liver disease[382], with examples of MMP-9 being positively associated with the raise in ALT and bilirubin[382] as seen in our cohort. Well documented is the increase of soluble mannose in liver disease, this must come from somewhere and with LSEC being one of the biggest expressors this may well

be the source. Enzymatic cleavage would not translate to any reduction in protein or mRNA expression in LSEC as this is happening after transcription and translation and the proteolytic enzymes may not be present in LSEC monocultures. To assess this, biopsies from very early onset of liver disease, possible multi-cultures like spheroids or early timepoint in rodent models would need to be examined. In ARLD tissue, the majority of the CD206 expression was seen concentrated within the scar, I believe this is due to either the abundance of infiltrating immune cells at the site of injury or sCD206. The antibody used in this staining protocol was polyclonal so could therefore bind to many epitopes along the receptor. Mentioned previously, CD206 is cut off at the very base with its ecto-domains still intact[349], so is still accessible to bind. Therefore, if sCD206 was concentrated in the scar our primary antibody would pick this up.

Immunofluorescence was performed on fixed LSEC (Figure 3.11C) to identify subcellular distribution of CD206. Here we observed punctate staining suggesting the receptor was intercellular within endosomes. Similar staining has been observed in other studies reporting considerable co-localisation with EEA-1, an early endosomal marker.[381] The cells used in this study were a macrophage-like hybridoma cell line so not fully comparable to LSEC. Nevertheless, this does confirm presence of CD206 in endosomes. Since the LSEC I used for immunofluorescence were isolated from diseased tissue; the mainly intracellular staining present may be a result of cleavage from the cell membrane by MMP.

No difference was observed between healthy and diseased LSEC regarding protein and mRNA expression. Again, the Ramachandran *et al*., liver atlas[114] also confirms this, with very little difference between injured and healthy LSEC. What was quite unexpected was the extent of expression (i.e., RNA copy number) seen within LSEC in comparison to whole liver tissue. As multiple cell types are present in the whole tissue, it would be expected overall to have a higher expression. This was not the case however and is what led us to investigate the difference between freshly isolated and passaged cells. CD206 was upregulated as cells were passaged in culture. Potential reasons for this could be

due to the upregulation of this receptor with stress through the act of trypsin or mechano-response from the plastic .

The fact the distribution of CD206 along the sinusoid is so continuous places this as a potential candidate for the off-target clearance of therapeutic antibodies within the liver. This may occur in both health and disease given the lack of change in mRNA or protein expression in cirrhosis. Due to its binding capacity, lysosomal enzyme capture and its distribution, this receptor would have sufficient access to circulating antibodies as they progress through the liver's vasculature.

Expression of LSIGN in the liver

LSIGN was considered due to its high expression on the LSEC and 34% homology with ASGPR.[352] ASGPR is associated with hepatic removal of antibodies that are glycosylated with either terminal galactose or N-acetylglucosamine.[39,75] LSIGN has been implicated in the binding and subsequent catabolism of glycoproteins containing mannose.[354,355] Internalisation of bound antibody is calcium dependent, however I was unable to find in the literature if this is associated with clathrin-coated pits. DC-SIGN however, which shares 77% homology with LSIGN, has been found to internalise HIV virions via clathrin-coated pits.[383] Therefore, this could possibly be a mechanism in which this receptor delivers antibodies to the lysosomes. Although there was a significant reduction in LSIGN protein expression between healthy and ARLD tissue, no difference was noted in mRNA expression. Our staining suggested a reduction in intensity and extent of staining in cirrhosis. This is in agreement with a review paper suggested LSIGN to be downregulated in cirrhosis in humans.[384] Regarding distribution, healthy tissue presented a uniform LSIGN expression surrounding the sinusoid, however less intense than that seen in CD206 or CD32b. ARLD displayed significantly less staining as evidenced with the % coverage quantification. Here, staining was on both the sinusoids (sporadic staining) and on the cells within. A potential explanation for both the presence of LSIGN within the sinusoids and higher protein expression in cirrhotic cells, may be that,

according to the MacParland *et al.,* scRNA-seq data[153], fibroblasts are the biggest expressors of LSIGN within the liver (refer to Figure 3.14B). With increased tissue turnover and myofibroblasts within injured liver, it is assumed to have an increased quantity of fibroblasts present that contribute to the levels of protein expression seen.

Regarding, expression in isolated LSEC no substantial difference was observed in mRNA between healthy and diseased LSEC. On average MASLD saw the lowest expression with ARLD and healthy being similar values. This is support by Ramachandran *et al.,* sc-RNA seq data.[114] MASLD exhibited the lowest expression of LSIGN, and this may be due to its downregulation in passaging. This aetiology was the only one to be reduced in passaging and culture, with both healthy and ARLD increased in mRNA expression.

Expression of CD32b by the liver

CD32b is the most extensively researched receptors with a role in the internalisation and catabolism of immune complexes. It has been known to impair antibody therapy[245-250] and is often used for the selection of LSEC from liver digests.[385] This is a low affinity receptor therefore is known to bind only to multimeric complexes. However, although we cannot say with absolute certainty, we assumed no complex formation or aggregation formed with our antibodies in functional assays which are presented later. CD32b, or FcγR in general, have be found to cluster and induce signalling with other receptors. For instance, macrophage-inducible C-type lectin (Mincle) is concomitant with inflammatory disease like hepatitis and obesity. Upon ligation of this lectin, induction of a signal cascade through both Mincle and FcγRs ITAM, causes NF-kB activation in macrophages.[386] Mincle is encoded by *CLEC4E*, however using a basic local alignment search tool (BLAST), no homology was found between CLEC4M encoding LSIGN and this gene (data not shown). Nor was it found to be expressed in LSEC on the Liver Atlas.[114] A common feature of CD32b, CD206 and Mincle is these receptors all rely on the association of co-receptors to transduce a signal cascade.[333,334] Interestingly in 1995, it was suggested CD206 was involved in the activation of FcγR-mediated phagocytosis of

IgG opsonised sheep red blood cells.[387] With inhibition of CD206, leading to a reduction of catabolism of these red blood cells.[387] 15 years later, it was found that CD206$^{-/-}$ macrophages, despite having equal numbers of FcγR receptors as WT macrophages, had reduced function of FcγR. Both Fc-mediated phagocytosis and oxygen burst was significantly abridged in comparison to WT.[388] Co-localisation was also found between CD206, CD32b and opsonised IgG sheep red blood cells.[388] Just as complexes of anti-CD20-CD20-CD32b that lead to rapid internalisation and lysosomal degradation[250], maybe clustering of CD206, CD32b and antibody may have the same response.

Distribution of CD32b within healthy tissue was similar to LSIGN and CD206, in that it was uniformly expressed throughout the sinusoids. However, an absence of staining was observed in zone 1. This is in alignment with other publications whereby CD32b is noted to prefer oxygen deficient regions.[142,153,154] Tissue from MASLD and ARLD cases showed a drastic reduction in CD32b staining. No difference was observed in mRNA, however protein expression was significantly reduced in MASLD and ARLD. Here, the preferential expression of CD32b was detected in zone 3; this area sees the start and most extensive damage in many liver diseases. Scarring, infiltrate and steatosis in zone 3 is often associated with the early progression of fibrosis to cirrhosis[257,389], this leads to the loss of structure integrity and often AST is highly concentrated here.[257] With ARLD being characterised by its extensive scarring, this may be the reason for reduced CD32b expression.

The homology between CD32a and CD32b has found to be significant, and often commercial antibodies are unable to distinguish the two receptors. We wanted to see the difference in gene expression in LSEC, to ensure the results we were seeing were due to CD32b and not CD32a. Very little CD32a was expressed in LSEC, and minimal differences were observed between each aetiology. CD32b on the other had showed a significant difference between healthy and diseased liver, similar to that seen in whole liver lysates. Alongside the reasons stated previously, the lack of protein expression in CD32b in cirrhotic LSEC may be due to the loss seen through passage and culturing.

To attempt to recapitulate the expression pattern seen within the freshly isolated diseased cells we looked to investigate how oxygen depletion regulated expression of CD32b. To achieve this, IOX2 a potent inhibitor of the enzyme prolyl hydroxlases-2 that regulates the abundance of hypoxia inducible factor (HIF)[364,376], was used. This elicits an artificial hypoxic environment that induces transcription of genes involved in glycolysis and angiogenesis.[364] Here we found IOX2 at 100nM treatment for 48-hours induced CD32b, but not CD32a expression compared to the non-treated equivalent. A similar effect has been seen in the literature with both LSEC under hypoxia and with IOX2 treatment, both upregulating CD32 alongside LYVE1 and CD31.[376] These will therefore be useful in subsequent chapters to explore how the increased expression of CD32b alters antibody internalisation.

Finally, immunofluorescence was performed on healthy isolated LSEC to contextualise the localisation within the cells. Here we either permeabilised the cells or not before staining for CD32b. This was so we could understand the trafficking of this receptors. Both showed extensive diffuse staining throughout the cytoplasm. This appeared somewhat fibrous in non-permeabilised cells. On the other hand, when permeabilised the extent of staining was similar but appeared more as puncta. This could possibly be in alignment with vesicles as CD32b is able to recycle back to the cell surface. Internalisation, like CD206 and LSIGN, is clathrin and calcium dependent.[377] Calcium is depleted in cirrhosis[378], which may affect their ability to transduce signal upon ligation.

CD32b saw a considerable loss in cirrhotic cells at an mRNA level, this along with the surmountable evidence that this receptor clears immune complexes places it as a prime receptor of interest. With the loss in disease, any difference seen in therapeutic uptake may be due to the loss of expression of this receptor.

3.8 Summary

The aim of this chapter was to justify the interest in the chosen receptors alongside exploring how their expression differs in health and disease. For ease this has been summarised into Table 3.2. We also explored how passaging and culture can affect these receptors. To try and recapitulate the regular phenotype within each aetiology, emphasis was made on using the cells at as low a passage as possible. However, this was not always possible. Nevertheless, the data confirms that LSEC in tissue express an extensive portfolio of scavenger type receptors which have the potential to bind and internalize therapeutic antibody. The expression of some of these changes significantly in disease. Isolated LSEC recapitulate many of the features of cells in tissue and we shall use these to explore receptor function further in subsequent chapters.

Table 3. 2: Summary of chapter 3 results

Receptor	Protein (comparable to Healthy)		mRNA (comparable to Healthy)		Passaging		
	Whole Liver	LSEC	Whole Liver	LSEC	Healthy	ARLD	MASLD
FcRn	+/-	+/-	+/-	+/-	-	+	-
CD206	+/-	+	+/-	+/-	+	+	+
LSIGN	++	N/A	+	+/-	+	+	-
CD32b	---	N/A	+/-	---	+/-	-	-
CD32a	N/A	N/A	N/A	+	-	-	-
B2M	+/-	+/-	+/-	+/-	-	+	-

This shows a summary of the trends seen throughout Chapter 3. +/-=no difference, +=positive increase (not significant), ++= significantly increased, -=reduced on trend (not significant) ---=significantly decreased, N/A=data not available.

Chapter Four: The binding and processing of therapeutic antibody

Now we have established the differences in receptor expression between cirrhotic and healthy liver, the next step is to ascertain if there is any difference in the binding, internalisation, and processing of therapeutic antibodies in diseased vs healthy individuals. One novel aspect of this thesis is the fact very little has been explored in terms of understanding the role of human LSEC in the pharmacokinetics of these antibodies. Studies have been done in mice, rats and cynomolgus monkeys where antibody localisation on the lining of sinusoids has been observed[104,160,162] but no one yet has considered human LSEC alone. Therefore, the first sections of this chapter are going to interrogate LSECs ability to interact and internalise antibodies, and the latter half will focus on the end fate of these mAbs/bsAbs.

To begin this chapter, we need to introduce the mAbs and bsAbs that will be utilised throughout the rest of this thesis. Table 4.1 shows a summary of each antibody used alongside what they target, format, clearance rate, pI and % hydrophobicity. These commercially relevant antibodies were provided by our collaborator GSK, and thus all antibodies have been anonymised. Clearance rates, net charge, and pI (fab region) were obtained via GSK or through literature.[390] % hydrophobicity was attained through running the antibodies sequences through Prot pi.[391] % hydrophobicity describes what proportion of total amino acid composition is classed as hydrophobic according to this software. Anti-CD20 and Anti-CD20 LAGA are the same antibody, however, the latter's Fc has been disabled via assumed mutations of L235A and G237A.[70] This will also be compared with **antibody C**, as this is a humanised mAb targeting the same CD20 antigen. This will allow for useful comparisons since 3 antibodies all target the same epitope but differ slightly in either Fc region or variable region allowing use to determine the scope of how one factor effects non-specific (off-target i.e. engages with a receptor not targeted for) clearance. Of note, the anti-CD20 was often used in my preliminary

experiments before using the therapeutic antibodies (A-I sourced from GSK) due to the limited amount available of these mAbs/bsAbs.

Table 4. 1: Therapeutic antibody characteristics.

Origin	Name	Isotype	Target	Clearance mL/day/Kg	Net charge	pI (overall)	pI (Fab region)	Hydrophobicity (%)
Tester Abs Believed to be chimeric	Anti-CD20*	IgG1	CD20	2.96	-	8.56	7.76	42.29
	Anti-CD20 LAGA*	IgG1	CD20	-	-	-	-	-
Chimeric	Antibody A	IgG1	Phosphatidyl-serine	31.22	5.4	8.22	6.80	38.23
Humanised	Antibody B	IgG1k	SLAMF7	5.95	5.2	8.22	6.71	43.37
	Antibody C *	IgG1	CD20	0.85	9.2	8.70	6.95	43.72
	Antibody D	IgG1	IL-4	7.08	5.2	8.24	-	-
Human	Antibody E	IgG1 kappa	CCL2	12.82	3.3	7.91	-	42.98
	Antibody F	IgG1	IGF-1R	12.59	11.4	8.92	7.14	40.70
	Antibody G	IgG1 kappa	CD38	1.60	-	7.01	6.90	4.21
Bispecific	Antibody H	IgG + dAb	IL-5/IL-13 (dAb)	159.30	-	-	-	-
	Antibody I	IgG + dAb	IL-4/IL-13 (dAb)	6.72	3.4	7.91		-

This table defines the mAbs and bispecific antibodies used throughout this thesis. Therapeutic antibodies have been anonymised, but targets and clearance data have been provided. pI of the overall antibody at a *p*H of 7 was obtained through Prot pi alongside the % hydrophobicity. pI of the Fab region was provided by GSK. % hydrophobicity related to what proportion of the total amino acid composition is classed as hydrophobic. * Identifies the 3 antibodies all targeted at the same epitope. – means data was unable to be obtained.

4.1 The trials and tribulations of the HERA assay

The human endothelial recycling assay (HERA) was first described by Grevys and colleagues.[50,455] This cellular assay was suggested as a screening tool to assess the extent of FcRn-dependent rescue of therapeutic IgG from degradation within cells. Here they

used a modified cell line, HMEC1 that stably expressed B2M and the full-length heavy chain of FcRn. They reported a >100-fold increase in expression of FcRn in comparison to parental cells.[50] Next IgG antibodies were incubated with confluent cells for 4-hours before media was removed, and cells were lysed and marked as the 'uptake' group. In parallel wells, following incubation with antibody, fresh media was added, and a further 4-hour incubation took place. From here the authors lysed the cells and took the media. The cell lysate at this 8-hour time-point was referred to as 'residual amount' and the IgG concentration within the media connoted 'recycled.' Each sample was analysed via ELISA. Thus, the authors could quantify how much antibody internalised at the 4-hour mark, how much antibody was recycled back into the media at the subsequent 4-hour mark and how much was left in the cell. Any concentration left unaccounted for was considered degraded by the cell.[50]

We attempted to adapt this assay to reflect more of a physiological setting and therefore exchanged the genetically modified HMEC1 cells for primary isolated LSEC. A schematic of the adapted protocol is shown in Figure 2.3. Cells were serum starved for 1-hour and washed profusely prior to starting this assay due to the abundance of IgG within human serum in the media. We initially incubated the cells with ligand in prewarmed HBSS adjusted to the *p*H of 7.4 to ensure this recapitulated the environment at the surface of the cell. Adaptations were made to this, including incubating at *p*H 6.0 to favour FcRn recycling, however none of the data presented here is with that condition. Anti-CD20 antibody was chosen to optimise this assay as it was the most abundant antibody available.

4.1.1 An ELISA approach to quantifying the HERA assay

Initial interrogation of HERA assay samples was performed using a Human IgG ELISA. As anti-CD20 was of an IgG1 isotype this allowed for quantitative detection and measurement of IgG within the cell lysates and media. Figure 4.1 shows a pie chart representing the % distribution of anti-CD20 (applied at 500ng/mL) in a typical assay

with healthy and cirrhotic LSEC. 'Recovered' refers to the amount of anti-CD20 not taken up by LSEC, equivalent to what remained in the media at the 4-hour point. 'Recycled' shows how much antibody was recycled into the media at the second (8-hour) time point and 'lysate' refers to how much antibody was left in the cell at the close of experiment (Supplementary Figure S.2 shows examples of the raw date acquired). Healthy LSEC, on the left, exhibited a more efficient internalisation process, leaving less anti-CD20 in the media at 4-hours (blue segment) in comparison to that of cirrhotic LSEC (right side). It also showed a higher distribution of antibody recycled back into the fresh media by the 8th hour. Cirrhotic cells appeared to accumulate the antibody within for a longer period evidenced by its larger lysate segment.

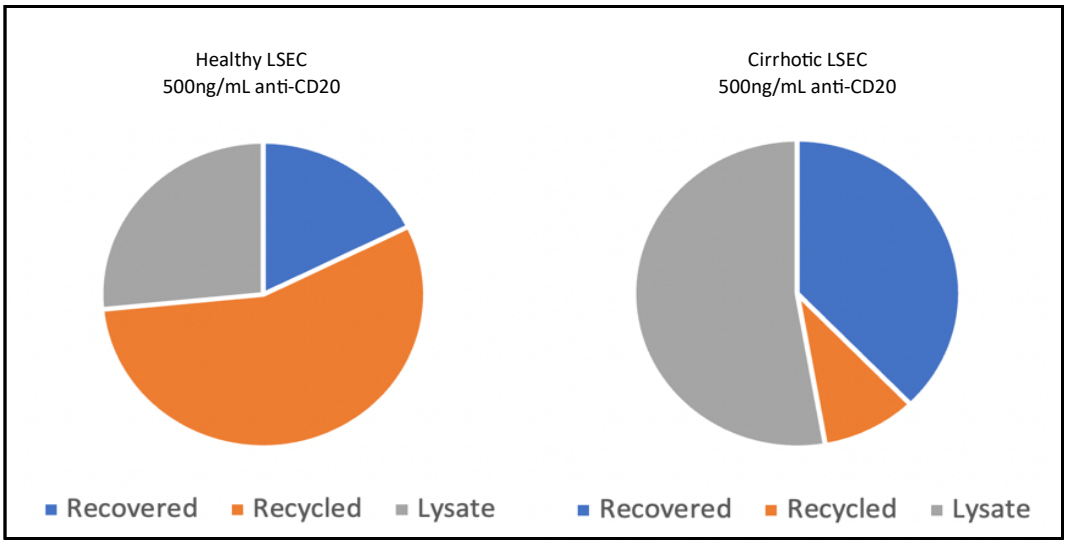


Figure 4. 1: HERA assay determined by a human IgG ELISA. These pie charts present the distribution of anti-CD20 quantified at each time point of the HERA assay. 500ng/mL of anti-CD20 in pre-warmed HBSS (*p*H 7.4) were incubated on either healthy (left) or cirrhotic (right) LSEC for 4 hours before the media was removed to assess the amount of antibody not taken up by the cell (recovered). Next cells were washed before fresh media was added and further incubated for 4 hours. At this time point media was again taken to quantify the amount of antibody recycled out of the cell and cells were lysed using RIPA buffer to ascertain how much anti-CD20 antibody remained within the cells. This data represents averages of triplicate wells of 1 liver each.

Repeating this experiment several times we noticed even after background subtraction the samples that were taken from cells incubated with no anti-CD20 treatment (negative controls) gave quite a substantial absorbance reading. We sought to fix this through using a more specific ELISA and a longer serum starve step (2-hours). The ELISA next utilised was a rituximab ELISA rather than standard IgG in an effort to reduce background, and representative results are shown in Figure 4.2.

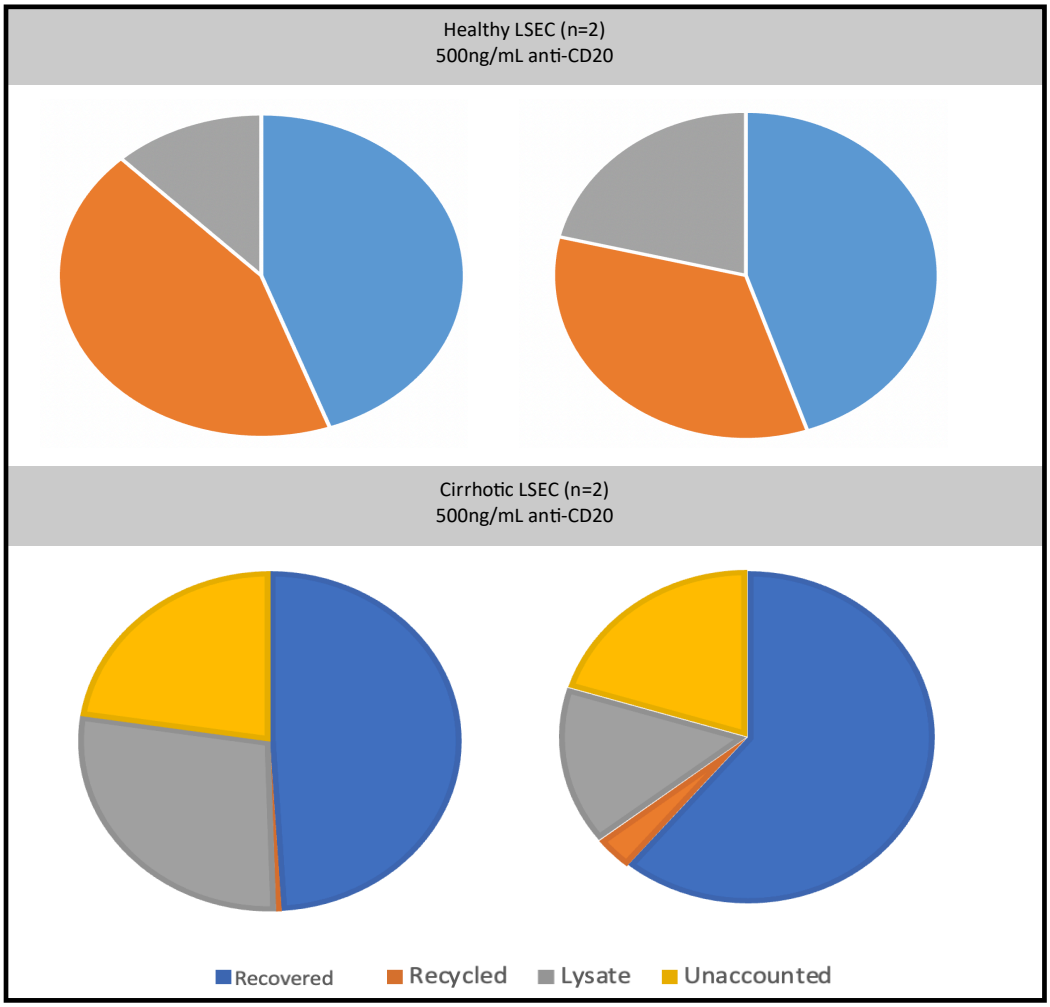


Figure 4. 2: HERA assay determined by Rituximab ELISA. Here are representative pie charts of the distribution of anti-CD20 quantified from the HERA assay, using a rituximab ELISA. 500ng/mL of anti-CD20 in pre-warmed HBSS (*p*H 7.4) were incubated on either healthy (top n=2 livers from averages of triplicate wells each) or cirrhotic (bottom, n=2 livers from averages of triplicate wells each) LSEC for 4 hours before the media was removed to assess the amount of antibody not taken up by the cell (recovered). Next cells were washed before fresh media was added and further incubated for 4 hours. At this time point media was again taken to quantify the amount of antibody recycled out of the cell and cells were lysed using RIPA buffer to ascertain how much anti-CD20 remained within the cells. For the cirrhotic samples the sum of the recovered recycled and lysate was less than was originally added (500 ng/mL) therefore the remaining quantity was reported as unaccounted for (yellow slice).

Focusing on the healthy LSEC first, a greater proportion of anti-CD20 was reported in the recovered segment compared to that observed for the IgG ELISA (Fig 4.1). However, an extensive amount of recycling was present in both. The smallest segment for Rituximab ELISA was what remained within the cell at the 8-hour time point. For cirrhotic LSEC, like the previous ELISA, these cells had a reduced ability to internalise anti-CD20 evidenced by the large blue 'recovered' proportion. Very little recycling was reported this time and again a large amount was concentrated in the cell lysates at the 8-hour point. In contrast to previous data however, cirrhotic cells yielded an unaccounted-for concentration of anti-CD20, meaning the sum of all segments did not equate to the initial concentration added. Therefore, the difference was marked as unaccounted; this made up a considerable proportion within cirrhotic LSEC. This assay also exhibited high background signal from the negative control, similar to that obtained with the total IgG ELISA, therefore we decided to use another approach to quantify our outcome (MSD).

4.1.2 A Meso-Scale Discovery (MSD) approach to quantifying the HERA assay

To overcome the issue with the negative control, we turned to a more sensitive approach to ascertain if this could discriminate between our samples. MSD uses electrochemiluminescence for detection as opposed to ELISA's colorimetric reaction; increasing sensitivity and dynamic range.[393] Unfortunately, the standards barely registered using this approach meaning a standard curve could not be made for concentration determination. However, Figure 4.3 shows the raw data plotted as a pie chart for cirrhotic cells. The data for healthy cells could not be plotted as nothing registered for the outputs on the 8-hour time point. In contrast to that seen in the ELISAs, the amount recovered was minimal from the media collected from cirrhotic cells at 4-hours (Figure 4.3). Recycled anti-CD20 made up a large proportion of the antibody detected and together with that accumulated within the cells (lysate segment) accounted for >95% of the total signal.

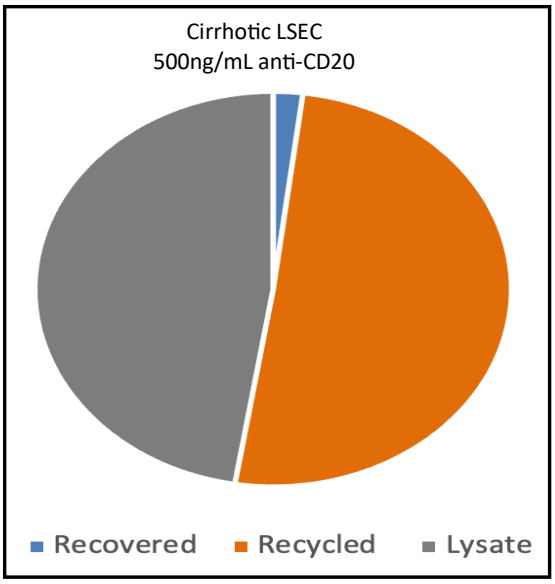


Figure 4. 3: MSD determination of HERA assay. Here is a representative pie chart of the distribution of anti-CD20 quantified from the HERA assay, using Meso-Scale discovery. 500ng/mL of anti-CD20 in pre-warmed HBSS (*p*H 7.4) were incubated on cirrhotic LSEC for 4 hours before the media was removed to assess the amount of antibody not taken up by the cell (recovered). Next cells were washed before fresh media was added and further incubated for 4 hours. At this time point media was again taken to quantify the amount of antibody recycled out of the cell and cells were lysed using MSD lysis buffer to ascertain how much anti-CD20 remained within the cells. N=1 Liver gained from triplicate wells averaged.

4.1.3 Interpretation of the HERA findings

Despite months of optimisation, we were unable to achieve satisfactory results. Either the negative control read too high, or the combined concentration returned was higher than the original amount added. We started with the IgG ELISA and although not presented, a range of concentrations were examined (both high and lower than 500ng/mL) and all within range of the ELISAs detection limits. Although we saw a dose response (i.e. 500ng/mL read higher than 50ng/mL), often the combined analysis did not work out. This ELISA was designed for the use with serum, plasma, and cell supernatants. but not validated for the measure of IgG in cell lysates. This may explain the problem except that the readings from our supernatants were also askew. Next, we reasoned that the IgG ELISA was not specific enough so moved to a Rituximab ELISA. The anti-CD20 used was supplied by GSK as a 'Rituximab-type' molecule (i.e. not definitively rituximab). However, this ELISA was well cited in publications, and reported to detect anti-CD20 mAbs, Ocrelizumab and Rituximab, in breast milk.[393] Therefore we reasoned this would

be acceptable for our needs. Again, this ELISA was only optimised for serum, plasma, and cell supernatants. The outputs here showed a similar trend to that seen in the previous ELISA with an increased amount still left in the media of cirrhotic samples following the initial 4-hour incubation, suggesting cirrhotic LSEC had a reduced capacity to internalise antibody. They also displayed an inability to 'process' the antibody post internalisation with accumulation within the cell. Healthy cells however, showed a higher capacity to recycle antibody back into the media, evidenced by the much larger proportion of anti-CD20 found in the media post 8-hours. This may suggest that despite there being no difference in FcRn expression between healthy and cirrhotic LSEC (Figure 3.7), the function of FcRn may be dampened in liver injury. Alternatively, the delivery via either pinocytosis or another receptor into the internalised space may be altered in cirrhosis. We have discussed in Chapter 3, research showing mannosylated glycoproteins bound to CD206 were fated to undergo degradation in comparison to sulphated proteins.[328] In cirrhosis, fibrosis and MASLD it has been noted that there is an increase in protein glycosylation.[394-396] Reported increases in glycosyltransferases[394], fucosylation and bisecting GlcNAc are present in liver injury.[397] Antibodies produced in CHO cells are susceptible to modifications depending on the additives in the media.[398] For example, addition of dexamethasone leads to the increase in sialyation and galactose and uridine presence increase galactosylation.[398] With antibodies so susceptible to post-translational modification, maybe the supernants of cirrhotic LSEC modify these antibodies leading to a reduction in recycling.

Next, we moved to an assay with reported higher sensitivity, therefore chose meso-scale discovery. Once again, the same issues prevailed. For each method used, the blank from the standards gave the expected low readings, however the negative control (cells with no treatment) still gave high positive concentrations. Subtraction of this from other data points as an extra form of background subtraction was not an option as it would often lead to negative concentrations in samples. Increased washing steps and serum starvation had no effect. Media with no human serum and the *p*H adjusted HBSS gave readings similar to the blank, so these weren't responsible for the discrepancies seen.

Evidently this was a result of the cells being present in the wells, but whether the increased background was elicited through secretions due to a stress response to serum starvation is unknown. What was determined however, was this assay was not translational for use with primary LSEC. Although a general trend was observed in both ELISAs, MSD showed completely opposite results in cirrhotic cells. Therefore, we chose not to consider data from this method. One possible confounder is that the anti-CD20 antibodies supplied from GSK were stated to be fully human in origin. Upon investigation and testing with different secondaries however, we found this antibody to only be detected via dot blot with an anti-mouse secondary and not an anti-human secondary. We are unsure why this is the case however it could explain why the human IgG and MSD did not work, although we did see a dose response. This also does not necessarily account for false positives seen in the rituximab-like ELISAs.

4.2 Alternative approach to measuring therapeutic antibody's interaction with LSEC

We needed another approach to assess how LSEC interacted with therapeutic antibodies. The literature suggests flow cytometry is often used as a mode to evaluate mAb binding, uptake, and effector function in cells.[399,400,414] Therefore, we adapted a protocol to suit this output whereby cells were seeded until confluent and then treated with a therapeutic antibody for 4- or 8-hours. Cells were harvested at each time point and binding of antibody was assessed via flow cytometry. While this was useful for establishing the extent of interaction of antibody bound over the time course, this approach did not provide any context on antibody location i.e., on the surface or internalised. Therefore, we also performed immunofluorescence staining and microscopy to establish the location of these antibodies. This began as a fixed and indirect process, however, progressed to live imaging through conjugation of a fluorophore.

4.2.1 Validation of methods.

4.2.1.1 Analysis of anti-CD20 interaction with LSEC via flow cytometry

Anti-CD20 was initially used to validate each methodology. Initial stages of optimisation of flow cytometry were performed on the Cyan ADP cytometer, this was accompanied by analysis on Summit software. At this point only % of fluorescence was reported, this provided an estimate for the % of cells that were positive for antibody binding over 4- and 8-hours. Cells were treated with either 50ng/mL or 500ng/mL of anti-CD20 antibody and comparisons were made between healthy and cirrhotic cells. Figure 4.4 panel A shows the difference at 4 hours. A dose response Figure 4.4 (A and E) was observed in both cirrhotic (n=8) and healthy LSEC (n=9), evidenced by the increased % fluorescence for 500ng/mL in comparison to 50ng/mL. On average a greater % of healthy cells were positive for anti-CD20 than cirrhotic cells. Anti-CD20 0ng/mL was used as a control with all other conditions the same. Here the highest value of 0.33% was considered background staining. Panel B shows LSEC incubated with anti-CD20 antibody for 8-hours. A significant difference can be seen at 500ng/mL between cirrhotic and healthy LSEC. LSEC isolated from healthy donors saw the largest loss in anti-CD20 positive cells between 4 and 8-hours (Figure 4.4 D and F). The loss in cirrhotic cells was not significant. For the 50ng/mL anti-CD20 treatment group, very few cells were positive for anti-CD20, and no loss was observed between 4 and 8-hours (Figure 4.4 C).

We had noted difference in mRNA expression of key receptors of LSEC through culture and passaging (Figure 3.19), so we wanted to see if this impacted ability to interact with anti-CD20. Therefore, we took healthy and cirrhotic cells between passage 1 to 3 (P1-3) and compared to passage 4 and 5 (P4-5). Figure 4.5A, shows the difference in passaging has on the percentage of anti-CD20 positive cells in healthy LSEC. More cells were positive for anti-CD20 on average in healthy LSEC at passage 4-5, but this was not significant. Again, we noted a decrease in positivity between 4- and 8-hours. In contrast there was more interaction with low passage cirrhotic LSEC at both timepoints. Here passaging beyond P3 caused a loss in % positive anti-CD20 cells particularly evident in the 8-hour time point.

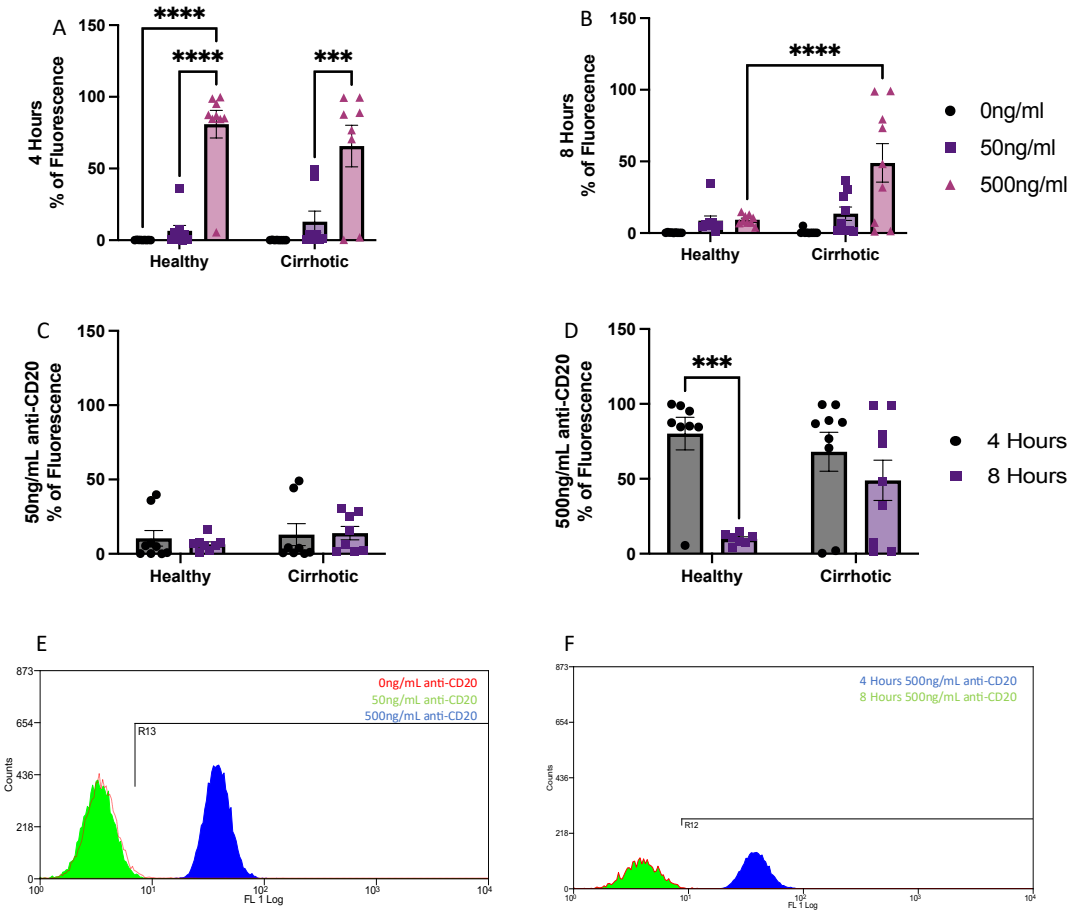


Figure 4. 4: Validation of flow-based method in LSEC with anti-CD20. LSEC were isolated from either healthy (n=9) or cirrhotic (n=8) tissue. Cells were seeded at 50,000/ well in a 24 well plate and left until 80% confluent. Cells were then treated with 50ng/mL or 500ng/mL of anti-CD20 antibody for 4- or 8- hours. Each point represents cells isolated from an individual liver and was pooled from two wells each. Following incubation, cells were washed and dissociated from the wells using TrypLE express. Cells were placed into appropriate FACs tubes and washed 2x with FACs buffer. Following this process every step was done on ice. Cells were fixed using 4% PFA for 20 minutes before being washed. Cells were permeabilised using 0.1% Triton X-100 for 5 minutes before being incubated with anti-mouse IgG1 Alexa fluor 488 for 30 minutes. Cells were washed thrice more before being analysed on the cyan ADP cytometer. Analysis was performed on Summit software and plotted in Prism. A) shows the % of cells positive for Alexafluor 488 symbolising anti-CD20 at the 4-hour time point for healthy and cirrhotic cells. Significance was found in healthy LSEC between the control 0ng/mL and 500ng/mL (p=<0.0001) and 50ng/mL and 500ng/mL (p=<0.0001) and in cirrhotic cells between 50ng/mL and 500ng/mL (p=0.0004). B) shows the similar but at an 8-hour time point. Significance was seen between healthy and cirrhotic LSEC at 500ng/mL treatment concentration (p=<0.0001). C) is extracted from the above panels to show difference in 4- and 8-hours following treatment with 50ng/mL of anti-CD20. D) same as C but regarding 500ng/mL. Significance is seen between healthy LSEC at 4 and 8 hours (p=0.0006). Panels E and F are histograms obtained through summit software to show the difference at 4-hours at each concentration (0ng/mL= red; 50ng/mL= green; 500ng/mL= blue) of anti-CD20 (E) and between 4 (blue) and 8 (green) hours at 500ng/mL treatment of anti-CD20 (F). Significance was calculated using 2-way ANOVA and error bars represent SEM.

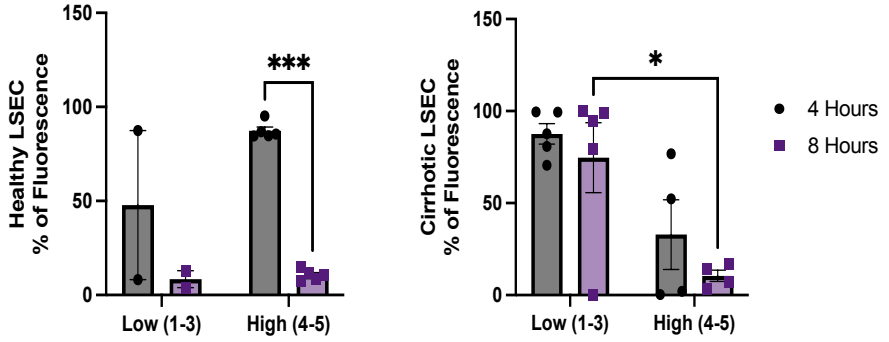


Figure 4. 5 Flow based evaluation of passaging in LSEC ability to bind anti-CD20 antibody. LSEC were isolated from either healthy or cirrhotic tissue. Cells were seeded at 50,000/ well in a 24 well plate and left until 80% confluent. Cells were then treated with 500ng/mL of anti-CD20 antibody for 4- or 8- hours. Each point represents cells isolated from an individual liver and was pooled from two wells each. Following incubation, cells were washed and dissociated from the wells using TrypLE express. Cells were placed into appropriate FACs tubes and washed 2x with FACs buffer. Following this process every step was done on ice. Cells were fixed using 4% PFA for 20 minutes before being washed. Cells were permeabilised using 0.1% triton for 5 minutes before being incubated with anti-mouse IgG1 Alexa fluor 488 for 30 minutes. Cells were washed thrice more before being analysed on the cyan ADP cytometer. Analysis was performed on summit software and plotted in Prism. A) shows the % of cells positive for Alexafluor 488 symbolising anti-CD20 at the 4-hour time point for healthy cells passage between 1 to 3 and 4 to 5. Significance was shown between the 4- and 8-hour time points in high passage cells (p=0.0003). B) shows similar but in cirrhotic cells, significance was noted between the 8-hour time point between low and high passaged cells (p=0.272). Significance was calculated by 2way ANOVA and error bars show SEM.

4.2.1.2 Analysis of anti-CD20 interaction with LSEC via microscopy

Following the flow cytometry, we wanted to see if we could determine where the antibody was localising, either within or on the cell. Therefore, we turned to microscopy and an indirect immunofluorescence approach. Cells were treated with 500ng/mL of anti-CD20 antibody for 4- or 8-hours prior to being fixed with 4% PFA. LSEC were then permeabilised and stained using an anti-mouse IgG secondary Alexa fluor 488. Figure 4.6 shows anti-CD20 was internalised by 2x healthy LSEC. The top two rows present internalisation in the first 4-hours from 2 different donors. Despite both being healthy donors, the staining pattern was completely different. The top row shows fibrous-like staining throughout the cell, whereas the second row shows punctate anti-CD20 staining resembling vesicular staining. Here, anti-CD20 positive structures tend towards a perinuclear pattern, excluding the cluster of cells (white arrow) where the staining is more dispersed.

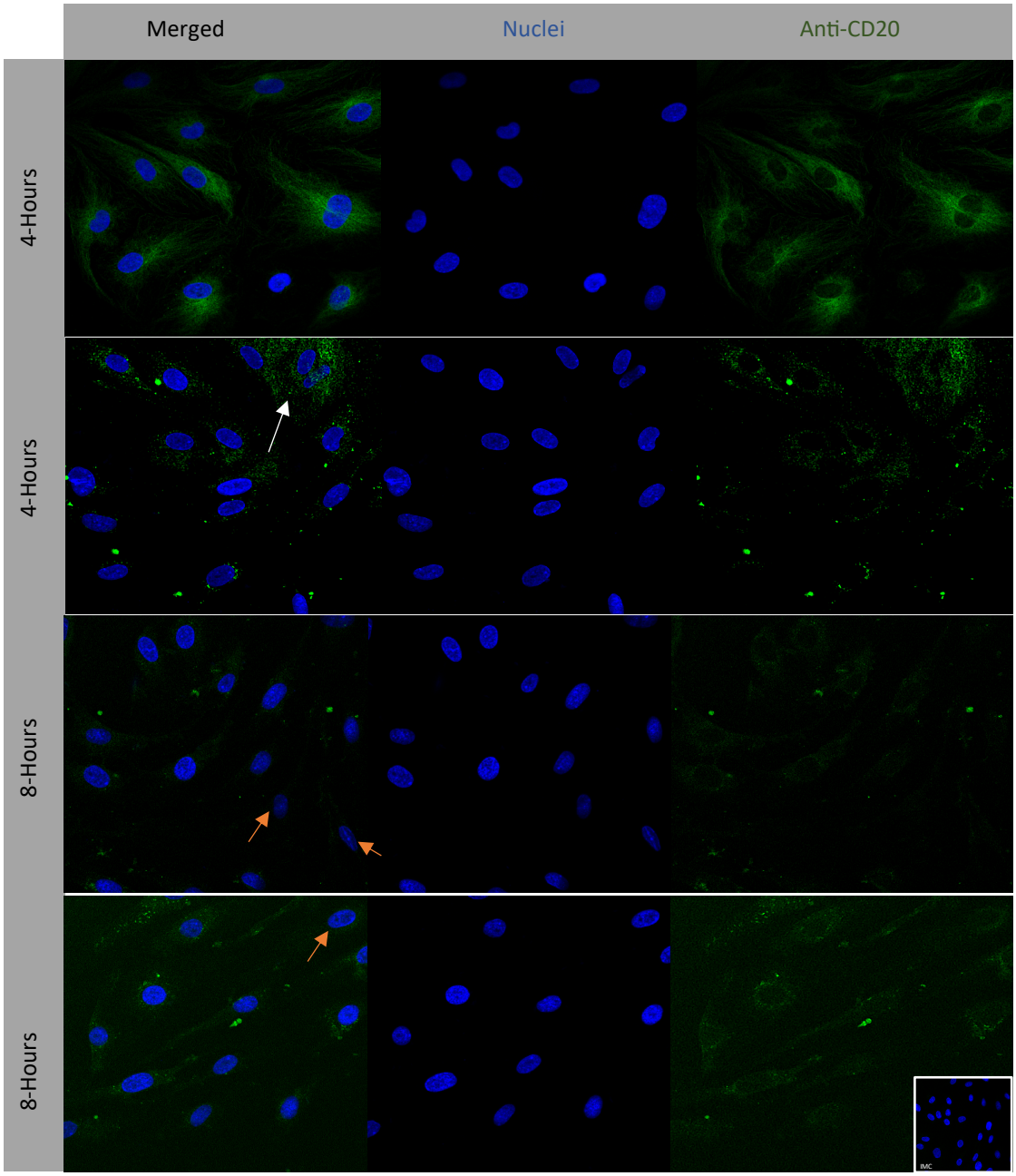


Figure 4. 6: Confocal images of anti-CD20 internalisation into healthy LSEC. LSEC were isolated from 2 healthy donor. Cells were seeded 70,000 per chamber in Ibitreat IBIDI vi chamber slide and grown until confluent. Treatment with anti-CD20 commenced for 4- and 8 hours. At each time point cells were fixed with 4% PFA for 5 minutes at 37 degrees. Following this, cells were permeabilised with 0.1% Triton X-100 for 5 minutes at RT. Incubation with anti-mouse IgG Alexa fluor 488 for 1 hour took place to allow detection of the anti-CD20 (green). Nuclei (blue) was counterstained with DAPI for 5 minutes. Images taken on LSM780 confocal, 40x with water immersion. Top two panels show 4-hours of anti-CD20 incubation. The bottoms two panels show healthy LSEC incubated with anti-CD20 for 8-hours. Bottom right panel contains the IMC. White arrows show a cluster of anti-CD20 positive cells; orange arrows indicate no staining present.

The two bottom rows show healthy cells incubated with anti-CD20 antibody for 8-hours. In comparison to the top two panels (4-hours) and agreement with our other findings, there is a considerable loss in staining at 8-hours. The staining present is vesicular and is

scattered throughout the cell, and not every cell has positive staining in evidence (e.g., negative cell indicated by the orange arrow).

Figure 4.7 shows representative images of both ARLD and MASLD cirrhotic cells after anti-CD20 treatment at 4- and 8-hours. The top two rows show ARLD LSEC stained with anti-CD20 (green) with very few cells positive for anti-CD20. Like donor cells, this staining was vesicular and mostly centred around the nucleus. The 8-hour ARLD panel shows per cell an equal intensity of staining, however more cells have internalised anti-CD20 over time. The following two panels are representative examples of MASLD isolated LSEC incubated with anti-CD20. The 4-hour time point shows anti-CD20 has internalised into very few cells in comparison to healthy cells. One cell though in particular, indicated by the blue arrow, exhibited extensive staining throughout the cytoplasm. All staining present is vesicular. At the 8-hour time point MASLD cells show a loss of internalised anti-CD20 evidenced by the reduction of green punctate staining in the bottom row.

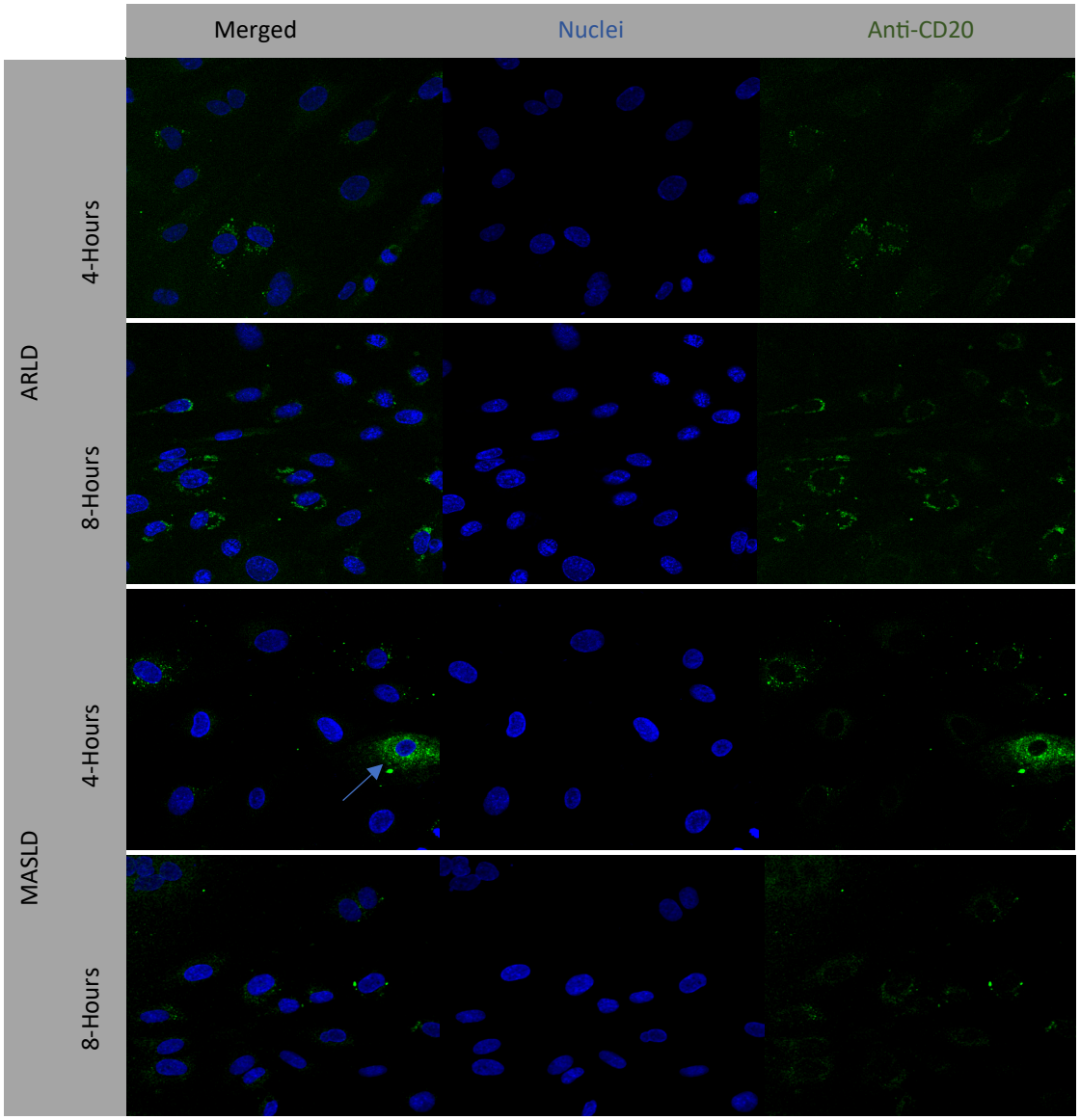


Figure 4. 7: Confocal images of anti-CD20 internalisation into cirrhotic LSEC. LSEC were isolated from ARLD and MASLD donors. Cells were seeded 70,000 per chamber in Ibitreat IBIDI vi chamber slide and grown until confluent. Treatment with anti-CD20 commenced for 4- and 8 hours. At each time point cells were fixed with 4% PFA for 5 minutes at 37 degrees. Following this, cells were permeabilised with 0.1% triton for 5 minutes at RT. Incubation with anti-mouse IgG Alexa fluor 488 for 1 hour took place to allow detection of the anti-CD20 (green). Nuclei (blue) was counterstained with DAPI for 5 minutes. Images taken on LSM780 confocal, 40x with water immersion. Top two panels show ARLD treated cells at 4 hours (top) and 8 hours (second panel). The bottom two panels show MASLD representative images (third panel 4-hour; fourth panel 8-hour).

From these images we were able to quantify the corrected total cell fluorescence (CTCF) to allow numerical comparison between variables. Figure 4.8A shows the difference between healthy (n=31) and cirrhotic (n=21) LSEC and their ability to internalise anti-CD20 antibody within the first 4-hours. Fluorescence is considerably higher in healthy

LSEC in comparison to cirrhotic cells (Figure 4.8A). Individual variation is more apparent in healthy LSEC. The opposite is true at 8-hours, where fluorescence is higher in cirrhotic cells than healthy (Figure 4.8B). A significant loss of signal is seen in healthy cells over time. Cirrhotic cells accumulate signal over time, although here display a wider range of individual variability in the 8-hour data set. The second row shows CTCF values in ARLD (Figure 4.8C) and MASLD (Figure 4.8D) livers specifically. Here each data point equates to a technical replicate mean and 2 livers were assessed in total. ARLD cells at the 4- and 8-hour time points, show a loss in fluorescence over time. MASLD cells, however, behave differently in that similar levels of fluorescence are observed between each time point. MASLD cells overall are generally more consistent than the ARLD samples. Finally, we also compared healthy cells over P2 and P3 for 4- and 8-hours. P2 LSEC demonstrated a complete loss in fluorescence over time. P3 also exhibited significant loss over time, but to a lesser extent than P2 LSEC. It is important to note the axis scales in each of these panels however which mean that uptake is considerably less at 8 hours for all healthy and ARLD cells. MASLD LSEC are the notable outlier with much more signal than ARLD at 4 hours, with no change at 8 hours.

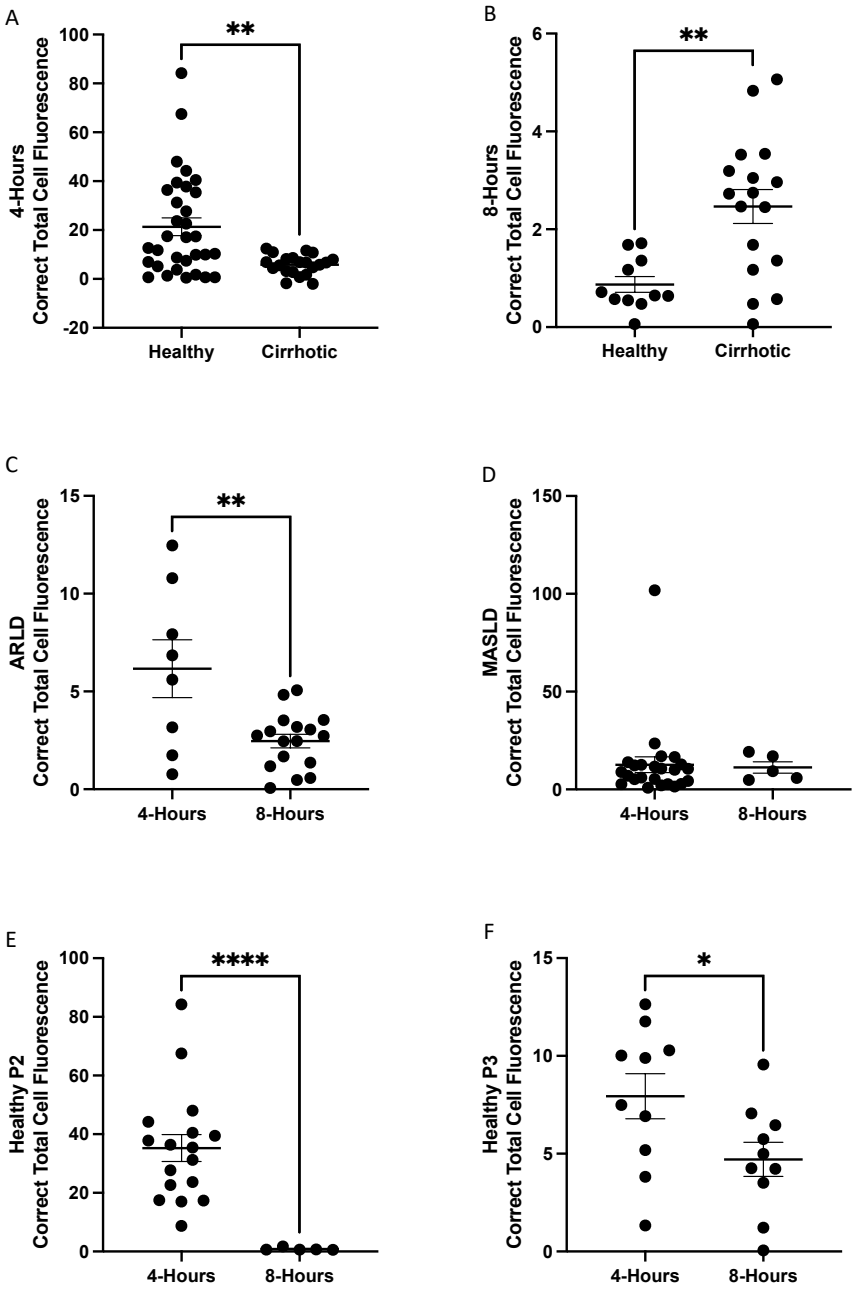


Figure 4. 8: Corrected Total Cell Fluorescence quantification of anti-CD20 internalisation. LSEC were incubated with 500ng/mL of anti-CD20 antibody for 4- and 8- hours. Following fixation, permeabilization and staining using an anti-mouse IgG Alexafluor 488, images were taken on the LSM780 confocal microscope at 40x with water immersion. Images were then quantified in ImageJ. CTCF is calculated by integrated density – (area of selected cells x mean fluorescence of background readings). For this every cell drawn around, an area of background is taken and read, this allows for sufficient background subtraction. A) shows healthy vs cirrhotic LSEC at the 4-hour treatment time point of anti-CD20. Each point represents LSEC from a different liver (n=31 and n=21 respectively). Significance was found between the two (p=0.0023). B) is the same comparison but made at the 8-hour time point (healthy n=11; cirrhotic n=17). Again, significance was found between healthy and cirrhotic (p=0.0016). C and D) shows the CTCF of ARLD and MASLD fluorescence of 4- and 8- hours. Each point here was averaged from 5 FOV per chamber of an IBIDI. Significance was found between 4- and 8-hour for ARLD (p=0.0030). E and F show comparison between 4- and 8- hour CTCF of healthy LSEC at P2 and P3 respectively. E saw significance at p=<0.0001 and F at p=0.0390. Significance was calculated through unpaired T tests or Mann-Whitney depending on normality. Plotted as mean with SEM.

4.2.2 Interpretation of findings using antibody uptake assays

Following analysis of these results, we decided to proceed with this combined methodology to assess whether the GSK assets were internalised and processed by human LSEC. Anti-CD20 was chosen as the trial antibody as it has clinical relevance and its target antigen is not expressed by LSEC, therefore any signal is reflective of the off-target interaction we are investigating. Corrected total cell fluorescence (CTCF) was chosen as the quantification method due to the amount of background we observed. CTCF is a manual process and allows for efficient background subtraction, even when staining is less abundant, and contrast is less clear for thresholding. Another reason is the morphology of LSEC, as often in culture some cells are flatter or more spread than others. This means that for cells that are flatter but containing equal amounts of fluorophores, the pixels are more distributed, meaning quantification would give a lower reading of fluorescence. With CTCF, the area of a cell is considered making it a more accurate tool to quantify our results.

Interestingly, although the ELISA assays were not optimal, the trends we observed in those assays were mirrored in both our microscopy and cytometry outputs. For instance, in every protocol, cirrhotic cells were seen to accumulate more antibody at 8 hours in comparison to healthy cells. Healthy LSEC were also seen as more efficient at 'processing', this is suggestive in the loss of % cells positive for anti-CD20 in flow, the large amount of anti-CD20 recovered in media in the ELISAs and loss of fluorescence over time through immunofluorescent quantification. This 'lost' antibody could either be recycled or degraded by LSEC, so we have termed these antibodies as 'processed.' This shall be addressed in Section 4.4. Similarities were also observed between microscopy and flow data. Cirrhotic cells at 4-hours often showed less than 100% of cells being positive for anti-CD20. This was also seen in the sporadic staining within a few cells in both ARLD and MASLD panels in Figure 4.7. Whereas healthy cells with very close to 100% cell positivity, showed far more consistent staining throughout the two 4-hour panels in Figure 4.6. By our isolation method we do not distinguish the different possible subpopulations of LSEC (e.g., periportal vs pericentral cells) meaning our culture

population is considered heterogenous. This may explain this difference in why some cells internalise antibody and some do not, but zonal markers would be required for confirmation. It also suggests healthy LSEC overall have a higher ability to interact with and internalise antibody throughout the sinusoid. Regarding healthy LSEC, the first panel that presents as fibrous staining is the first and only time, we observed staining like that. Majority of staining presented, similar to that in the below panel, as a vesicular pattern throughout the cell. Both 4-hour images were taken on the same day and treated equally with cells seeded into the same IBIDI, in separate chambers and from different livers. A look into the literature I found one possible explanation, Falkowska-Hansen and colleagues described similar intracellular distribution of clathrin heavy chains associated along the microtubules within the cell.[401] This looked somewhat similar to our observation for this particular donor and as previously described every receptor of interest throughout Chapter 3 alongside pinocytosis is trafficked through clathrin coated pits; suggesting in this case anti-CD20 may have been partition into this particular mechanism of internalisation. Worthy of note, this staining pattern also doesn't look too dissimilar to that seen in Figure 3.18 C of CD32b (nonpermeabilized) suggesting possible colocalisation here. In hindsight, this should have been done at the time.

Overall, our healthy donor cohort demonstrated a broad spread of data potentially due to the variability often seen in donated human samples, particularly in healthier donors.[403] As often to be diagnosed with a disease one must meet a certain clinical criteria so this can lead to a more homogenous population of individuals explaining why in figures such as 4.8A the grouping for cirrhotic cells is far tighter than that in their healthier counterparts. This was also observed in our clinical and expression data throughout Chapter 3. Cirrhotic cells were more impacted by the process of culture and passaging than healthy LSEC. At high passage (P4-5), cirrhotic LSEC showed less antibody uptake. Due to the accumulation of evidence throughout Chapters 3 and 4 for LSEC's changes in culture and passaging we ensured where possible, cells were used at P1-P2 as much as functionality allowed. Where cells were P3-P4 this will now be highlighted throughout.

4.3 LSEC can internalise and traffic IgG-based therapeutic antibodies.

Following our successful trials with anti-CD20, we applied these methodologies to the GSK assets. The following section will detail each antibody separated by origin (i.e. chimeric, humanised etc.). Here data points highlighted in red indicate cells were P3-P4. Flow cytometry from this point onwards was performed on the BD LSR Fortessa and analysed using Flowjo. For fluorescent microscopy, all cells were fixed and due to antibody availability, we chose to extensively investigate one antibody per category.

4.3.1 Chimeric antibodies

An initial time course was performed with **Antibody A** incubated on P4 MASLD cells, taken at 1-, 2-, 4-, and 8-hours at concentrations of 50ng/mL and 500ng/mL (Figure 4.9A), with median fluorescence intensity (MFI) recorded. 0ng/mL is plotted throughout as it allows comparison to the background fluorescence. Here, we observed 500ng/mL accumulating more so over the 8-hours in comparison to the 50ng/mL sample.

Figure 4.9B shows data for pooled cells incubated with 500ng/mL and 50ng/mL of **Antibody A** (healthy n=5 and cirrhotic n=6). Again, cirrhotic cells showed a dose dependent response with **antibody A** at 4- and 8-hours. Overall, healthy LSEC exhibited higher MFI on average than cirrhotic cells. At 8-hours 500ng/mL of **Antibody A** resulted in higher fluorescence for both cell types. The red data points indicate P3-P4 LSEC, in general all these high passage cells show the highest uptake in both healthy and cirrhotic cells.

Panel D and E show the same data as A and B but allows for clearer comparison between 4- and 8-hour time points in each treatment group: 50ng/mL and 500ng/mL of **Antibody A**. D shows the 50ng/mL treated cells, here a clear reduction in MFI is observed in the healthy LSEC in comparison to no difference presented in cirrhotic cells. In the 500ng/mL group, on average there was a lower MFI observed; with the slightest reduction in average MFI over 4- and 8-hours.

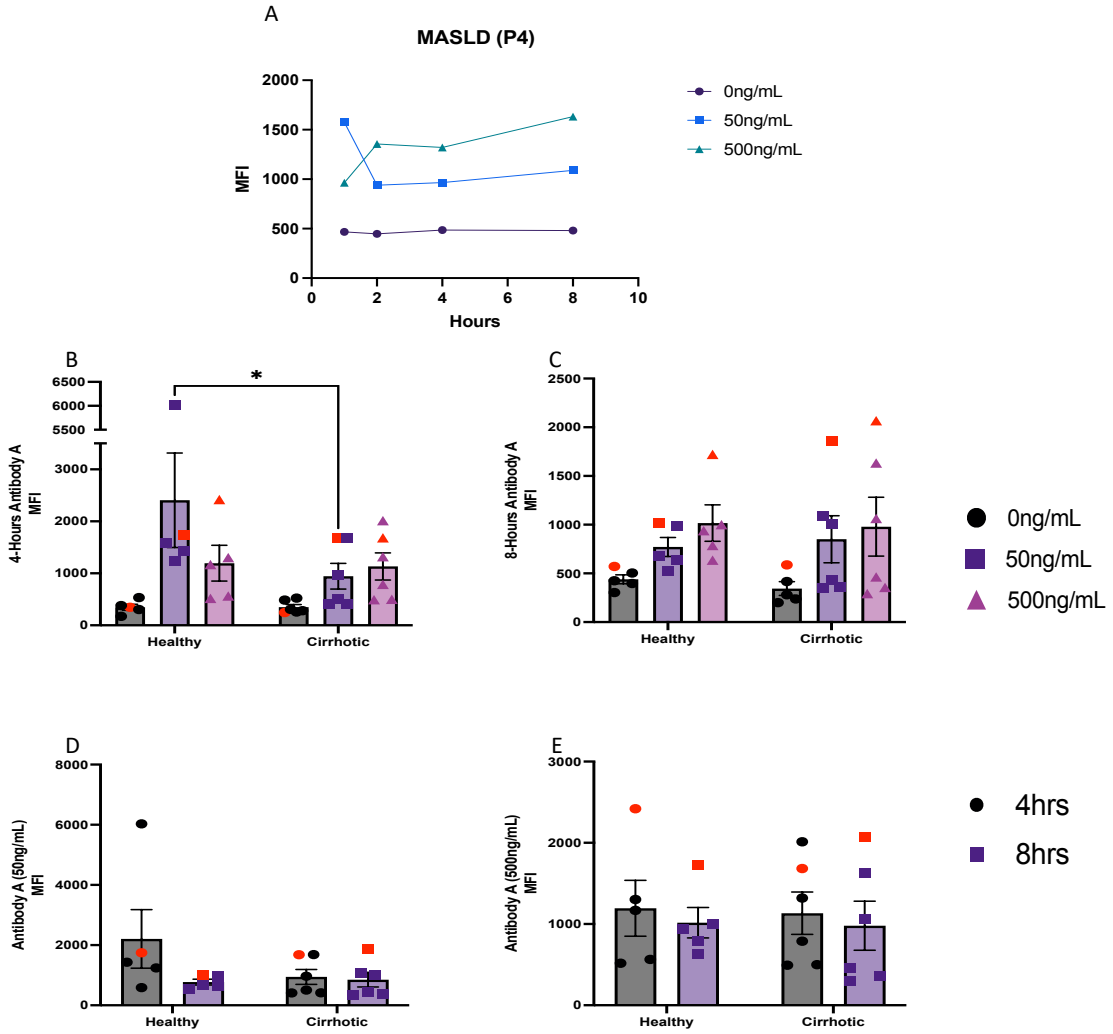


Figure 4. 9: Flow cytometric analysis of Antibody A in healthy and cirrhotic LSEC. LSEC were seeded into 24 well plates and treated with concentrations of 50ng/mL or 500ng/mL of Antibody A. Following each time point, cells were dissociated from each well and pooled with its corresponding doublet. Each data point corresponds to an individual liver (healthy n=5, cirrhotic n=6). All steps were performed on ice. Cells were washed with FACs buffer before being fixed for 20 minutes with 4% PFA. Cells were washed twice more, before being permeabilised with 0.1% Triton for 10-mintues and incubated with anti-mouse IgG1 Alexafluor 488 for 30 minutes. Cells were then washed 3x before being analysed using the LSR Fortessa. Flowjo software was used to obtain MFI with data plotted on Prism. A) is a time course of treatment over 1-, 2-, 4- and 8-hours of Antibody A on MASLD isolated LSEC.B) shows healthy and cirrhotic cells incubated with Antibody A for 4-hours with 50ng/mL and 500ng/mL. C)shows the equivalent at 8-hours. D & E are the same data plotted as in B and C but allows for better comparison between time points for both 50ng/mL and 500ng/mL of Antibody A. Red data points represent cells P3 or above. Significance was calculated using 2way ANOVA and error bars show SEM.

Other mAbs included in the chimeric category are the anti-CD20 and anti-CD20 LAGA. Figure 4.10 shows that Anti-CD20 treatment in healthy LSEC (n=2; Figure 4.10A) showed MFI was highest in cells treated with the highest concentration. For cells treated with 50ng/mL very little was observed above that of the background (0ng/mL) in healthy

LSEC. Over 4- and 8-hours, the top concentration saw a minor loss in MFI in both healthy and diseased LSEC within a small sample size.

The anti-CD20 LAGA is based on the parent anti-CD20 mAb, however through point mutations, the Fc region has been disabled. A considerably higher MFI was observed in every timepoint for both healthy and cirrhotic LSEC for anti-CD20 LAGA when compared to the unmodified Fc (Compare Figures 4.10A,B and C,D). Nevertheless, no significance was seen between healthy and diseased LSEC. Immunofluorescence staining using anti-CD20 LAGA showed a very similar localization to that of anti-CD20. Figure 4.11 shows a representative image of LAGA internalised into MASLD LSEC. Staining here is vesicular and mostly localised around the nucleus (indicated by white arrow) with some staining present in the cytoplasm.

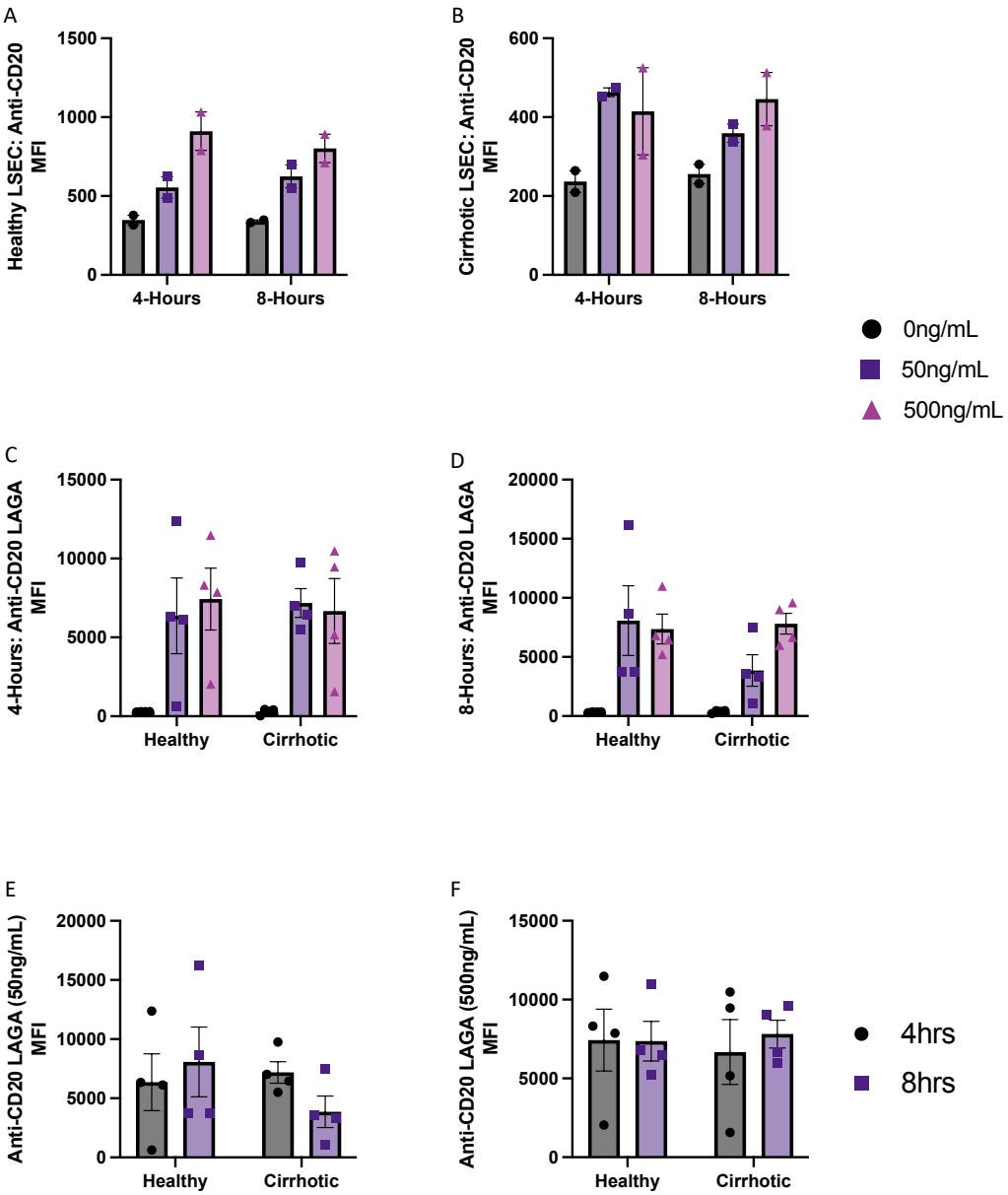


Figure 4. 10: Flow cytometric analysis of anti-CD20 and anti-CD20 LAGA in healthy and cirrhotic LSEC. LSEC were seeded into 24 well plates and treated with concentrations of 50ng/mL or 500ng/mL of anti-CD20 or Anti-CD20 LAGA. Following each time point cells were dissociated from each well and pooled with its corresponding doublet. Each point corresponds to an individual liver (n=2 each for anti-CD20; n=4 for each LAGA). All steps were performed on ice. Cells were washed with FACs buffer before being fixed for 20 minutes with 4% PFA. Cells were washed twice more, before being permeabilised with 0.1% Triton for 10-mintues and incubated with anti-mouse IgG1 Alexafluor 488 for 30 minutes. Cells were washed 3x before being analysed using the LSR Fortessa. Flowjo software was used to obtain MFI with data plotted on Prism. A) shows healthy LSEC incubated for 4- and 8-hours with 50ng/mL and 500ng/mL of anti-CD20. B) shows the equivalent in cirrhotic cells. C) shows healthy and cirrhotic LSEC incubated with for 4-hours with 50ng/mL and 500ng/mL of anti-CD20 LAGA. D) shows the equivalent at 8-hours. E & F are the same data plotted in C and D but allows for better comparison between time points for both 50ng/mL and 500ng/mL of LAGA. No significance was observed. Error bars show SEM.

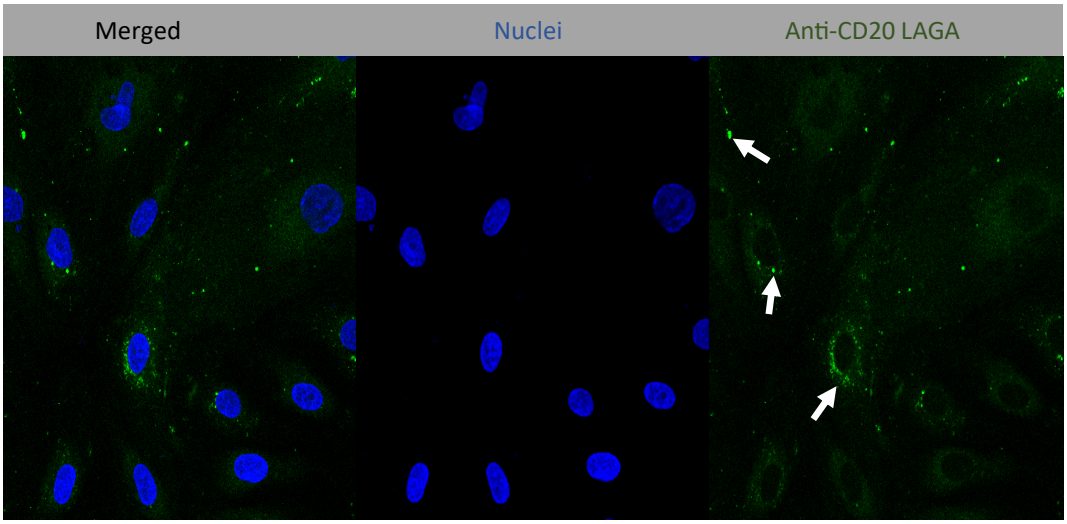


Figure 4. 11: Immunofluorescence of internalised anti-CD20 LAGA at 4-hours. LSEC were isolated from MASLD tissue. Cells were seeded 70,000 per chamber in Ibitreat IBIDI vi chamber slide and grown until confluent, then treated with 500ng/mL anti-CD20 LAGA for 4 hours. Cells were then fixed with 4% PFA for 5 minutes at 37 degrees. Following this, cells were permeabilised with 0.1% Triton x100 for 5 minutes at RT. Incubation with anti-mouse IgG Alexa fluor 488 for 1 hour took place to allow detection of the anti-CD20 LAGA (green). Nuclei (blue) was counterstained with DAPI for 5 minutes. Images taken on LSM780 confocal, 40x with water immersion. White arrows indicate perinuclear puncta staining of anti-CD20 LAGA

4.3.2 Humanised antibodies.

Antibody B was the first humanised antibody tested. From here onwards, each antibody was detected using an anti-human IgG secondary Alexafluor 488 unless stated otherwise. Referring to figure 4.12 little difference was observed at 4-hours. Both healthy and cirrhotic LSEC saw a loss in MFI over time, although no significance was calculated. Passage number (red dots) showed no difference.

Regarding immunofluorescence, a representative image of internalisation in healthy LSEC can be seen in Figure 4.13. Taken at 4-hours, **Antibody B** was distributed in a similar manner to that observed for other antibody preparations, specifically internalisation into vesicles mostly centred around the nucleus with some present throughout the cytoplasm. Here **Antibody B** is identified in green.

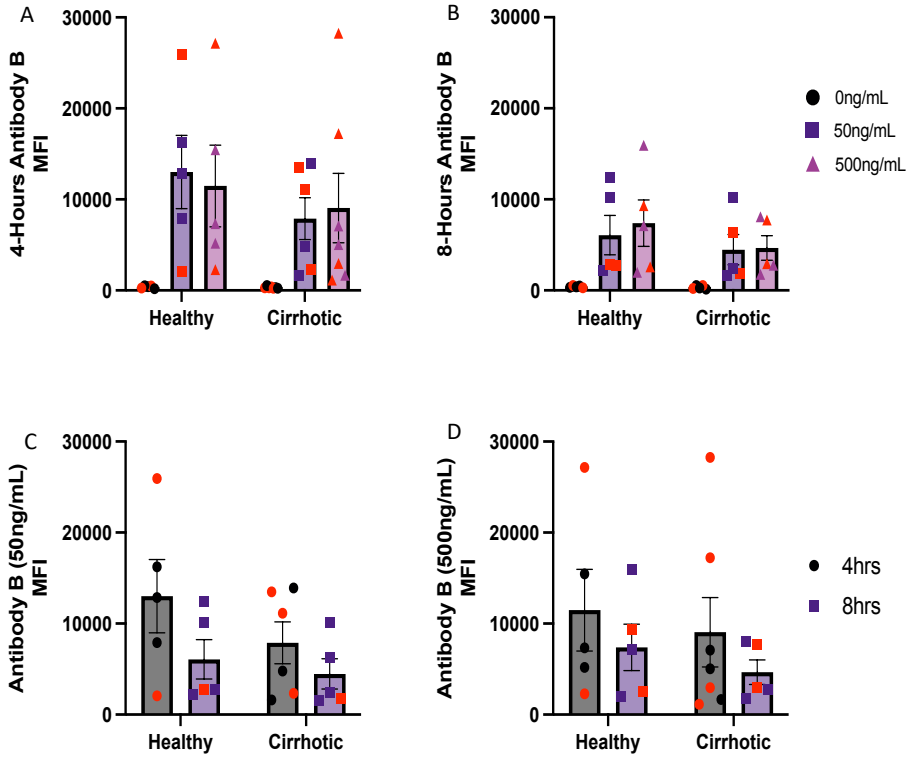


Figure 4. 12: Flow cytometric analysis of Antibody B in healthy and cirrhotic LSEC. LSEC were seeded into 24 well plates and treated with concentrations of 50ng/mL or 500ng/mL of antibody B. Following each time point cells were dissociated from each well and pooled with its corresponding doublet. Each point corresponds to an individual liver (Healthy n=5; Cirrhotic n=6). All steps were performed on ice. Cells were washed with FACs buffer before being fixed for 20 minutes with 4% PFA. Cells were washed twice more, before being permeabilised with 0.1% Triton for 10-mintues and incubated with anti-human IgG1 Alexafluor 488 for 30 minutes. Cells were washed 3x before being analysed using the LSR Fortessa. Flowjo software was used to obtain MFI with data plotted on Prism. A) shows healthy and cirrhotic LSEC incubated with for 4-hours with 50ng/mL and 500ng/mL of antibody B. B) shows the equivalent at 8-hours. C and D are the same data plotted in A and B but allows for better comparison between time points for both 50ng/mL and 500ng/mL of antibody B. No significance was observed. Error bars show SEM.

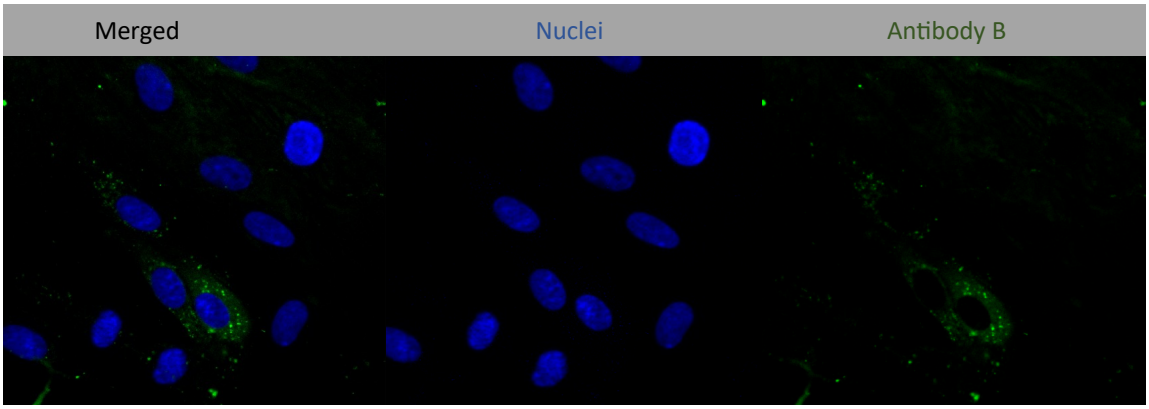


Figure 4. 13: Representative image of Antibody B internalised into healthy LSEC at 4-hours. LSEC were isolated from healthy tissue. Cells were seeded 70,000 per chamber in Ibitreat IBIDI vi chamber slide and grown until confluent. Treatment with 500ng/mL of antibody B commenced for 4 hours. Cells were then fixed with 4% PFA for 5 minutes at 37 degrees C. Following this, cells were permeabilised with 0.1% triton for 5 minutes at RT. Incubation with anti-human IgG Alexa fluor 488 for 1 hour took place to allow detection of the antibody B (green). Nuclei (blue) was counterstained with DAPI for 5 minutes. Images taken on LSM780 confocal, 40x with water immersion.

No significance was observed throughout. On average cirrhotic LSEC reported less MFI than healthy cells. Little difference was observed over the time course.

Similar was perceived in the staining of the therapeutic in healthy LSEC incubated with 500ng/mL of **Antibody C (Figure 4.15)**. Very little fluorescence was observed in the first 4-hour treatment panel, indicated by the white arrows. The cells treated for 8-hours, however, saw an increase in vesicles positive with antibody. Staining is present throughout the cell. The orange arrow shows signal at the cell surface.

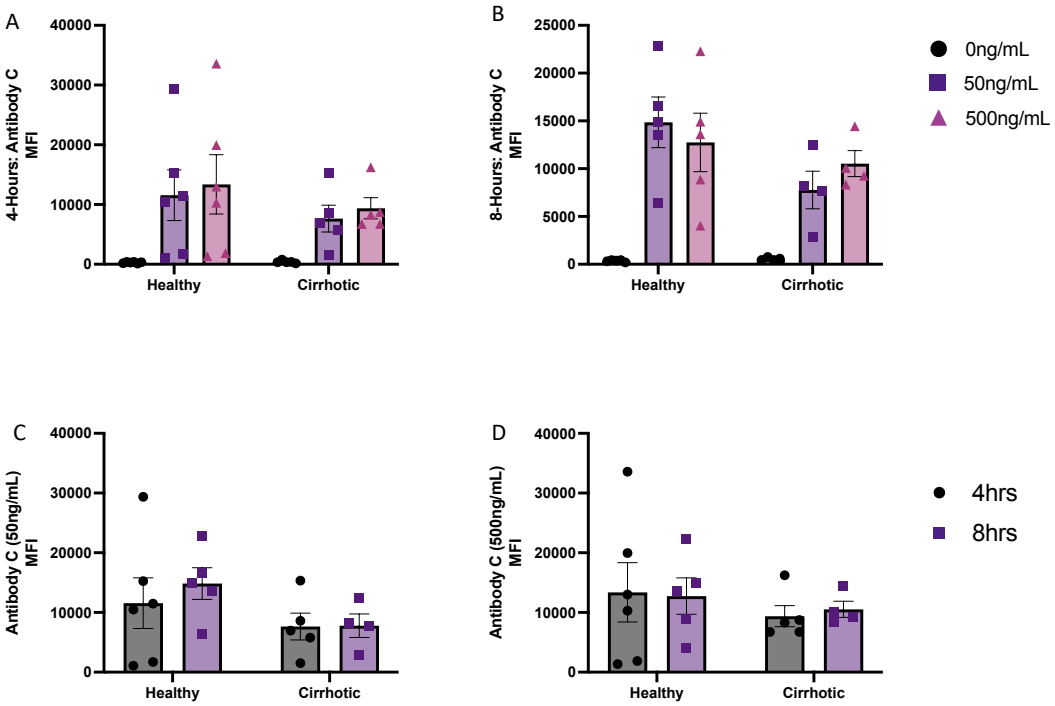


Figure 4. 14: Flow cytometric analysis of Antibody C in healthy and cirrhotic LSEC. LSEC were seeded into 24 well plates and treated with concentrations of 50ng/mL or 500ng/mL of antibody C. Following each time point cells were dissociated from each well and pooled with its corresponding doublet. Each point corresponds to an individual liver (Healthy n=5; Cirrhotic n=5). All steps were performed on ice. Cells were washed with FACs buffer before being fixed for 20 minutes with 4% PFA. Cells were washed twice more, before being permeabilised with 0.1% Triton for 10-mintues and incubated with anti-human IgG1 Alexafluor 488 for 30 minutes. Cells were washed 3x before being analysed using the LSR Fortessa. Flowjo software was used to obtain MFI with data plotted on Prism. A) shows healthy and cirrhotic LSEC incubated with for 4-hours with 50ng/mL and 500ng/mL of antibody C. B) shows the equivalent at 8-hours. C and D are the same data plotted in A and B but allows for better comparison between time points for both 50ng/mL and 500ng/mL of antibody C. No significance was observed. Error bars show SEM.

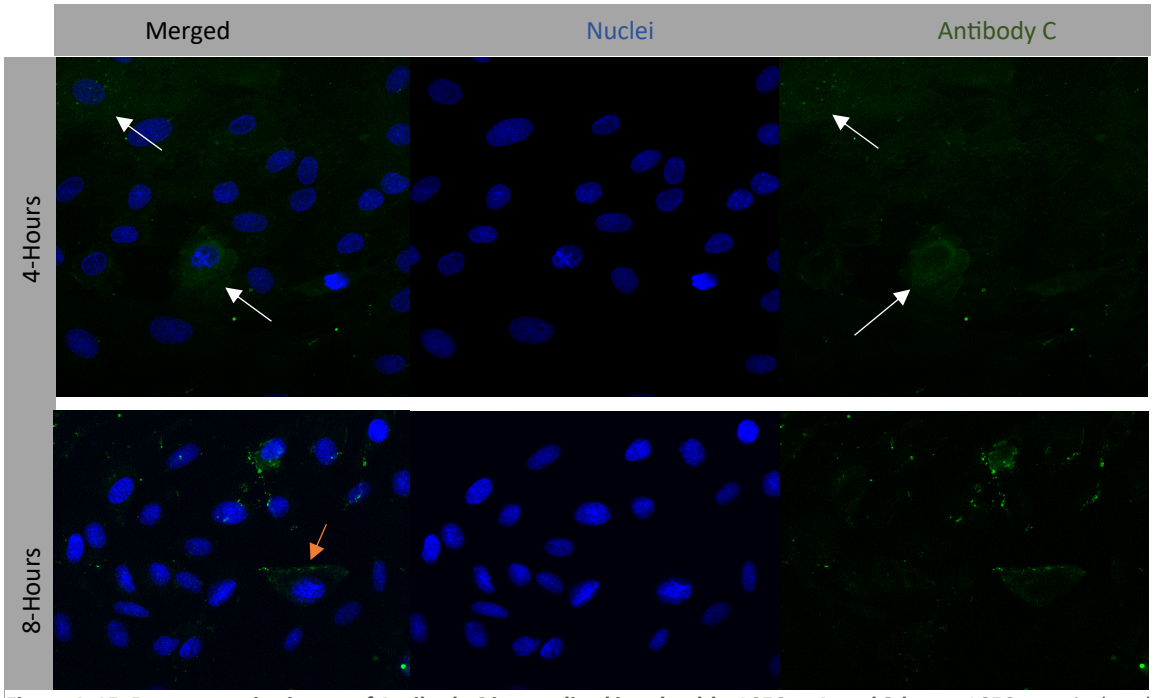


Figure 4. 15: Representative image of Antibody C internalised into healthy LSEC at 4- and 8-hours. LSEC were isolated from healthy tissue. Cells were seeded 70,000 per chamber in Ibitreat IBIDI vi chamber slide and grown until confluent. Treatment with 500ng/mL of antibody C commenced for 4 and 8 hours. Cells were then fixed with 4% PFA for 5 minutes at 37 degrees. Following this, cells were permeabilised with 0.1% triton for 5 minutes at RT. Incubation with anti-human IgG Alexa fluor 488 for 1 hour took place to allow detection of the antibody C (green). Nuclei (blue) was counterstained with DAPI for 5 minutes. Images taken on LSM780 confocal, 40x with water immersion. Top panel shows 4-hour incubation time, here minimal staining was observed (indicated by white arrows). Bottom panel shows 8-hours incubation with antibody C. More vesicular staining was evident here with some localised on the cell surface membrane indicated by the orange arrow.

Antibody D also exhibits a minimal dose dependent response in both normal and cirrhotic liver in the first 4-hour incubation period (Figure 4.16A). Over time, 50ng/mL treated cells exhibit the same MFI in healthy, with a slight increase observed in cirrhotic cells. Regarding the higher concentration of **Antibody D**, a loss in fluorescence was seen in both, however less evident in cirrhotic LSEC (Figure 4.16D).

Due to the large quantities of **Antibody D** sent by GSK, more immunofluorescence was able to be undertaken with this antibody. Figure 4.17 shows representative images of internalisation of antibody at 4- and 8-hours. The 4-hour panel (top) appears to show antibody accumulating at the cell membrane. The lower panel shows an example of the 8-hour time point. Here vesicular staining is seen, in closer proximity to the nucleus but staining is evident throughout the cytoplasm of the cell. As more staining was able to be

conducted, CTCF quantification was possible. Here as seen with the flow cytometry marginal differences were observed in 500ng/mL uptake of **Antibody D** at the 4-hour mark. However, the difference here was that cirrhotic LSEC exhibited higher fluorescence. Furthermore, a time course of fluorescence was taken over 2-, 3-, 4- and 8-hours in healthy LSEC (Figure 4.18). Here internalisation of **Antibody D** decreased over time.

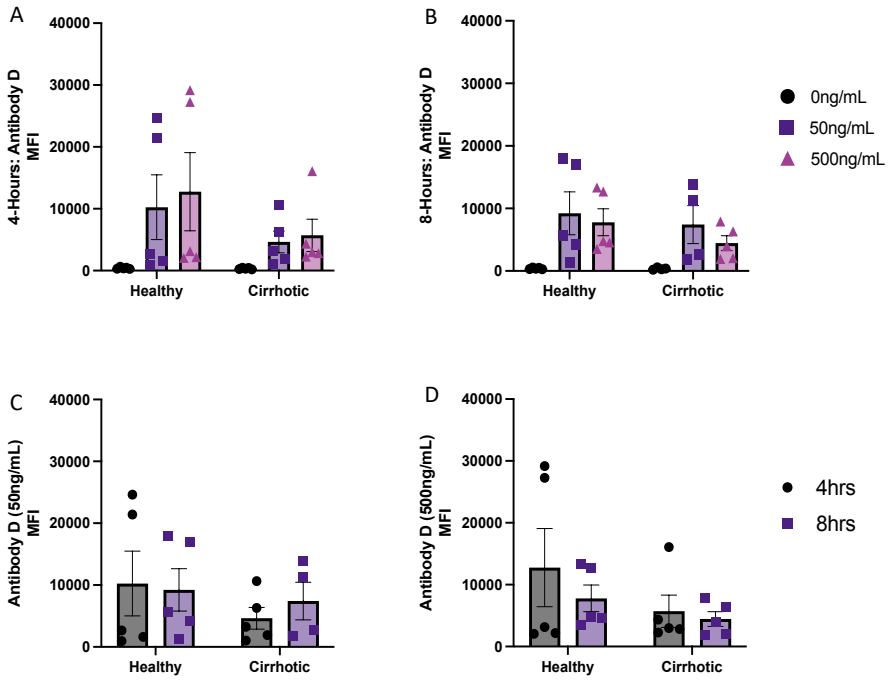


Figure 4. 16 Flow cytometric analysis of Antibody D in healthy and cirrhotic LSEC. LSEC were seeded into 24 well plates and treated with concentrations of 50ng/mL or 500ng/mL of antibody D. Following each time point cells were dissociated from each well and pooled with its corresponding doublet. Each point corresponds to an individual liver (Healthy n=5; Cirrhotic n=5). All steps were performed on ice. Cells were washed with FACs buffer before being fixed for 20 minutes with 4% PFA. Cells were washed twice more, before being permeabilised with 0.1% Triton for 10-mintues and incubated with anti-human IgG1 Alexafluor 488 for 30 minutes. Cells were washed 3x before being analysed using the LSR Fortessa. Flowjo software was used to obtain MFI with data plotted on Prism. A) shows healthy and cirrhotic LSEC incubated with for 4-hours with 50ng/mL and 500ng/mL of antibody D. B) shows the equivalent at 8-hours. C and D are the same data plotted in A and B but allows for better comparison between time points for both 50ng/mL and 500ng/mL of antibody D. No significance was observed. Error bars show SEM.

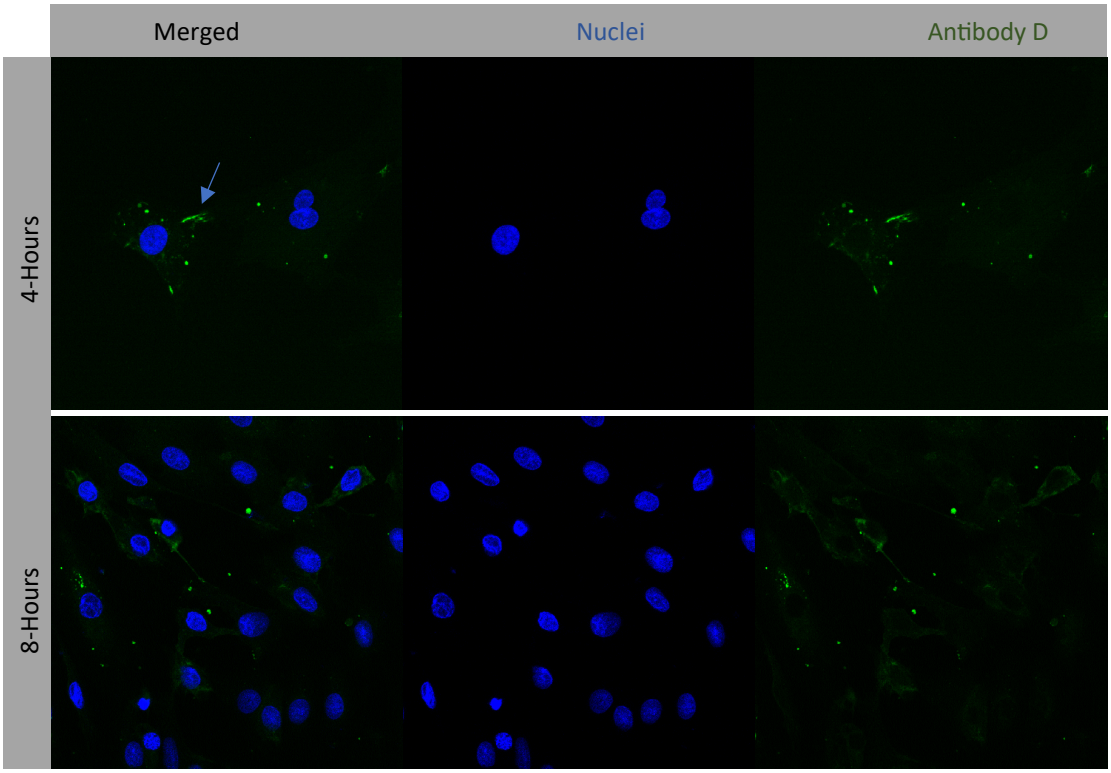


Figure 4. 17: Representative image of Antibody D internalised into healthy LSEC at 4- and 8-hours. LSEC were isolated from healthy tissue. Cells were seeded 70,000 per chamber in Ibitreat IBIDI vi chamber slide and grown until confluent. Treatment with 500ng/mL of antibody D commenced for 4 and 8 hours. Cells were then fixed with 4% PFA for 5 minutes at 37 degrees. Following this, cells were permeabilised with 0.1% triton for 5 minutes at RT. Incubation with anti-human IgG Alexa fluor 488 for 1 hour took place to allow detection of the antibody D (green). Nuclei (blue) was counterstained with DAPI for 5 minutes. Images taken on LSM780 confocal, 40x with water immersion. Top panel shows 4-hour incubation time, here presumed accumulation at the cell membrane can be observed (indicated by the blue arrow). Bottom panel shows 8-hours incubation with antibody D.

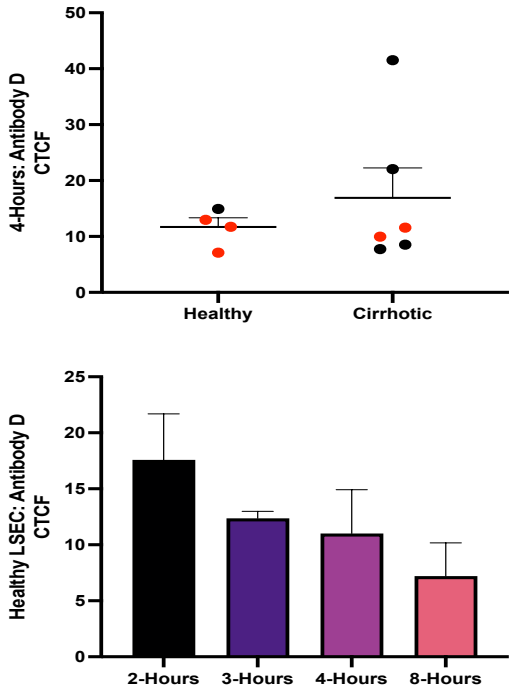


Figure 4. 18: Corrected Total Cell Fluorescence quantification of Antibody D internalisation. LSEC were incubated with 500ng/mL of Antibody D for 4- and 8- hours. Following fixation, permeabilization and staining using an anti-human IgG Alexafluor 488, images were taken on the LSM780 confocal microscope at 40x with water immersion. Images were then quantified in ImageJ. CTCF is calculated by integrated density – (area of selected cells x mean fluorescence of background readings). For this every cell drawn around, an area of background is taken and analysed, this allows for sufficient background subtraction. A) shows healthy vs cirrhotic LSEC at the 4-hour treatment time point of Antibody D. Each point represents LSEC from a different liver (n=4 and n=6 respectively). No significance was found. Red data points indicate P3-P4. B) shows healthy LSEC (n=4) incubated with antibody D over 2-, 3-, 4- and 8-hours and CTCF quantified. Plotted as mean with SEM.

4.3.3 Fully Human antibodies.

Antibody E presented a mild dose dependent response in healthy, however this was blunted in cirrhotic cells at the 4-hour mark (Figure 4.19). At the lower concentration of **antibody E**, very similar levels of interaction were seen with both healthy and cirrhotic LSEC over 4- and 8-hours (Figure 4.19C). However, with 500ng/mL, an increase in accumulation of antibody was observed in healthy, with the opposite true in cirrhotic cells (Figure 4.19D). To note significance was calculated. The higher passaged cells here presented the lowest levels of MFI. Regarding immunofluorescence very little was noted in the first 2-hours of incubation with antibody E (Figure 4.20 & 4.21). This was increased in the following 2-hours however, by 8-hours had decreased again. Staining at early and

late time points was vesicular, with staining localised on the edge of the cell for the 8-hour time point. The 4-hour panel however presents a distinctly different staining pattern to that seen previously. **Antibody E** is localised throughout the cell, in a fibrous like pattern similar to that seen in the outlier healthy donor treated with anti-CD20 in Figure 4.6. This pattern was present through many fixed stained Antibody E treated cells from both cirrhotic and healthy livers.

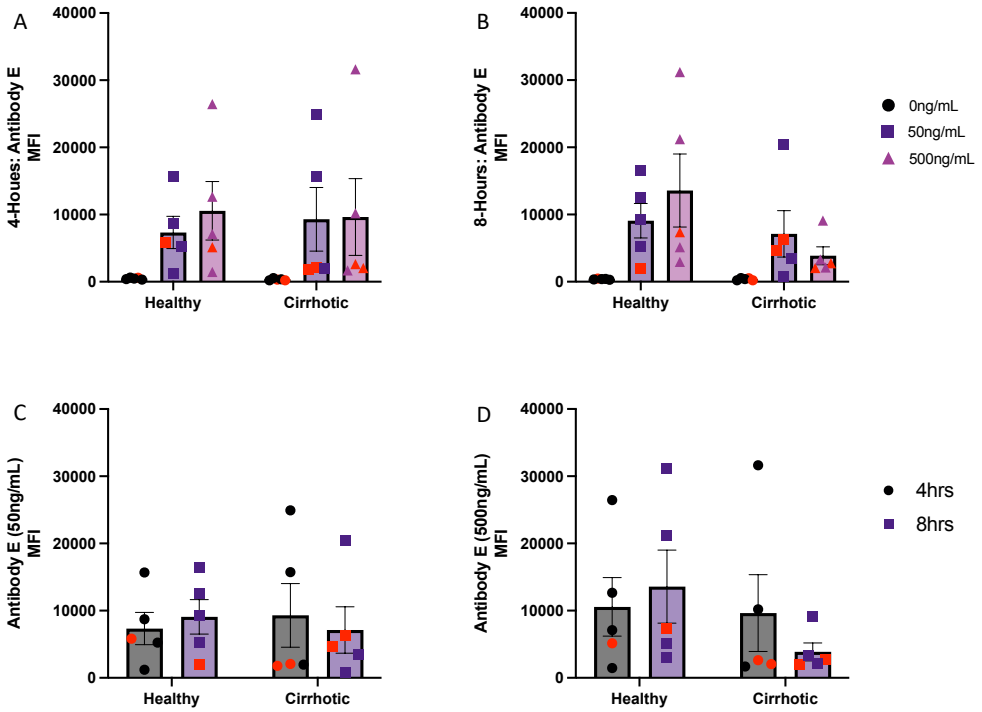


Figure 4. 19: Flow cytometric analysis of Antibody E in healthy and cirrhotic LSEC. LSEC were seeded into 24 well plates and treated with concentrations of 50ng/mL or 500ng/mL of antibody E. Following each time point cells were dissociated from each well and pooled with its corresponding doublet. Each point corresponds to an individual liver (Healthy n=5; Cirrhotic n=5). All steps were performed on ice. Cells were washed with FACs buffer before being fixed for 20 minutes with 4% PFA. Cells were washed twice more, before being permeabilised with 0.1% Triton for 10-mintues and incubated with anti-human IgG1 Alexafluor 488 for 30 minutes. Cells were washed 3x before being analysed using the LSR Fortessa. Flowjo software was used to obtain MFI with data plotted on Prism. A) shows healthy and cirrhotic LSEC incubated with for 4-hours with 50ng/mL and 500ng/mL of antibody E. B) shows the equivalent at 8-hours. C and D are the same data plotted in A and B but allows for better comparison between time points for both 50ng/mL and 500ng/mL of antibody E. No significance was observed. Error bars show SEM. Red data points indicate cells passaged 3-4.

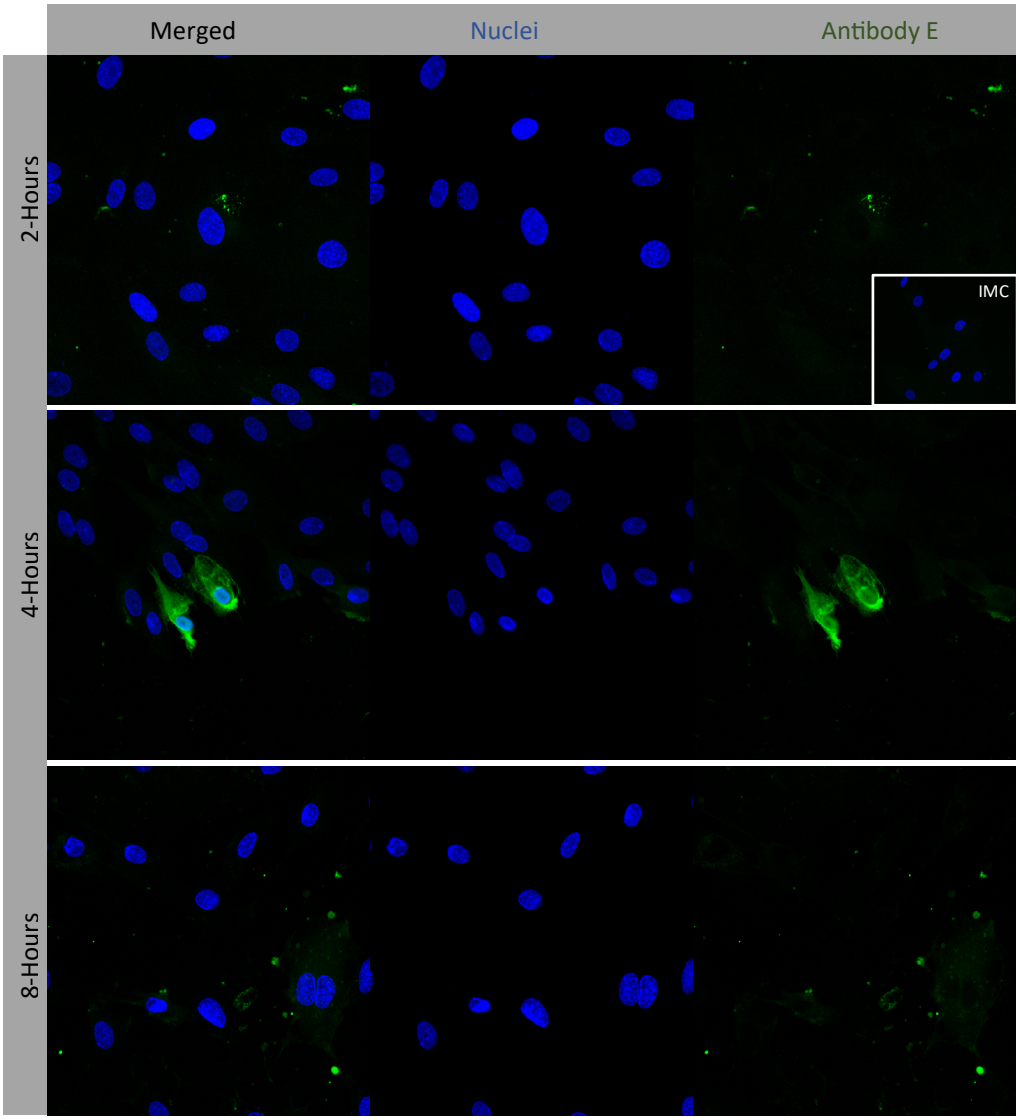


Figure 4. 20: Representative image of Antibody E internalised into healthy LSEC at 4- and 8-hours. LSEC were isolated from healthy tissue. Cells were seeded 70,000 per chamber in Ibitreat IBIDI vi chamber slide and grown until confluent. Treatment with 500ng/mL of antibody E commenced for2-, 4- and 8-hours. Cells were then fixed with 4% PFA for 5 minutes at 37 degrees. Following this, cells were permeabilised with 0.1% Triton x100 for 5 minutes at RT. Incubation with anti-human IgG Alexa fluor 488 for 1 hour took place to allow detection of the antibody E (green). Nuclei (blue) was counterstained with DAPI for 5 minutes. Images taken on LSM780 confocal, 40x with water immersion. Top panel shows 2-hour incubation time, here accumulation at the cell membrane can be observed. Middle panel exhibits LSEC treated for 4-hours, here the antibody appears fibrous throughout the cell. The bottom panel shows 8-hours incubation with antibody E, some punctate fluorescence is observed here. Insert panel shows the isotype matched control (IMC).

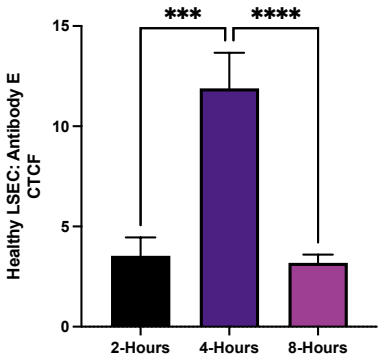


Figure 4. 21: Corrected Total Cell Fluorescence quantification of Antibody E internalisation. LSEC were incubated with 500ng/mL of Antibody E for 2-, 4- and 8- hours. Following fixation, permeabilization and staining using an anti-human IgG Alexafluor 488, images were taken on the LSM780 confocal microscope at 40x with water immersion. Images were then quantified in ImageJ. CTCF is calculated by integrated density – (area of selected cells x mean fluorescence of background readings). For this every cell drawn around, an area of background is taken and read, this allows for sufficient background subtraction. CTCF was quantified for each time point and plotted as mean with SEM. Here significance was calculated through Brown-Forsythe and Welch ANOVA test; ***=0.0002, ****=<0.0001.

Antibody F exhibited a non-significant dose dependent response in both healthy and cirrhotic LSEC (Figure 4.22). High uptake was observed in healthy cells. Comparatively over time, the 50ng/mL treatment group saw similar retention throughout. In the higher concentrated antibody group, some loss of MFI was observed but nothing significant. Overall, retention at the 8-hour time point was high. Here passaged cells, saw the lowest fluorescence excluding one individual which scored high for uptake in both the 50ng/mL and 500ng/mL categories.

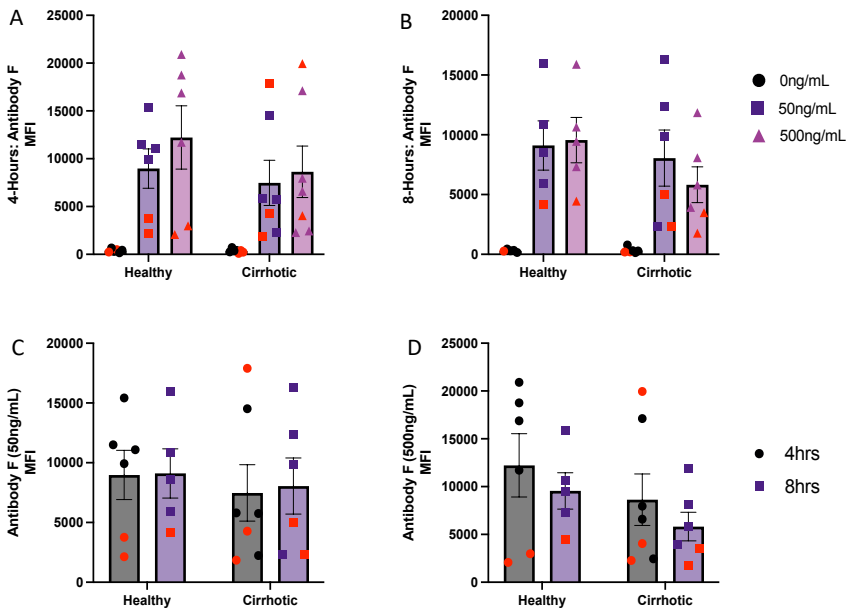


Figure 4. 22: Flow cytometric analysis of Antibody F in healthy and cirrhotic LSEC. LSEC were seeded into 24 well plates and treated with concentrations of 50ng/mL or 500ng/mL of antibody F. Following each time point cells were dissociated from each well and pooled with its corresponding doublet. Each point corresponds to an individual liver (Healthy n=6; Cirrhotic n=6). All steps were performed on ice. Cells were washed with FACs buffer before being fixed for 20 minutes with 4% PFA. Cells were washed twice more, before being permeabilised with 0.1% Triton for 10-mintues and incubated with anti-human IgG1 Alexafluor 488 for 30 minutes. Cells were washed 3x before being analysed using the LSR Fortessa. Flowjo software was used to obtain MFI with data plotted on Prism. A) shows healthy and cirrhotic LSEC incubated with for 4-hours with 50ng/mL and 500ng/mL of antibody F. B) shows the equivalent at 8-hours. C and D are the same data plotted in A and B but allows for better comparison between time points for both 50ng/mL and 500ng/mL of antibody F. No significance was observed. Error bars show SEM. Red data points indicate cells passaged 3-4.

Antibody G was the only nonchimeric antibody that could not be detected using a human IgG secondary. It was detected however, by an anti-mouse IgG. Therefore, analysis was carried out using this detection method. Excluding the anti-CD20 antibodies, **antibody G** showed the lowest MFI therefore the weakest interaction with LSEC than any other antibody. This was particularly evident in the first 4-hours of incubation in cirrhotic LSEC (Figure 4.23). Here very little fluorescence was present beyond the negative control. Interaction with antibody was not dose-dependent, with 50ng/mL of **antibody G** reading the highest MFI, this was slightly reduced by the 8-hour mark. Cirrhotic cells read very similar throughout the time course for both concentrations. The only group to show a trend in increase of fluorescence was healthy

LSEC treated with 500ng/mL of **Antibody G**. This data set showed the least variability comparatively to the rest of the antibodies studied.

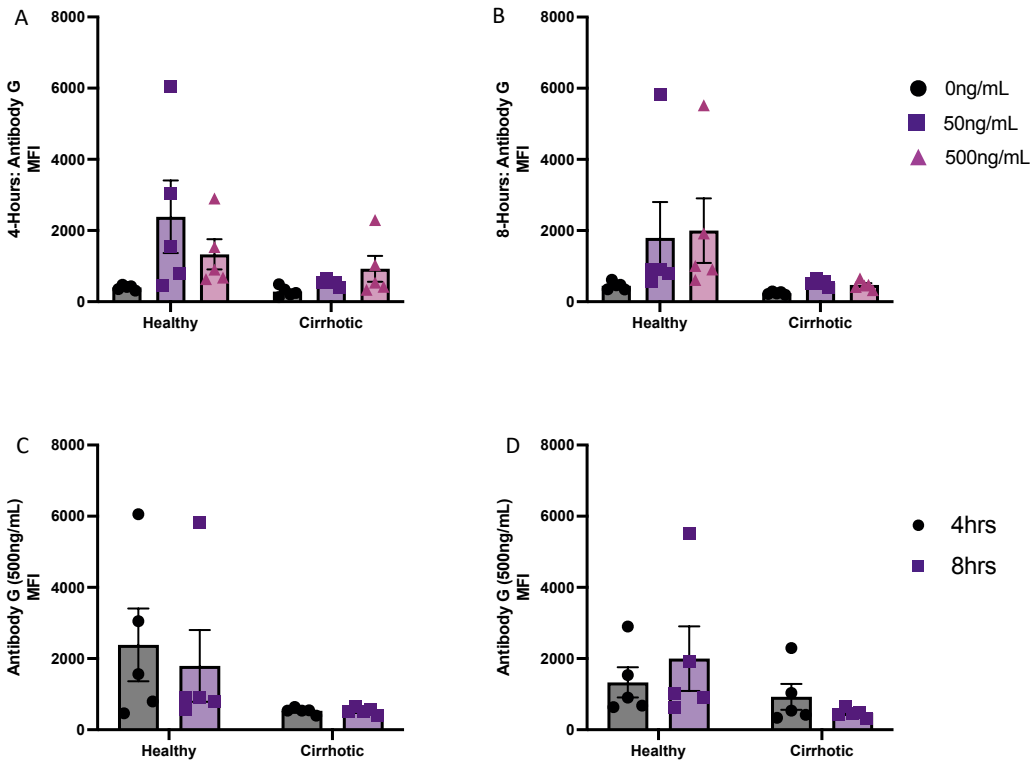


Figure 4. 23: Flow cytometric analysis of Antibody G in healthy and cirrhotic LSEC. LSEC were seeded into 24 well plates and treated with concentrations of 50ng/mL or 500ng/mL of antibody G. Following each time point cells were dissociated from each well and pooled with its corresponding doublet. Each point corresponds to an individual liver (Healthy n=5; Cirrhotic n=5). All steps were performed on ice. Cells were washed with FACs buffer before being fixed for 20 minutes with 4% PFA. Cells were washed twice more, before being permeabilised with 0.1% Triton for 10-mintues and incubated with anti-human IgG1 Alexafluor 488 for 30 minutes. Cells were washed 3x before being analysed using the LSR Fortessa. Flowjo software was used to obtain MFI with data plotted on Prism. A) shows healthy and cirrhotic LSEC incubated with for 4-hours with 50ng/mL and 500ng/mL of antibody G. B) shows the equivalent at 8-hours. C and D are the same data plotted in A and B but allows for better comparison between time points for both 50ng/mL and 500ng/mL of antibody G. No significance was observed. Error bars show SEM.

4.3.4 Bispecific antibodies.

Antibody H presented the highest disparity between healthy and cirrhotic LSEC, with the non-injured liver cells, showing the highest MFI at 500ng/mL in 4-hours (Figure 4.24). In contrast, 50ng/mL of **Antibody H** presented the highest fluorescence in cirrhotic cells. By 8-hours, healthy cells had partially 'processed' antibody H showing a reduction in MFI (Figure 4.24B-D). This was the case for the lower concentration in cirrhotic cells,

however, with 500ng/mL treated cells a further accumulation of antibody was noted. (Figure 4.24D).

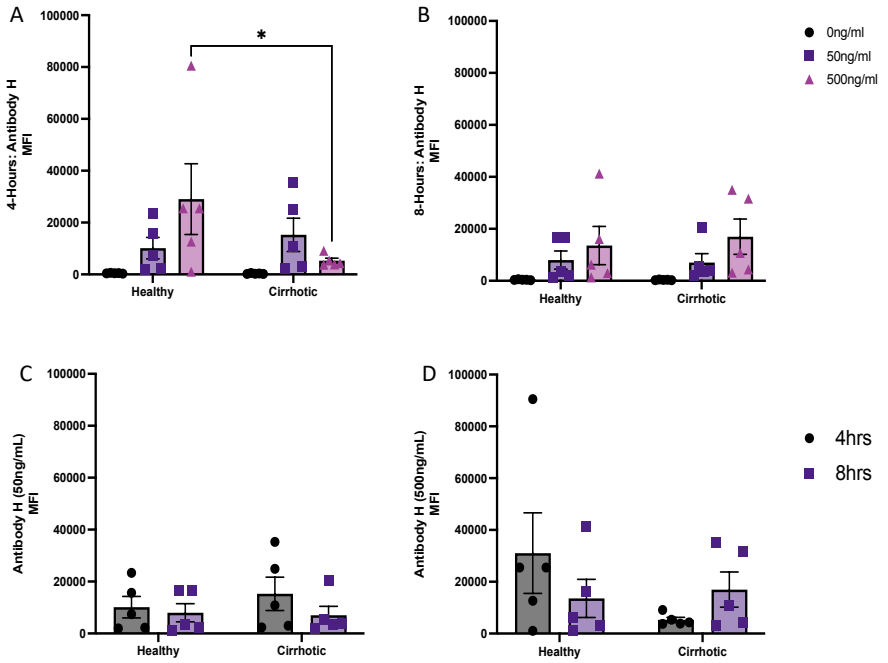


Figure 4. 24: Flow cytometric analysis of Antibody H in healthy and cirrhotic LSEC. LSEC were seeded into 24 well plates and treated with concentrations of 50ng/mL or 500ng/mL of antibody H. Following each time point cells were dissociated from each well and pooled with its corresponding doublet. Each point corresponds to an individual liver (Healthy n=5; Cirrhotic n=5). All steps were performed on ice. Cells were washed with FACs buffer before being fixed for 20 minutes with 4% PFA. Cells were washed twice more, before being permeabilised with 0.1% Triton for 10-mintues and incubated with anti-human IgG1 Alexafluor 488 for 30 minutes. Cells were washed 3x before being analysed using the LSR Fortessa. Flowjo software was used to obtain MFI with data plotted on Prism. A) shows healthy and cirrhotic LSEC incubated with for 4-hours with 50ng/mL and 500ng/mL of antibody H. B) shows the equivalent at 8-hours. C and D are the same data plotted in A and B but allows for better comparison between time points for both 50ng/mL and 500ng/mL of antibody H. Significance was calculated using 2way ANOVA (p=0.044) . Error bars show SEM.

An identical pattern occurred with the second bispecific investigated, **Antibody I**. Significance was observed at 4-hours between healthy and cirrhotic LSEC at the top concentration of antibody. Over the time-course, healthy LSEC treated with 500ng/mL of antibody saw a decrease. Conversely, cirrhotic observed a minor increase in MFI.

Immunofluorescent staining of ARLD LSEC at 4- and 8-hours confirmed this increase in internalisation over time (Figure 4.26). Here, **Antibody I** was detected in vesicles internalised within the cell. At 4-hours this appeared to be more on the peripheral of the

cell, in opposed to the 8-hour localisation which is in closer proximity to the nucleus. In opposition to the flow cytometry data above, when imaging was quantified, the CTCF for healthy vs cirrhotic per cell was on average lower in the non-injured LSEC at 4-hours (Figure 4.27).

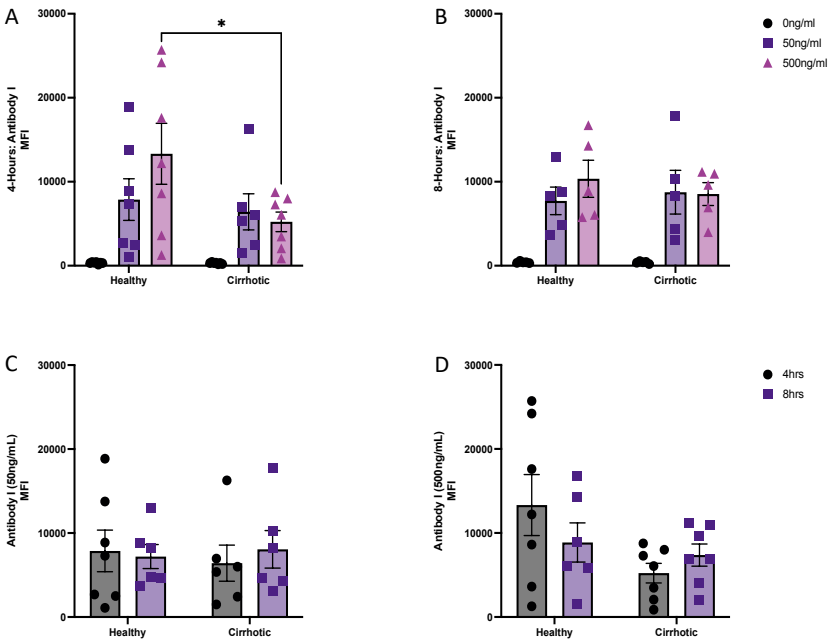


Figure 4. 25: Flow cytometric analysis of Antibody I in healthy and cirrhotic LSEC. . LSEC were seeded into 24 well plates and treated with concentrations of 50ng/mL or 500ng/mL of antibody I. Following each time point cells were dissociated from each well and pooled with its corresponding doublet. Each point corresponds to an individual liver (Healthy n=7; Cirrhotic n=6). All steps were performed on ice. Cells were washed with FACs buffer before being fixed for 20 minutes with 4% PFA. Cells were washed twice more, before being permeabilised with 0.1% Triton for 10-mintues and incubated with anti-human IgG1 Alexafluor 488 for 30 minutes. Cells were washed 3x before being analysed using the LSR Fortessa. Flowjo software was used to obtain MFI with data plotted on Prism. A) shows healthy and cirrhotic LSEC incubated with for 4-hours with 50ng/mL and 500ng/mL of antibody I. B) shows the equivalent at 8-hours. C and D are the same data plotted in A and B but allows for better comparison between time points for both 50ng/mL and 500ng/mL of antibody I. Significance was calculated using 2way ANOVA (p=0.0231). Error bars show SEM.

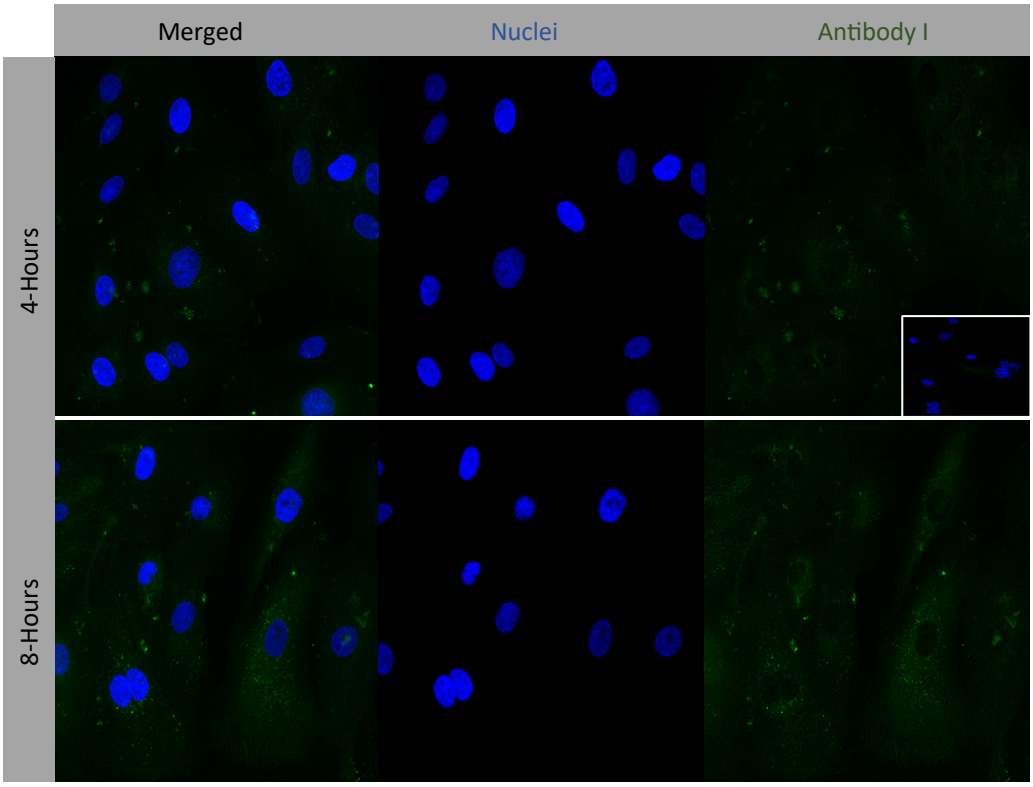


Figure 4. 26: Representative image of Antibody I internalised into healthy LSEC at 4- and 8-hours. LSEC were isolated from healthy tissue. Cells were seeded 70,000 per chamber in Ibitreat IBIDI vi chamber slide and grown until confluent. Treatment with 500ng/mL of antibody I commenced for 4- and 8- hours. Cells were then fixed with 4% PFA for 5 minutes at 37 degrees. Following this, cells were permeabilised with 0.1% Triton x100 for 5 minutes at RT. Incubation with anti-human IgG Alexa fluor 488 for 1 hour took place to allow detection of the antibody I (green). Nuclei (blue) was counterstained with DAPI for 5 minutes. Images taken on LSM780 confocal, 40x with water immersion. Top panel shows 4-hour incubation time, here slight accumulation at the cell membrane can be observed in puncta. The bottom panel shows 8-hours incubation with antibody I, increased levels of punctate fluorescence is observed here. Insert panel shows the isotype matched control (IMC).

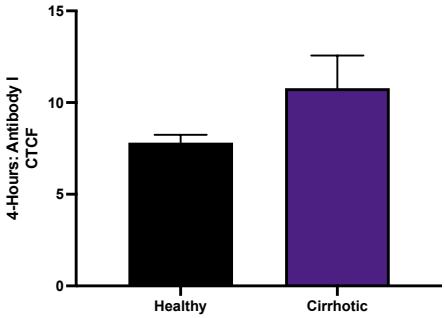


Figure 4. 27: Corrected Total Cell Fluorescence quantification of Antibody I internalisation. Healthy and cirrhotic LSEC (n=4) were incubated with 500ng/mL of Antibody I for 4-hours. Following fixation, permeabilization and staining using an anti-human IgG Alexafluor 488, images were taken on the LSM780 confocal microscope at 40x with water immersion. Images were then quantified in ImageJ. CTCF is calculated by integrated density – (area of selected cells x mean fluorescence of background readings). For this every cell drawn around, an area of background is taken and read, this allows for sufficient background subtraction. CTCF was quantified for each aetiology plotted as mean with SEM. No significance was calculated using Mann-Witney test.

4.3.5 Origin of antibody affects its internalisation and processing rate.

Using the equation outlined in section 2.7.3.3, MFI for each time point was used to assess the capacity of healthy and cirrhotic LSEC to 'process' therapeutic antibodies. Those with a negative % value (green) suggests accumulation of antibody over 8-hours; conversely a positive % value (red) indicates antibody that has been 'processed' so has either recycled back into the media or degraded through lysosomal action. Anti-CD20, Anti-CD20 LAGA and **Antibody G** was not accounted for in this comparison.

Apart from humanized antibodies, all cells treated with 50ng/mL of antibody, behaved similarly (Figure 4.28 upper panel). For example, both human and bispecific antibodies accumulated over time in cells from both aetiologies. Whereas antibodies of chimeric origin saw a loss of ~20% of MFI in healthy and ~13% in cirrhotic cells (i.e., were processed over time). Humanised antibodies were the only therapeutics partitioned differently in cirrhotic and healthy cells. The latter accumulated these antibodies within the cell over 8-hours whereas, their cirrhotic counterparts saw a loss of ~8% of fluorescence over time.

On the other hand, higher concentrations of antibody treatment highlighted more discrepancies in processing mechanisms between normal and cirrhotic cells (Figure 4.28 lower panel). At 500ng/mL of antibody treatment, only humanised antibodies were handled the same by the two cell types. With both exhibiting accumulation over 8-hours. For chimeric antibodies ~20% of MFI was lost in cirrhotic cells, whereas healthy accumulated a small amount of antibody (2%). Bispecific antibodies saw an opposite action with healthy cells showing a higher capacity to sort antibodies with a loss of 25% of MFI, and a gain of ~5% presented in cirrhotic cells. Fully human antibodies saw the most significant difference with a 25% loss in MFI in cirrhotic cells, but a vast ~63% accumulation of human origin antibody in healthy LSEC.

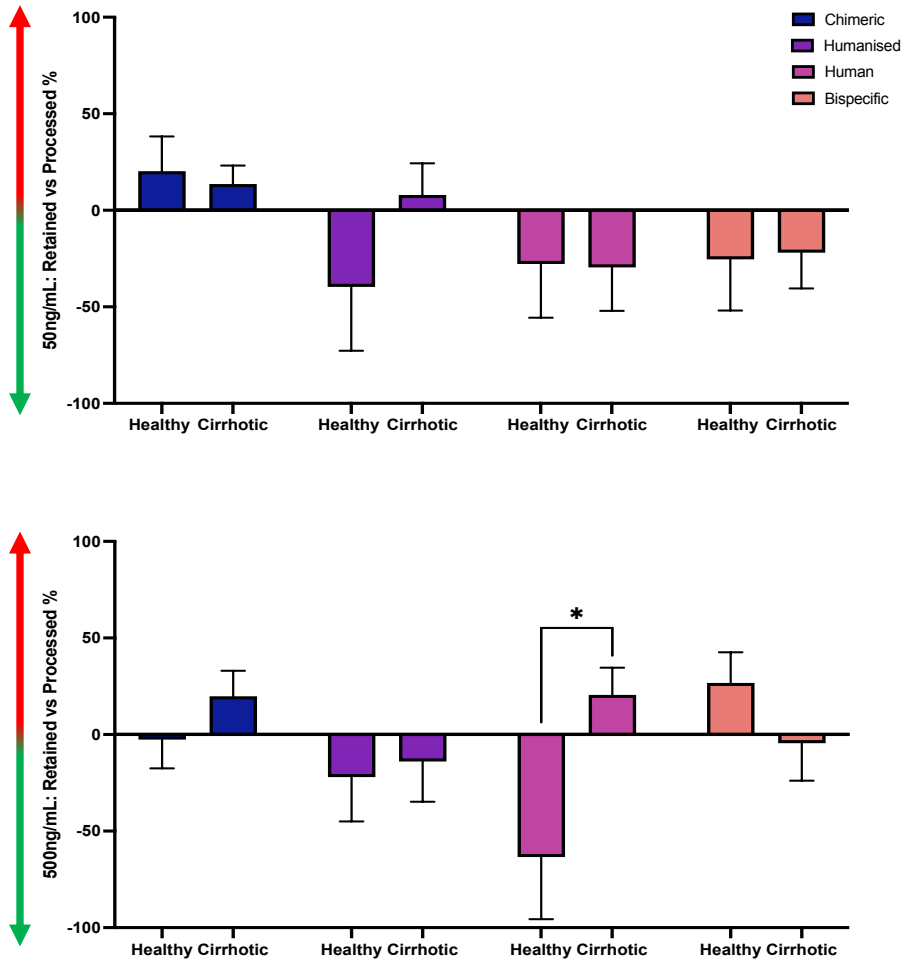


Figure 4. 28: Summary of % Process of MFI. This the shows the average difference in MFI over 4- and 8-hours per each antibody origin for 50ng/mL (top) and 500ng/mL (bottom). To obtain the % process, the 8- hour MFI was subtracted from the 4-hour total then divided by the 4-hour MFI and multiplied by 100 to gain a %. Here positive % (shown by red arrow) shows a loss in fluorescence over time indicating the antibody has been processed. The negative % connoted by the green end of the arrow shows accumulation of the antibody within the cell. The data is plotted as mean with SEM and significance was calculated by 2way ANOVA.

Further comparisons were made between the three antibodies that all targeted the same antigen, CD20. Comparisons between uptake at 4- and 8-hours in healthy and cirrhotic cells with incubation of **Antibody C**, anti-CD20 and anti-CD20 LAGA can be found in Figure 4.29. **Antibody C** of humanised origin consistently presented the highest MFI throughout, with the chimeric anti-CD20 consistently exhibiting the lowest interaction with LSEC. Anti-CD20 LAGA, the equivalent of anti-CD20 with the Fc disabled, saw increased levels of fluorescence to similar of that seen with **antibody C**. Here LAGA antibody at lower concentration was handled similarly by both cell types at 4 hours but by 8-hours cirrhotic LSEC showed a reduction in comparison.

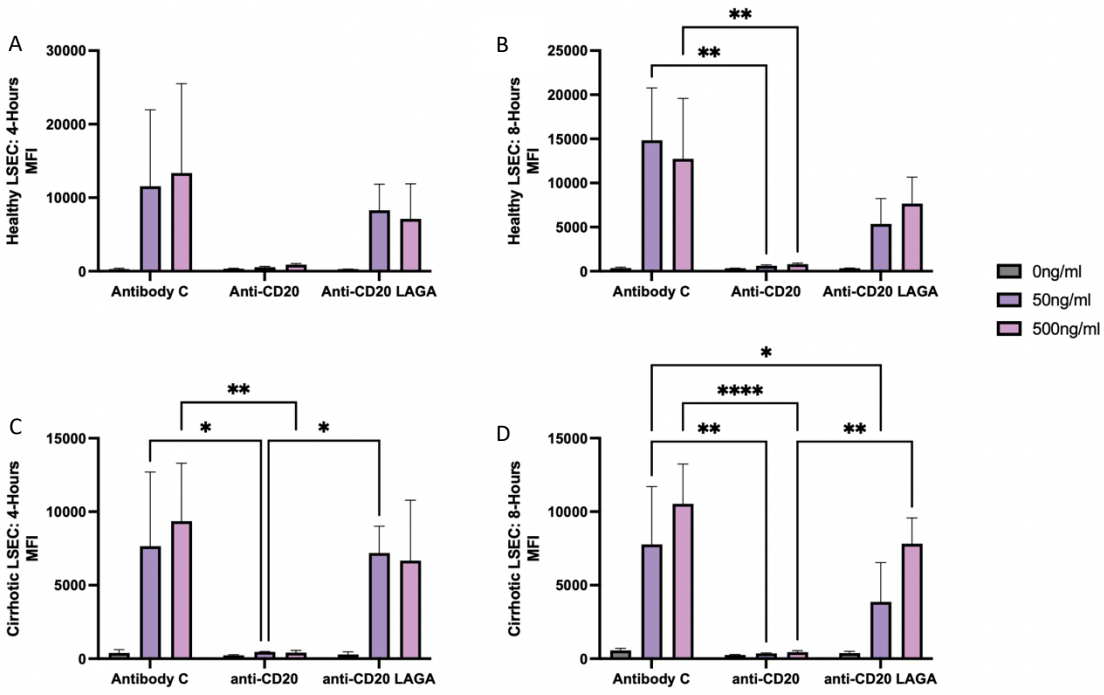


Figure 4. 29: MFI comparison for CD20 targeting antibodies. This figure shows the comparisons of MFI at 4- and 8-hour time points for both cirrhotic and healthy LSEC for antibody C, anti-CD20 and anti-CD20 LAGA which all target CD20. A) shows 4-hours for treatment of all three antibodies at 50ng/mL and 500ng/mL in healthy isolated LSEC. B) shows the equivalent at 8-hours of treatment. C and D show the equivalent in cirrhotic LSEC. Summary of data is plotted as mean and error bars show SD. Significance was calculated using 2way ANOVA.

4.3.6 Discussion

This section aimed to confirm LSEC's ability to bind and internalise therapeutic antibodies and note any discrepancies seen in disease. Here we assessed every GSK asset under consideration over both a 4- and 8-hour period and noted its median fluorescent

intensity by flow cytometry and where able, used immunofluorescence microscopy to contextualise where the antibody localised with the cells over time. This confirmed that LSEC do internalise therapeutic antibody and that discrepancies between healthy and cirrhotic LSEC become evident in a dose dependent manner. Treatment of antibodies at 50ng/mL often led to an increase of accumulation over time, whereas 500ng/mL treated cells exaggerated a varied response, particularly that seen in fully human antibodies. This could be in response to a threshold amount leading to receptor clustering often needed to stimulate a receptor mediated response as discussed in Chapter 3. Regarding % positive we saw no difference over antibodies, and as before there was a discrepancy in an increased number of positive cells when treated with the higher concentration. Furthermore, we also compared LSEC ability to interact with antibodies in the presence of HepG2s (Hepatocyte-like cell line) in a Transwell co-culture. Here we saw no significant effect on HepG2 presence with LSEC on antibody uptake (Supplementary Figure S.3 & Figure S.4).

On average, cirrhotic LSEC processed more antibodies leading to a loss in MFI over time compared to healthy cells. This was in direct contrast to our earlier findings in the HERA ELISA assays but here we have used a more diverse panel of reagents. It would be interesting to revisit the HERA and ELISA assays with some of the bispecific and human antibodies. One of many possible explanations for enhanced processing in cirrhosis may be the on average higher CD206 expression (particularly in protein expression) of cirrhotic LSEC as seen in Chapter 3. This may have led to increased lysosomal enzyme accumulation gearing these cells to have a higher capacity to degrade antibodies rather than accumulate them. To test this though we would need to compare the abundance of these enzymes between healthy and cirrhotic cells to be sure. Healthy LSEC however, showed the largest recorded clearance/processing of bispecific antibodies. This fits with observations that bsAbs are often known for their poor stability and pharmacokinetics.[404] What was interesting was the retention of antibody in cirrhotic cells. Often bispecifics antibodies fail to meet desirable clinical cut offs due to poor PK which is mostly tested in healthy models. The data for cirrhotic LSEC suggests that more

relevant diseased models for preclinical testing may be worthwhile as patients who may have some degree of underlying liver disease are often the target market for said therapeutics.

We also attempted to correlate overall net charge and clearance rates of each antibody to the % processed and initial 4-hour uptake by LSEC and found no association (data not shown). This suggests these are not the cause for the noticeable LSEC uptake and processing discrepancies. However, worthy of note we have no information of any charge clusters or true glycosylation patterns of these antibodies therefore cannot conclude whether this has any influence on disposal in healthy vs diseased cells. What we did observe however, was the association with antibody origin and how healthy and cirrhotic LSEC processed these therapeutics. For instance, despite having the largest clearance rate (31.22mL/day/kg) **Antibody A** and the chimeric antibodies in general exhibited the lowest MFI and therefore the lowest interaction with cells compared to any other antibody class. This was negated when the Fc region was disabled with anti-CD20 LAGA showing similar interaction with LSEC as **Antibody C**. Fab fragments are known to clear from the periphery quite rapidly[404], however in this case our antibody still had its Fc region present, it had just been rendered non-functional. Another possible suggestion for this accumulation of LAGA within the cell is that with a redundant Fc region, FcRn is unable to bind, meaning the antibody cannot be recycled back into the extracellular space. LSEC are known to be incredibly efficient endocytes with some studies suggesting they can internalise cargo and have it processed through to the recycling endosomal compartments within 20 minutes.[405] If this is the case then it is possible, we may have missed this with our time points and the rapid recycling meant that anti-CD20 had already been and gone. Another noteworthy comparison may be that of **Antibody G**, despite being presented as a fully human antibody this could not be detected with an anti-human IgG secondary. Instead via a dot blot I confirmed binding to anti-mouse IgG. This suggests either that the mouse secondary may be causing the low MFI observed (disputed by LAGA MFI though) or this antibody may have originated from humanised mice and this has affected the outcome of the extent of human element to this antibody.

Due to this, **Antibody G** was excluded from the summary seen in Figure 4.28 and will not be considered from this point onwards. Anti-CD20 LAGA was excluded on the basis that it was the only modified antibody present so therefore may skew results and anti-CD20 was excluded also due to its questionable origins similar to that of **Antibody G**.

Fluorescent microscopy was a useful tool to contextualise the location of the antibody within the cells at a small snapshot in time. Often punctate staining of internalised antibody was observed encircling the nucleus within the cell. This has been described previously with clathrin pits associated with adaptor protein 2 (AP-2) in the perinuclear regions. Here this suggested cargo was within the early endosomal compartments as AP-2 is a known adaptor subunit located at the plasma membrane responsible for the initial stages of endocytosis.[406] It would therefore be interesting to colocalize staining for AP-2 with our internalised antibodies and assess whether there are changes in quantity of AP-2 vesicles in cirrhosis.

Both methods used throughout this section were effective tools to quickly screen whether LSEC could interact with therapeutic antibodies and whether they possess the capacity to process these antibodies. As seen throughout this chapter sometimes the MFI obtained via flow cytometry did not always concur with the levels of staining acquired via confocal microscopy, such as seen in Figure 4.14 and Figure 4.15. A possible explanation for this may lay in the fact that flow cytometry is superior in sensitivity and the data is displayed on a log scale in comparison to microscopy.

What we could not confirm via these methods was whether these antibodies underwent lysosomal degradation or were recycled back into the extracellular space. We also possibly limited ourselves by only focusing on two time points as some literature suggests that LSEC may take up to 16 hours (in rat) to transport material to the lysosomes.[405] We sought to rectify this in the following Section 4.4.

4.4 LSEC can divert therapeutic antibody for lysosomal degradation.

As mentioned in the previous section, we were able to observe a loss of interaction between the LSEC and antibody which we termed processing, however we were unable to say whether this loss was due to recycling or via degradation mechanisms. Therefore, we proposed using lysosomal markers to determine the fate of our antibodies and whether there were any differences between healthy and cirrhotic LSEC. As the largest responses had previously been observed for antibody concentrations of 500ng/mL, we decided to use this concentration and initial experiments were ran with anti-CD20 and anti-CD20 LAGA antibodies.

Incubation of anti-CD20 with both healthy and cirrhotic LSEC for 4- and 8-hours was undertaken prior to fixation with 4% PFA. Following this, indirect detection of anti-CD20 via an anti-mouse IgG 488 secondary (AF488) was performed alongside staining for LAMP1, a marker associated with late endosomes/lysosomes (Figure 4.30). At 4-hours very little colocalization is seen however by 8-hours colocalization is evident as indicated by the white arrow in the panel (Fig 4.30). Anti-CD20 LAGA also undergoes lysosomal degradation by the 2nd hour (Figure 4.31). The bottom panel shows a close-up example of said colocalization, for both antibodies with this association occurring in the perinuclear space. Figure 4.31 (middle) shows the CTCF quantification of LAMP1 through 4- and 8-hour treatments with anti-CD20. Here a significant drop in LAMP1 expression is seen over time in healthy cells, this is less prevalent in cirrhotic LSEC but a decrease in expression is evident here too.

To assess the capacity of LSEC to transport cargo to the lysosome we wanted to compare the mRNA expression of *AP3M1* between cirrhotic and healthy cells (Figure 4.31 right panel). This gene encodes adaptor protein 3 (AP-3); this subunit is responsible for the budding of vesicles and involved in the trafficking of lysosomes. The gene was expressed in both healthy and diseased cells with no significant difference between each aetiology. However, the median expression and variation in expression was marginally higher in cirrhotic LSEC.

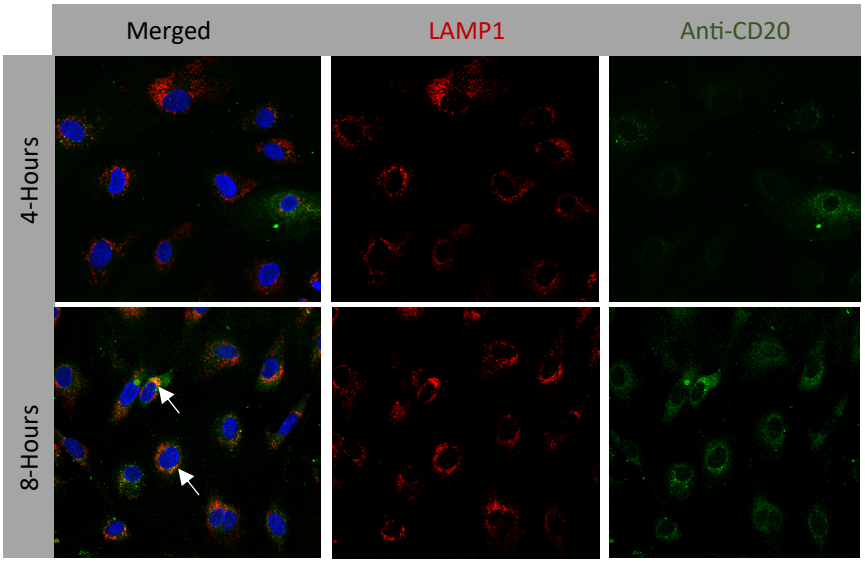


Figure 4. 30: Representative images of CD20 colocalising with lysosomal marker LAMP1. Healthy isolated LSEC were seeded at 70,000 per chamber in Ibidi vi slide and left overnight to settle. The following day cells were treated for 4- and 8-hours with anti-CD20 before being washed and fixed with 4% PFA. Subsequent immunofluorescent staining was then performed by first permeabilising the cells with 0.1% Triton x100 for 5minutes at room temp. Following this incubation with LAMP1 took place for 1hr before washing and then further incubation with a cocktail of anti-mouse AF488 and anti-Rabbit AF647 secondaries to detect anti-CD20 and Lamp1 respectively. Nucleus was counterstained using DAPI. Images were taken on the LSM780 40x with water immersion. White arrows indicate the points of colocalisation.

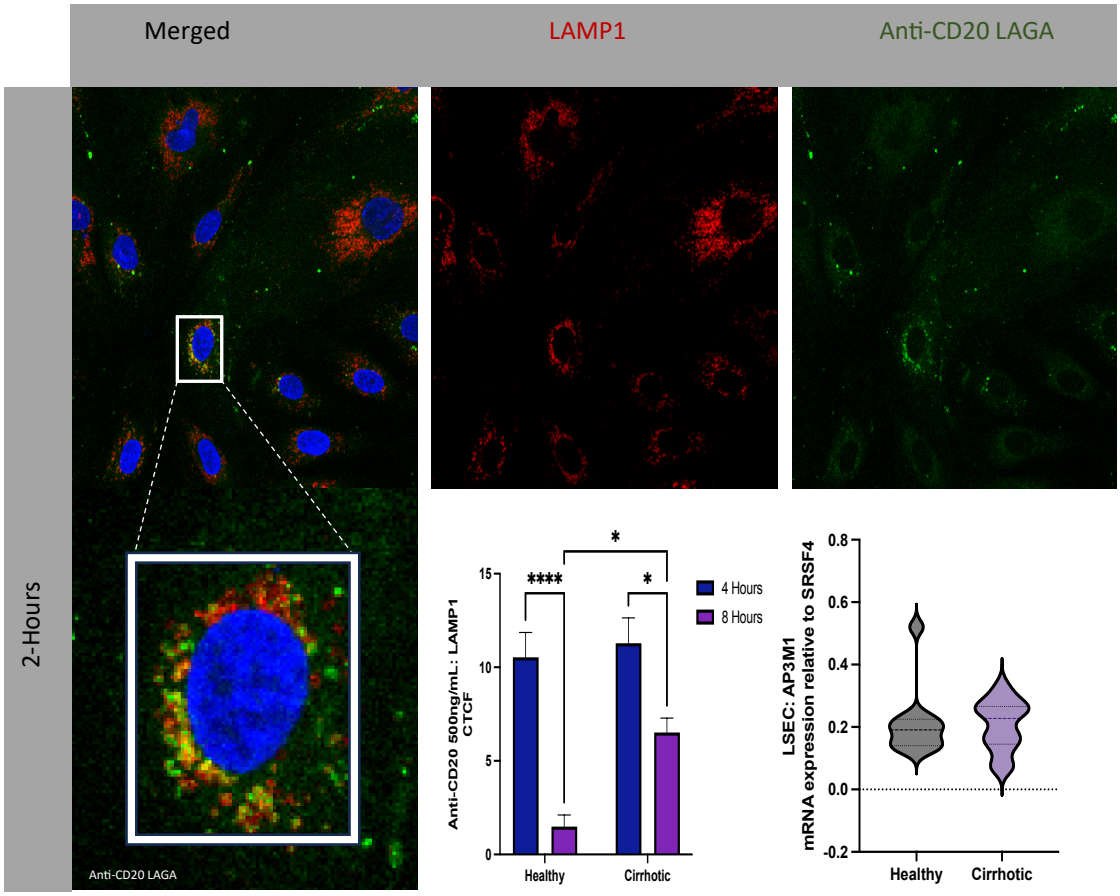


Figure 4. 31: LSEC capacity for lysosomal degradation. Healthy isolated LSEC were seeded at 70,000 per chamber in Ibidi vi slide and left overnight to settle. The following day cells were treated for 4- and 8-hours with anti-CD20 LAGA before being washed and fixed with 4% PFA. Subsequent immunofluorescent staining was then performed by first permeabilising the cells with 0.1% Triton x100 for 5minutes at room temp. Following this incubation with LAMP1 took place for 1hr before washing and then further incubation with a cocktail of anti-mouse AF488 and anti-Rabbit AF647 secondaries to detect anti-CD20 and Lamp1 respectively. Nucleus was counterstained using DAPI. Images were taken on the LSM780 40x with water immersion. White box leads to a zoomed-out example of co-localisation of LAGA and LAMP-1. The bar chart to the right shows the CTCF of LAMP1 over a 4- and 8- treatment period with healthy and cirrhotic LSEC, here significance was calculated using 2-way ANOVA *p= <0.05; **** p=<0.0001. The violin graph shows the mRNA expression of *AP3M1* relative to *SRSF4* between healthy (n=11) and cirrhotic (n=14) LSEC.

For better resolution we next sought to live image LSEC using conjugated therapeutic antibodies. The chosen antibodies: D (humanised), E (human) and I (bispecific) were conjugated to Alexafluor 647 (AF647) prior to being incubated on cirrhotic and healthy LSEC. Images were taken at 2-, 8- and 22-hours. Quantification of AF647 vesicles showed **antibody D** treatment in healthy LSEC led to a continual significant increase of vesicle burden over time (Figure 32A). Conversely, following an increase in antibody internalisation in cirrhotic LSEC, by 22-hours this was reduced.

Figure 4.32B and C depict the colocalisation seen between lysoview (lysosomal stain) and vesicles positive with **antibody D**. Here -1 indicates a perfect negative correlation, +1 shows absolute positive association and 0 equals no relationship. Positive correlation was seen with all 3 therapeutics. In the case of **Antibody D,** both healthy and cirrhotic cells saw an increase association over time. Representative images of **Antibody D** internalised in both healthy and cirrhotic LSEC are shown in Figure 4.33 over the time course. The top two panels show healthy LSEC stained with cell tracker green internalising AF647 conjugated **Antibody D** at the 2-hour time point. This highlights the vesicular staining of the internalised antibody often present in what appears to be vacuoles within the cell. Most is localised around the nucleus but staining is also seen throughout. The panels below show example images from which the quantification of vesicles and co-localisation were obtained. Here blue shows the lysosomes (lysoview) and red depicts the AF647 labelled **Antibody D**. Upon colocalisation this appears purple. Here co-localisation is present throughout each panel, however, is more prevalent in the 22-hour incubation point for both cirrhotic and healthy LSEC. The cirrhotic cells are not all positive unlike that healthy LSEC where antibody is present in all cells.

The fully human antibody, **E**, was found in a larger number of vesicles in cirrhotic in comparison to healthy cells. On average for both cell types a reduction in vesicles was seen overtime, although this was more significant in cirrhotic LSEC. Again, cirrhotic cells exhibited the highest association with lysosomes by the 22nd hour (Figure 4.32B). But both, showed equal increases over time. Exemplar images of this therapeutic can be found in Figure 4.34, here the top panel shows 63x magnified image of healthy LSEC incubated with **Antibody E** for 22-hours. This panel allows for interpretation between what is colocalised (purple) and what is not (red). As shall be seen throughout the live imaging data, all antibody appears to be internalised into vesicles. These antibody-loaded vesicles increase over time for both healthy and cirrhotic panels alongside evidence of colocalisation with lysosomes. Once again, more healthy cells contain antibody than cirrhotic cells.

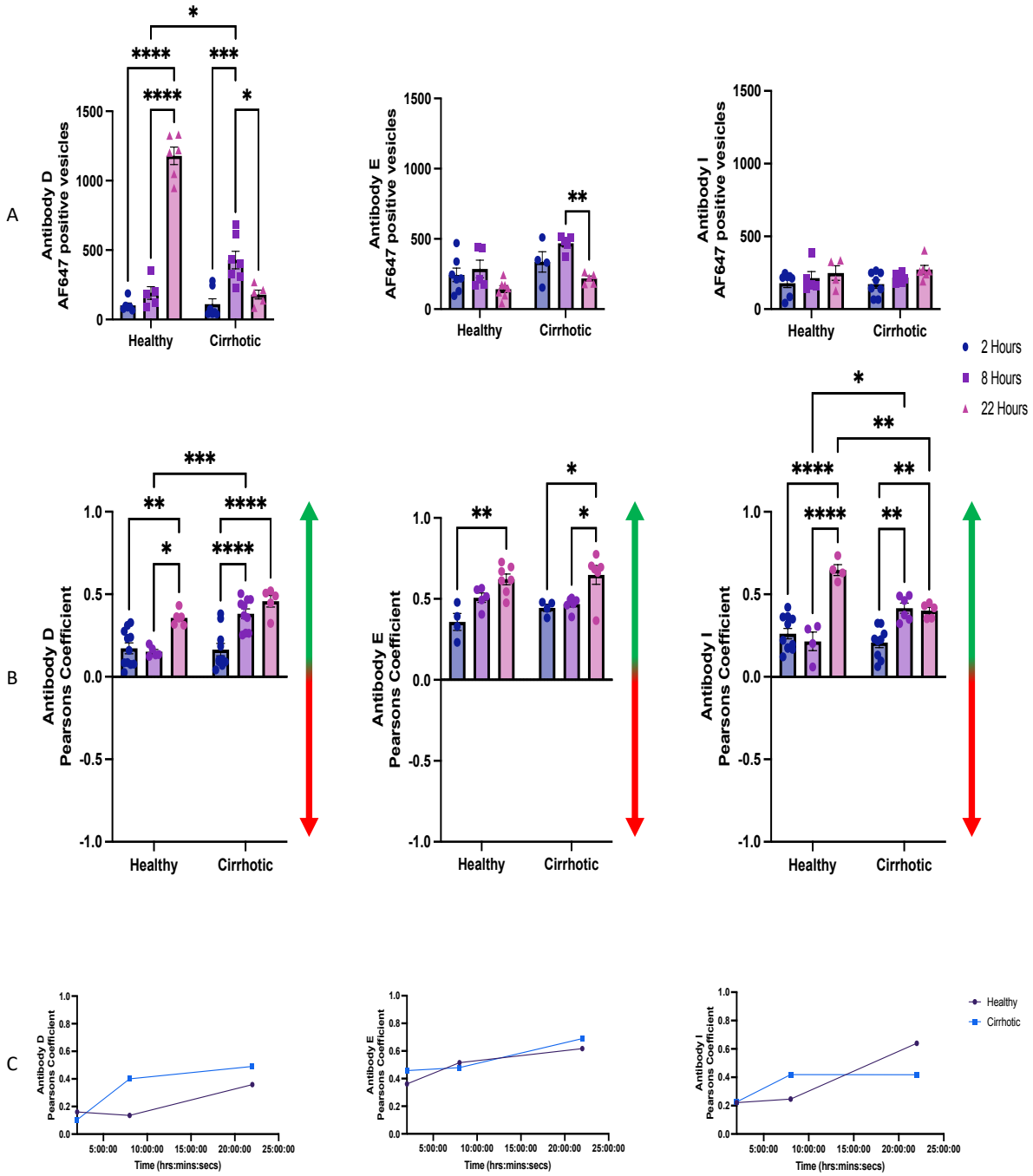


Figure 4. 32: Colocalisation of Antibody D, E, and I with lysosomes in LSEC. LSEC were seeded at 70,000 per chamber in IBIDI and left overnight to settle. The following day, 500ng/mL antibody D, E, and I conjugated to Alexafluor 647 was incubated on cells alongside the addition of lysoview DND. Live imaging was taken at time points 2-, 8- and 22-hours. Row A (top) shows the quantification of AF647 positive vesicles. Row B shows the Pearson coefficient showing the colocalisation with lysoview at each time point. Here the range runs from -1 (perfect negative correlation; red arrow) to +1 (absolute correlation between the two; green arrow). Row C shows the same data as Row B but in a different layout to allow side by side comparison between healthy and cirrhotic cells.

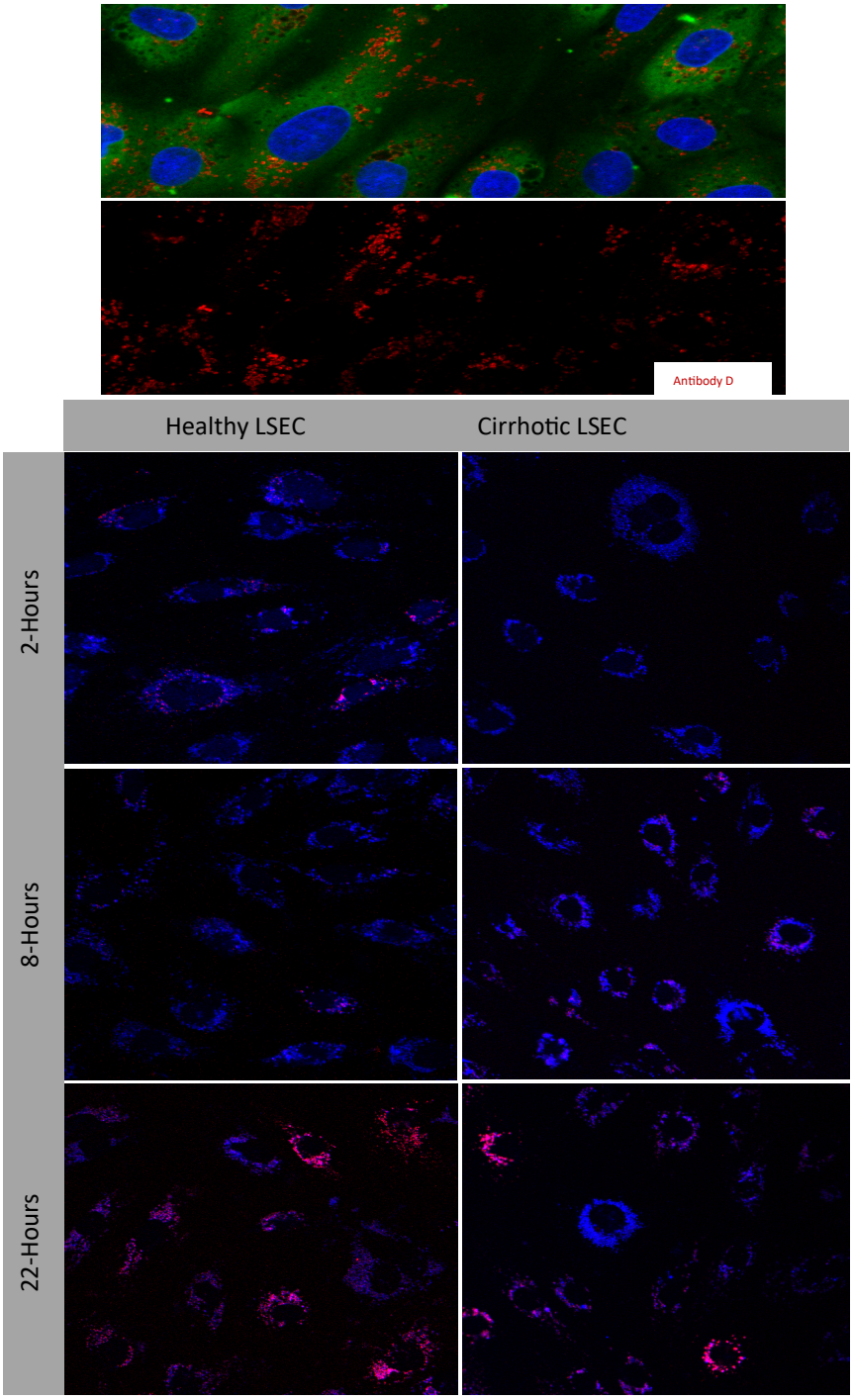


Figure 4. 33: Antibody D localisation within the lysosomes. The very top two images shows LSEC stained with cell tracker green incubated with Antibody D (red) for 2-hours. Nuclei counterstained with DAPI. The below panels show LSEC incubated with antibody D AF647 (red) and lysoview DND (blue) for 2-, 8- and 22-hours. Images were captures on the LSM780 40x with water immersion.

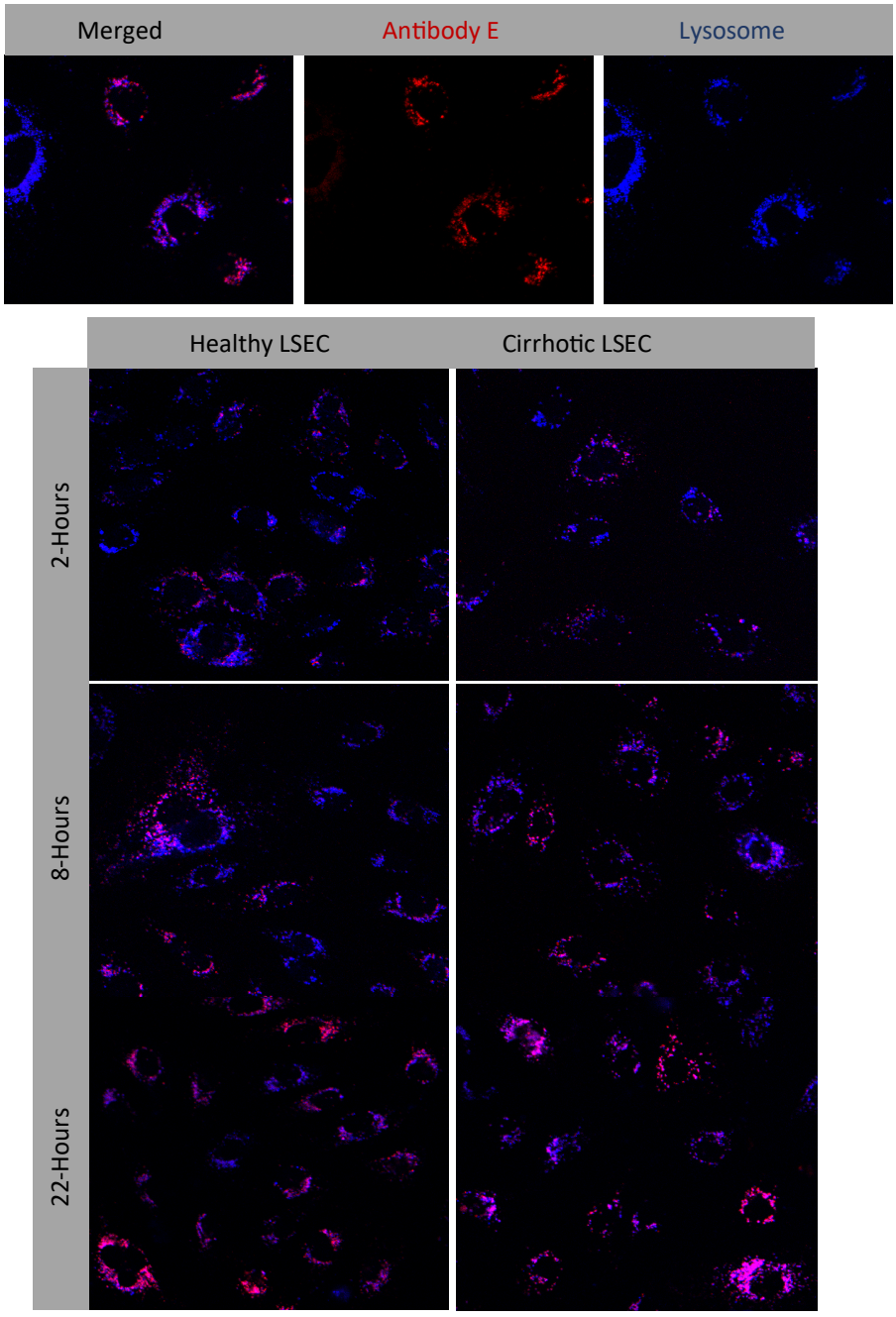


Figure 4.34: Antibody E localisation within the lysosomes. The very top images show LSEC stained with Antibody E (red) and lysoview DND (blue) for 22-hours imaged at 63x. This allows comparison between the signal channel read and merged to be contrasted for the below images. The below panels show LSEC incubated with antibody E AF647 (red) and lysoview DND (blue) for 2-, 8- and 22-hours. Images were captured on the LSM780 40x with water immersion.

The bispecific **Antibody I** was found in the lowest number of vesicles in comparison to the other two antibodies; however, it did still increase in abundance over time. Healthy LSEC shows a significantly higher association between antibody and lysosome than cirrhotic cells particularly at the 22-hour point. At the 8-hour point a higher association with **Antibody I** and the lysosomes are seen within cirrhotic cells, however this levels out over the rest of the time course. Representative images of localisation staining can be found in Figure 4.35. The top panel shows cell tracker green stained LSEC incubated with the bsAb for 2-hours. Punctate staining is present throughout the cells and also encircles the nucleus. This image shows antibody loaded vesicles are found near the lysosomes but not fully co-localised at this point. There are time course differences between healthy and cirrhotic LSEC. At 2-hours, most cirrhotic cells show little colocalisation between therapeutic and lysosome, whilst the opposite is the case for healthy LSEC. By 4-hours, both see an increase in colocalization, and this is further exaggerated by the 22-hour end point.

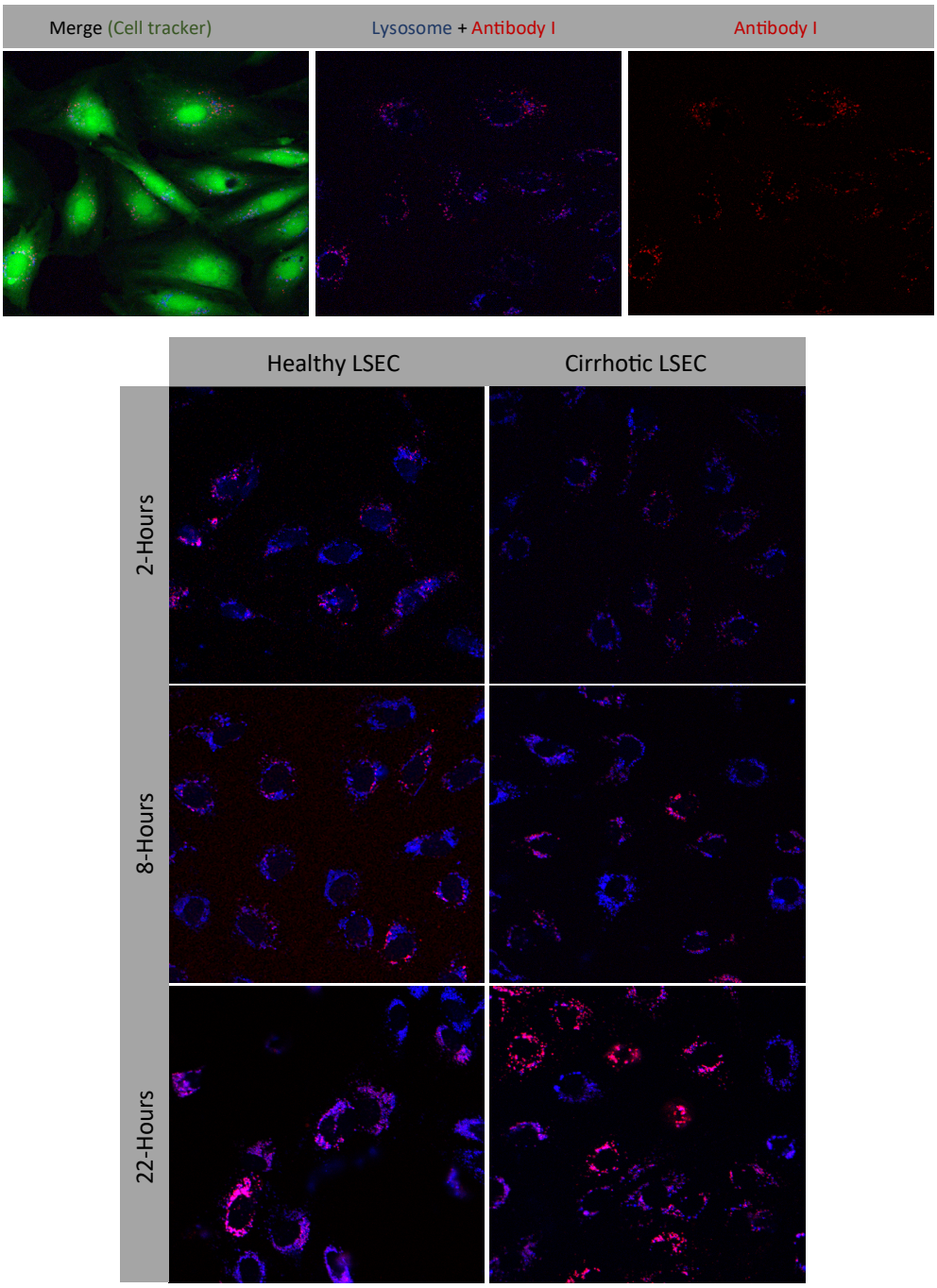


Figure 4. 35: Antibody I localisation within the lysosomes. The very top panel shows LSEC stained with cell tracker green incubated with Antibody I (red) for 2-hours at 40x . The below panels show LSEC incubated with antibody I AF647 (red) and lysoview DND (blue) for 2-, 8- and 22-hours. Images were captures on the LSM780 40x with water immersion.

4.4.1 Discussion

LSEC are known for their high functionality in the process of endocytosis, however despite knowledge that they hold ~17% of the liver's lysosomal volume[407], these cells are often overlooked regarding their role in the non-specific clearance of therapeutic antibodies. By incorporating lysoview into our immunofluorescence assay, we were able to conclude that LSEC trafficked most internalised therapeutic antibodies towards the route of lysosomal degradation.

Initially we used a fixed imaging method whereby we localised the antibodies to LAMP-1 positive structures. During the maturation of endosomes, they acquire new markers in which allows us to differentiate between early and late endosomes. LAMP-1 was initially chosen as its very closely associated with lyso-endosomes[408], a pathway we were interested. As an added benefit the antibody isotype matched the needs for our co-localisation studies with other antibodies. Initially we also attempted to measure colocalisation with the early endosomal marker, EEA-1. Despite successful single staining of cells with this reagent, when incorporated with the secondary used to detect anti-CD20 we were unable to see any signal of this endosomal marker. The hosts of both staining regents were different and changing order of staining primaries and secondaries didn't prevent this loss in signal. Therefore, we relied on staining with the later marker. Here we saw LAMP1 expression fall considerably over the 8-hour anti-CD20 treatment period in healthy cells but not as significantly in cirrhotic LSEC. Referring to the initial proof of concept flow cytometry data obtained on the Cyan, here we also saw a vast loss in % positivity of cells with anti-CD20 in healthy than in cirrhotic, this corresponds suggesting that this loss here was due to degradation within the lysosomes. It has been found that among alcohol abusing HIV-induced liver injury patients that alcohol damages and suppresses lysosomal biogenesis and function.[409] It was found under alcohol exposure that lysosomal leakage and apoptosis was increased and defective migration of the lysosome biogenesis transcription factor, TFEB along the microtubules was observed.[409] Furthermore, the repressor of TFEB, ZKSCAN3 was upregulated under alcohol intake.[409] Majority of our cirrhotic cohort was made up of ARLD patients

therefore, this dysfunction in the lysosomes may have resulted in our delayed loss of LAMP1 expression. To note, cirrhotic LSEC capacity for clearance was not uniform, for some antibodies it showed increased lysosomal association and loss of antibody laden vesicles over time. This is suggestive of pathway being dependent on antibody specificity.

LAMP-1 expression is expected to be upregulate during the trafficking process and often stays at this level to maintain the lysosomal compartments following degradation.[410] The fact we are seeing such an exaggerated response once again suggests we may be possibly missing the earlier trafficking and degradation stages of these antibodies. Anti-CD20 LAGA was also seen to be co-localised with LAMP-1 within 2-hours, this is vastly different to the expected time points seen in other studies. Although, to my knowledge this has not been investigated in human LSEC, in rat models and M1LEC (immortalised LSEC mouse cell line), internalisation and transportation to the late endosomes took ~20minutes.[401,405] By 2-hours this process was complete, however, at this timepoint only 2.5% of ligand was trafficked to the lysosome.[405] This increased to 53% by 16-hours. This slow process was not reflective of any of our findings, often with positive correlation with the lysosomes seen within 2-hours. This may be due to the human element of our experiment or factors in how we isolate/ grow our cells in comparison to that seen in the above studies.

Fixed imaging often leads to considerable background staining therefore this process could not be automated for quantification. Due to this we moved to a live imaging approach using conjugated antibodies and lysoview DND. We only received enough antibody to conjugate for a very select number of antibodies therefore we had to narrow our experiments down to focus on three key therapeutics. **Antibody D**, **E**, and **I** were chosen as they were of different origins: humanised, human, and bispecific respectively and gave the most interesting variances in the flow cytometry data. We understood that using a non-specific NHS ester kit to conjugate these antibodies may cause changes in properties and function. However, this was allayed when imaging and flow data corresponded with our live imaging trends.

We adapted the time points which we imaged to 2-, 8- and 22-hours through optimisation. At the 1-hour timepoint we often saw no signal of antibody within the cell, therefore 2-hours was chosen. This was interesting as in humans we saw rapid partition into the lysosomes in comparison to rat LSEC, however, here observed a far slower internalisation in the initial stages. Rat LSEC saw cargo within the late endosomes within 20-minutes[401,405], no signal was obtained by us until 2-hours. Again, this further suggests animal vectors are no appropriate for PK analysis regarding LSEC functionality. We kept the 8-hour time point as often this was the key differentiator between healthy and cirrhotic LSEC. Then 22-hours was added as this was an overnight incubation step in which cells were still 'happy' with having a concentrated therapeutic and lysoview still incubated on them but also allowed us to investigate the reduction or gain over an extended period.

We found as the humanisation proportion of the antibody increased so did the colocalisation with lysosomes over time. For instance, **antibody D** of humanised origin exhibited the lowest colocalisation overall whereas **antibody E**, a fully human mAb showed consistently the highest colocalisation in both healthy and cirrhotic LSEC. **Antibody D** also, showed the most dramatic divergence between healthy and cirrhotic cells in terms of number of vesicles positive for the antibody. In healthy cells this shows a slow rate of internalisation with a mass increase by the 22-hour mark, whereas in cirrhotic cells it appears this had already met its threshold of internalisation and had already begun lysosomal degradation as evidenced by the increased levels of colocalisation at the 8- and 22-hour point. Healthy LSEC only demonstrated a rise in lysosomal colocalisation by the 22-hour mark just as abundance of antibody had soared. This heightened clearance response was also seen in cirrhotic cells treated with antibody E. Looking at the mRNA expression levels of *AP3M1*, a gene encoding for AP-3 an integral subunit of the internalisation and trafficking process to the lysosome[411], cirrhotic cells saw a higher expression on average of this gene than healthy LSEC. Although not significant, it suggests a possible reason why cirrhotic cells were capable of increased levels of clearance in both the flow cytometry data and in reduction of vesicle count.

Suggesting they have more endosomal machinery adept to traffic these mAbs to the lysosome than healthy LSEC. Although this was not an exhaustive look at this pathway, further research would need to be carried out to assess how the AP-3 trafficking pathway was affected in cirrhosis. As mentioned previously, the bispecifics were the type of antibody where healthy LSEC showed the highest association between therapeutic and lysosome. This matched the difference observed in the % processed summary from the flow cytometry data; here healthy LSEC saw a loss in MFI over time which correlates with the increase in lysosomal localisation. Thus, healthy cells were particularly able to process bispecific antibody, as seen in the *in vivo* clearance rates seen in table 4.1. I could not find any literature relating to antibody type and handling in lysosomes, excluding one study where it was suggested larger antibody (in this case nanoparticles attached to a mAb) led to increased accumulation within the lysosomes.[412] However, as our bispecifics are only slightly larger than the mAbs in this panel, we saw no real difference between antibody type and association rates.

In a study using cell surface labelling and electron microscopy, a surface charge distribution was obtained across healthy LSEC.[413] Here it was found that cationic residues resided within coated pits, whereas negatively charged patches were sporadically spaced throughout the entire cell membrane including these pits.[413] Despite no statistical significance noted with overall net charge and MFI earlier, it is worth mentioning here that **Antibody D** had the highest overall net charge and pI (5.2 and 8.23 respectively). This could possibly be an explanation for the increased amount of **Antibody D** positive vesicles observed over the 22-hour period. With increased basic residues on the antibody this would mean increased electrostatic attraction leading to increased internalisation. **Antibody E** and **I** both have similar net charge at 3.3 and 3.4 with the same pI at 7.9, possibly explaining the similar numbers of vesicles observed. It is unknown whether this charge distribution changes in liver injury, if so this may explain some of the differences observed in uptake of therapeutics in cirrhotic cells.

4.5 Summary

A summary of findings for each antibody can be found in Table 4.2. The aim of this chapter was to establish whether LSEC could internalise and process therapeutic antibodies. Initial experimentation through the HERA and ELISA assays were unsuccessful, however through flow cytometry we were able to confirm LSEC could indeed interact in a non-antigen specific way with therapeutic antibodies. Through microscopy it was confirmed that these antibodies were internalised into vesicles within the cells. Both methods showed that in a dose dependent manner, LSEC isolated from cirrhotic and normal liver processed these antibodies differently and at different rates. For instance, fully human antibodies exhibited the most significant discrepancy in health and disease with the former leading to the accumulation within the cell over 8-hours and the latter having most likely begun the process of being degraded by lysosomes as per the positive colocalisation correlation. Human LSEC presented a much faster mechanism for trafficking antibody to the lysosomes than previously described in animal and immortal cell lines, with association present within the lysosomes by the 2nd hour of incubation for both cirrhotic and healthy cells.

The following chapter looks to interrogate the route of internalisation to further elucidate why this partitioning into degradation differs between health and diseased LSEC.

Table 4.2: Summary of Chapter 4 results

Origin	Name	Isotype	Target	Findings
Chimeric	Anti-CD20	IgG1	CD20	Dose-dependent response Low uptake overall; loss in MFI over time Staining: Vesicular and perinuclear.
	Anti-CD20 LAGA	IgG1	CD20	Dose dependent response High uptake similar to antibody C. Increase in MFI for healthy cells. For cirrhotic cells- low concentration sees reduction in MFI, high concentration shows an increase in MFI. Staining: Perinuclear and vesicular.
	Antibody A	IgG1	Phosphatidyl-serine	Dose depend in cirrhotic, blunted in NL. Similar response in both, minimal reduction in MFI at 500ng/mL
Humanised	Antibody B	IgG1k	SLAMF7	Blunted dose response in NL, not cirrhotic. Both aetiologies saw MFI reduction over time. Staining: Perinuclear and vesicular.
	Antibody C	IgG1	CD20	Dose dependent response. Both aetiologies show increase over time. Staining: Localisation at cell membrane at 8-hours.
	Antibody D	IgG1	IL-4	Dose dependent uptake in both. Accumulation over time in lower concentrations, loss at high concentrations in NL. Staining: present at the membrane at 4-hours, increased vesicles number up until 22-hours. Slow degradation rate.
Human	Antibody E	IgG1 kappa	IL-6	Dose dependent uptake. Gained MFI over time in NL, lost in cirrhotic LSEC. Fixed imaging: Fibrous throughout the cell. Live imaging: vesicular Max fluorescence/vesicular and CTCF at 4hours reduced by 8-hours Degradation via lysosomes
	Antibody F	IgG1	IGF-1R	Dose dependent uptake. Similar MFI over time at low concentrations; gain at 500ng/mL in NL.
	Antibody G	IgG1 kappa	CD38	Blunted dose response in NL, not cirrhotic. Cirrhotic MFI similar over time, low concentrations saw a loss of MFI, high concentration saw a gain in NL.
Bispecific	Antibody H	IgG + dAb	IL-4/IL-13 (dAb)	Dose dependent uptake in healthy but not cirrhotic. Significance seen in 4-hour uptake at 500ng/mL between NL and cirrhotic. Healthy loss in MFI over time, cirrhotic gained
	Antibody I	IgG + dAb	IL-5/IL-13 (dAb)	Same as above Staining: Vesicular Higher lysosomal degradation evidenced in healthy LSEC.

Chapter Five: Mechanism elucidation for Internalisation of antibody by LSEC.

The previous chapter established that LSEC possessed the ability to internalise and catabolise therapeutic antibodies. This capacity and rate of internalisation/clearance was determined by origin of antibody and differed between healthy and cirrhotic cells. In this chapter we seek to answer the 4th aim set out in this thesis: to elucidate the means responsible for off-target clearance. In doing so, this will extend our knowledge of clearance mechanisms and may inform preclinical therapeutic design to improve PK and clinical success. This chapter will look at exploring whether antibody uptake is a receptor mediated or fluid phase pinocytic process. We have studied the binding kinetics and capacity of each receptor investigated in Chapter 3 alongside using both direct and indirect techniques to interrogate individual proteins involved in potential internalisation mechanisms. This was undertaken in both healthy and cirrhotic LSEC to distinguish whether the difference in processing we have reported, is associated with the method by which each internalises these mAbs and bsAbs. To note, due to availability of reagent, not every antibody was assessed, where possible justification for using particular antibodies will be discussed in the relevant section.

5.1 Each receptor can bind to the Fab region of antibodies

In previous comparisons between anti-CD20, anti-CD20 LAGA, and **antibody C** (Figure 4.29), we observed that disabling the Fc of this chimeric antibody led to similar uptake at 4-hours as seen for the humanised antibody, **C.** Therefore, we next wanted to briefly explore how the Fab regions of these two anti-CD20 antibodies differed in binding to the three receptors of interest: CD206, CD32b and LSIGN. Computational modelling was utilised with protein docking by PIPER through the server ClusPro (AbeMAP)[415,416], and structures were obtained from the protein data bank (Pymol was used to remove ligands and domains where needed). For each receptor modelled consisted of: LSIGN carbohydrate recognition domain and two repeating units of the neck was modelled. For

CD32b the interaction site consisted of its ectodomain, and CD206 was split into different C-type lectin domains (CTLD): 2 (pH 4; including the CysR), 3 (*p*H 7;including CysR) and 4. The ClusPro system ranks the top 30 docked models and reports the most residual members within the cluster alongside the lowest energy required to bind, taking into account the attraction and repulsion of Van der Waals, electrostatic energy (Coulombin and Born approximations) and structure based potential generated by the Decoys as the reference state (DARS) to show the solvation effects.[417] To note this data is only predictive, to truly ascertain whether these clusters are able to bind these Fab fragments, site directed mutagenesis would need to be performed. Figure 5.1 shows an example image of the top ranked docked model for anti-CD20 and **antibody C** Fabs bound to CTLD2 of CD206, the red mesh area shows the binding site.

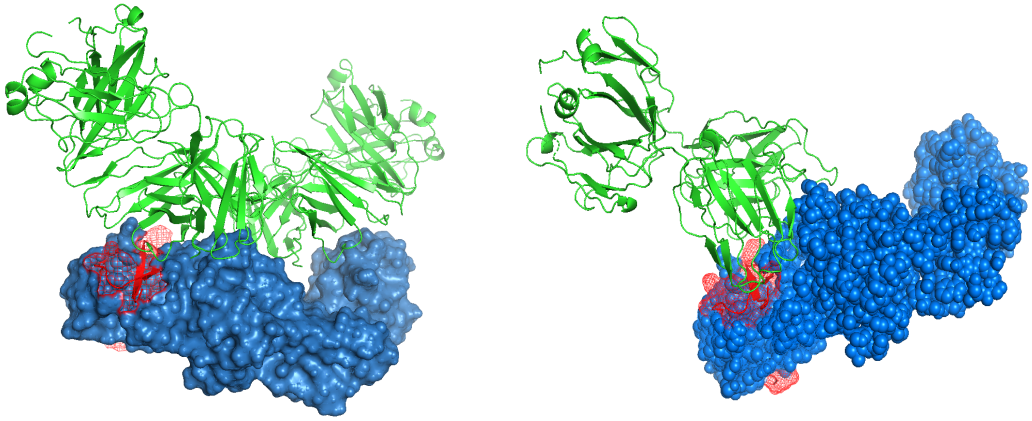


Figure 5. 1 Fab fragments docking to CD206. Left shows CD20 Fab fragment (green) bound to c-type lectin domain 2 (blue), the red mesh highlights the area of interaction. Right shows similar with **antibody C** (green). Proteins were available in the protein data bank and manipulated in Pymol. Each ligand was added into the ClusPro software where the PIPER algorithm rotated the receptor around the Fab fragment 70,000 times noting the top 1000 clusters able to bind. This then bottlenecked down to 10 through assessment of number of members within a cluster and the lowest required energy needed to bind. This image shows the top ranked docked model from this software.

Table 5.1 shows the topped ranked models for each receptor per mAb Fab and how they ranked in terms of members within the cluster alongside the energy required for binding from the centre of the cluster. The more members and the lower the energy the better. For both mAbs, CD32b provided the highest number of members per cluster but not the lowest energy required to bind. For anti-CD20 this was found to be with LSIGN which

also had the second largest cluster size. **Antibody C** on the other hand saw the lowest energy expenditure with the CTLD2 at *p*H 4 (modelled in Figure 5.1B).

Table 5. 1 ClusPro analysis of Antibody C and anti-CD20 fab fragments to receptors.

		Antibody C (Fab only)		Anti-CD20 (Fab only)	
Receptor (Domain)		Cluster Members	Centre energy	Cluster Members	Centre energy
CD32b		128	-270.9	75	-291.5
LSIGN		74	-338.2	70	-446.9
CD206	CysR-CTLD2 (pH 4)	108	-402	59	-282.6
	CysR-CTLD3 (pH 7)	67	-279.0	52	-271.6
	CTLD4	82	-397.0	60	-325.5

CysR- cysteine residues, CTLD- C-type lectin domain

This showed the predicted ability of all receptors able to bind to the Fab region of these two antibodies. Therefore, we undertook the following functional tests described in the following sections to investigate which if any receptor was primarily responsible.

5.2. Direct approaches to determine receptors responsible for antibody internalisation

5.2.1 Impact of CD206 siRNA on antibody traffic

To assess the role of CD206 in the off-target uptake of antibodies we used siRNA to silence this receptor via transient knockdowns (KD). These cells underwent the same assay as described throughout Chapter 4 whereby flow cytometry was performed at 4- and 8-hours to assess association with the therapeutics and MFI was documented and compared to cells without siRNA knock down. Gene and protein silencing through knockdown was confirmed and validated using qPCR and western blots respectively (Supplementary Figure S.5). Flow cytometry analysis was also carried out on scrambled siRNA treated LSEC to control for non-specific lipofectamine effects.

With **antibody B**, data showed *MRC1* KD LSEC overall saw a reduction in average MFI for antibody accumulation in both healthy and cirrhotic cells (Figure 5.2). Hence antibody uptake at early timepoints was reduced in MRC1 KD cells. Significance was calculated in cirrhotic LSEC at 4-hours at a treatment concentration of 500ng/mL. This difference was less evident at the 8-hour time point in cirrhotic cells due to the loss of MFI over time in the non-treated cells.

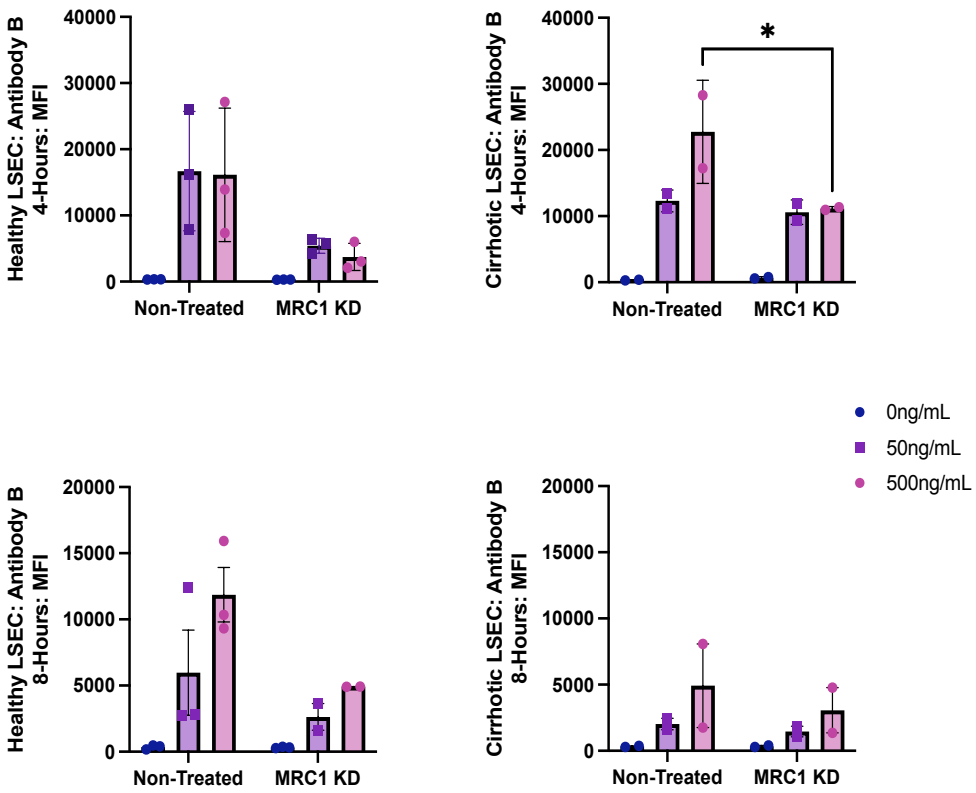


Figure 5. 2 Flow cytometry analysis of *MRC1* KD LSEC. Healthy and cirrhotic LSEC underwent siRNA knockdown for *MRC1* prior to being treated with antibody B (humanised) for 4- (upper panel) and 8-hours (lower panel). Following this flow cytometry analysis was performed and MFI was recorded and compared to untreated LSEC. Error bars indicate SEM, significance calculated through 2-way ANOVA. Significance seen at 500ng/mL at 4-hours in cirrhotic LSEC p=0.0393.

A similar trend in healthy LSEC was seen with **antibodies A** (chimeric) and **F** (fully human)(Figure 5.3). **Antibody I** however, showed an increase in MFI in *MRC1* KD LSEC at the first time point (4-hours) but then presented a loss in MFI at the latter time point in

comparison to normal healthy LSEC (figure 5.3). No significance was observed throughout.

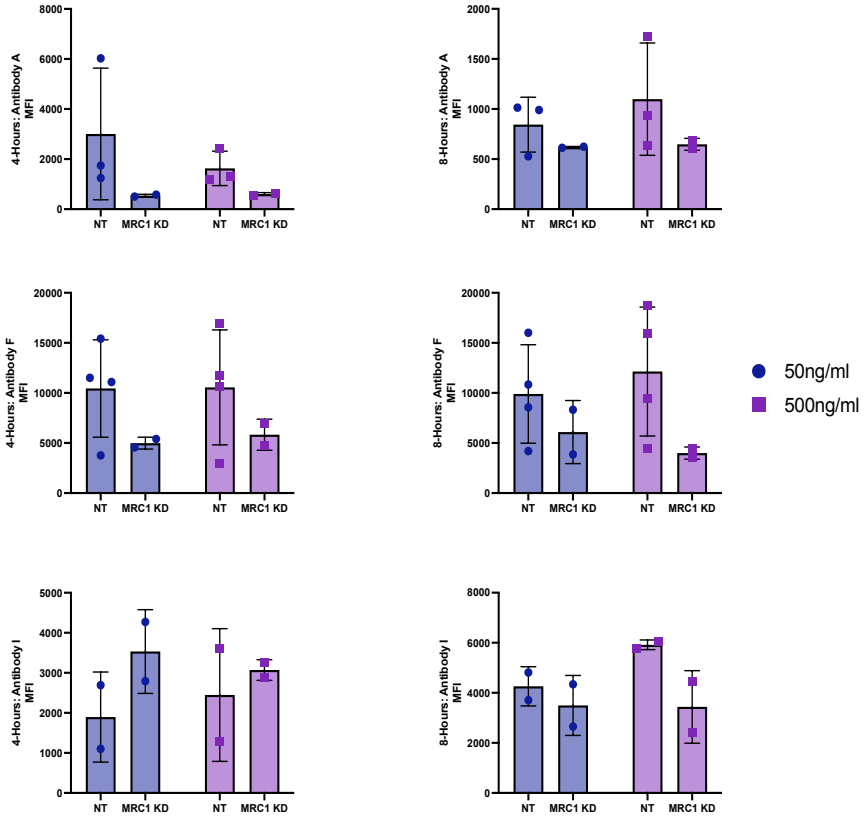


Figure 5. 3: Flow cytometry analysis for *MRC1* KD healthy LSEC. Healthy LSEC underwent siRNA knockdown for *MRC1* prior to being treated with antibodies A (chimeric), F (human), and I (bispecific) for 4- and 8-hours. Following this flow cytometry analysis was performed and MFI was recorded and compared to untreated LSEC. Error bars indicate SD, no significance was calculated through 2-way ANOVA. Each point indicates a separate liver.

Next, I used SPR to assess the binding kinetics of CD206 with 6 chosen antibodies, here RSV LAGA and RSV wildtype (WT) were used as controls. This experiment did not go as expected and of the 6 antibodies used, none, even the controls, registered either association or dissociation data. **Antibody A** was excluded due to off-target binding. **Antibody B** and **D** were the only antibodies to show a slight change in the sensograms but following subtraction of the baseline no meaningful data was obtained (all sensograms are available in Supplementary Figure S.6, those for antibodies **A, B** and **D**

can be seen in Figure 5.4). Thus, we cannot be sure of any direct interaction between CD206 and our test reagents using this methodology.

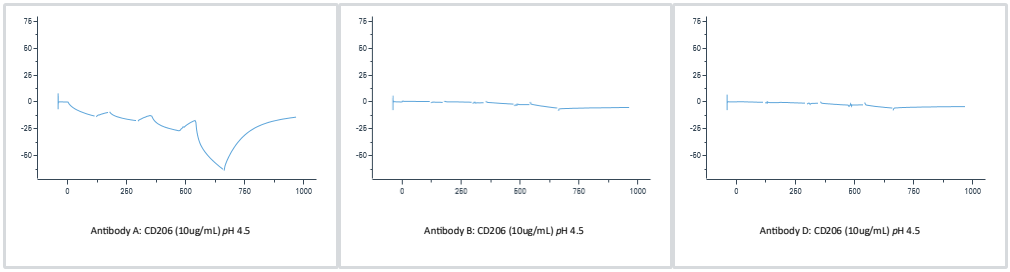


Figure 5. 4: SPR sensograms for CD206: Single cycle kinetics were performed on 8K Biacore SPR instrument at *p*H 4.5 for antibody A, B and D on CD206. Here antibody A (chimeric) was excluded for off target (chip) binding. Very little interaction was evident for antibody B (humanised) and D (humanised). Plotted for the 1:1 Langmuir equation to attempt to determine K_D.

Thus, we returned to a whole cell uptake approach with fluorescently conjugated antibodies. Unfortunately, not enough **antibody B** was available to conjugate however, as shown previously **antibody D** was successfully conjugated to Alexafluor 647 (AF647). Therefore, we assessed whether this mAb was still internalised following *MRC1* KD in LSEC and compared colocalisation with the lysosomal compartments. Alongside **Antibody I** which showed a varying response in the *MRC1* KD cells through flow cytometry, we incubated these antibodies for 4-hours on healthy LSEC to compare number of AF647 positive vesicles between KD and non-KD cells, reflecting differential uptake of the antibody (Figure 5.5).

No difference was seen in quantity of vesicles between non-treated (n=3) and *MRC1* knockdown (n=3) cells with either antibody **D** or **I**, nor was any difference observed in the extent of colocalisation between each treatment group. The representative images below reflect this finding with AF647 often being located close to the lysosomes however, very little overlap was seen at this time point. Importantly here the comparison “control” cells had been treated with scrambled siRNA to compare the effects of lipofectamine on uptake. These looked very much like untreated cells. To ensure knockdowns did not impact lysosomal quantity, these were quantified and

compared between each treatment group, and on average per cell was shown to be equal. Thus, KD or lipofectamine did not alter lysosome number or ability of **antibodies D** and **I** to internalise.

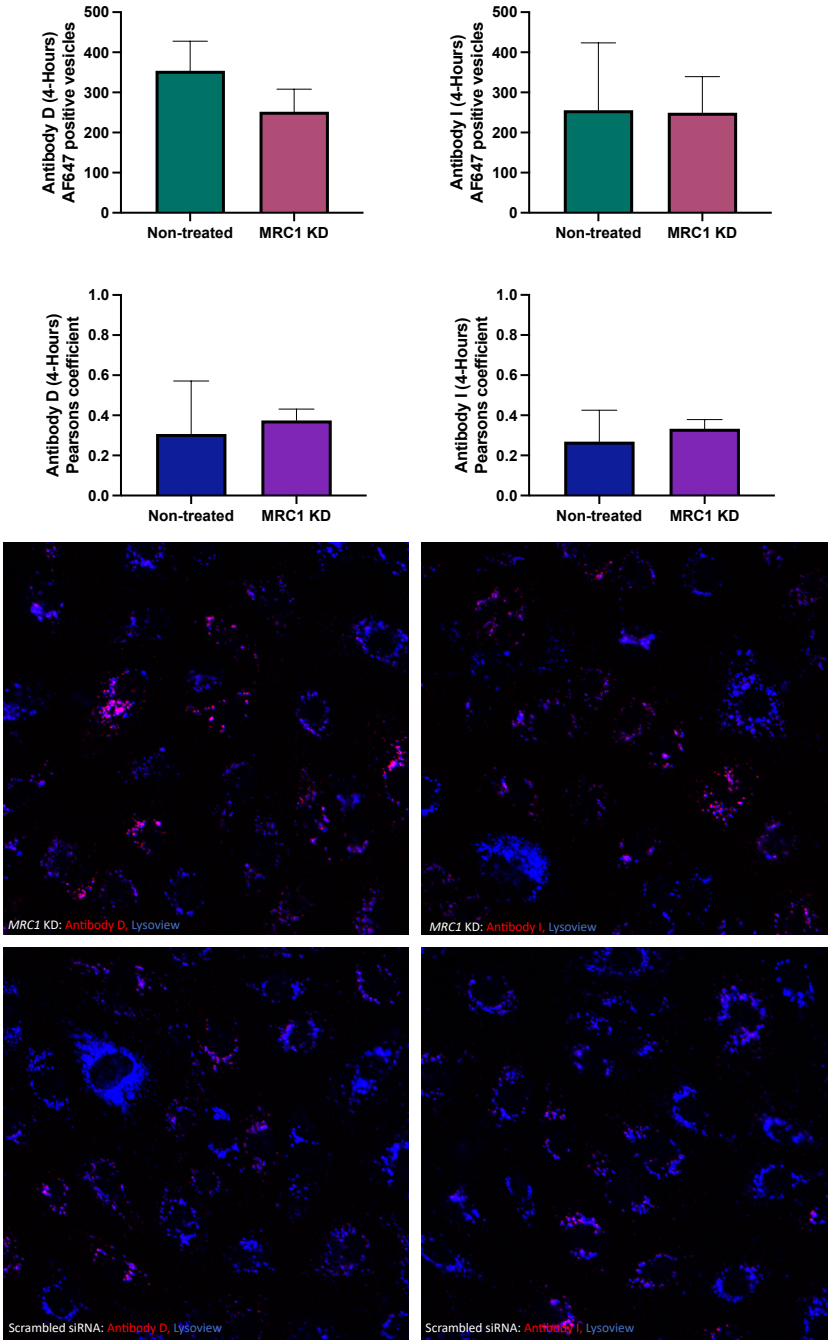


Figure 5. 5 Confocal analysis of *MRC1* KD on cirrhotic LSEC. LSEC were isolated from cirrhotic livers. Following culture and passaging cells were separated into *MRC1* siRNA knock down group (n=3) and scrambled siRNA (n=3). LSEC were then treated with 500ng/mL of conjugated antibody D and I (red) alongside lysoview DND (blue). Images were taken on the LSM780 confocal at 4-hours (40x, water immersion). 5 fields of view per n was taken and averaged. Quantification was undertaken in ImageJ whereby AF647 positive vesicles were counted and colocalisation quantified for antibody and lysosome.

5.2.2 Impact of LSIGN (*CLEC4M*) siRNA on antibody traffic

Knockdowns were performed silencing *CLEC4M*, with validation of loss of expression confirmed by qPCR (Supplementary Figure S.7). Following flow cytometry analysis, at 4-hours all antibodies showed a trend for reduction of MFI in KD cells. However, this was only significant for **antibody I** at 500ng/mL (Figure 5.6). Unfortunately, samples were lost for **antibody A** and **C** at the 8-hour mark therefore are not shown. Uptake of **Antibody F** was reduced by KD at 4- and 8-hours, with overall accumulation of antibody similar at both time points. **Antibody I** however showed a slight increase in fluorescence over time in the knockdown cells, whilst control cells showed the highest signal at the earlier timepoint. As with the *MRC1* KD cells, only a small number of replicates were possible so results may not be fully representative.

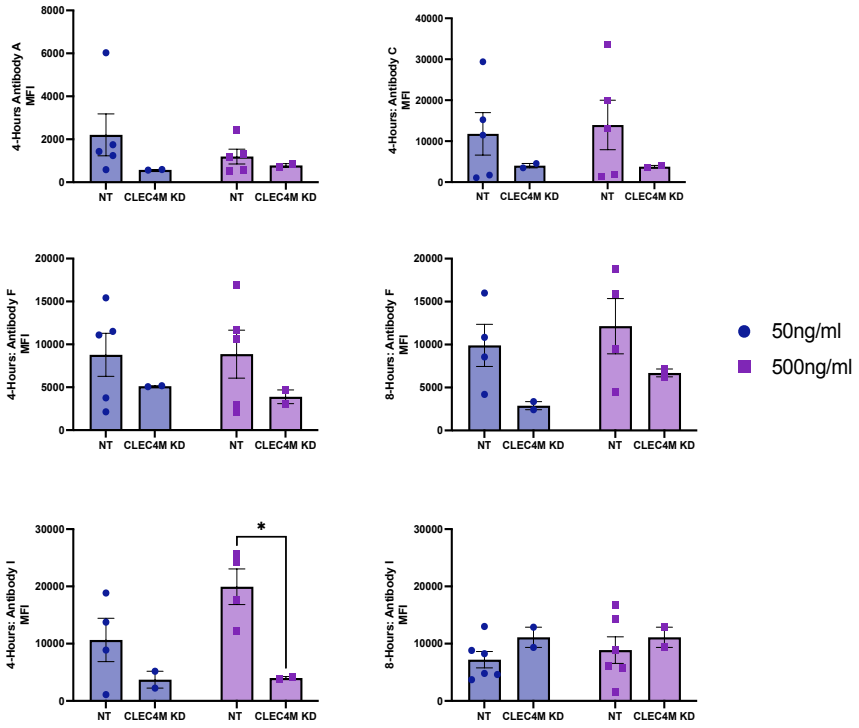
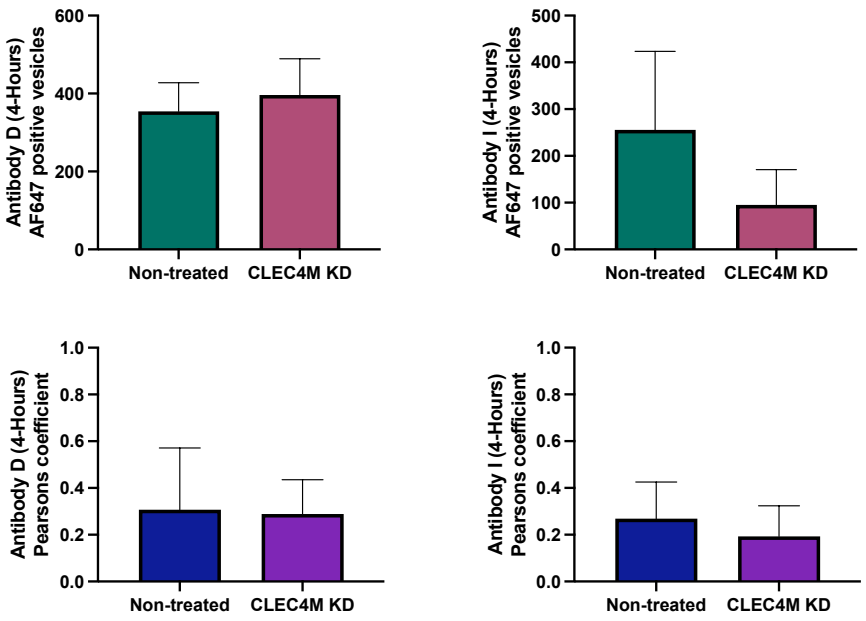


Figure 5. 6 Flow cytometry analysis for LSEC with reduced *CLEC4M* expression. Cirrhotic LSEC underwent siRNA knockdown for *CLEC4M* prior to being treated with antibodies A, F, and I for 4- and 8-hours. Following this flow cytometry analysis was performed and MFI was recorded and compared to untreated LSEC. Significance was calculated through 2-way ANOVA with significance seen at 500ng/mL for 4-hour treated with antibody I ($p=0.0317$). Error bars show SEM.

SPR was also performed using a recombinant CD209 and the same 6 antibodies alongside RSV WT and RSV LAGA. Observations were the same as before with **antibody A** exhibiting high off target binding and no data being able to be obtained from this protocol. Sensograms can be viewed in Supplementary Figure S.8. Immunofluorescence uptake of conjugated AF647 **antibody D** and **I** in non-treated and *CLEC4M* KD LSEC was once again performed considering the failure of the SPR. No statistical significance was observed. However, image analysis suggested there was a decrease in **antibody I** positive vesicles after knockdown in the 4-hour samples, as hinted in the flow cytometry data. However, there was quite large variation, particularly in the control cells. **Antibody D** uptake appeared unaffected by knockdown. Both antibodies were still found within lysosomes after knockdown and this association was unchanged by treatment (Figure 5.7).



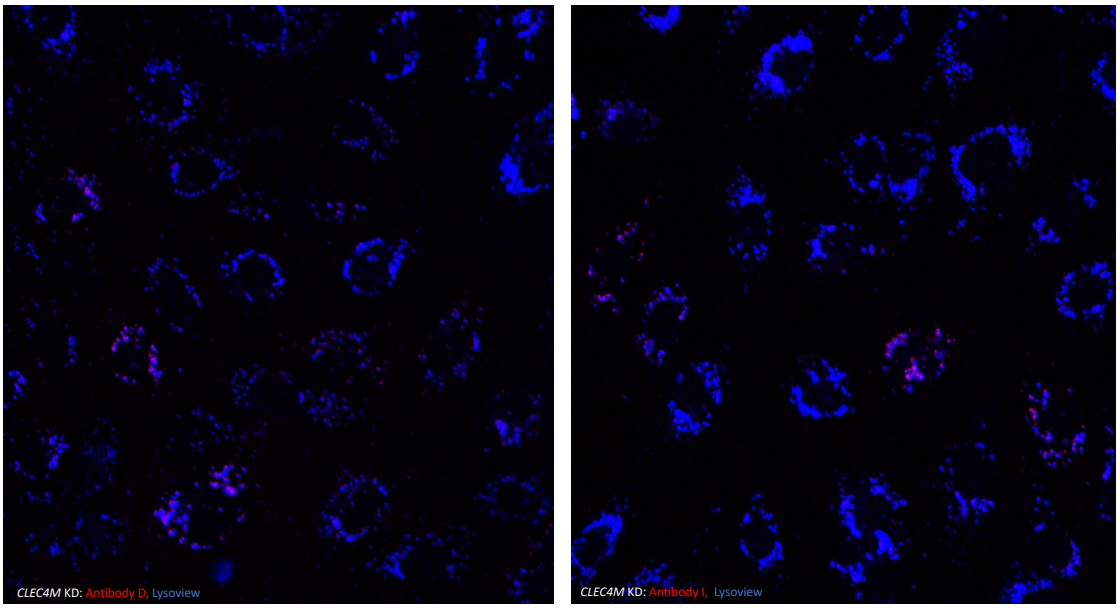


Figure 5. 7: Confocal analysis of *CLEC4M* KD on cirrhotic LSEC. LSEC were isolated from cirrhotic livers. Following culture and passaging cells were separated into *CLEC4M1* siRNA knock down group (n=3) and scrambled siRNA (n=3). LSEC were then treated with 500ng/mL of conjugated antibody D and I (red) alongside lysoview DND (blue). Images were taken on the LSM780 confocal at 4-hours (40x, water immersion). 5 fields of view per n was taken and averaged. Quantification was undertaken in ImageJ whereby AF647 positive vesicles were counted and colocalisation quantified between antibody and lysosome.

5.2.3 The impact of CD32b on antibody traffic

As CD32b was often completely lost in passaged LSEC (Figure 3.19), particularly in cirrhotic cells, we approached analysing this receptor differently. Firstly, we sought to assess the binding kinetics of all 6 antibodies with CD32b via SPR as we had with the other receptors. However, for this protein we did see successful interactions within the flow cell. Here the equilibrium dissociation K_D constant and R_{max} (maximal response when all ligand is occupied) was reported. Data for CD32aR and CD32aH was also generated (Table 5.2). Antibody **A** and **F** were rejected due to off target binding. Data are shown in Table 5.2 and here lower K_D values indicate stronger binding affinity. Overall, CD32aH displayed the highest affinity for all antibodies, with **antibody C** having the highest affinity. This was followed by CD32aR, here **antibody D** exhibited the strongest affinity for this receptor and **antibody I** having the lowest. Regarding CD32b, this displayed the lowest affinities in total of the 3 receptors. Here **antibody C** exhibited the highest affinity, with **antibody D** presenting the lowest.

Table 5. 2: SPR analysis of binding kinetics for CD32aH, CD32aR and CD32b

Receptor	Antibody	KD (M)	R_{max}
CD32aH	Antibody A	Rejected	Rejected
	Antibody B	$3.66x10^{-6}$	119.9
	Antibody C	$1.90x10^{-6}$	123.1
	Antibody D	$2.76x10^{-6}$	151.5
	Antibody F	Rejected	Rejected
	Antibody I	$3.48x10^{-6}$	135.8
CD32aR	Antibody A	Rejected	Rejected
	Antibody B	$1.22x10^{-5}$	146.2
	Antibody C	$3.84x10^{-3}$	31747.1
	Antibody D	$5.89x10^{-6}$	103.7
	Antibody F	Rejected	Rejected
	Antibody I	$2.48x10^{-2}$	294842.5
CD32b	Antibody A	Rejected	Rejected
	Antibody B	$6.08x10^{-2}$	312128.0
	Antibody C	$1.08x10^{-2}$	96385.3
	Antibody D	$8.69x10^{-2}$	487397.2
	Antibody F	Rejected	Rejected
	Antibody I	$7.60x10^{-2}$	272608.4

KD- equilibrium dissociation constant; R_{max} – maximal response when all ligand is occupied. M- molarity.

Regarding assessing CD32b function in cells, we first went for an indirect non-specific approach and incubated LSEC with Fc blocker prior to and during incubation with anti-CD20. Following this, we chose a fixed stain microscopy approach alongside flow

cytometry. This was performed on the Cyan cytometer prior to gaining access to the Fortessa, therefore as before only % of cell fluorescence was recorded (Figure 5.8).

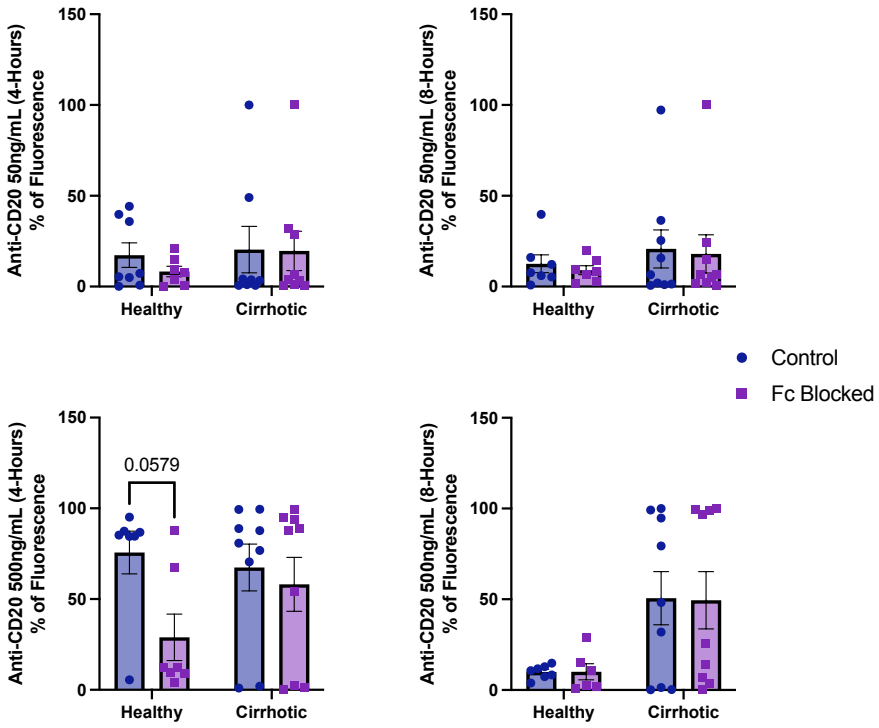


Figure 5. 8: Fc block effects on internalisation in cells. Fc block was incubated on both healthy (n=8) and cirrhotic (n=9) LSEC for 30-minutes prior and during incubation with anti-CD20 for 4- and 8-hours. Following to this cell were dissociated from the 24-well plate, stained with a secondary anti-mouse Alexafluor 488, and analysed using the CyAn cytometer and % of fluorescent cells recorded. No significance was found with 2-way ANOVA and error bars show SEM.

Here very little difference was observed when Fc block was used, with the exclusion of the 4-hour treatment with 500ng/mL of anti-CD20. Here a close to significant reduction in the % of cells positive for anti-CD20 was observed. For the microscopic approach, CTCF quantification of anti-CD20 antibody internalised into cirrhotic LSEC (Figure 5.9), suggested no difference after Fc blockade. Number of LAMP1 positive vesicles was unchanged by treatment also. These were quantified per cell of LSEC isolated from one liver and separated over several technical replicates. Therefore, comparisons between treatment can be made for the same donor. A representative image of 500ng/mL of anti-CD20 treated, Fc-blocked LSEC can be found below. Imaging was similar to that seen in the non-treated cells shown in Chapter 4, with vesicular staining present in the

perinuclear region at the 4-hour timepoint shown. Thus, FC blockade had little impact on antibody internalization.

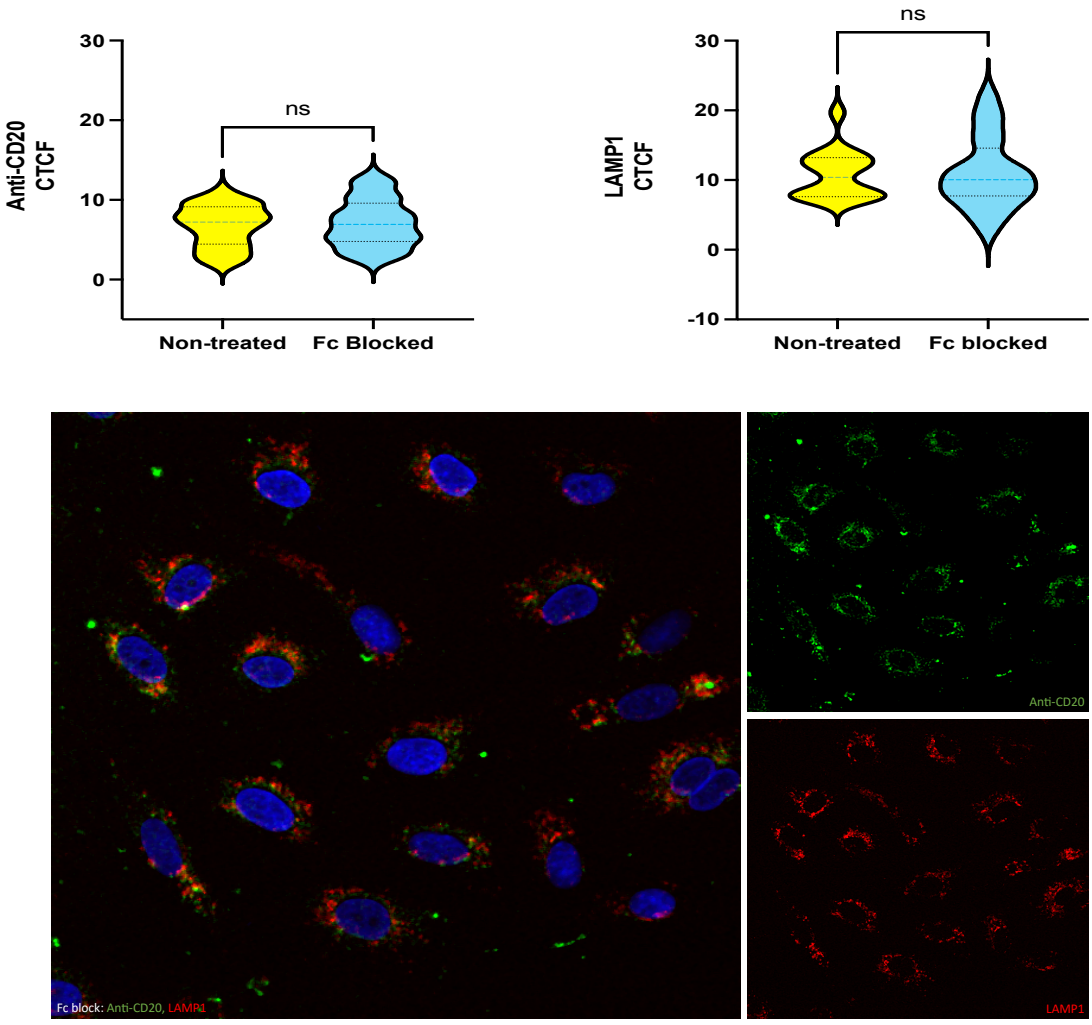


Figure 5. 9: Confocal analysis of impact of Fc-block on anti-CD20 internalisation. LSEC were seeded 70,000 per chamber into an Ibitreat Ibidi chamber. Fc block was incubated on cells for 30 minutes prior to the addition of anti-CD20 (Fc block was added into the media here too). Following incubation for 4-hours cells were fixed using 4% PFA. LSEC were then permeabilised with 0.1% Triton X-100 for 5 minutes prior to staining with anti-mouse IgG Alexafluor 488 and LAMP1 for 30 minutes at room temperature. Nuclei were counterstained with DAPI. Cells were imaged on the LSM780, and images were quantified via ImageJ. CTCF for both antibody and LAMP1 were recorded. No significance was confirmed.

In Chapter 3, we described how IOX2 led to an increased expression of CD32b at both the mRNA and protein levels. With this information we employed the gain in expression to assess how this impacted the uptake of anti-CD20. Although we were only able to do pilot experiments given the time available, **Antibody C** (Figure 5.10) showed reduced

fluorescence in IOX2 treated cells at every time point excluding that of 50ng/mL at 8-hours in cirrhotic LSEC.

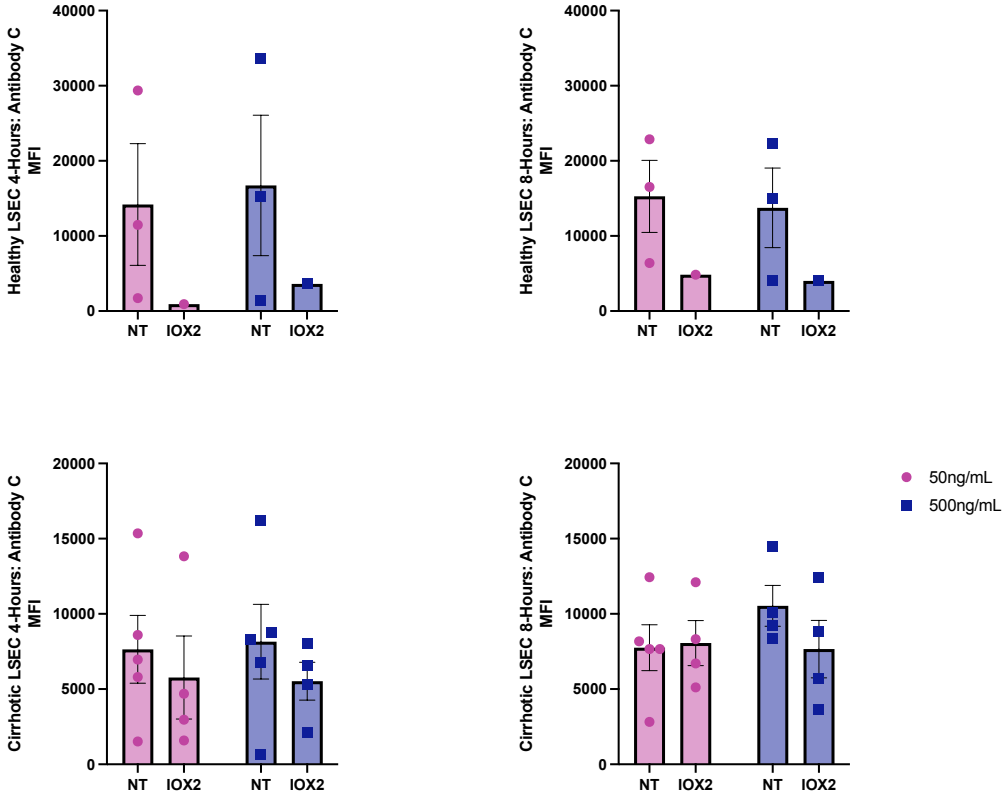


Figure 5. 10: IOX2 effects on internalisation of Antibody C. Healthy (n=3/ 1(IOX2)) and cirrhotic (N=5/4 (IOX2)) LSEC were isolated and pre-treated with IOX2 for 24-hours prior to being incubated with antibody C (50ng/mL and 500ng/mL) for 4- and 8-hours. Cells were then taken flow cytometry analysis and MI was reported. No significance was established, and error bars show SEM.

A similar theme was present for **antibody F** with a nonsignificant reduction in MFI for IOX2 treated cells (Figure 5.11). Once again, the low the number of repeats for healthy LSEC lessens our confidence in this data.

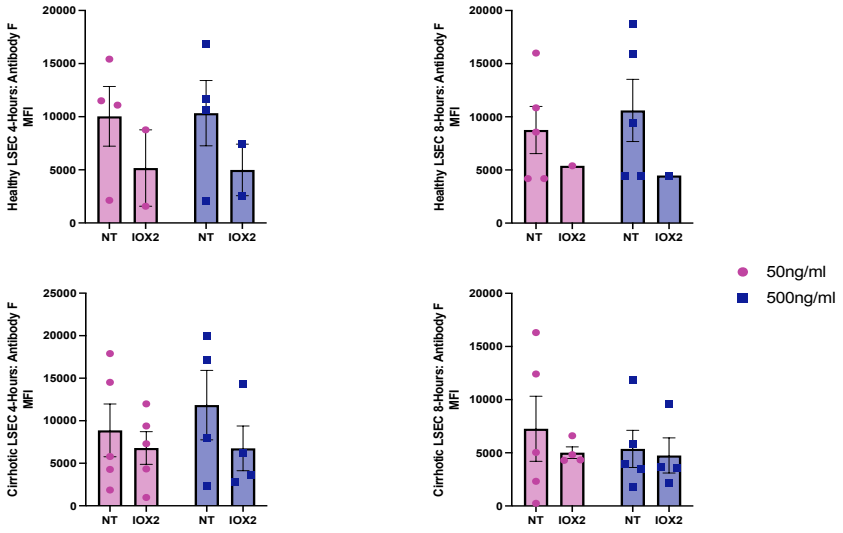


Figure 5. 11 IOX2 effects on internalisation of Antibody F. Healthy (n=5/ 1(IOX2)) and cirrhotic (N=5/4 (IOX2)) LSEC were isolated and pre-treated with IOX2 for 24-hours prior to being incubated with antibody F (50ng/mL and 500ng/mL) for 4- and 8-hours. Cells were then taken flow cytometry analysis and MI was reported. No significance was established, and error bars show SEM.

Only healthy LSEC were available for investigating uptake of **antibody A** and **H** after IOX treatment (Figure 5.12)**.** Again, small sample size was an issue, however a similar reduction in MFI was observed in IOX treated cells.

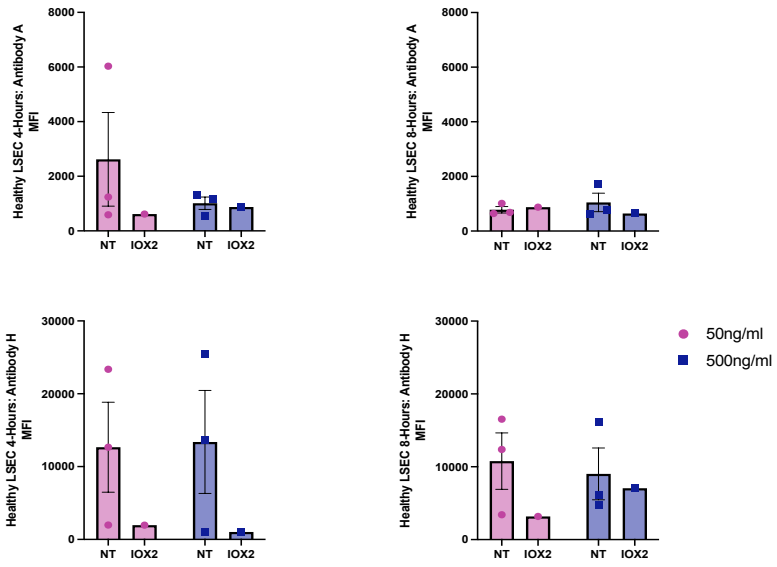


Figure 5. 12: IOX2 effects on internalisation of Antibody A and H. Healthy (n=3/ 1(IOX2)) LSEC were isolated and pre-treated with IOX2 for 24-hours prior to being incubated with antibody (50ng/mL and 500ng/mL) for 4- and 8-hours. Cells were then taken flow cytometry analysis and MI was reported. No significance was established, and error bars show SEM.

Our final use of IOX2 was in healthy LSEC (n=3) treated with **antibody D** with a fixed microscopy output (Figure 5.13). CTCF was calculated at 2-, 4- and 8-hours for both LAMP1 positivity and antibody fluorescence. A reduction in antibody fluorescence was observed at 2- and 8-hours in IOX-treated cells. There was no change at 4 hours, however when we considered LAMP1 positivity, we observed a significant increase at this same 4 hour timepoint.

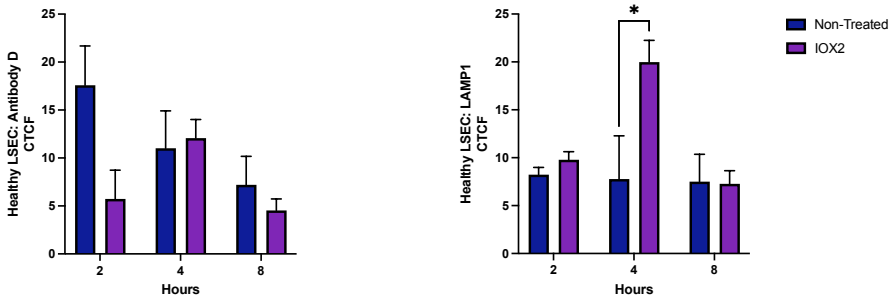


Figure 5. 13: Fixed microscopy quantification of antibody D fluorescence following IOX treatment. Healthy LSEC (n=3) were seeded into IBIDI chambers and treated with IOX2 for 24-hours. The following day antibody D (500ng/mL) was incubated on the cells and fixed at 2-, 4- and 8-hour time points. LAMP1 and anti-human IgG Alexafluor 488 was used to identify both lysosomal compartment and antibody. Quantification was performed on ImageJ for the corrected total cell fluorescence (CTCF) of both targets and plotted via Prism. 2-way ANOVA was used to assess significance. This was found at the 4-hour point between IOX2 and non-treated LSEC in the quantification of LAMP1 (P=0.0103). Error bars show SEM.

Our final cellular approach to try and identify antibody-binding surface receptors was the use of DTSSP to crosslink therapeutic antibody to the cell membrane. This crosslinker is thiol-cleavable therefore, following cell lysis in the presence of a reducing agent (β-mercaptoethanol) the receptor and antibody become dissociated. Comparing bands between reduced and non-reduced lysates on a western blot allowed us to determine whether a protein was conjugated to an antibody or not. This was performed on antibodies for both CD206 and CD32b (over multiple blots; we also investigated stabilin 1 and 2) at early passages. Figure 5.14 shows the gel results for both bispecifics, **Antibody H** and **I,** incubated on LSEC prior to being blotted for CD32b. Here a higher mass protein was seen in the non-reduced lysates (blue box Fig 5.14) , possibly representing the weight of CD32b conjugated to an IgG. The bands for Antibody H and I

were of similar size. This was only seen on membranes from LSEC treated with these two antibodies, all the other antibodies exhibited no second band in the non-reduced lysates. This experiment was repeated to ascertain the binding of CD206, LSIGN, and Stabilin-1 and -2, however no binding was displayed on the gels.

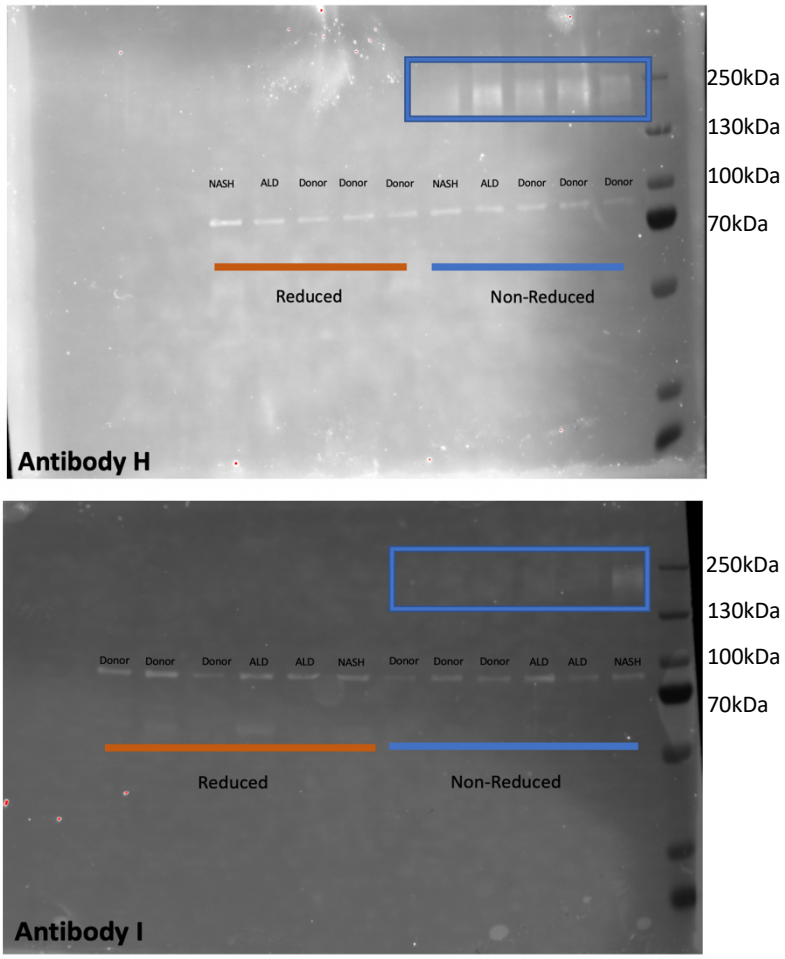


Figure 5. 14: CD32b crosslinked to bsAbs H and I: DTSSP forms crosslinks between antibody and receptor on the cell surface of healthy and cirrhotic LSEC. Following this, cells were lysed using RIPA buffer and two wells were pooled per donor. Matched lysates underwent different treatments with one being reduced by incubation with β-mercaptoethanol and the other non-reduced prior to boiling. Lysates were the quantified and concentration matched before running on a SDS-PAGE blot to separate proteins. Blots were transferred to nitrocellulose membrane before being incubated with different receptors. This figure depicts two blots detecting for CD32b following incubation with DTSSP and antibody H (top) and antibody I (below). Here the non-reduced samples show two bands with one heavy band indicating IgG bound to CD32b (blue box).

Following the blotting data indicating possible CD32b interaction with both bispecifics, we then sought to explore this process further. To do so we obtained the structure of the Fc and Fab regions of **antibody I** (dAb and linker structural information was unavailable) and docked these to the CD32b ectodomain via ClusPro as described in Section 5.1 (Figure 5.15A). We then proceeded with the highest ranked docked model and ran this through the online database, PDBsum.[418] This allows for estimation of the type of interactions formed between each chain alongside the residues responsible. Figure 5.15B shows the data obtained, here chain A represents CD32b ectodomain, chain L is the light chain and chain H shows the heavy chain of antibody H. In total 69 interactions are present between 11 and 10 residues of CD32b and the heavy chain of **antibody I** respectively. This consisted solely of hydrogen bonds and non-bonded contacts. The light chain had 63 contact points with CD32b with a mixture of salt bridges, hydrogen bonds and non-bonded contacts. Here Lys156 was the only residue that was able to bind both chains of the mAb. With all the bonds present, this is a robust and viable interaction between CD32b and the mAb.

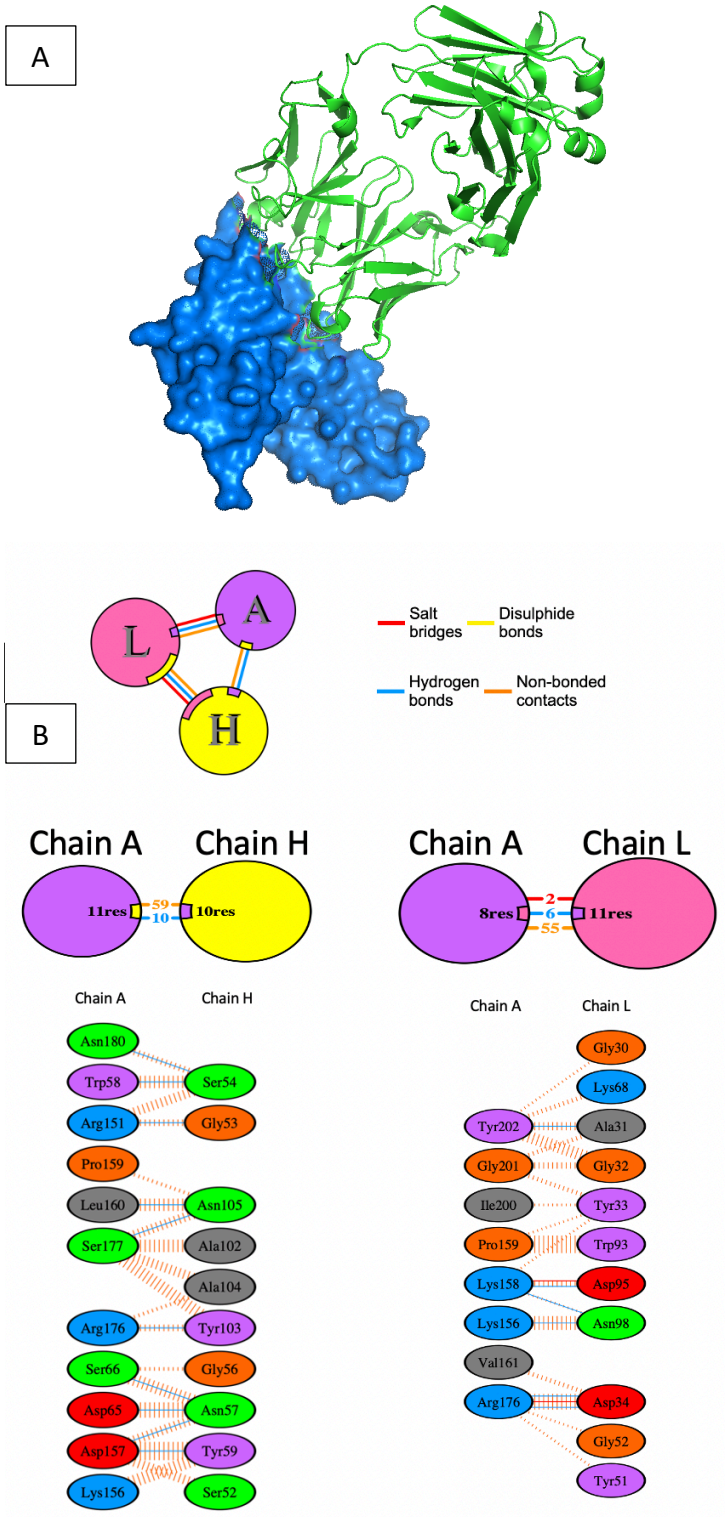


Figure 5. 15: Interactions between CD32b and the mAb portion of antibody I. Protein bank and Pymol was utilised to put the structures of CD32b ectodomain and the mAb portion of antibody H into ClusPro. The topped docked model can be found in point A, with red and green areas indicating docking sites. Following this the docked model was ran through the PDBsum software to gain an idea for the types of bonds and residues responsible for this binding. Chain A showing CD32b, chain L as the IgG light chain and chain H as the IgG heavy chain. The key above indicated bonds between residues with salt bridges in red, non-contact as orange vertical lines and blue to signify hydrogen bonds.

5.2.4 Interactions between FcRn and our antibodies

The final receptor of interest was FcRn. Here we utilised SPR to observe the binding kinetics of 6 antibodies at a *p*H of 6 (Table 5.3). Here the equilibrium dissociation constant KD, the association rate constant (k_{on}) and dissociation rate constant (k_{off}) were all able to be reported. RSV WT was used as a control and reported $1.05x10^{-8}$, $1.74x10^{6}$ and $1.84x10^{-2}$ for KD, k_{on} and k_{off} respectively. The lower the KD, the higher the affinity, therefore here **antibody A** presented the highest affinity to FcRn (*p*H 6) with **antibody I** exhibiting the lowest. Similar was seen in association rate (k_{on}) with **antibody A** have the fastest association to ligand and **antibody I** having the slowest association rate. A difference was observed in the dissociation rate, with the fastest to leave FcRn being **antibody B** and **antibody A** having the slowest dissociation rate.

Table 5. 3: SPR analysis of FcRn interaction with antibodies at a *p*H of 6.

Receptor	Antibody	KD (M)	K_{on} (1/ms)	K_{off} (1/s)
FcRn (*p*H 6)	Antibody A	$4.03x10^{-9}$	$2.29x10^{6}$	$9.20x10^{-3}$
	Antibody B	$1.09x10^{-8}$	$1.79x10^{6}$	$1.95x10^{-2}$
	Antibody C	Rejected	Rejected	Rejected
	Antibody D	$7.17x10^{-9}$	$1.47x10^{6}$	$1.05x10^{-2}$
	Antibody F	$5.20x10^{-9}$	$2.21x10^{6}$	$1.15x10^{-2}$
	Antibody I	$1.65x10^{-8}$	$8.03x10^{5}$	$1.33x10^{-2}$

FcRn= neonatal Fc receptor; KD (M)- equilibrium dissociation constant; K_{on}= association rate and K_{off}=dissociation rate.

5. 3 Discussion: Receptor mediated clearance by LSEC

This section aimed to elucidate whether a particular receptor was responsible for off-target clearance of therapeutics by LSEC. Initial *in silico* investigations were performed to assess whether the Fab region of an antibody was able to bind to the receptors of interest. We chose to look at this since results gained in the previous chapter for anti-CD20, anti-CD20 LAGA and **antibody C** suggested the extent of humanisation within this particular region affected its PK but Fc loss did not. To ensure this was the case we wanted to assess the binding capacity of the Fab region between anti-CD20 and **antibody C**, all structures were gained from the protein bank database. We found that interactions were possible between each antibody's fab region and receptor, with CD32b being ranked the highest for both with the largest number of members within the cluster. To reach a signal transduction threshold, CD32b needs a clustering of receptors[419] to cascade a phosphorylation chain leading to effector function. With the knowledge that CD32b binds the CH2-CH3 region of the Fc[420], it is not out of scope to consider that clustering may be a result of an antibody being able to bind receptors at both terminals of the IgG. In Figure 5.15A, the top ranked docked model of **antibody I** with the ectodomain of CD32b can be observed, here only one Fab arm is docked to the receptor, meaning the equivalent region is available on the second Fab arm. This allows for 3 possible binding sites available for CD32b. In literature there is evidence that anti-CD20 such as rituximab engages CD32b via bipolar antibody bridging, leading to internalisation of the complete complex of CD32b, CD20 and anti-CD20.[421,250] Since our docking data raises the possibility of 3 binding domains for interaction between CD32b and our reagents, this suggests the interaction would reach threshold for internalisation. Thus, CD32b is a good candidate to drive antibody internalization into our cells.

However, we also got mixed results when investigating CD32b as the receptor responsible. Non-specific blocking of all Fc receptors showed no difference. To note we did not use any confirmation assays to prove Fc was blocked therefore it is possible this reagent was ineffective.

Overexpressing CD32b via IOX2 often led to a paradoxical average loss of fluorescence (non-significant). This suggests that increasing CD32b expression reduced antibody accumulation, but we did not check expression levels post treatment on the cells used for functional uptake assays. Very low numbers of repeats were performed due to tissue availability at the time so we would need to confirm these findings, but we may have accelerated antibody recycling out of the cell or destruction by lysosomal clearance. Interestingly LAMP1 fluorescence was significantly upregulated at 4-hours in LSEC treated with IOX2 when observed via confocal. LAMP1 is a known marker for lysosomal activity[422], possibly suggesting that the reduction observed in MFI by each antibody in the cytometry data maybe the consequence of faster clearance as often FcR endocytosis is said to be geared more towards degradation.[423] This would have to be further investigated by both increasing numbers of donor cells used alongside, performing microscopy analysis on more mAbs/bsAbs than just **antibody D** and testing whether antibody was recycled into the supernatant faster after IOX treatment.

Using the crosslinker DTSSP, indicated that the two bsAbs, **antibody H** and **antibody I** bound to CD32b at the cell surface membrane. Interestingly, **antibody D** which makes up the mAb part of **antibody I** did not present a band in the non-reduced blots (data not shown). This suggests as both **H and I** possess the same dAb portion, that this addition is possibly the site for the CD32b interaction. In addition, **antibody D** showed the lowest affinity for CD32b when compared to the other 5 mAbs examined, further evidencing the addition of the dAb changes the PK of this bsAb. Therefore, an interesting experiment would have been to explore the dAb region in its own right, and perform identical experiments as seen throughout this thesis with this region. Another important point to make is that CD32b has been identified, as with our *in silico* investigations, to bind to a vast number of mAbs triggering a phosphorylation cascade.[251] Notwithstanding, often this does not result in the internalisation of said mAb[251] suggesting antibody chemistry is the determining factor for uptake. This could be due to residue charge or specificity within the variable region influencing non-specific clearance. It also questions whether our interaction present at the cell surface (established by DTSSP) with the bsAbs would

lead to internalisation, or just stimulate a phosphorylation cascade. This would explain why little affect was seen in the Fc block and IOX assays. In rats, CD32b recycling was due to clathrin invagination. Here ITIM phosphorylation was notably absent.[252]

Given the more complex structural nature of a bsAbs, it is plausible that under serum and *p*H conditions such as those in the human body, conformational changes as well as aggregation in the bsAbs could occur This provides a further explanation for CD32b possibly being responsible as often this receptor is credited for the clearance of immune aggregates in general[164] particularly by LSEC.[246,252] Further, FcRn interactions with the bsAbs format could well be compromised, which coincides with **antibody I** displaying the lowest affinity for FcRn in our SPR studies and supports the concept that bsAbs rather than being recycled undergoes lysosomal degradation as suggested in Chapter 4 whereby healthy LSEC showed significant clearance of this antibody. At this point there is no explanation as to why cirrhotic LSEC accumulated this antibody rather than clearing it. However, CD32b showed reduced expression in cirrhotic LSEC, it was also less continuously expressed along the sinusoids than that seen with healthy LSEC. With the indication that CD32b interacts with the with bsAbs, this loss of expression may explain altered traffic of these reagents in cirrhotic cells.

CD206 was confirmed to also bind to the Fab region of **antibody C** and anti-CD20. As mentioned in an earlier chapter CTLD 4,5 and 7 are considered the most important regions for binding glycoproteins.[331] Due to lack of structural information for CTLD 5 and 7 we could only model docking studies with CTLD4. This domain ranked highest for binding between anti-CD20 and CD206, however this was not the case for the humanised **antibody C**. Here the CTLD2 was considered the best domain for binding. Both antibodies target the same epitope and although the domains of CD206 exhibited similar binding energy, they differed in number of members per cluster suggesting higher affinity for the humanised antibody. This possibly explains why as the rodent proportion of engineered antibodies reduces, more LSEC uptake is seen (Figure 4.28).

The other chimeric antibody in this thesis was **antibody A,** which showed little uptake in LSEC throughout Chapter 4. By SPR this antibody exhibited high off-target binding and often had to be ruled out from data sets for this reason. It is perhaps unsurprising therefore that this antibody failed the serum stability test in preclinical testing at GSK. With the unstable and 'sticky' nature of this antibody it is possible to suggest that it exhibited low internalisation rates as it may have stuck to the well during experimentation or that conformational changes *in situ* may have reduced its ability to bind. **Antibody B** in cirrhotic LSEC was the only antibody to exhibit significant reduction in uptake following *MRC1* knockdown. This may reflect marginal increases in CD206 expression seen in cirrhotic cells (Figure 3.11). Unfortunately, binding kinetics was unable to be precured by SPR, possibly due poor selection of recombinant protein used. Alongside this and the low experimental repeats we cannot say for certain whether this CD206 is responsible for the internalisation of this antibody. Referred to previously, CD206 is the sole receptor responsible for the intake of lysosomal enzymes.[94] Therefore, we wanted to see if transiently silencing *MRC1* would affect the lysosomal capabilities with LSEC. As shown in Figure 5.5, no difference was observed in association between lysosome and antibody. However, this is not to say this may play a role in a more complex physiology relevant *in vivo* model.

SPR proved to be unsuccessful in our hands, with our recombinant receptors and antibodies unable to ascertain any interactions. SPR is an excellent tool for quick screening of binding of an array of antibodies to targets. However, it is inadequate when recapitulating true physiological reactions failing to consider receptor clustering, varying flow rates seen within the sinusoid alongside the fluidity of the cellular membrane.[424] Therefore, just because no binding was seen here does not necessarily mean this interaction isn't happening within the actual liver. A study looking into DC-SIGN, which shares homology with LSIGN also found no interaction with human IgG.[425] This used a FACS and SPR approach and found despite favourable glycosylation patterns no binding took place.[425] This may explain why we found little evidence of binding between with our mAbs and receptor. Another possibility is that as both manipulation of CD32b and

LSIGN showed effects on the binding of **antibody I,** maybe both receptors need to be present to cluster. This has been seen with CD32b, which is able to cluster with other receptors such as with Mincle receptor to trigger internalisation.[426] This however would need to be explored further through more targeted experimental approaches such as membrane preps followed by mass spectrometry.

To conclude this section, we had some indication of CD32b binding to bsAbs however, could not determine whether this interaction led to the internalisation and thus degradation of these antibodies within LSEC. Nor could we 100% rule in or out CD206 or LSIGN playing some kind of role. This points more towards antibody specificity/chemistry being the key determinant for uptake however, again more research needs to be done to truly rule out different factors that may cause this off-target clearance. Factors such as residue cluster charges and hydrophobicity patches would need to be considered to help predict uptake. Regarding these receptors, no convincing evidence could be found to distinguish why cirrhotic and healthy LSEC behaved differently with different antibodies. Therefore, in the following section we propose using indirect approaches to truly interrogate individual pathways to determine why rates of internalisation and clearance in both aetiologies differ.

5.4 Indirect approaches which could explain LSEC antibody uptake

Contrasting results when studying specific receptors led us to explore other downstream internalisation mechanisms in healthy and cirrhotic LSEC. Numerous pathways for endocytosis co-exist in a single cell and can operate concurrently.[423] Particles more than 500nm are known to internalise via a 'trigger' process known as macropinocytosis.[423] Whereas anything below this size, such as mAbs internalised into LSEC are sorted through varying processes. One mechanism of interest somewhat explored in the above Section 5.2, is receptor mediated clathrin-dependent internalisation. The most explored receptors in this pathway are the Fc receptors such as CD32b. This was found to occur

through a 'zipper' like process, where cytosolic ITAMS/ITIMS mediate signal transduction resulting in F-actin rearrangement extending the membrane to engulf the ligand.[423,427] This action is controlled by actin remodelling GTPases[427], and uniquely regulated by Cdc42.[427,428] Cdc42 activation determines the opening of the phagosomal/endosomal cup with subsequential deactivation, by PI3K, leading to the scission (closing) of said cup and internalisation of the phagosome.[429] PI3K involvement is well established in FcyR mediated phagocytosis with upregulation correlating with higher levels of PIP3[430-431], a product of PI3K activity as described in Chapter 3. Phagosomes formed by FcR mediated internalisation are fated for degradation. [432]

The second main mechanism of interest for entry into a cell, is the microscale clathrin-dependent internalisation enabled by coat accumulation leading to lipid arrangement in a pinch like process. This pathway can be divided into 6 steps: initiation, growth, stabilization, budding, scission and uncoating.[433] Similar to our receptors of interest, clathrin cannot associate directly with lipids or proteins so relies on a vast network of adaptor proteins such as AP2.[434] These proteins react with moieties on the membrane and recruit clathrin triskelions to form a lattice coated structure. Following engulfment of cargo, dynamin and actin polymerization drives scission and coated vesicle are released intracellularly. These vesicles then rely on the recruitment of other proteins to drive them down particular pathways. For instance, AP-3 which we considered in Chapter 4, is associated with the lysosomal fate.

To explore these pathways we used inhibitors for particular proteins of interest throughout and quantified the amount of internalised conjugated antibody within the cell. **Antibodies D** (humanised)**, E** (human) and **I** (bsAb) were chosen as these were the only antibodies we could conjugate.

5.4.1 Cirrhotic LSEC have a delayed signal transduction response.

Both healthy and cirrhotic LSEC were treated with 500ng/mL **antibody I** for 15- and 45-minutes prior to being lysed and assessed using a human tyrosine phosphorylation proteome profiler. Results can be seen in Figure 5.16 which illustrates that cirrhotic LSEC

treated with this antibody saw a delay in phosphorylation in comparison to healthy cells, evidenced by the reduced signal across each receptor at the 15-minute treatment time compared to that seen at 45-minutes. On the other hand, healthy LSEC saw a reduction over these time points. The FcyRs, CD32a and CD16a/b (signalled by blue vertical line on the left-hand labels), showed phosphorylation at every time point after antibody exposure in both healthy and cirrhotic cells. These were one of the first receptors seen in cirrhotic LSEC at 15-minutes and remained at 45-minutes in healthy cells when majority of receptors had already undergone phosphorylation. The SLAM family also underwent phosphorylation in healthy and diseased cells treated with **antibody I**. LAIR-1 was the only individual receptor that was phosphorylated in cirrhotic cells but not healthy LSEC over each treatment timepoint.

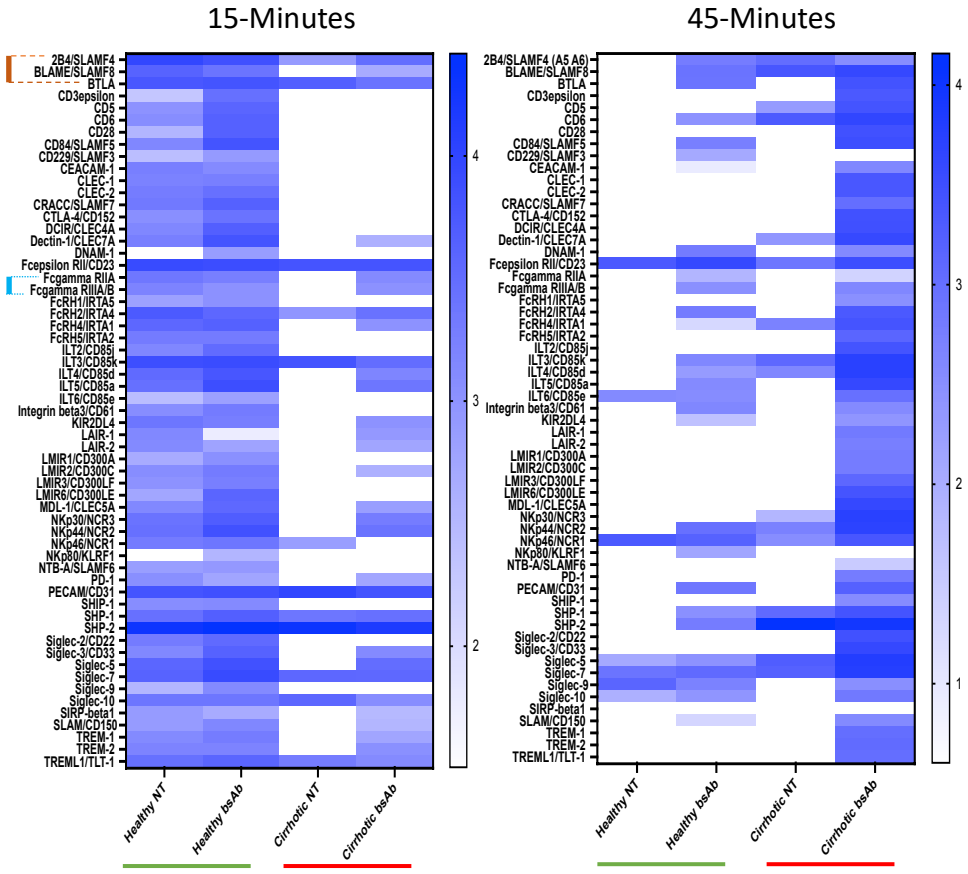


Figure 5. 16: Human phospho-immunoreceptor profile following Antibody I treatment. Healthy and cirrhotic LSEC were treated with 500ng/mL of antibody I for 15- and 45-minutes. Prior to being lysed using buffer from the provided kit. Per manufacturers instructions a proteome profiler was performed, and images taken on the chemidoc. Analysis was performed using Biotechne online dot blot software and plotted as a heatmap on Prism. NT- non-treated control LSEC and bsAb- bispecific antibody I. Data was log2 transformed and displayed as a heatmap.

5.4.2 Dextran Sulfate suggested a receptor mediated mechanism of antibody internalisation

Dextran Sulfate (DxS) is considered a non-specific inhibitor of receptor-mediated endocytosis. With the mixed results in the direct approaches seen in the beginning of this chapter, we used DxS to explore whether therapeutic antibody uptake was due to receptor mediated processes. Figure 5.17 shows the quantification of vesicles positive for antibody following 15-minutes of Dextran Sulfate incubation vs the non-treated control LSEC. **B**oth healthy and cirrhotic cells showed a considerable reduction in internalisation of **antibody D** in LSEC treated with DxS. Similar was observed for

antibody I, however by the 8th hour particularly in the healthy LSEC, function was regained, and vesicle count began to increase. **Antibody E** saw the largest difference in internalisation rate between healthy and cirrhotic LSEC. The former, exhibited little effect when dosed with DxS compared to non-treated LSEC, whereas the cirrhotic cells treated with DxS showed an initial reduction at 2-hours but returned to similar levels by 22-hours for both healthy and cirrhotic LSEC.

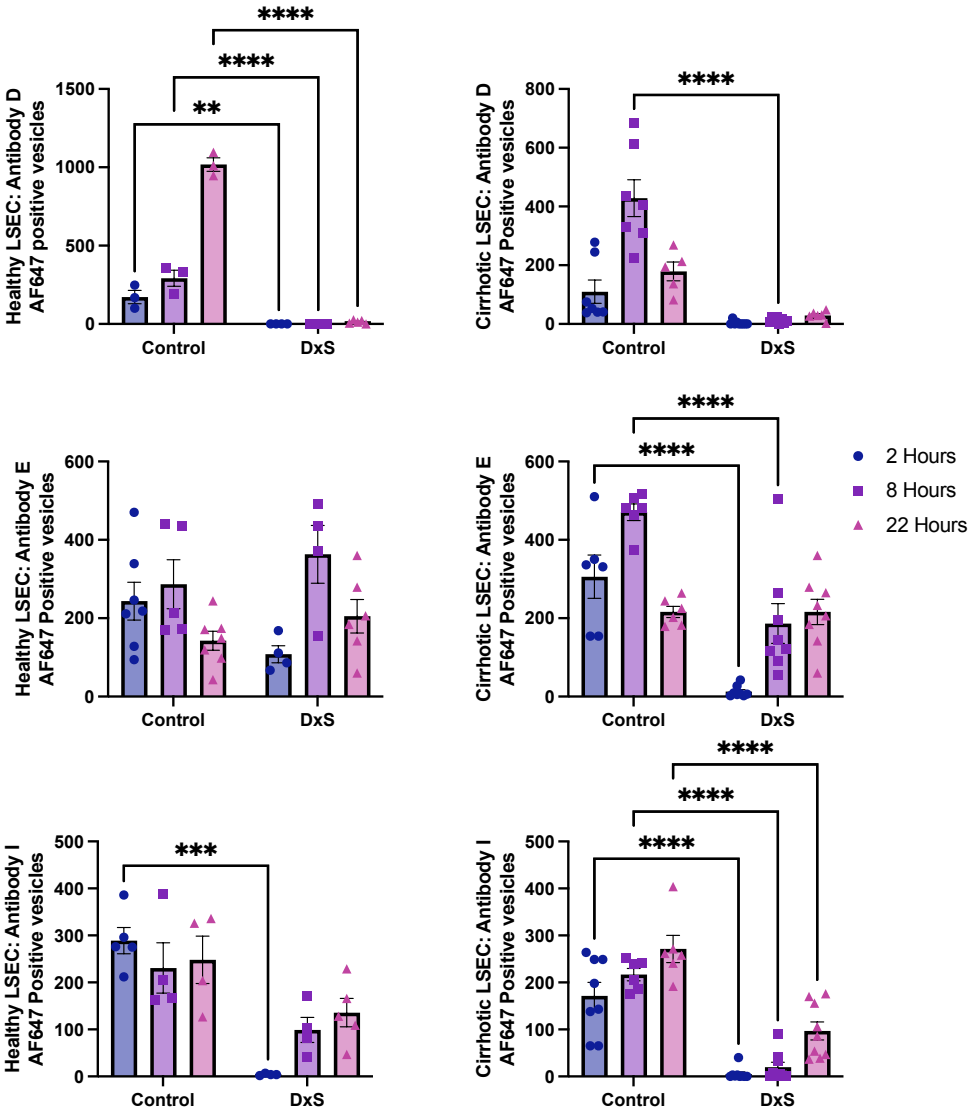


Figure 5. 17: Dextran sulfate effects on therapeutic internalisation. 100ug/mL of Dextran sulfate was incubated with healthy and cirrhotic LSEC for 15 minutes prior to incubation with 500ng/mL of antibodies D (humanised), E (human) and I (bsAb) conjugated with Alexafluor 647. Live images were taken at 2-, 8- and 22-hours on the LSM780 at 40x and image analysis was performed with ImageJ. Each point marks an individual liver. Error bars show SEM and significance was calculated using 2-way ANOVA. *= p<0.05; **=p<0.01; ***=p<0.001; ****=p<0.0001.

5.4.3 Sucrose significantly affected cirrhotic LSECs ability to internalise mAbs

Following further evidence of a receptor-mediated internalisation mechanism, we next sought to explore whether this was clathrin-dependent. Hyperosmolarity interferes with the normal recycling of clathrin and reformation of coated pits[435,436], therefore 0.45M of sucrose used to investigate clathrin's role in the internalisation of therapeutic antibodies by LSEC. At the initial 2-hour point of incubation with mAb/bsAb following sucrose incubation, cirrhotic LSEC saw the most significant reduction in vesicles positive for the therapeutics (Figure 5.18). This was evident for all 3 antibodies chosen. Healthy LSEC however, showed varying responses. **Antibody D** was not plotted as no positive vesicles were present in n=3 healthy livers. With **antibody I** both cirrhotic and healthy LSEC showed reduced antibody uptake. Interestingly, healthy LSEC incubated with **antibody E,** displayed very little difference in positive vesicular count. Following this we wanted to investigate how long after sucrose treatment the effect persisted in cirrhotic LSEC (2-, 8- and 22-hours). Representative images of the sucrose treatment group for each antibody can be seen in Figure 5.19. Quantification of vesicular number can be found in Figure 5.20. For **antibody D** and **E,** reduction in mAb internalisation is retained significantly up until the 8-hour time point. After this uptake is similar in the control and sucrose treated cells. Regarding **antibody I,** sucrose effects on cirrhotic cells are only present until the 2-hour incubation point, beyond this equivalent bsAb uptake is observed between the two groups.

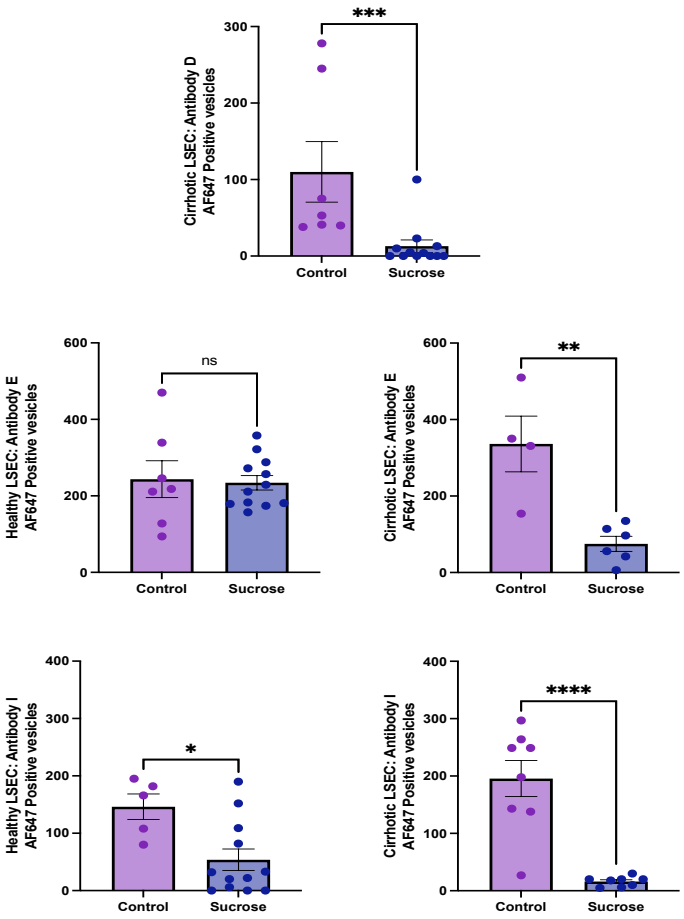


Figure 5. 18: 2-Hour incubation of antibodies following sucrose treatment. Healthy (left) and cirrhotic (right) LSEC were treated with 0.4M of sucrose for 2-hours prior to being incubated with conjugated antibodies D (humanised), E (human) and I (bsAb). Images were taken on the LSM780 at 40x with water immersion. ImageJ was used to count AF647 positive vesicles. Each point represents an individual liver (5 FOV averaged) and error bars show SEM. Significance was determined through unpaired T-tests. *= p<0.05; **=p<0.01; ***=p<0.001; ****=p<0.0001.

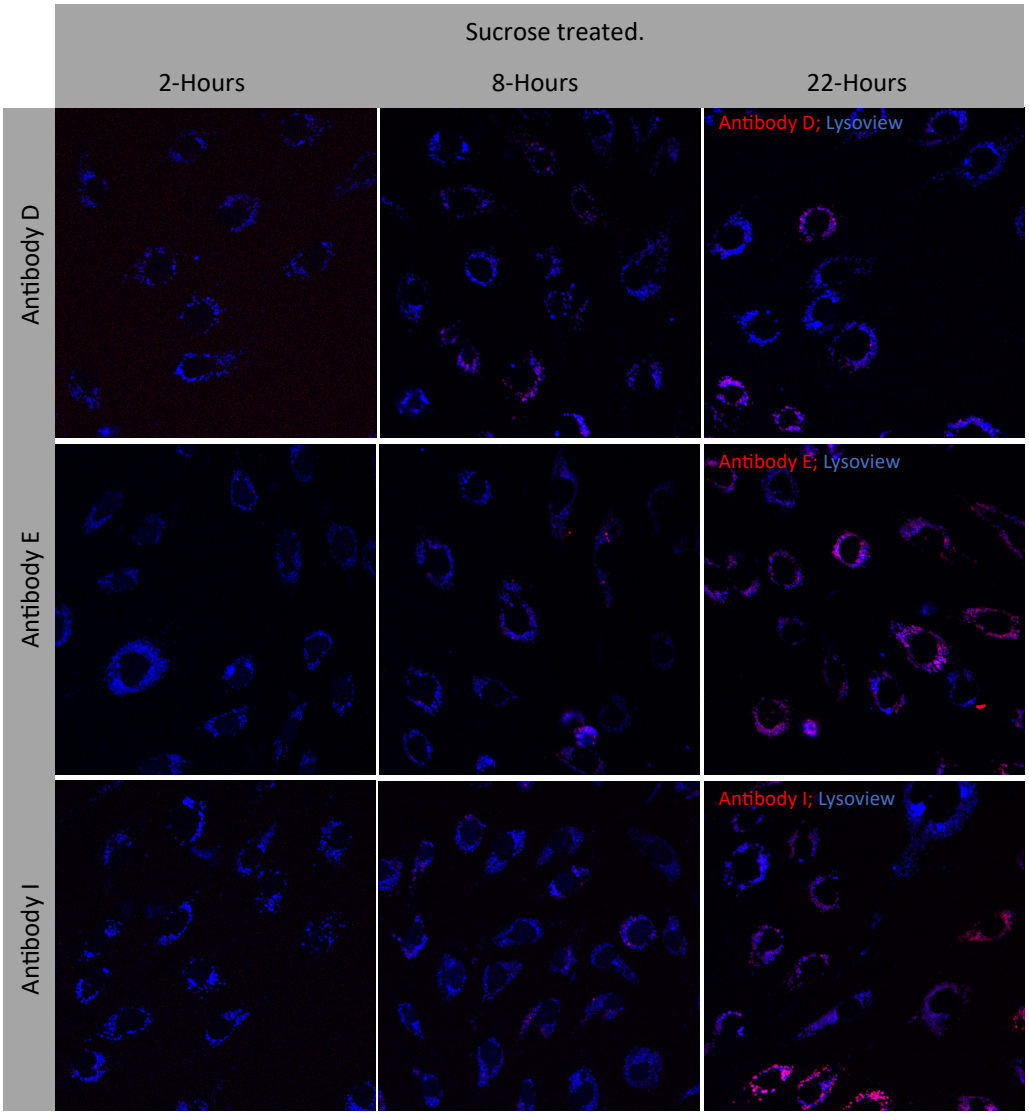


Figure 5. 19: Representative images of sucrose treated LSEC internalising antibodies. LSEC were treated with 0.4M of sucrose for 2-hours prior to being incubated with lysoview (blue) and conjugated antibodies D (humanised), E (human), and I (bsAb) (red). Live images were taken on the LSM780 at 40x with water immersion at 2-, 8- and 22-hours.

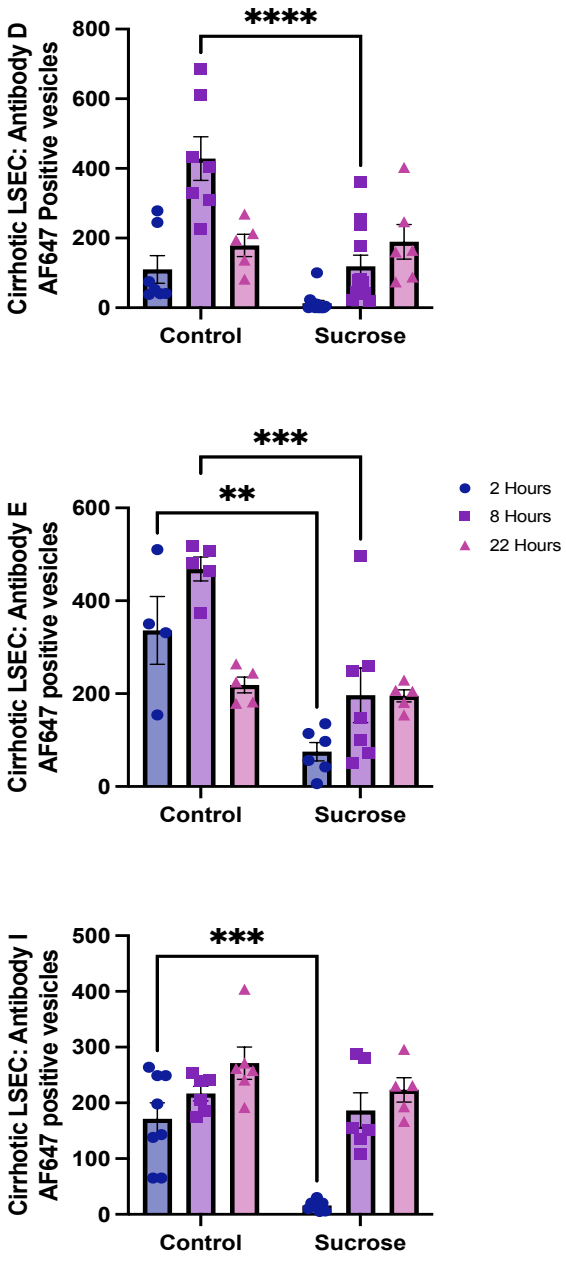


Figure 5. 20: Quantification of AF647 positive vesicles post sucrose treatment. LSEC were treated with 0.4M of sucrose for 2-hours prior to being incubated with Lysoview (blue) and conjugated antibodies D (humanised), E (human), and I (bsAb) (red). Live images were taken on the LSM780 at 40x with water immersion at 2-, 8- and 22-hours. Quantification was performed with ImageJ. 2-way ANOVA was used to determine significance. *= $p<0.05$; **=$p<0.01$; ***=$p<0.001$; ****=$p<0.0001$. Error bar shows SEM.

5.4.4 Cirrhotic LSEC need microtubules to internalise therapeutic antibodies

Following determination of the possible clathrin-dependent nature of internalisation, we next explored whether this involved a clathrin-net structure along the microtubules as previously described in rat LSEC.[401] Nocodazole reversibly interferes with the polymerisation with microtubules. Therefore, we utilised this anti-mitotic agent to assess the role of microtubules in the uptake of therapeutic antibodies.

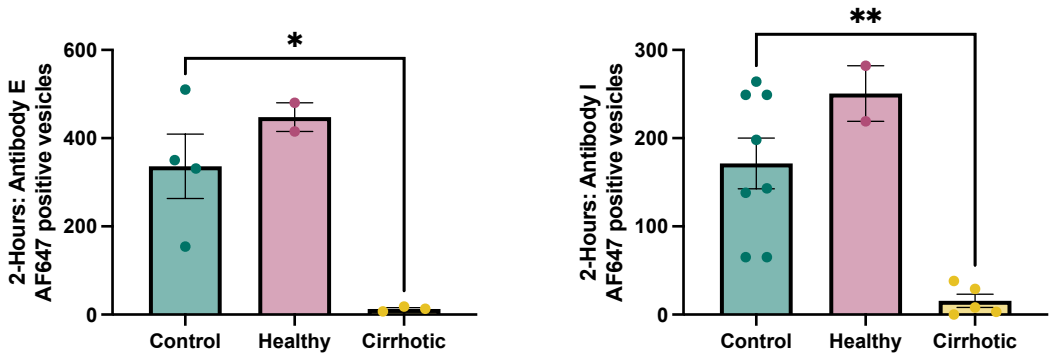


Figure 5. 21: 2-Hour incubation with antibody post nocodazole treatment. Healthy (n=2) and cirrhotic (n=3/5) LSEC were treated with 0.2ug/mL nocodazole for 1-hour prior to incubation with antibody E (human) and I (bsAb). Following a 2-hour incubation cells were imaged on the LSM780 at 40x. Quantification was performed through ImageJ. 2-way ANOVA was used to calculate significance. *= $p<0.05$ and **=$p<0.01$. Error bars show SEM.

Initially in the first 2-hour incubation of **mAb E** and **bsAb I** Nocodazole caused a significant reduction in internalisation in cirrhotic LSEC only (Figure 5.21). Here the control consisted of an untreated mixture of healthy and cirrhotic LSEC. Since this was not evident in healthy LSEC, we only used cirrhotic cells for subsequent experiments. All three antibodies were mostly blocked at the 2-hour point by nocodazole; and significant reduction was still present at 8-hours for antibodies **D** and **E.** This was not the case for **antibody I** where similar quantities of internalised bsAb was observed at 8- and 22-hours. As seen in Figure 5.22, the quantity of lysosomes was unaffected through this treatment.

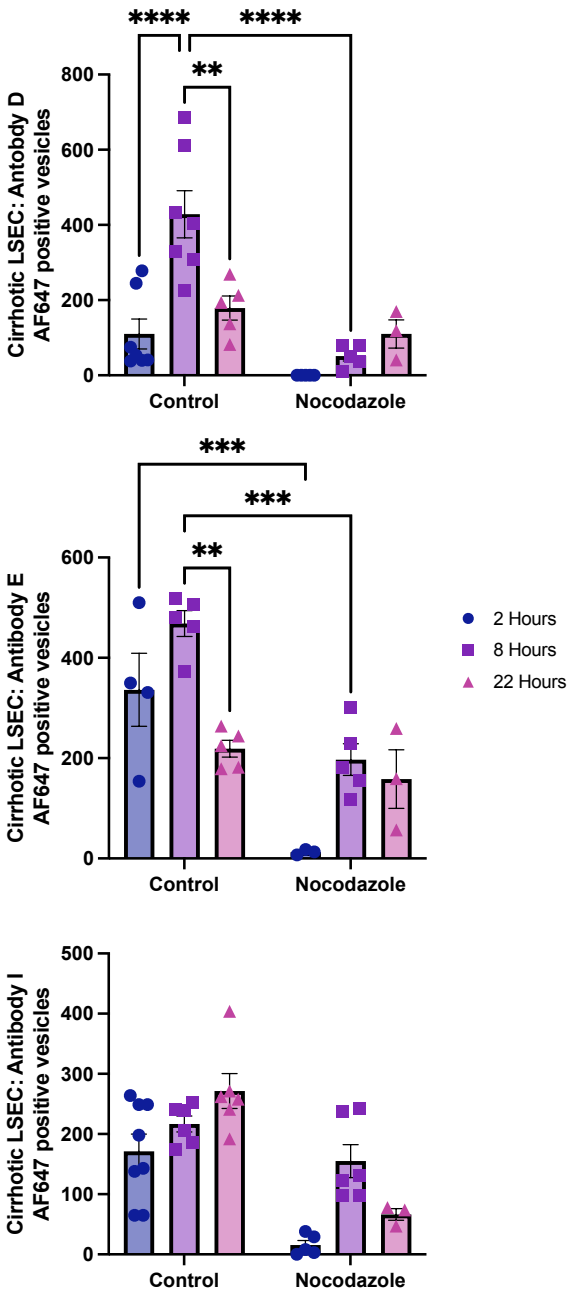


Figure 5. 22: Time course quantification of internalised antibody post nocodazole treatment. Cirrhotic LSEC were treated with 0.2ug/mL nocodazole for 1-hour prior to incubation with antibody D (humanised), E (human), and I (bsAb). Following a 2-, 8- and 22-hour incubation cells were liver imaged on the LSM780 at 40x. Quantification was performed through ImageJ. 2-way ANOVA was used to calculate significance. *= p<0.05; **=p<0.01; ***=p<0.001; ****=p<0.0001. Error bar shows SEM. Each represents an individual liver (5 FOV averaged).

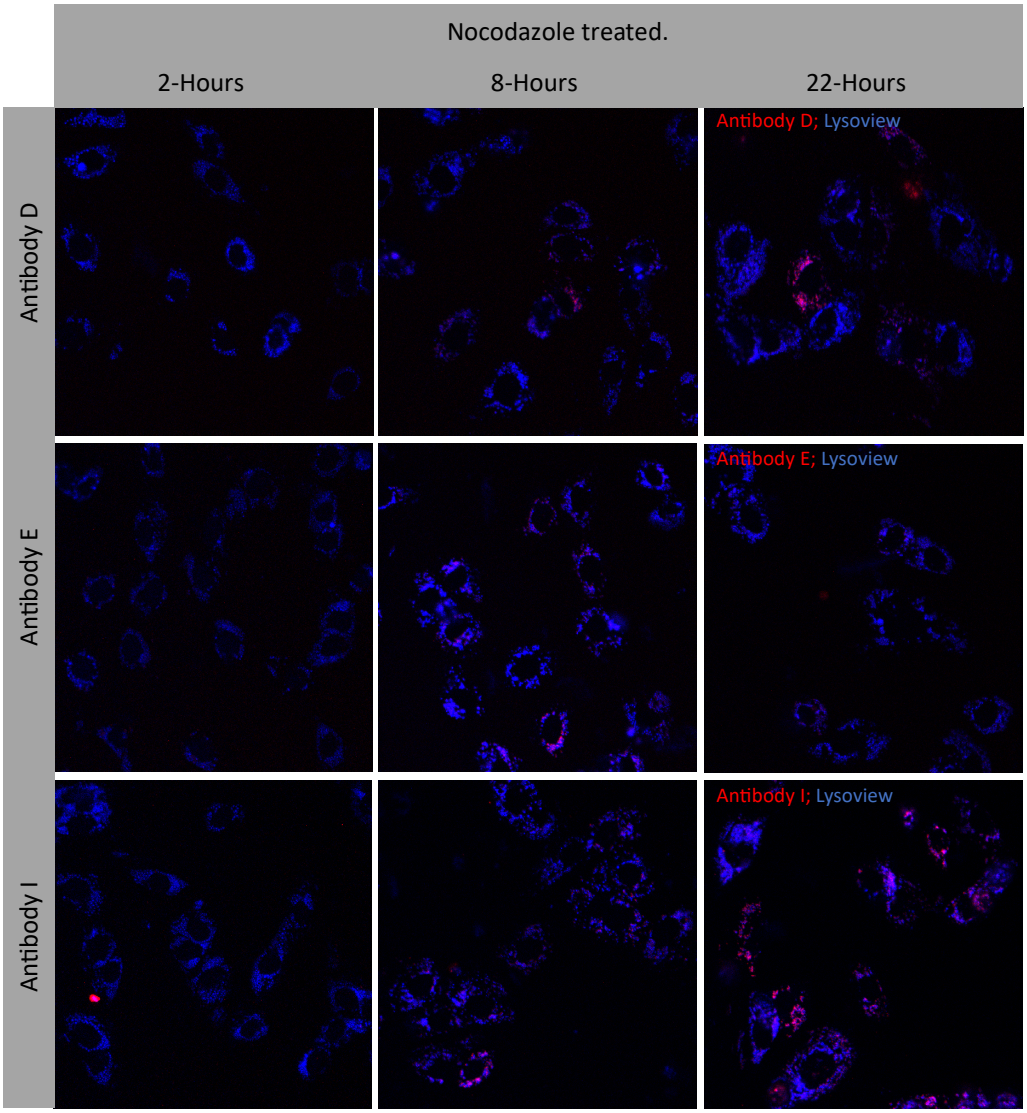


Figure 5. 23: Representative images of nocodazole treated LSEC internalising antibodies. LSEC were treated with 0.2ug/mL nocodazole for 1-hour prior being incubated with lysoview (blue) and conjugated antibodies D, E, and I (red). Live images were taken on the LSM780 at 40x with water immersion at 2-, 8- and 22-hours.

5.4.5 PI3K played a more important role in cirrhotic LSEC internalisation

PI3K plays a key role in endocytosis within cells particularly in F-actin formation. We wanted to investigate whether this kinase affects LSECs ability to internalise therapeutic antibodies. Therefore, wortmannin a non-specific PI3K inhibitor was used to investigate

this. **Antibody D** showed a continual reduction in vesicles positive with antibody over the 22-hours after wortmannin treatment of healthy cells (Figure 5.24). Cirrhotic LSEC conversely only displayed significant reduction at 8-hours. Regarding **antibody E**, no difference was observed in healthy LSEC, whereas cirrhotic cells showed considerable loss of vesicles at 2- and 8-hours post treatment. There was no impact of wortmannin on the internalisation of **antibody I** by healthy cells. Interestingly, at the 8-hour time point in cirrhotic LSEC the abundance of vesicles positive for antibody within the cell was significantly higher than in the control non-treated group. No differences were seen in lysosomal colocalisation at each time point (data not shown).

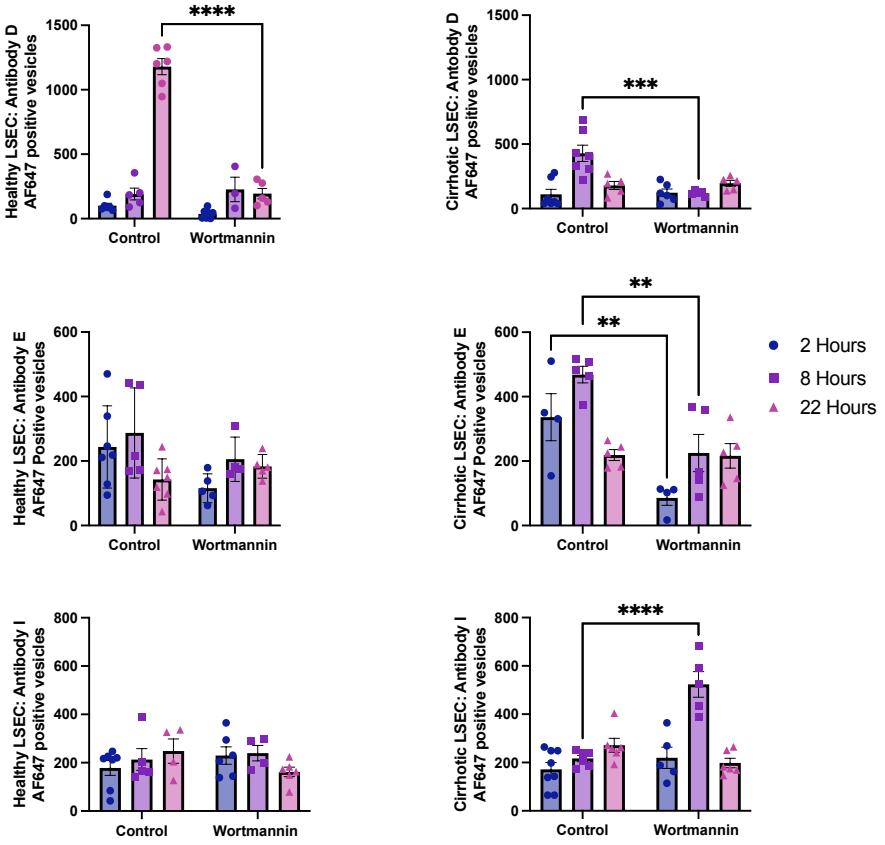


Figure 5. 24: PI3K inhibition effects on therapeutic internalisation. Healthy and cirrhotic LSEC were pre-treated for 1-hour of 1uM of wortmannin prior to incubation 500ug/mL of antibody D (Humanised), E (human), and I (bsAb). Following a 2-, 8- and 22-hour incubation cells were live imaged on the LSM780 at 40x. Quantification was performed through ImageJ. 2-way ANOVA was used to calculate significance. *= p<0.05; **=p<0.01; ***=p<0.001; ****=p<0.0001. Error bar shows SEM. Each represents an individual liver (5 FOV averaged).

5.4.6 Cdc42 plays a vital role in Antibody E internalisation

In section 5.4, we described how PI3K deactivated Cdc42 allowing for the scission of the vesicle bud intracellularly. Following the results seen with non-specific inhibition of PI3K, particularly with **antibody I**, we next wanted to investigate if the inhibition of Cdc42 would yield the same results. Therefore, we incubated ML141, a specific non-competitive inhibitor of Cdc42 with LSEC for 24-hours prior to antibody treatment. Cirrhotic LSEC was used for this investigation as at the time no healthy donor tissue was available (Figure 2.25). A slight reduction of positive vesicle number was evident for **antibody D** and **antibody I** at the 2-hour timepoint. Internalisation of **antibody E** was completely abrogated in ML141 treated cells at this point. There was some recovery at the 8-hour timepoint but remained significantly reduced compared to control LSEC. On average a marginal increase of **antibody I** abundance was evident in ML141 incubated LSEC**.** As seen in panel D, after treatment with ML141, the lysosomes appeared less formed and vesicular appearing instead as homogenous staining within cells.

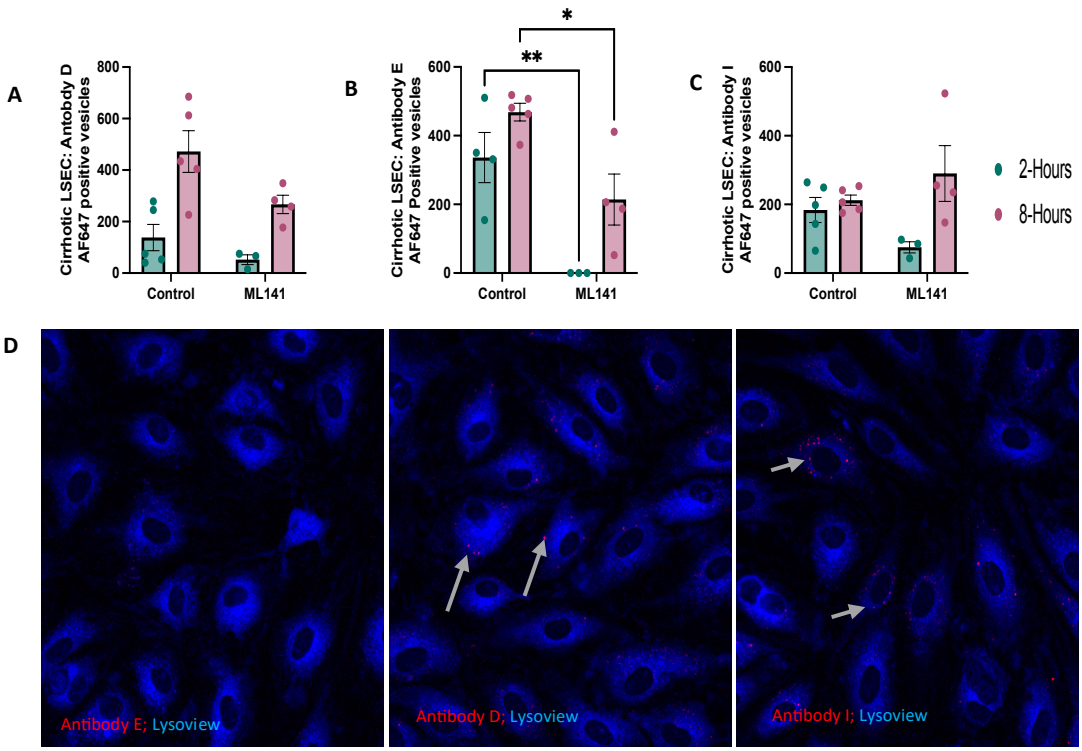


Figure 5. 25: Cdc42 inhibition on cirrhotic LSEC at 4-hours. Cirrhotic LSEC were incubated with 15uM of ML141 for 24-hours prior to incubation with Lysoview (blue) and conjugated AF647 antibodies D (humanised), E (human), and F (bsAb) (red). Live images were taken on the LSM780 at 40x with water immersion at 2- and 8-hours. Quantification performed using ImageJ. Error bars show SEM. Significance calculated with 2-way ANOVA. *= p<0.05 and **=p<0.01.

Colocalisation analysis never reached perfect correlation (Pearsons= 1) between antibodies and lysosomal compartments. With this and the previous literature suggesting FcRn was able to deliver cargo to the lysosomes, we wanted to see if blocking this interaction had any affect. Initial observation of antibody positive vesicles suggested **antibody D** in healthy LSEC was reduced in FcRn blocked cells (Figure 5.26). This was mirrored in the cirrhotic cells for the first 8-hours, however by the 22nd hour of incubation, an increased number of vesicles were noted in the treated cells in comparison to the control non-treated group. In FcRn blocked healthy cells, an increase of vesicles at 22-hours was present with **antibody E**. The opposite was observed in cirrhotic cells with the initial 2- and 8-hour time points showing a loss in vesicle abundance in comparison to the control cells. This normalised by the 22nd hour. **Antibody I** overall showed a reduction in healthy cells particularly at the 2-hour point. No difference was observed in the cirrhotic cells for this bsAb.

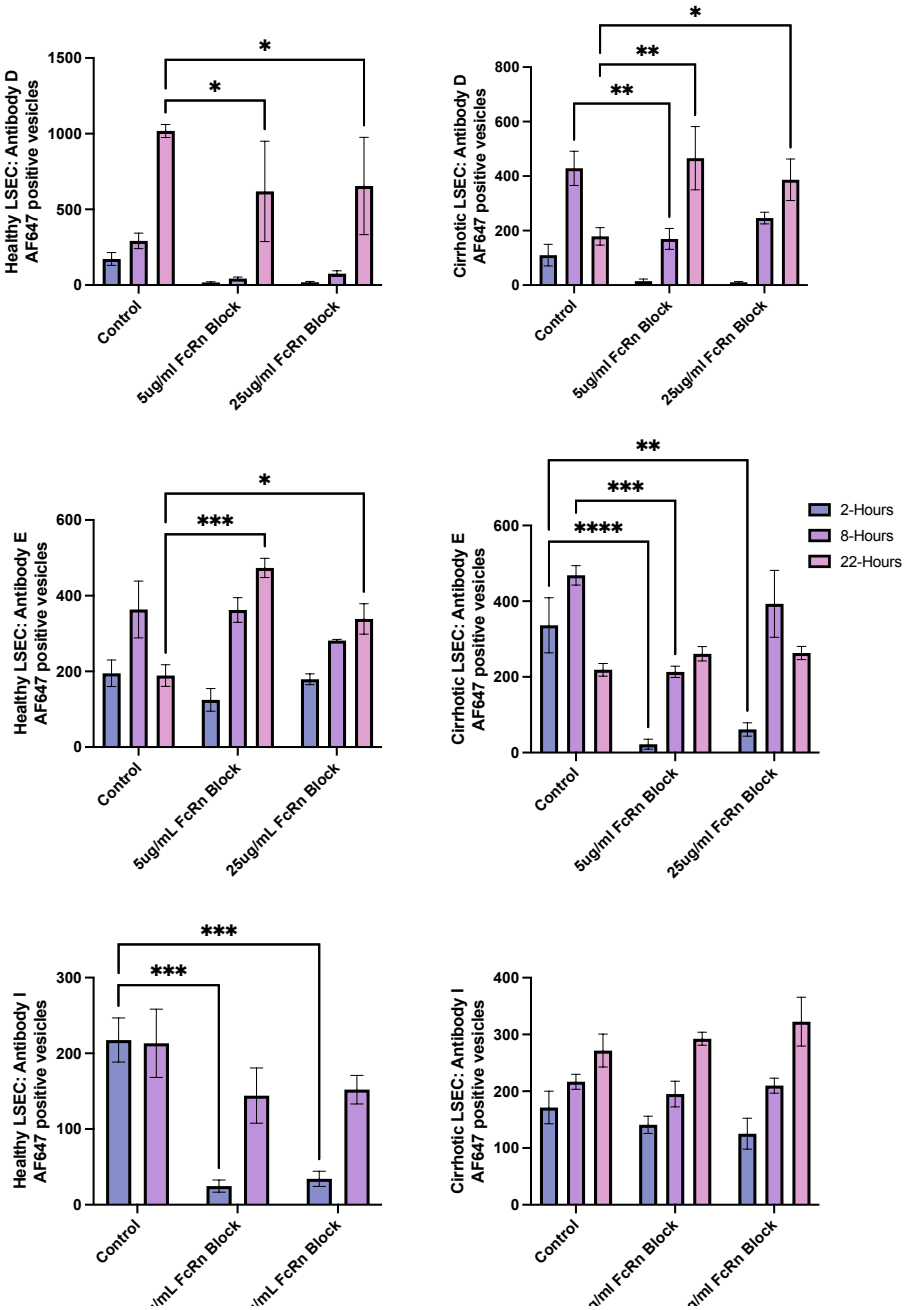


Figure 5. 26: FcRn blocker effect on antibody internalisation. Healthy and cirrhotic LSEC were pre-treated for 1-hour of 5ug/mL and 25ug/mL of FcRn blocker prior to incubation 500ug/mL of antibody D (humanised), E (human), and I (bsAb). Following a 2-, 8- and 22-hour incubation cells were live imaged on the LSM780 at 40x. Quantification was performed through ImageJ. 2-way ANOVA was used to calculate significance. *= p<0.05; **=p<0.01; ***=p<0.001; ****=p<0.0001. Error bar shows SEM. N=4 for each aetiology (5 FOV averaged).

Following this, we next wanted to see whether blocking FcRn binding led to an increase in lysosomal degradation of antibody. Therefore, we next explored the colocalisation between AF647 conjugated antibody and the lysosomal compartment (Figure 5.27).

For both healthy and cirrhotic LSEC, after 2-hours of incubation with **antibody D** there was a significant loss of antibody within the lysosomes. This had levelled out by the 8-hour and was equivalent between control and treated cells at the 22-hour point. For **antibody E**, both healthy and cirrhotic LSEC saw a reduction in lysosomal association in cells whose FcRn interaction was blocked. Less discrepancy was evident in cells incubated with **antibody I** with a significant reduction seen at 2-hours but not at the later time point. Cirrhotic cells on the other hand, saw an increase at 22-hours under treatment with the lowest concentration of FcRn blocker but not the highest concentration.

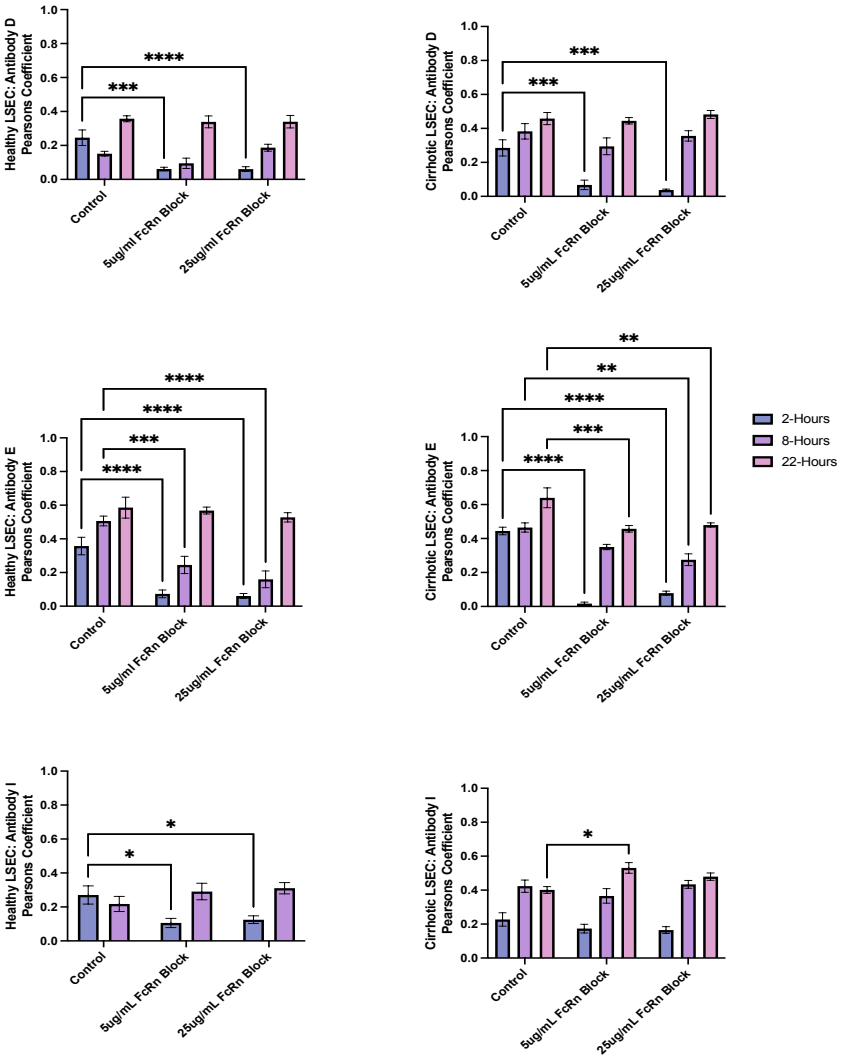


Figure 5. 27: Co-localisation of lysosomes and antibody under FcRn block. Healthy and cirrhotic LSEC were pre-treated for 1-hour of 5ug/mL and 25ug/mL of FcRn blocker prior to incubation 500ug/mL of antibody D (humanised), E (human), and I (bsAb). Following a 2-, 8- and 22-hour incubation cells were live imaged on the LSM780 at 40x. Quantification of colocalisation was performed through ImageJ using JACOP plugin. 2-way ANOVA was used to calculate significance. *= p<0.05; **=p<0.01; ***=p<0.001; ****=p<0.0001. Error bar shows SEM. N=4 for each aetiology (5 FOV averaged).

5.5 Indirect Approaches: Discussion

The aim of this section was to see if we could discriminate which internalisation pathway three conjugated antibodies used and if there was any discernible difference between healthy and cirrhotic LSEC. Through use of a proteome profiler assay, we initially established that regarding **antibody I**, cirrhotic LSEC showed a delayed capacity to

initiate a signal cascade in comparison to healthy LSEC. Often the activation of tyrosine phosphorylation requires calcium as described in Chapter 3. Patients with cirrhosis are often associated with hypocalcaemia[437], this may be a reason for the delay in signal transduction seen. Possibly unlikely due to both being in the same media through culture, however it may reflect inherent changes in calcium channel expression. I could not find any literature regarding the changes of this expression in disease. LAIR1, leukocyte associated immunoglobulin like receptor 1, was the only receptor to show activation in cirrhotic cells and not healthy cells. This transmembrane glycoprotein consists of a single extracellular IgG binding domain and signals through the ITIM motif similar to that of CD32b. According to both the human protein atlas[130] and the liver cell atlas[114], LAIR1 is not expressed on LSEC. This receptor, however, is associated with increased expression in infiltrating human blood monocytes in early and late-stage cirrhosis.[438] Its expression levels are also associated with poor survival rates with hepatocellular carcinoma.[439] With its ability to bind IgG and strong association with cirrhosis, this would possibly be a receptor to explore further in the future. Particularly to establish whether it is expressed by LSEC.

As previously we couldn't prove which of our chosen receptors were responsible for antibody uptake, we went for a more generic approach to assessing whether these antibodies were internalised via a receptor mediated mechanism. Dextran sulfate was shown in previous studies to completely inhibit the uptake of albumin and mannan in LSEC[440], cementing its role as a non-specific inhibitor of receptor mediated endocytic pathways namely the scavenger and mannose (CD206) receptors. Here we saw considerably discrepancies in our data. Healthy LSEC with **antibody E** showed little difference when treated with DxS, suggesting uptake of this antibody is possibly more of a fluid mediated pinocytic process rather than due to a receptor. Cirrhotic cells incubated with this antibody were inhibited by DxS for at least 8-hours, indicating a different internalisation route into the diseased cell. Regarding **antibody I,** again difference was observed between healthy and cirrhotic LSEC. Possible reasons for this may be different entry routes into the cell or that cirrhotic cells are unable to withstand the change in

charge that comes with DxS incubation. Charge distribution studies of LSEC, showed that sporadic negative charge clusters were present across the cell surface interspersed with positively charged coated pits.[413] This was performed on healthy LSEC therefore it is unknown if the distribution/ charge of cirrhotic LSEC reflects normal cells or has a distinct pattern. However, in immunoelectron microscopy studies it was found in liver disease that LSEC had increased numbers of micro-pinocytic vesicles[441-442], the vacuolar apparatus including endosomes and lysosomes was underdeveloped and this was associated with an increase in frequency of positively charged caveolin-1 pits.[441] Clathrin coated pits were unaccounted for. With DxS being a negatively charged polysaccharide, its blockade of available pits for internalisation and improperly formed internal network of endosomes in cirrhosis may account for the differences between healthy and cirrhotic LSEC. An interesting finding was that with the increased negative charge due to DxS, it would be expected that the antibody with the more basic charge of the three would most likely show increased internalisation, however this was not the case. **Antibody D** had both the highest net charge and pI however uptake was completely obliterated by DxS in both healthy and cirrhotic LSEC. This suggests this process is strongly associated with either scavenger/CD206 mediated uptake or there is a particular residue charge/ factor responsible for this.

As discussed, LSEC possess the ability to intake cargo via either pinocytic or receptor mediated processes. Similar mechanisms are possible in hepatocytes and previous literature have proven that hyperosmolarity induced via sucrose obstructs clathrin coated pit-mediated internalisation.[436,443] As pinocytosis is a clathrin-independent mechanism this allows us to distinguish between the two. Once again **antibody E** in healthy LSEC pre-treated with sucrose showed no difference in uptake to the control LSEC. This along with the DxS data, strongly indicates that healthy LSEC internalise and process this human antibody differently to cirrhotic LSEC which showed significant reduction up to 8-hours post sucrose treatment. This alongside the % cleared MFI shown in Figure 4.28, further suggests these cells partition this antibody differently leading to the increased degradation observed in cirrhotic LSEC. Moreover, our data showing

antibody E to be internalised via a receptor and clathrin independent mechanism strongly suggest healthy LSEC clear this antibody via pinocytosis.

Sucrose is a polar molecule possessing areas of both negative and positive charge[444], therefore should not have as strong inhibitory action as possible with DxS, suggesting charge is not the cause for inhibition of uptake in cirrhotic cells. Again though, it may be the case that due to the dysfunctional nature of LSEC seen within liver injury, they are unable to cope with the change in osmolarity.

Next, we investigated the role of microtubules on the internalisation process. This was of interest as previous studies in rat LSEC suggested clathrin coated pits localised along the microtubules to transport cargo.[401] Firstly, it must be stated that interfering with a major component of the cytoskeleton had detrimental effects on cellular morphology, therefore any results seen may possibly be in response to that rather than the actual mechanism of intake. However, again healthy LSEC saw little impact with intake of **antibodies E** and **I** at the early time points. Whereas again cirrhotic cells were significantly affected. A longer time course in cirrhotic LSEC was performed with similar results showing initial reduction in uptake of all antibodies excluding **antibody I**. By 22-hours that had returned to normal values, which may be due to the reversible nature of nocodazole.[445] As no colocalization was done between clathrin and antibody it cannot be conclusively determined to date that the microtubules were supporting clathrin transport in LSEC.

PI3K plays a considerably role in endocytosis within cells but is not distinguishable from pinocytosis and receptor-mediated internalisation. Cirrhotic LSEC treated with wortmannin, a potent PI3K inhibitor, saw a decrease in internalisation of **antibody D** and **E.** PI3K inhibition leads to the continual activation of Cdc42, leading to the inability to close the vesicular cup.[429] With cirrhotic LSEC already described to have an underdeveloped endosomal system[441], this could explain why they were more impacted by PI3K inhibition than healthy LSEC. Conversely, with cirrhotic LSEC treated with

wortmannin, an increase in vesicles was present for **antibody I.** Without further investigation, the reasons as to why is unknown. However, it may be possible that as this bsAb was implicated to interact with CD32b which does not strongly rely on PI3K but rather SHP-1[242-244] this allows its continual internalisation. Furthermore, in a study on the ghrelin pathway, it was found that SHP-1 regulated PI3K subunit 85; when in the absence of SHP-1, PI3K and thus its downstream AKT activity was increased and the opposite true when SHP-1 was overexpressed.[446] **Antibody I** was indicated by DTSSP to be associated with CD32b, it could be theorised that inhibition of PI3K, would lead to the increase of SHP-1 and thus the increase of CD32b internalisation explaining the significant increase in **antibody I** in wortmannin treated cells. Worthy of note, wortmannin is a reversible inhibitor, meaning it might have been more advantageous to have incubated the cells with both antibody and wortmannin for prolonged observations. Cdc42 is closely regulated by PI3K, and thus as before **antibody I** saw an increase in internalisation abundance at 8-hours. ML141 occasionally exerts influence on other GTPases such as Rac1 and Rab7 etc.[447] Due to this, the lysosomal compartments are unable to form, hence the difference in lysoview staining we observed in Figure 5.25 This could possibly describe the accumulation rather than the lysosomal degradation of **antibody I**.

The final inhibition tool we utilised was a FcRn blocker. With the knowledge that FcRn is the saviour for IgG catabolism it was surprising to find that under inhibition of this interaction we often saw a reduction in internalisation and lysosomal co-localisation of antibody. At the time of writing this I could only find one similar finding in the literature. Whereby knocking out FcRn in podocytes led to a reduction in lysosomal degradation of IgG opsonised complexes and an overall loss of LAMP1 expression.[448] Both our and this research support the possibility that FcRn does play a role in delivering internalised cargo to the lysosomes.[449]

A summary of all findings gained throughout this chapter can be found in Table 5.4.

Table 5. 4: Summary of finding throughout chapter for each antibody

Name	Healthy	Cirrhotic
Antibody A (Chimeric)	Failed serum stability (GSK) Exhibited off target binding in SPR MFI reduced in *MRC1* KD LSEC Reduction in MFI for *CLEC4M* KD LSEC Highest affinity towards FcRn (SPR) Fastest association and slowest dissociation to FcRn	Reduced MFI for both *CLEC4M* and *MRC1* KD LSEC
Antibody B (Humanised)	Reduction in MFI for *MRC1* KD Fastest dissociation from FcRn	**Significant** reduction in MFI at 4-hours in *MRC1* KD LSEC
Antibody C (Humanised)	Highest affinity towards CD32b (SPR) Highest affinity towards CD32aH (SPR)	
Antibody D (Humanised)	No difference observed for *MRC1 and CLEC4M* KD with imaging Lowest affinity to CD32b (SPR) DxS showed a loss of internalisation (**receptor mediated**) PI3K involved in endocytic process FcRn blocked reduced internalisation at 22hrs =FcRn blocker reduced lysosomal degradation	DxS showed a loss of internalisation (**receptor mediated**) Affected by sucrose (**Clathrin dependent mechanism**) Microtubule dependent PI3K affect internalisation at 8-hours Cdc42 inhibition had no affect Affected by microtubules FcRn blockage reduced uptake at later time-points =Initial reduction in lysosomal association
Antibody E (Human)	No difference under DxS (**not receptor dependent**) No affect with sucrose (**clathrin independent**) No microtubules involvement Not affected by PI3K inhibition Affected by FcRn blocker =Less lysosomal association up to 8-hours **Most likely Pinocytosis**	First 8-hours significantly affected by DxS (**receptor mediated**) Affected by sucrose (**clathrin dependent**) Affected by microtubules (l**ocalised on tubules**) Affected by PI3K inhibition Affected by Cdc42 inhibition Affected by FcRn block =Less lysosomal degradation initially
Antibody F (Human)	Reduced MFI in *MRC1* KD LSEC (ss) Rejected from FcyR (SPR) Failed serum stability (GSK)	Reduced MFI in *MRC1* KD LSEC (ss)
Antibody H (bsAb)	Crosslinker showed interaction with CD32b Fab region able to bind CD32b ectodomain	Crosslinker showed interaction with CD32b
Antibody I (bsAb)	*MRC1* KD led to increased MFI Imaging *showed CLEC4M* and *MRC1* KD had no affect Crosslinker showed interaction with CD32b Lowest affinity to FcRn (SPR) DxS: 2-hours loss of internalisation but regains over time Marginal affect by sucrose No microtubules involvement Unaffected by PI3K inhibition Affected by FcRn blocker =Less lysosomal association initially	Imaging showed *LSIGN* and *MRC1* KD had no affect Crosslinker showed interaction with CD32b Delayed signal transduction (proteome) Complete loss with DxS treatment (**receptor mediated**) Affected by sucrose (**Clathrin dependent**) Marginally affected by microtubule inhibition Increased with PI3K inhibition No affect by Cdc42 inhibition (increase at 8-hours) Not affected by FcRn blocker =Increased lysosomal association at the end time points

GSK- per in house GSK testing; SPR- surface plasmon resonance; MFI- median fluorescent intensity; KD- knockdown; DxS- dextran sulfate. = related to following colocalisation studies following FcRn block.

Chapter Six: Conclusion and Considerations

Therapeutic antibodies make up the majority share of the drug industry, estimated to be worth $495 billion by 2030.[1] Yet challenges persist such as poor *in vivo* pharmacokinetics caused by non-specific clearance preventing many therapeutics achieving clinical success. The liver has been implicated as the organ responsible for early catabolism, and in this thesis, we suggest that LSEC play a role in this off-target clearance. We also sought to look at the implications of liver disease and establish if the changes of this complex cellular landscape led to alterations in clearance and its internalisation mechanisms.

At the start of this thesis, we set out to investigate 4 aims. Table 6.1 shows an overview of each aim and the conclusions we have drawn from such.

Table 6. 1: Conclusions made from each aim set out by this thesis

Aims	Findings
1. **To assess expression of key receptors thought to be involved in the scavenging of antibodies within healthy and diseased tissue and cells**	• LSEC **express an extensive portfolio of receptors** able to bind and internalize biotherapeutics • **FcRn:** Gene and protein expression similar in both aetiologies. Similar distribution in both tissue types. Therefore, **not responsible** for the discrepancies in clearance. • **CD206:** No difference in mRNA expression; protein expression marginally elevated in cirrhosis. Majority expression continuous on healthy tissue LSEC, sporadic in cirrhotic tissue (IHC). • **LSIGN:** No real difference in expression profile. Majority expression continuous on healthy tissue LSEC, sporadic in cirrhotic tissue (IHC). • **CD32b:** Gene expression significantly reduced in cirrhotic LSEC. Majority expression continuous on healthy tissue LSEC, sporadic in cirrhotic tissue (IHC).
2. **Quantify LSEC's ability to bind and uptake mAbs/bsAbs**	• Confirmation on the ability to internalize therapeutic antibody by microscopy and flow cytometry. • **Healthy and cirrhotic LSEC process antibody differently** in varying rates and clearance patterns at higher doses.
3. **Elucidate the mechanisms by which LSEC internalize antibody**	• Healthy and cirrhotic LSEC **utilize different internalization** pathways. • Cirrhotic shows a delayed signal transduction and tends to be clathrin dependent, involve microtubule localization, PI3K dependent and likely receptor mediated. • BsAbs may internalize through CD32b • FcRn may play a role in delivery to the lysosomes.
4. **To track the fate of internalized therapeutics within the cell**	• **LSEC can partition mAbs/bsAbs towards lysosomal degradation**. • This rate is altered between healthy and cirrhotic LSEC, and origin of antibody plays a role.

6.1 Clinical implications

Throughout researching and attempting to contextualise some of the data we obtained, I often came across the same issue. To my knowledge very little has been studied on the complex mechanism of how the cellular scope of the human liver causes the off-target clearance of therapeutic antibodies. There is however a plethora of evidence that the liver endothelium plays some capacity of clearance in immune complexes in an array of animal models. Often these immune complexes studied include complexes of mAb and antigen leading to the desired target-mediated clearance. Excluding one paper that observed tumour burden affecting antibody clearance[103], I have not seen any literature that considers how liver injury affects the PK and clearance rates of biotherapeutics. The data obtained throughout this thesis highlights the needed consideration for both the role of human LSEC in PK but also questions if the pre-clinical models used to assess and score antibodies are effective enough to achieve clinical success.

Here we show cirrhosis not only alters internalisation and clearance rates, but clearly internalises antibodies through a different mechanism than that seen in healthy LSEC. Here, cirrhotic LSEC preferred a receptor-mediated clathrin-dependent internalisation mechanism associated with microtubules and PI3K association. Whereas healthy LSEC, in particularly the case of **antibody E**, strongly indicated a pinocytic mode of entry.

This difference has considerable implications in clinical relevancy as it is not healthy individuals who often require antibody-based treatment. With the rising burden of liver injury and disease, individuals are often not diagnosed until the irreversible cirrhotic stage meaning many are left asymptomatic but with altered liver function. This also holds implications in a toxicology sense too. Accumulation within the liver, off-target toxicities and further aggravation of underlying liver injury can have detrimental effects.

Although this thesis does not definitively answer how LSEC internalise and degrade these biotherapeutics and why the changes in liver disease affect this clearance, it does provide a good scope to take this research further. This can have major implications

down the line, for instance if the bsAbs from this thesis are proven to be cleared by CD32b as suggested by our DTSSP crosslinker experiment. Then antibody engineering, like that seen in the anti-CD20 LAGA, can be implemented removing the ability of these therapeutics to bind to FcRs and hopefully increasing their half-life. Increasing half-life of antibody-based therapies is vital as it allows better dosing routines allowing for patient comfort, compliance, but most importantly more effective treatment. Overall, improving knowledge of PK and distribution profiles within the body, helps in the design of better therapeutics.

6.2 Limitations and future research

Hindsight and critically evaluating this thesis has allowed me to gain oversight of where this research is lacking and allowed me to suggest some possible further experiments that would allow more clarity and give more strength to the data presented throughout these chapters.

Firstly, it is important to note, during the project we were subject to a global pandemic resulting in both inaccessibility to the lab during this time but also loss of access to tissue that extended beyond us re-entering the lab space. Although this gained momentum later there are points (particularly in the direct approaches section 5.2) where the sample size is not large enough due to availability to allow for true conclusions as representation is not present. This has meant for instance with the case of CD206, I cannot truly draw any inferences to how these knockdowns affected internalisation despite early data looking promising.

Another limitation to this research was the lacking concentration of antibodies and the time in which they were received. Due to Covid and other factors, I gained access to much of this antibody panel in my 3rd year meaning I had to be conservative on some of the experiments ran. This was somewhat alleviated by using the anti-CD20 as a preliminary testing agent, however in experiments requiring larger concentrations these

had to be set aside. For instance, initially we began this thesis with the intention to perfuse antibodies through *ex vivo* wedges of liver, however this was not feasible with the concentrations provided. Therefore, we moved to inject these antibodies into blocks of tissue. Despite some promising results (see Supplementary Figure S.9), we couldn't afford the opportunity to optimise this to reduce background staining for instance, again due to the concentrations available.

This thesis focuses mainly on the monoculture of LSEC with some supplementary mention of THP-1 and co-cultures assays with HepG2 (Supplementary Figures S1-3). For these co-cultures we saw very little difference in LSEC uptake of therapeutics. However, if I was afforded the time to do this research again, I would endeavour to make these models and assays more relevant to recapitulating the complex histoarchitecture of the liver. Further research, primarily running a HERA-like assay on co-cultures housing both primary hepatocytes and LSEC would be informative. This is important as within the liver, the crosstalk between hepatocytes is vital for their function and in these condition phenotype retains truer than that seen in monocultures. I would also suggest using a modelling system akin to an organ-on-a-chip with co-cultures of relevant cells under a microfluidic system. The flow rate within the liver sinusoids is of high importance and has major effects on the phenotype of LSEC. We mentioned previously how rates differ in these vessels and flow can sometimes be stopped or reversed, this gives some relevance to how we designed our experiments. However, in other research where microfluidic systems have been applied, demonstrated far better retention of expression profile more akin to that seen in the liver.[224] I understand the relevance of outcomes this thesis has made is more orientated for a pharmaceutical industry setting and therefore high throughput is desired, consequently this approach may not be favoured. Nevertheless, it may be a careful consideration to make in the future.

Often in the microscopy internalisation studies, particularly with cirrhotic LSEC, we observed not all cells were positive for internalised antibody. We described previously that the phenotype of LSEC differed along the sinusoid depending on the metabolic zone

and access to oxygen/nutrients. As we isolate a heterogenous population of LSEC, it would have been interesting to have investigated further which population of LSEC in particular was responsible for the internalisation of antibody. This would allow use to understand the location of uptake and allow us to investigate further the receptor responsible. For instance, if LAIR1 was expressed in cells of a particular zone positive for uptake, would allow us to validate the proteome profile data further. This could be visualised through colocalisation with known markers or a tighter regulated selection in the isolation of said cells.

Another improvement I would make is regarding the timings of fixation during the initial flow cytometry and microscopy experiments. Here we fixed cells at the 4- and 8-hour incubation time-points, in which we got very little fluorescence intensity during chimeric antibodies binding. **Antibody A** had its own problems with being a poorly stable antibody and had the tendency to stick to surfaces evidenced in the SPR. However, with the anti-CD20 and anti-CD20 LAGA chimeras, these were both evidenced to be within the lysosomes within 2-hours. Therefore, it is possible that we had missed the processing point of these antibodies. The cost and practicality of access to the confocal microscope was not feasible to extend these time periods. However, If I was to rerun this experiment, I would design a more high-throughput approach and set more timepoints throughout.

Through crosslinker binding we showed possible evidence that the bsAbs interacted with CD32b. Although useful data, I do believe this could be further validated using mass spectrometry to confirm binding. I would propose to adapt this protocol and still using a crosslinker, this time with both DTSSP and DSP to assess binding both internally and on the surface of the cell. This approach would allow us to explore beyond the receptors we investigated in this thesis. The LSEC play host to a large system of scavenger receptors; any one of these may be responsible. With the DxS data suggesting cirrhotic LSEC often internalised via a receptor-mediated process, and CD206 not giving any significant findings in our knockdowns, this leaves the scavenger receptors as possible targets.

Furthermore, this method may also elucidate if CD32b was responsible but can also show if clustering of multiple receptors was also present.

Moreover, we know that therapeutic antibodies are susceptible to post translational modifications. Biotherapeutics are prone to glycosylation and even has been reported to undergo this under particular media compositions.[398] It would be interesting to perfuse/ incubate antibody within liver tissue of both cirrhotic and healthy origin and afterwards somehow retrieve said antibody and explore any differences in sugar additives. Soluble mannose is a known characteristic in cirrhosis, the extent this may interact with a therapeutic may be interesting to explore. Particularly if this addition leads to conformational changes leading to different internalisation mechanisms and clearance rates. Furthermore, it is unknown how the charge distribution across LSEC changes under liver injury so this could be another factor to interrogate further.

Our data suggested that FcRn may be complicit in the delivery of mAb to the lysosomal compartment. As very little literature is published on this especially in a liver context, I do believe this is worthy of more exploration. I think colocalisation tracking of FcRn, mAb and lysosomal compartment would be of interest. It may be that the FcRn within LSEC, as with shown in podocytes[448], may not function to conventional mechanism as normally described. Again, this would require further research.

6.3 Concluding statements

In this thesis I have investigated the role of LSEC in the off-target clearance of therapeutic antibodies. We also sought to see how chronic liver injury affects this internalisation and clearance. We concluded that LSEC express an extensive portfolio of receptors capable of binding to IgG-based therapies. Often mRNA and protein expression were not significantly different, but we did observe considerably different distribution of these receptors between healthy and cirrhotic liver tissue by IHC. We were also able to confirm that LSEC internalised these mAbs and often partitioned them for lysosomal degradation. We also established that cirrhotic and healthy LSEC pathway of

internalisation was distinctly different from one another. Cirrhotic preferred entry by a receptor-mediated, clathrin-dependent means, whereas healthy LSEC often skew towards receptor and clathrin-independent mechanisms.

In conclusion, mAbs and bsAbs development was revolutionary in the therapeutic industry. They hold mass potential, however a vast number of these antibodies developed fail to translate from bench to bedside. This is often due to limited comprehension of PK profiles leading to off-target clearance and poor half-lives. Here we characterise LSEC's capacity to internalise and degrade these antibodies. We have also shown that under chronic liver injury these cells alter in their internalisation profiles. Consequently, we suggest both considerations need to be implemented in future antibody research to truly understand the effects of PK and mechanisms of clearance, allowing these therapeutics to maximise their potential.

References

1. Grandview Research. (2022, August). *https://www.grandviewresearch.com/press-release/global-monoclonal-antibodies-market*. Monoclonal Antibodies Market Growth & Trends.
2. Lu, R.-M., Hwang, Y.-C., Liu, I.-J., Lee, C.-C., Tsai, H.-Z., Li, H.-J., & Wu, H.-C. (2020). Development of therapeutic antibodies for the treatment of diseases. *Journal of Biomedical Science*, *27*(1), 1. https://doi.org/10.1186/s12929-019-0592-z
3. Kaplon, H., Crescioli, S., Chenoweth, A., Visweswaraiah, J., & Reichert, J. M. (2023). Antibodies to watch in 2023. *MAbs*, *15*(1). https://doi.org/10.1080/19420862.2022.2153410
4. Behring, E. & Kitasato, S. Über das Zustandekommen der Diphtherie- Immunität und der Tetanus-Immunität bei Thieren. *Dtsch. Med. Wschr* 16, 1113–1114 (in German) (1890).
5. Behring, E. Untersuchungen über das Zustandekommen der Diphtherie-Immunität bei Thieren. *Dtsch. Med. Wschr.* 16, 1145–1147 (in German) (1890).
6. Ehrlich, P. Die Seitenkettentheorie und ihre Gegner. *Münch. Med. Wschr.* 18, 2123 (in German) (1901).
7. Ehrlich, P. Die Schutzstoffe des Blutes. *Dtsch. Med. Wschr.* 27, 865 (in German
8. Hess, V. (2008). The Administrative Stabilization of Vaccines: Regulating the Diphtheria Antitoxin in France and Germany, 1894–1900. *Science in Context*, *21*(2), 201–227. https://doi.org/10.1017/S0269889708001695
9. Leavy, O. (2016). The birth of monoclonal antibodies. *Nature Immunology*, *17*(S1), S13–S13. https://doi.org/10.1038/ni.3608
10. Köhler, G. and Milstein, C (1975). Continuous cultures of fused cells secreting antibody of predefined specificity. *Nature*, *256*(5517), 495–497. https://doi.org/10.1038/256495a0
11. Todd, P. A., & Brogden, R. N. (1989). Muromonab CD3. A review of its pharmacology and therapeutic potential. *Drugs*, *37*(6), 871–899. https://doi.org/10.2165/00003495-198937060-00004
12. Brennan, F. R., Morton, L. D., Spindeldreher, S., Kiessling, A., Allenspach, R., Hey, A., Muller, P. Y., Frings, W., & Sims, J. (2010). Safety and immunotoxicity assessment of immunomodulatory monoclonal antibodies. *MAbs*, *2*(3), 233–255. https://doi.org/10.4161/mabs.2.3.11782
13. Sgro, C. (1995). Side-effects of a monoclonal antibody, muromonab CD3/orthoclone OKT3: bibliographic review. *Toxicology*, *105*(1), 23–29. https://doi.org/10.1016/0300-483X(95)03123-W

14. Morrison, S. L., Johnson, M. J., Herzenberg, L. A., & Oi, V. T. (1984). Chimeric human antibody molecules: mouse antigen-binding domains with human constant region domains. *Proceedings of the National Academy of Sciences*, *81*(21), 6851–6855. https://doi.org/10.1073/pnas.81.21.6851
15. Lacy, H. M., Gunnell, M. G., Laurenzana, E. M., & Owens, S. M. (2008). Engineering and characterization of a mouse/human chimeric anti-phencyclidine monoclonal antibody. *International Immunopharmacology*, *8*(1), 1–11. https://doi.org/10.1016/j.intimp.2007.09.020
16. Epic Investigators, 1994. Use of a monoclonal antibody directed against the platelet glycoprotein IIb/IIIa receptor in high-risk coronary angioplasty. *New England Journal of Medicine*, *330*(14), pp.956-961
17. Maloney DG, Grillo-López AJ, White CA, Bodkin D, Schilder RJ, Neidhart JA, Janakiraman N, Foon KA, Liles TM, Dallaire BK, Wey K, Royston I, Davis T, Levy R. IDEC-C2B8 (Rituximab) anti-CD20 monoclonal antibody therapy in patients with relapsed low-grade non-Hodgkin's lymphoma. Blood. 1997 Sep 15;90(6):2188-95. PMID: 9310469.
18. Jones, P. T., Dear, P. H., Foote, J., Neuberger, M. S., & Winter, G. (1986). Replacing the complementarity-determining regions in a human antibody with those from a mouse. *Nature*, *321*(6069), 522–525. https://doi.org/10.1038/321522a0
19. Mayrhofer, P., & Kunert, R. (2018). Nomenclature of humanized mAbs: Early concepts, current challenges and future perspectives. *Human Antibodies*, *27*(1), 37–51. https://doi.org/10.3233/HAB-180347
20. Milo, R. (2014). The efficacy and safety of daclizumab and its potential role in the treatment of multiple sclerosis. *Therapeutic Advances in Neurological Disorders*, *7*(1), 7–21. https://doi.org/10.1177/1756285613504021
21. U.S. Food and Drug Administration. 2018. *CDER Statement Zinbryta Withdrawal*. [online] Available at: <https://www.fda.gov/drugs/drug-safety-and-availability/fda-working-manufacturers-withdraw-zinbryta-market-united-states> [Accessed 28 October 2020].
22. Smith, G. P. (1985). Filamentous Fusion Phage: Novel Expression Vectors That Display Cloned Antigens on the Virion Surface. *Science*, *228*(4705), 1315–1317. https://doi.org/10.1126/science.4001944
23. Winter, G., Griffiths, A. D., Hawkins, R. E., & Hoogenboom, H. R. (1994). Making Antibodies by Phage Display Technology. *Annual Review of Immunology*, *12*(1), 433–455. https://doi.org/10.1146/annurev.iy.12.040194.002245
24. Kempeni, J. (1999). Preliminary results of early clinical trials with the fully human anti-TNFalpha monoclonal antibody D2E7. *Annals of the Rheumatic Diseases*, *58*(Supplement 1), i70–i72. https://doi.org/10.1136/ard.58.2008.i70
25. Jakobovits, A., Amado, R. G., Yang, X., Roskos, L., & Schwab, G. (2007). From XenoMouse technology to panitumumab, the first fully human antibody product

from transgenic mice. *Nature Biotechnology*, *25*(10), 1134–1143. https://doi.org/10.1038/nbt1337

26. Lonberg, N., Taylor, L. D., Harding, F. A., Trounstine, M., Higgins, K. M., Schramm, S. R., Kuo, C.-C., Mashayekh, R., Wymore, K., McCabe, J. G., Munoz-O'Regan, D., O'Donnell, S. L., Lapachet, E. S. G., Bengoechea, T., Fishwild, D. M., Carmack, C. E., Kay, R. M., & Huszar, D. (1994). Antigen-specific human antibodies from mice comprising four distinct genetic modifications. *Nature*, *368*(6474), 856–859. https://doi.org/10.1038/368856a0
27. Edelman, G. M., Cunningham, B. A., Gall, W. E., Gottlieb, P. D., Rutishauser, U., & Waxdal, M. J. (1969). THE COVALENT STRUCTURE OF AN ENTIRE γG IMMUNOGLOBULIN MOLECULE. *Proceedings of the National Academy of Sciences*, *63*(1), 78–85. https://doi.org/10.1073/pnas.63.1.78
28. Silverton, E. W., Navia, M. A., & Davies, D. R. (1977). Three-dimensional structure of an intact human immunoglobulin. *Proceedings of the National Academy of Sciences*, *74*(11), 5140–5144. https://doi.org/10.1073/pnas.74.11.5140
29. Cain, P., Huang, L., Tang, Y., Anguiano, V. and Feng, Y. (2023) Impact of IgG subclass on monoclonal antibody developability. *mAbs* 15(1) 2191302. doi: 10.1080/1940862.2023.2191302
30. de Lau, W. B., Heije, K., Neefjes, J. J., Oosterwegel, M., Rozemuller, E., & Bast, B. J. (1991). Absence of preferential homologous H/L chain association in hybrid hybridomas. *Journal of Immunology (Baltimore, Md. : 1950)*, *146*(3), 906–914.
31. Manzke, O., Tesch, H., Lorenzen, J., Diehl, V., & Bohlen, H. (2001). Locoregional treatment of low-grade B-cell lymphoma with CD3xCD19 bispecific antibodies and CD28 costimulation. II. Assessment of cellular immune responses. *International Journal of Cancer*, *91*(4), 516–522. https://doi.org/10.1002/1097-0215(200002)9999:9999<::aid-ijc1069>3.0.co;2-a
32. Ma, J., Mo, Y., Tang, M., Shen, J., Qi, Y., Zhao, W., Huang, Y., Xu, Y., & Qian, C. (2021). Bispecific Antibodies: From Research to Clinical Application. *Frontiers in Immunology*, *12*. https://doi.org/10.3389/fimmu.2021.626616
33. Nisonoff, A., Wissler, F. C., & Lipman, L. N. (1960). Properties of the Major Component of a Peptic Digest of Rabbit Antibody. *Science*, *132*(3441), 1770–1771. https://doi.org/10.1126/science.132.3441.1770
34. Nisonoff, A., & Rivers, M. M. (1961). Recombination of a mixture of univalent antibody fragments of different specificity. *Archives of Biochemistry and Biophysics*, *93*(2), 460–462. https://doi.org/10.1016/0003-9861(61)90296-X
35. Wolf, E., Hofmeister, R., Kufer, P., Schlereth, B., & Baeuerle, P. A. (2005). BiTEs: bispecific antibody constructs with unique anti-tumor activity. *Drug Discovery Today*, *10*(18), 1237–1244. https://doi.org/10.1016/S1359-6446(05)03554-3
36. Ross, S. L., Sherman, M., McElroy, P. L., Lofgren, J. A., Moody, G., Baeuerle, P. A., Coxon, A., & Arvedson, T. (2017). Bispecific T cell engager (BiTE®) antibody

constructs can mediate bystander tumor cell killing. *PLOS ONE*, *12*(8), e0183390. https://doi.org/10.1371/journal.pone.0183390

37. Arvedson, T. L., Balazs, M., Bogner, P., Black, K., Graham, K., Henn, A., Friedrich, M., Hoffmann, P., Kischel, R., Kufer, P., Lutterbuese, R., Muenz, M., Raum, T., Rattel, B., Rex, K., Rock, D., Thomas, O., Wahl, J., Wolf, A., & Coxon, A. (2017). Generation of half-life extended anti-CD33 BiTE® antibody constructs compatible with once-weekly dosing. *Cancer Research*, *77*(13_Supplement), 55–55. https://doi.org/10.1158/1538-7445.AM2017-55
38. Scott, M. J., Lee, J. A., Wake, M. S., Batt, K. v., Wattam, T. A., Hiles, I. D., Batuwangala, T. D., Ashman, C. I., & Steward, M. (2017). 'In-Format' screening of a novel bispecific antibody format reveals significant potency improvements relative to unformatted molecules. *MAbs*, *9*(1), 85–93. https://doi.org/10.1080/19420862.2016.1249078
39. Datta-Mannan, A. (2019). Mechanisms Influencing the Pharmacokinetics and Disposition of Monoclonal Antibodies and Peptides. *Drug Metabolism and Disposition*, *47*(10), 1100–1110. https://doi.org/10.1124/dmd.119.086488
40. Dostalek, M., Gardner, I., Gurbaxani, B. M., Rose, R. H., & Chetty, M. (2013). Pharmacokinetics, pharmacodynamics and physiologically-based pharmacokinetic modelling of monoclonal antibodies. *Clinical Pharmacokinetics*, *52*(2), 83–124. https://doi.org/10.1007/s40262-012-0027-4
41. Kamath, A. v. (2016). Translational pharmacokinetics and pharmacodynamics of monoclonal antibodies. *Drug Discovery Today: Technologies*, *21–22*, 75–83. https://doi.org/10.1016/j.ddtec.2016.09.004
42. Leipold, D., & Prabhu, S. (2019). Pharmacokinetic and Pharmacodynamic Considerations in the Design of Therapeutic Antibodies. *Clinical and Translational Science*, *12*(2), 130–139. https://doi.org/10.1111/cts.12597
43. Wines, B. D., Powell, M. S., Parren, P. W. H. I., Barnes, N., & Hogarth, P. M. (2000). The IgG Fc Contains Distinct Fc Receptor (FcR) Binding Sites: The Leukocyte Receptors FcγRI and FcγRIIa Bind to a Region in the Fc Distinct from That Recognized by Neonatal FcR and Protein A. *The Journal of Immunology*, *164*(10), 5313–5318. https://doi.org/10.4049/jimmunol.164.10.5313
44. Deisenhofer, J. (1981). Crystallographic refinement and atomic models of a human Fc fragment and its complex with fragment B of protein A from Staphylococcus aureus at 2.9- and 2.8-A resolution. *Biochemistry*, *20*(9), 2361–2370.
45. Shields, R. L., Namenuk, A. K., Hong, K., Meng, Y. G., Rae, J., Briggs, J., Xie, D., Lai, J., Stadlen, A., Li, B., Fox, J. A., & Presta, L. G. (2001). High resolution mapping of the binding site on human IgG1 for Fc gamma RI, Fc gamma RII, Fc gamma RIII, and FcRn and design of IgG1 variants with improved binding to the Fc gamma R. *The Journal of Biological Chemistry*, *276*(9), 6591–6604. https://doi.org/10.1074/jbc.M009483200

46. BRAMBELL, F. W. R. (1958). THE PASSIVE IMMUNITY OF THE YOUNG MAMMAL. *Biological Reviews*, *33*(4), 488–531. https://doi.org/10.1111/j.1469-185X.1958.tb01412.x
47. Simister, N. E., & Mostov, K. E. (1989). An Fc receptor structurally related to MHC class I antigens. *Nature*, *337*(6203), 184–187. https://doi.org/10.1038/337184a0
48. Qiao, S.-W., Kobayashi, K., Johansen, F.-E., Sollid, L. M., Andersen, J. T., Milford, E., Roopenian, D. C., Lencer, W. I., & Blumberg, R. S. (2008). Dependence of Antibody-Mediated Presentation of Antigen on FcRn. *Proceedings of the National Academy of Sciences of the United States of America*, *105*(27), 9337–9342. http://www.jstor.org/stable/25462970
49. Vaughn, D. E., & Bjorkman, P. J. (1998). Structural basis of pH-dependent antibody binding by the neonatal Fc receptor. *Structure*, *6*(1), 63–73. https://doi.org/10.1016/S0969-2126(98)00008-2
50. Grevys, A., Frick, R., Mester, S., Flem-Karlsen, K., Nilsen, J., Foss, S., Sand, K. M. K., Emrich, T., Fischer, J. A. A., Greiff, V., Sandlie, I., Schlothauer, T., & Andersen, J. T. (2022). Antibody variable sequences have a pronounced effect on cellular transport and plasma half-life. *IScience*, *25*(2), 103746. https://doi.org/10.1016/j.isci.2022.103746
51. Kamath, A. v. (2016). Translational pharmacokinetics and pharmacodynamics of monoclonal antibodies. *Drug Discovery Today: Technologies*, *21–22*, 75–83. https://doi.org/10.1016/j.ddtec.2016.09.004
52. Baxter, L. T., Zhu, H., Mackensen, D. G., & Jain, R. K. (1994). Physiologically based pharmacokinetic model for specific and nonspecific monoclonal antibodies and fragments in normal tissues and human tumor xenografts in nude mice. *Cancer Research*, *54*(6), 1517–1528.
53. Ryman, J. T., & Meibohm, B. (2017). Pharmacokinetics of Monoclonal Antibodies. *CPT: Pharmacometrics & Systems Pharmacology*, *6*(9), 576–588. https://doi.org/10.1002/psp4.12224
54. Kraft, T. E., Richter, W. F., Emrich, T., Knaupp, A., Schuster, M., Wolfert, A., & Kettenberger, H. (2020). Heparin chromatography as an *in vitro* predictor for antibody clearance rate through pinocytosis. *MAbs*, *12*(1). https://doi.org/10.1080/19420862.2019.1683432
55. Thorsteinson, N., Gunn, J. R., Kelly, K., Long, W., & Labute, P. (2021). Structure-based charge calculations for predicting isoelectric point, viscosity, clearance, and profiling antibody therapeutics. *MAbs*, *13*(1). https://doi.org/10.1080/19420862.2021.1981805
56. Igawa, T., Tsunoda, H., Tachibana, T., Maeda, A., Mimoto, F., Moriyama, C., Nanami, M., Sekimori, Y., Nabuchi, Y., Aso, Y., & Hattori, K. (2010). Reduced elimination of IgG antibodies by engineering the variable region. *Protein*

Engineering Design and Selection, *23*(5), 385–392. https://doi.org/10.1093/protein/gzq009

57. Li, B., Tesar, D., Boswell, C. A., Cahaya, H. S., Wong, A., Zhang, J., Meng, Y. G., Eigenbrot, C., Pantua, H., Diao, J., Kapadia, S. B., Deng, R., & Kelley, R. F. (2014). Framework selection can influence pharmacokinetics of a humanized therapeutic antibody through differences in molecule charge. *MAbs*, *6*(5), 1255–1264. https://doi.org/10.4161/mabs.29809
58. Datta-Mannan, A., Thangaraju, A., Leung, D., Tang, Y., Witcher, D. R., Lu, J., & Wroblewski, V. J. (2015). Balancing charge in the complementarity-determining regions of humanized mAbs without affecting pI reduces non-specific binding and improves the pharmacokinetics. *MAbs*, *7*(3), 483–493. https://doi.org/10.1080/19420862.2015.1016696
59. Boswell, C. A., Tesar, D. B., Mukhyala, K., Theil, F.-P., Fielder, P. J., & Khawli, L. A. (2010). Effects of Charge on Antibody Tissue Distribution and Pharmacokinetics. *Bioconjugate Chemistry*, *21*(12), 2153–2163. https://doi.org/10.1021/bc100261d
60. Sampei, Z., Igawa, T., Soeda, T., Okuyama-Nishida, Y., Moriyama, C., Wakabayashi, T., Tanaka, E., Muto, A., Kojima, T., Kitazawa, T., Yoshihashi, K., Harada, A., Funaki, M., Haraya, K., Tachibana, T., Suzuki, S., Esaki, K., Nabuchi, Y., & Hattori, K. (2013). Identification and Multidimensional Optimization of an Asymmetric Bispecific IgG Antibody Mimicking the Function of Factor VIII Cofactor Activity. *PLoS ONE*, *8*(2), e57479. https://doi.org/10.1371/journal.pone.0057479
61. Schoch, A., Kettenberger, H., Mundigl, O., Winter, G., Engert, J., Heinrich, J., & Emrich, T. (2015). Charge-mediated influence of the antibody variable domain on FcRn-dependent pharmacokinetics. *Proceedings of the National Academy of Sciences*, *112*(19), 5997–6002. https://doi.org/10.1073/pnas.1408766112
62. Gan, Z., Ram, S., Vaccaro, C., Ober, R. J., & Ward, E. S. (2009). Analyses of the Recycling Receptor, FcRn, in Live Cells Reveal Novel Pathways for Lysosomal Delivery. *Traffic*, *10*(5), 600–614. https://doi.org/10.1111/j.1600-0854.2009.00887.x
63. Waibl, F., Fernández-Quintero, M. L., Wedl, F. S., Kettenberger, H., Georges, G., & Liedl, K. R. (2022). Comparison of hydrophobicity scales for predicting biophysical properties of antibodies. *Frontiers in Molecular Biosciences*, *9*. https://doi.org/10.3389/fmolb.2022.960194
64. Lyon, R. P., Bovee, T. D., Doronina, S. O., Burke, P. J., Hunter, J. H., Neff-LaFord, H. D., Jonas, M., Anderson, M. E., Setter, J. R., & Senter, P. D. (2015). Reducing hydrophobicity of homogeneous antibody-drug conjugates improves pharmacokinetics and therapeutic index. *Nature Biotechnology*, *33*(7), 733–735. https://doi.org/10.1038/nbt.3212
65. Amin, S., Barnett, G. v., Pathak, J. A., Roberts, C. J., & Sarangapani, P. S. (2014). Protein aggregation, particle formation, characterization & rheology. *Current*

Opinion in Colloid & Interface Science, *19*(5), 438–449. https://doi.org/10.1016/j.cocis.2014.10.002

66. Vugmeyster, Y., Szklut, P., Wensel, D., Ross, J., Xu, X., Awwad, M., Gill, D., Tchistiakov, L., & Warner, G. (2011). Complex Pharmacokinetics of a Humanized Antibody Against Human Amyloid Beta Peptide, Anti-Abeta Ab2, in Nonclinical Species. *Pharmaceutical Research*, *28*(7), 1696–1706. https://doi.org/10.1007/s11095-011-0405-x
67. Dobson, C. L., Devine, P. W. A., Phillips, J. J., Higazi, D. R., Lloyd, C., Popovic, B., Arnold, J., Buchanan, A., Lewis, A., Goodman, J., van der Walle, C. F., Thornton, P., Vinall, L., Lowne, D., Aagaard, A., Olsson, L.-L., Ridderstad Wollberg, A., Welsh, F., Karamanos, T. K., … Lowe, D. C. (2016). Engineering the surface properties of a human monoclonal antibody prevents self-association and rapid clearance in vivo. *Scientific Reports*, *6*(1), 38644. https://doi.org/10.1038/srep38644
68. Robbie, G. J., Criste, R., Dall'Acqua, W. F., Jensen, K., Patel, N. K., Losonsky, G. A., & Griffin, M. P. (2013). A Novel Investigational Fc-Modified Humanized Monoclonal Antibody, Motavizumab-YTE, Has an Extended Half-Life in Healthy Adults. *Antimicrobial Agents and Chemotherapy*, *57*(12), 6147–6153. https://doi.org/10.1128/AAC.01285-13
69. Liu, R., Oldham, R., Teal, E., Beers, S., & Cragg, M. (2020). Fc-Engineering for Modulated Effector Functions—Improving Antibodies for Cancer Treatment. *Antibodies*, *9*(4), 64. https://doi.org/10.3390/antib9040064
70. *WO2018029474A2 https://patents.google.com/patent/WO2018029474A2/en (PATENT)*
71. Zhang, Z., Shah, B., & Richardson, J. (2019). Impact of Fc N-glycan sialylation on IgG structure. *MAbs*, *11*(8), 1381–1390. https://doi.org/10.1080/19420862.2019.1655377
72. Hayes, J. M., Frostell, A., Karlsson, R., Müller, S., Martín, S. M., Pauers, M., Reuss, F., Cosgrave, E. F., Anneren, C., Davey, G. P., & Rudd, P. M. (2017). Identification of Fc Gamma Receptor Glycoforms That Produce Differential Binding Kinetics for Rituximab. *Molecular & Cellular Proteomics*, *16*(10), 1770–1788. https://doi.org/10.1074/mcp.M117.066944
73. Zou, G., Ochiai, H., Huang, W., Yang, Q., Li, C., & Wang, L.-X. (2011). Chemoenzymatic Synthesis and Fcγ Receptor Binding of Homogeneous Glycoforms of Antibody Fc Domain. Presence of a Bisecting Sugar Moiety Enhances the Affinity of Fc to FcγIIIa Receptor. *Journal of the American Chemical Society*, *133*(46), 18975–18991. https://doi.org/10.1021/ja208390n
74. Zheng, K., Bantog, C., & Bayer, R. (2011). The impact of glycosylation on monoclonal antibody conformation and stability. *MAbs*, *3*(6), 568–576. https://doi.org/10.4161/mabs.3.6.17922

75. Sinclair, A. M., & Elliott, S. (2005). Glycoengineering: The effect of glycosylation on the properties of therapeutic proteins. *Journal of Pharmaceutical Sciences*, *94*(8), 1626–1635. https://doi.org/10.1002/jps.20319
76. Lee, S. J., Evers, S., Roeder, D., Parlow, A. F., Risteli, J., Risteli, L., Lee, Y. C., Feizi, T., Langen, H., & Nussenzweig, M. C. (2002). Mannose Receptor-Mediated Regulation of Serum Glycoprotein Homeostasis. *Science*, *295*(5561), 1898–1901. https://doi.org/10.1126/science.1069540
77. Elliott, S., Pham, E., & Macdougall, I. C. (2008). Erythropoietins: A common mechanism of action. *Experimental Hematology*, *36*(12), 1573–1584. https://doi.org/10.1016/j.exphem.2008.08.003
78. Luo, C., Chen, S., Xu, N., Wang, C., Sai, W. bo, Zhao, W., Li, Y. chun, Hu, X. jing, Tian, H., Gao, X. dong, & Yao, W. bing. (2017). Glycoengineering of pertuzumab and its impact on the pharmacokinetic/pharmacodynamic properties. *Scientific Reports*, *7*(1), 46347. https://doi.org/10.1038/srep46347
79. Allavena, P., Chieppa, M., Monti, P., & Piemonti, L. (2004). From Pattern Recognition Receptor to Regulator of Homeostasis: The Double-Faced Macrophage Mannose Receptor. *Critical Reviews in Immunology*, *24*(3), 179–192. https://doi.org/10.1615/CritRevImmunol.v24.i3.20
80. Jones, A. J. S., Papac, D. I., Chin, E. H., Keck, R., Baughman, S. A., Lin, Y. S., Kneer, J., & Battersby, J. E. (2007). Selective clearance of glycoforms of a complex glycoprotein pharmaceutical caused by terminal N-acetylglucosamine is similar in humans and cynomolgus monkeys. *Glycobiology*, *17*(5), 529–540. https://doi.org/10.1093/glycob/cwm017
81. Huang, L., Biolsi, S., Bales, K. R., & Kuchibhotla, U. (2006). Impact of variable domain glycosylation on antibody clearance: An LC/MS characterization. *Analytical Biochemistry*, *349*(2), 197–207. https://doi.org/10.1016/j.ab.2005.11.012
82. Chen, X., Liu, Y. D., & Flynn, G. C. (2008). The effect of Fc glycan forms on human IgG2 antibody clearance in humans. *Glycobiology*, *19*(3), 240–249. https://doi.org/10.1093/glycob/cwn120
83. Harris, R. J. (2005). Heterogeneity of recombinant antibodies: linking structure to function. *Developments in Biologicals*, *122*, 117–127.
84. Wright, A., & Morrison, S. L. (1994). Effect of altered CH2-associated carbohydrate structure on the functional properties and in vivo fate of chimeric mouse-human immunoglobulin G1. *The Journal of Experimental Medicine*, *180*(3), 1087–1096. https://doi.org/10.1084/jem.180.3.1087
85. Yu, M., Brown, D., Reed, C., Chung, S., Lutman, J., Stefanich, E., Wong, A., Stephan, J.-P., & Bayer, R. (2012). Production, characterization and pharmacokinetic properties of antibodies with N-linked Mannose-5 glycans. *MAbs*, *4*(4), 475–487. https://doi.org/10.4161/mabs.20737

86. Kanda, Y., Yamada, T., Mori, K., Okazaki, A., Inoue, M., Kitajima-Miyama, K., Kuni-Kamochi, R., Nakano, R., Yano, K., Kakita, S., Shitara, K., & Satoh, M. (2007). Comparison of biological activity among nonfucosylated therapeutic IgG1 antibodies with three different N-linked Fc oligosaccharides: the high-mannose, hybrid, and complex types. *Glycobiology*, *17*(1), 104–118. https://doi.org/10.1093/glycob/cwl057
87. Goetze, A. M., Liu, Y. D., Zhang, Z., Shah, B., Lee, E., Bondarenko, P. v., & Flynn, G. C. (2011). High-mannose glycans on the Fc region of therapeutic IgG antibodies increase serum clearance in humans. *Glycobiology*, *21*(7), 949–959. https://doi.org/10.1093/glycob/cwr027
88. Liu, Y. D., van Enk, J. Z., & Flynn, G. C. (2009). Human antibody Fc deamidation in vivo. *Biologicals*, *37*(5), 313–322. https://doi.org/10.1016/j.biologicals.2009.06.001
89. Yan, Q., Huang, M., Lewis, M. J., & Hu, P. (2018). Structure Based Prediction of Asparagine Deamidation Propensity in Monoclonal Antibodies. *MAbs*, *10*(6), 901–912. https://doi.org/10.1080/19420862.2018.1478646
90. Abdel-Misih, S. and Bloomston, M., 2010. Liver Anatomy. *Surgical Clinics of North America*, 90(4), pp.643-653.
91. British Liver Trust. 2020. *About The Liver - British Liver Trust*. [online] Available at: <https://britishlivertrust.org.uk/information-and-support/liver-health-2/aboutheliver/> [Accessed 24 May 2020].
92. Mall, F., 1906. A study of the structural unit of the liver. *American Journal of Anatomy*, 5(3), pp.227-308.
93. Strauss, O., Phillips, A., Ruggiero, K., Bartlett, A. and Dunbar, P., 2017. Immunofluorescence identifies distinct subsets of endothelial cells in the human liver. *Journal of Hepatology*, 66(1), p.S654.
94. Elvevold, K., Simon-Santamaria, J., Hasvold, H., McCourt, P., Smedsrød, B. and Sørensen, K., 2008. Liver sinusoidal endothelial cells depend on mannose receptor-mediated recruitment of lysosomal enzymes for normal degradation capacity. *Hepatology*, 48(6), pp.2007-2015.
95. Sørensen, K. K., & Smedsrød, B. (2020). The Liver Sinusoidal Endothelial Cell. In *The Liver* (pp. 422–434). Wiley. https://doi.org/10.1002/9781119436812.ch34
96. MacPhee, P. J., Schmidt, E. E., & Groom, A. C. (1995). Intermittence of blood flow in liver sinusoids, studied by high-resolution in vivo microscopy. *American Journal of Physiology-Gastrointestinal and Liver Physiology*, *269*(5), G692–G698. https://doi.org/10.1152/ajpgi.1995.269.5.G692
97. Bhandari, S., Larsen, A. K., McCourt, P., Smedsrød, B., & Sørensen, K. K. (2021). The Scavenger Function of Liver Sinusoidal Endothelial Cells in Health and Disease. *Frontiers in Physiology*, *12*. https://doi.org/10.3389/fphys.2021.757469

98. Henderson, L. A., Baynes, J. W., & Thorpe, S. R. (1982). Identification of the sites of IgG catabolism in the rat. *Archives of Biochemistry and Biophysics*, *215*(1), 1–11. https://doi.org/10.1016/0003-9861(82)90272-7
99. Wright, A., Sato, Y., Okada, T., Chang, K. H., Endo, T., & Morrison, S. L. (2000). In vivo trafficking and catabolism of IgG1 antibodies with Fc associated carbohydrates of differing structure. *Glycobiology*, *10*(12), 1347–1355. https://doi.org/10.1093/glycob/10.12.1347
100. Yip, V., Palma, E., Tesar, D. B., Mundo, E. E., Bumbaca, D., Torres, E. K., Reyes, N. A., Shen, B. Q., Fielder, P. J., Prabhu, S., Khawli, L. A., & Boswell, C. A. (2014). Quantitative cumulative biodistribution of antibodies in mice. *MAbs*, *6*(3), 689–696. https://doi.org/10.4161/mabs.28254
101. Singh Jaggi, J., Carrasquillo, J. A., Seshan, S. v., Zanzonico, P., Henke, E., Nagel, A., Schwartz, J., Beattie, B., Kappel, B. J., Chattopadhyay, D., Xiao, J., Sgouros, G., Larson, S. M., & Scheinberg, D. A. (2007). Improved tumor imaging and therapy via i.v. IgG–mediated time-sequential modulation of neonatal Fc receptor. *Journal of Clinical Investigation*, *117*(9), 2422–2430. https://doi.org/10.1172/JCI32226
102. Eigenmann, M. J., Fronton, L., Grimm, H. P., Otteneder, M. B., & Krippendorff, B.-F. (2017). Quantification of IgG monoclonal antibody clearance in tissues. *MAbs*, *9*(6), 1007–1015. https://doi.org/10.1080/19420862.2017.1337619
103. Ferl, G. Z., Kenanova, V., Wu, A. M., & DiStefano, J. J. (2006). A two-tiered physiologically based model for dually labeled single-chain Fv-Fc antibody fragments. *Molecular Cancer Therapeutics*, *5*(6), 1550–1558. https://doi.org/10.1158/1535-7163.MCT-06-0072
104. Datta-Mannan, A., Molitoris, B. A., Feng, Y., Martinez, M. M., Sandoval, R. M., Brown, R. M., Merkel, D., Croy, J. E., & Dunn, K. W. (2023). Intravital Microscopy Reveals Unforeseen Biodistribution Within the Liver and Kidney Mechanistically Connected to the Clearance of a Bifunctional Antibody. *Drug Metabolism and Disposition*, *51*(3), 403–412. https://doi.org/10.1124/dmd.122.001049
105. Aschoff L. Das reticulo-endotheliale system. *Ergeb Inn Med Kinderheilkd* (1924) 26:1–118.
106. Seternes, T., Sørensen, K., & Smedsrød, B. (2002). Scavenger endothelial cells of vertebrates: A nonperipheral leukocyte system for high-capacity elimination of waste macromolecules. *Proceedings of the National Academy of Sciences*, *99*(11), 7594–7597. https://doi.org/10.1073/pnas.102173299
107. Kupffer, C. Ueber Sternzellen der Leber. *Archiv f. mikrosk. Anat.* 12, 353–358 (1876). https://doi.org/10.1007/BF02933897
108. Browicz. (1899). Ueber intravasculäre Zellen in den Blutcapillaren der Leberacini. *Archiv Für Mikroskopische Anatomie*, *55*(1), 420–426. https://doi.org/10.1007/BF02977740

109. Naito, M., Hasegawa, G., & Takahashi, K. (1998). Development, differentiation, and maturation of Kupffer cells. *Microscopy Research and Technique*, *39*(4), 350–364. https://doi.org/10.1002/(SICI)1097-0029(19971115)39:4<350::AID-JEMT5>3.0.CO;2-L
110. Biozzi G., Stiffel C. The physiopathology of the reticuloendothelial cells of the liver and spleen. *Progress in Liver Diseases.* 1965;2:p. 166
111. Aizarani, N., Saviano, A., Sagar, Mailly, L., Durand, S., Herman, J. S., Pessaux, P., Baumert, T. F., & Grün, D. (2019). A human liver cell atlas reveals heterogeneity and epithelial progenitors. *Nature*, *572*(7768), 199–204. https://doi.org/10.1038/s41586-019-1373-2
112. Andrews, T. S., Atif, J., Liu, J. C., Perciani, C. T., Ma, X., Thoeni, C., Slyper, M., Eraslan, G., Segerstolpe, A., Manuel, J., Chung, S., Winter, E., Cirlan, I., Khuu, N., Fischer, S., Rozenblatt-Rosen, O., Regev, A., McGilvray, I. D., Bader, G. D., & MacParland, S. A. (2022). Single-Cell, Single-Nucleus, and Spatial RNA Sequencing of the Human Liver Identifies Cholangiocyte and Mesenchymal Heterogeneity. *Hepatology Communications*, *6*(4), 821–840. https://doi.org/10.1002/hep4.1854
113. Guilliams, M., Bonnardel, J., Haest, B., Vanderborght, B., Wagner, C., Remmerie, A., Bujko, A., Martens, L., Thoné, T., Browaeys, R., de Ponti, F. F., Vanneste, B., Zwicker, C., Svedberg, F. R., Vanhalewyn, T., Gonçalves, A., Lippens, S., Devriendt, B., Cox, E., … Scott, C. L. (2022). Spatial proteogenomics reveals distinct and evolutionarily conserved hepatic macrophage niches. *Cell*, *185*(2), 379-396.e38. https://doi.org/10.1016/j.cell.2021.12.018
114. Ramachandran, P., Dobie, R., Wilson-Kanamori, J. R., Dora, E. F., Henderson, B. E. P., Luu, N. T., Portman, J. R., Matchett, K. P., Brice, M., Marwick, J. A., Taylor, R. S., Efremova, M., Vento-Tormo, R., Carragher, N. O., Kendall, T. J., Fallowfield, J. A., Harrison, E. M., Mole, D. J., Wigmore, S. J., … Henderson, N. C. (2019). Resolving the fibrotic niche of human liver cirrhosis at single-cell level. *Nature*, *575*(7783), 512–518. https://doi.org/10.1038/s41586-019-1631-3
115. Sharma, A., Seow, J. J. W., Dutertre, C.-A., Pai, R., Blériot, C., Mishra, A., Wong, R. M. M., Singh, G. S. N., Sudhagar, S., Khalilnezhad, S., Erdal, S., Teo, H. M., Khalilnezhad, A., Chakarov, S., Lim, T. K. H., Fui, A. C. Y., Chieh, A. K. W., Chung, C. P., Bonney, G. K., … DasGupta, R. (2020). Onco-fetal Reprogramming of Endothelial Cells Drives Immunosuppressive Macrophages in Hepatocellular Carcinoma. *Cell*, *183*(2), 377-394.e21. https://doi.org/10.1016/j.cell.2020.08.040
116. Guilliams, M., & Scott, C. L. (2022). Liver macrophages in health and disease. *Immunity*, *55*(9), 1515–1529. https://doi.org/10.1016/j.immuni.2022.08.002
117. Wu, X., Hollingshead, N., Roberto, J., Knupp, A., Kenerson, H., Chen, A., Strickland, I., Horton, H., Yeung, R., Soysa, R., & Crispe, I. N. (2020). Human Liver Macrophage Subsets Defined by CD32. *Frontiers in Immunology*, *11*. https://doi.org/10.3389/fimmu.2020.02108

118. Nakamoto, N., & Kanai, T. (2014). Role of Toll-Like Receptors in Immune Activation and Tolerance in the Liver. *Frontiers in Immunology*, *5*. https://doi.org/10.3389/fimmu.2014.00221
119. Tu, Z., Bozorgzadeh, A., Pierce, R. H., Kurtis, J., Crispe, I. N., & Orloff, M. S. (2008). TLR-dependent cross talk between human Kupffer cells and NK cells. *The Journal of Experimental Medicine*, *205*(1), 233–244. https://doi.org/10.1084/jem.20072195
120. Rivera, C. A., Adegboyega, P., van Rooijen, N., Tagalicud, A., Allman, M., & Wallace, M. (2007). Toll-like receptor-4 signaling and Kupffer cells play pivotal roles in the pathogenesis of non-alcoholic steatohepatitis. *Journal of Hepatology*, *47*(4), 571–579. https://doi.org/10.1016/j.jhep.2007.04.019
121. Kelley, J. L., Ozment, T. R., Li, C., Schweitzer, J. B., & Williams, D. L. (2014). Scavenger Receptor-A (CD204): A Two-Edged Sword in Health and Disease. *Critical Reviews in Immunology*, *34*(3), 241–261. https://doi.org/10.1615/CritRevImmunol.2014010267
122. Silverstein, R. L., & Febbraio, M. (2009). CD36, a Scavenger Receptor Involved in Immunity, Metabolism, Angiogenesis, and Behavior. *Science Signaling*, *2*(72). https://doi.org/10.1126/scisignal.272re3
123. Terpstra, V., van Amersfoort, E. S., van Velzen, A. G., Kuiper, J., & van Berkel, T. J. C. (2000). Hepatic and Extrahepatic Scavenger Receptors. *Arteriosclerosis, Thrombosis, and Vascular Biology*, *20*(8), 1860–1872. https://doi.org/10.1161/01.ATV.20.8.1860
124. Hoyle, G. W., & Hill, R. L. (1988). Molecular cloning and sequencing of a cDNA for a carbohydrate binding receptor unique to rat Kupffer cells. *Journal of Biological Chemistry*, *263*(16), 7487–7492. https://doi.org/10.1016/S0021-9258(18)68524-2
125. Coombs, P. J., Taylor, M. E., & Drickamer, K. (2006). Two categories of mammalian galactose-binding receptors distinguished by glycan array profiling. *Glycobiology*, *16*(8), 1C-7C. https://doi.org/10.1093/glycob/cwj126
126. Deppermann, C., Kratofil, R. M., Peiseler, M., David, B. A., Zindel, J., Castanheira, F. V. E. S., van der Wal, F., Carestia, A., Jenne, C. N., Marth, J. D., & Kubes, P. (2020). Macrophage galactose lectin is critical for Kupffer cells to clear aged platelets. *Journal of Experimental Medicine*, *217*(4). https://doi.org/10.1084/jem.20190723
127. Blériot, C., Barreby, E., Dunsmore, G., Ballaire, R., Chakarov, S., Ficht, X., de Simone, G., Andreata, F., Fumagalli, V., Guo, W., Wan, G., Gessain, G., Khalilnezhad, A., Zhang, X. M., Ang, N., Chen, P., Morgantini, C., Azzimato, V., Kong, W. T., … Ginhoux, F. (2021). A subset of Kupffer cells regulates metabolism through the expression of CD36. *Immunity*, *54*(9), 2101-2116.e6. https://doi.org/10.1016/j.immuni.2021.08.006
128. de Simone, G., Andreata, F., Bleriot, C., Fumagalli, V., Laura, C., Garcia-Manteiga, J. M., di Lucia, P., Gilotto, S., Ficht, X., de Ponti, F. F., Bono, E. B., Giustini, L.,

Ambrosi, G., Mainetti, M., Zordan, P., Bénéchet, A. P., Ravà, M., Chakarov, S., Moalli, F., … Iannacone, M. (2021). Identification of a Kupffer cell subset capable of reverting the T cell dysfunction induced by hepatocellular priming. *Immunity*, *54*(9), 2089-2100.e8. https://doi.org/10.1016/j.immuni.2021.05.005

129. Martens, J., Kzhyshkowska, J., Falkowski-Hansen, M., Schledzewski, K., Gratchev, A., Mansmann, U., Schmuttermaier, C., Dippel, E., Koenen, W., Riedel, F., Sankala, M., Tryggvason, K., Kobzik, L., Moldenhauer, G., Arnold, B., & Goerdt, S. (2006). Differential expression of a gene signature for scavenger/lectin receptors by endothelial cells and macrophages in human lymph node sinuses, the primary sites of regional metastasis. *The Journal of Pathology*, *208*(4), 574–589. https://doi.org/10.1002/path.1921
130. Digre, A., & Lindskog, C. (2021). The Human Protein Atlas—Spatial localization of the human proteome in health and disease. *Protein Science*, *30*(1), 218–233. https://doi.org/10.1002/pro.3987
131. Hume, D. A., Offermanns, S., & Bonnavion, R. (2022). Contamination of isolated mouse Kupffer cells with liver sinusoidal endothelial cells. *Immunity*, *55*(7), 1139–1140. https://doi.org/10.1016/j.immuni.2022.06.010
132. Shetty, S., Lalor, P. F., & Adams, D. H. (2018). Liver sinusoidal endothelial cells — gatekeepers of hepatic immunity. *Nature Reviews Gastroenterology & Hepatology*, *15*(9), 555–567. https://doi.org/10.1038/s41575-018-0020-y
133. Lalor, P. (2006). Human hepatic sinusoidal endothelial cells can be distinguished by expression of phenotypic markers related to their specialised functions *in vivo*. *World Journal of Gastroenterology*, *12*(34), 5429. https://doi.org/10.3748/wjg.v12.i34.5429
134. Wisse, E. (1970). An electron microscopic study of the fenestrated endothelial lining of rat liver sinusoids. *Journal of Ultrastructure Research*, *31*(1–2), 125–150. https://doi.org/10.1016/S0022-5320(70)90150-4
135. Szafranska, K., Kruse, L. D., Holte, C. F., McCourt, P., & Zapotoczny, B. (2021). The wHole Story About Fenestrations in LSEC. *Frontiers in Physiology*, *12*. https://doi.org/10.3389/fphys.2021.735573
136. Braet, F., & Wisse, E. (2002). Structural and functional aspects of liver sinusoidal endothelial cell fenestrae: a review. *Comparative Hepatology*, *1*(1), 1. https://doi.org/10.1186/1476-5926-1-1
137. Furuta, K., Guo, Q., Hirsova, P., & Ibrahim, S. H. (2020). Emerging Roles of Liver Sinusoidal Endothelial Cells in Nonalcoholic Steatohepatitis. *Biology*, *9*(11), 395. https://doi.org/10.3390/biology9110395
138. Smedsrød B, Eriksson S, Fraser JRE, Laurent TC, Pertoft H (1982) Properties of liver endothelial cells in primary monolayer cultures. In: Knook DL Wisse E (eds) Sinusoidal liver cells. Elsevier Biomedical Press, Amsterdam, pp 263–270

139. Sørensen, K. K., McCourt, P., Berg, T., Crossley, C., Couteur, D. le, Wake, K., & Smedsrød, B. (2012). The scavenger endothelial cell: a new player in homeostasis and immunity. *American Journal of Physiology-Regulatory, Integrative and Comparative Physiology*, *303*(12), R1217–R1230. https://doi.org/10.1152/ajpregu.00686.2011
140. Praaning-Van Dalen, D. P., & Knook, D. L. (1982). Quantitative determination of in Vivo endocytosis by rat liver kupffer and endothelial cells facilitated by an improved cell isolation method. *FEBS Letters*, *141*(2), 229–232. https://doi.org/10.1016/0014-5793(82)80054-9
141. Schroeder, B., & McNiven, M. A. (2014). Importance of Endocytic Pathways in Liver Function and Disease. In *Comprehensive Physiology* (pp. 1403–1417). Wiley. https://doi.org/10.1002/cphy.c140001
142. Strauss, O., Phillips, A., Ruggiero, K., Bartlett, A., & Dunbar, P. R. (2017). Immunofluorescence identifies distinct subsets of endothelial cells in the human liver. *Scientific Reports*, *7*(1), 44356. https://doi.org/10.1038/srep44356
143. McCourt, P. A. G., Smedsrød, B. H., Melkko, J., & Johansson, S. (1999). Characterization of a hyaluronan receptor on rat sinusoidal liver endothelial cells and its functional relationship to scavenger receptors. *Hepatology*, *30*(5), 1276–1286. https://doi.org/10.1002/hep.510300521
144. Li, R., Oteiza, A., Sørensen, K. K., McCourt, P., Olsen, R., Smedsrød, B., & Svistounov, D. (2011). Role of liver sinusoidal endothelial cells and stabilins in elimination of oxidized low-density lipoproteins. *American Journal of Physiology-Gastrointestinal and Liver Physiology*, *300*(1), G71–G81. https://doi.org/10.1152/ajpgi.00215.2010
145. Jeffers, S. A., Tusell, S. M., Gillim-Ross, L., Hemmila, E. M., Achenbach, J. E., Babcock, G. J., Thomas, W. D., Thackray, L. B., Young, M. D., Mason, R. J., Ambrosino, D. M., Wentworth, D. E., DeMartini, J. C., & Holmes, K. v. (2004). CD209L (L-SIGN) is a receptor for severe acute respiratory syndrome coronavirus. *Proceedings of the National Academy of Sciences*, *101*(44), 15748–15753. https://doi.org/10.1073/pnas.0403812101
146. Gardner, J. P., Durso, R. J., Arrigale, R. R., Donovan, G. P., Maddon, P. J., Dragic, T., & Olson, W. C. (2003). L-SIGN (CD 209L) is a liver-specific capture receptor for hepatitis C virus. *Proceedings of the National Academy of Sciences*, *100*(8), 4498–4503. https://doi.org/10.1073/pnas.0831128100
147. Pöhlmann, S., Soilleux, E. J., Baribaud, F., Leslie, G. J., Morris, L. S., Trowsdale, J., Lee, B., Coleman, N., & Doms, R. W. (2001). DC-SIGNR, a DC-SIGN homologue expressed in endothelial cells, binds to human and simian immunodeficiency viruses and activates infection in trans. *Proceedings of the National Academy of Sciences*, *98*(5), 2670–2675. https://doi.org/10.1073/pnas.051631398

148. Amraei, R., Yin, W., Napoleon, M. A., Suder, E. L., Berrigan, J., Zhao, Q., Olejnik, J., Chandler, K. B., Xia, C., Feldman, J., Hauser, B. M., Caradonna, T. M., Schmidt, A. G., Gummuluru, S., Muhlberger, E., Chitalia, V., Costello, C. E., & Rahimi, N. (2021). CD209L/L-SIGN and CD209/DC-SIGN act as receptors for SARS-CoV-2. *BioRxiv : The Preprint Server for Biology*. https://doi.org/10.1101/2020.06.22.165803
149. Smedsrød, B., Einarsson, M., & Pertoft, H. (1988). Tissue plasminogen activator is endocytosed by mannose and galactose receptors of rat liver cells. *Thrombosis and Haemostasis*, *59*(3), 480–484.
150. Shepherd, V. L., & Hoidal, J. R. (1990). Clearance of Neutrophil-derived Myeloperoxidase by the Macrophage Mannose Receptor. *American Journal of Respiratory Cell and Molecular Biology*, *2*(4), 335–340. https://doi.org/10.1165/ajrcmb/2.4.335
151. Malovic, I., Sørensen, K. K., Elvevold, K. H., Nedredal, G. I., Paulsen, S., Erofeev, A. v., Smedsrød, B. H., & McCourt, P. A. G. (2007). The mannose receptor on murine liver sinusoidal endothelial cells is the main denatured collagen clearance receptor. *Hepatology*, *45*(6), 1454–1461. https://doi.org/10.1002/hep.21639
152. March, S., Hui, E. E., Underhill, G. H., Khetani, S., & Bhatia, S. N. (2009). Microenvironmental regulation of the sinusoidal endothelial cell phenotype in vitro. *Hepatology*, *50*(3), 920–928. https://doi.org/10.1002/hep.23085
153. MacParland, S. A., Liu, J. C., Ma, X.-Z., Innes, B. T., Bartczak, A. M., Gage, B. K., Manuel, J., Khuu, N., Echeverri, J., Linares, I., Gupta, R., Cheng, M. L., Liu, L. Y., Camat, D., Chung, S. W., Seliga, R. K., Shao, Z., Lee, E., Ogawa, S., … McGilvray, I. D. (2018). Single cell RNA sequencing of human liver reveals distinct intrahepatic macrophage populations. *Nature Communications*, *9*(1), 4383. https://doi.org/10.1038/s41467-018-06318-7
154. Gage, B. K., Liu, J. C., Innes, B. T., MacParland, S. A., McGilvray, I. D., Bader, G. D., & Keller, G. M. (2020). Generation of Functional Liver Sinusoidal Endothelial Cells from Human Pluripotent Stem-Cell-Derived Venous Angioblasts. *Cell Stem Cell*, *27*(2), 254-269.e9. https://doi.org/10.1016/j.stem.2020.06.007
155. Ganesan, L. P., Kim, J., Wu, Y., Mohanty, S., Phillips, G. S., Birmingham, D. J., Robinson, J. M., & Anderson, C. L. (2012). FcγRIIb on Liver Sinusoidal Endothelium Clears Small Immune Complexes. *The Journal of Immunology*, *189*(10), 4981–4988. https://doi.org/10.4049/jimmunol.1202017
156. BENACERRAF, B., SEBESTYEN, M., & COOPER, N. S. (1959). The clearance of antigen antibody complexes from the blood by the reticuloendothelial system. *Journal of Immunology (Baltimore, Md. : 1950)*, *82*(2), 131–137.
157. Arend, W. P., & Sturge, J. C. (1979). Composition and biologic properties of soluble IgG-anti-IgG immune complexes: effects of variations in the specificity of rabbit antibodies to different structural components of human IgG. *Journal of Immunology (Baltimore, Md. : 1950)*, *123*(1), 447–454.

158. Kurlander, R. J., Ellison, D. M., & Hall, J. (1984). The blockade of Fc receptor-mediated clearance of immune complexes in vivo by a monoclonal antibody (2.4G2) directed against Fc receptors on murine leukocytes. *The Journal of Immunology*, *133*(2), 855–862. https://doi.org/10.4049/jimmunol.133.2.855
159. Skogh, T., Blomhoff, R., Eskild, W., & Berg, T. (1985). Hepatic uptake of circulating IgG immune complexes. *Immunology*, *55*(4), 585–594.
160. BOGERS, W. M. J. M., STAD, R.-K., JANSSEN, D. J., van ROOIJEN, N., van ES, L. A., & DAHA, M. R. (2008). Kupffer cell depletion *in vivo* results in preferential elimination of IgG aggregates and immune complexes via specific Fc receptors on rat liver endothelial cells. *Clinical and Experimental Immunology*, *86*(2), 328–333. https://doi.org/10.1111/j.1365-2249.1991.tb05818.x
161. van Rooijen, N. (1989). The liposome-mediated macrophage 'suicide' technique. *Journal of Immunological Methods*, *124*(1), 1–6. https://doi.org/10.1016/0022-1759(89)90178-6
162. Kasturirangan, S., Rainey, G. J., Xu, L., Wang, X., Portnoff, A., Chen, T., Fazenbaker, C., Zhong, H., Bee, J., Zeng, Z., Jenne, C., Wu, H., & Gao, C. (2017). Targeted Fcγ Receptor (FcγR)-mediated Clearance by a Biparatopic Bispecific Antibody. *Journal of Biological Chemistry*, *292*(10), 4361–4370. https://doi.org/10.1074/jbc.M116.770628
163. Datta-Mannan, A., Croy, J. E., Schirtzinger, L., Torgerson, S., Breyer, M., & Wroblewski, V. J. (2016). Aberrant bispecific antibody pharmacokinetics linked to liver sinusoidal endothelium clearance mechanism in cynomolgus monkeys. *MAbs*, *8*(5), 969–982. https://doi.org/10.1080/19420862.2016.1178435
164. Ganesan, L. P., Kim, J., Wu, Y., Mohanty, S., Phillips, G. S., Birmingham, D. J., Robinson, J. M., & Anderson, C. L. (2012). FcγRIIb on Liver Sinusoidal Endothelium Clears Small Immune Complexes. *The Journal of Immunology*, *189*(10), 4981–4988. https://doi.org/10.4049/jimmunol.1202017
165. Johansson, A. G., Sundqvist, T., & Skogh, T. (2000). IgG Immune Complex Binding to and Activation of Liver Cells. *International Archives of Allergy and Immunology*, *121*(4), 329–336. https://doi.org/10.1159/000024347
166. Jepsen, P., & Younossi, Z. M. (2021). The global burden of cirrhosis: A review of disability-adjusted life-years lost and unmet needs. *Journal of Hepatology*, *75*, S3–S13. https://doi.org/10.1016/j.jhep.2020.11.042
167. British Liver Trust. (2022). *Liver disease in numbers – key facts and statistics*. https://britishlivertrust.org.uk/information-and-support/statistics/#:~:text=Liver%20disease%20is%20a%20silent%20killer%20and%20it's%20on%20the%20increase&text=That's%20more%20than%2027%20deaths,the%20last%2050%20years%202. [accessed January 2023]
168. Williams, R., Aspinall, R., Bellis, M., Camps-Walsh, G., Cramp, M., Dhawan, A., Ferguson, J., Forton, D., Foster, G., Gilmore, S. I., Hickman, M., Hudson, M., Kelly,

D., Langford, A., Lombard, M., Longworth, L., Martin, N., Moriarty, K., Newsome, P., … Smith, T. (2014). Addressing liver disease in the UK: a blueprint for attaining excellence in health care and reducing premature mortality from lifestyle issues of excess consumption of alcohol, obesity, and viral hepatitis. *The Lancet*, *384*(9958), 1953–1997. https://doi.org/10.1016/S0140-6736(14)61838-9

169. Liver disease: Applying All Our Health, Office for Health Improvement and Disparities https://www.gov.uk/government/publications/liver-disease-applying-all-our-health/liver-disease-applying-all-our-healthaccessed Sept 2022
170. British Liver Trust analysis of UK deaths from liver disease 2016-2020. All data accessed 20th July 2022. Data sources: England and Wales data were accessed from NOMIS mortality statistics by year, sex, age and underlying cause (ICD-10 K70-77) https://www.nomisweb.co.uk/. Northern Ireland data were taken from the Registrar General Annual Reports 2016 to 2020 (ICD-10 K70, K73-74) https://www.nisra.gov.uk/statistics/births-deaths-and-marriages/registrar-general-annual-report. Scotland data were taken from National Records of Scotland vital events data sets 2016-2020 (ICD K70, K73-74) https://www.nrscotland.gov.uk/statistics-and-data/statistics/statistics-by-theme/vital-events/general-publications/vital-events-reference-tables/2020/list-of-data-tables#section6.
171. Choudhary, N. S., Saraf, N., Saigal, S., Gautam, D., Lipi, L., Rastogi, A., Goja, S., Menon, P. B., Bhangui, P., Ramchandra, S. K., & Soin, A. S. (2015). Rapid Reversal of Liver Steatosis With Life Style Modification in Highly Motivated Liver Donors. *Journal of Clinical and Experimental Hepatology*, *5*(2), 123–126. https://doi.org/10.1016/j.jceh.2015.04.002
172. Germani, G., Hytiroglou, P., Fotiadu, A., Burroughs, A. K., & Dhillon, A. P. (2011). Assessment of Fibrosis and Cirrhosis in Liver Biopsies: An Update. *Seminars in Liver Disease*, *31*(01), 082–090. https://doi.org/10.1055/s-0031-1272836
173. Suk, K. T. (2015). Staging of liver fibrosis or cirrhosis: The role of hepatic venous pressure gradient measurement. *World Journal of Hepatology*, *7*(3), 607. https://doi.org/10.4254/wjh.v7.i3.607
174. Forner, A., Llovet, J. M., & Bruix, J. (2012). Hepatocellular carcinoma. *The Lancet*, *379*(9822), 1245–1255. https://doi.org/10.1016/S0140-6736(11)61347-0
175. Semmler, G., Wernly, B., & Datz, C. (2024). What's in a name? New nomenclature for steatotic liver disease - to be or not to be? *Journal of Hepatology*, *80*(2), e56–e58. https://doi.org/10.1016/j.jhep.2023.07.035
176. Burton, Robyn & Henn, Clive & Lavoie, Don & Wolff, Alanna & Marsden, John & Sheron, Nick. (2016). The public health burden of alcohol and the effectiveness and cost-effectiveness of alcohol control policies: an evidence review.

177. Obed, A. (2015). Six month abstinence rule for liver transplantation in severe alcoholic liver disease patients. *World Journal of Gastroenterology*, *21*(14), 4423. https://doi.org/10.3748/wjg.v21.i14.4423
178. Roberts, S. E., John, A., Brown, J., Napier, D. J., Lyons, R. A., & Williams, J. G. (2019). Early and late mortality following unscheduled admissions for severe liver disease across England and Wales. *Alimentary Pharmacology & Therapeutics*, *49*(10), 1334–1345. https://doi.org/10.1111/apt.15232
179. Cheemerla, S., & Balakrishnan, M. (2021). Global Epidemiology of Chronic Liver Disease. *Clinical Liver Disease*, *17*(5), 365–370. https://doi.org/10.1002/cld.1061
180. Riazi, K., Azhari, H., Charette, J. H., Underwood, F. E., King, J. A., Afshar, E. E., Swain, M. G., Congly, S. E., Kaplan, G. G., & Shaheen, A.-A. (2022). The prevalence and incidence of NAFLD worldwide: a systematic review and meta-analysis. *The Lancet Gastroenterology & Hepatology*, *7*(9), 851–861. https://doi.org/10.1016/S2468-1253(22)00165-0
181. Morgan, A., Hartmanis, S., Tsochatzis, E., Newsome, P. N., Ryder, S. D., Elliott, R., Floros, L., Hall, R., Higgins, V., Stanley, G., Cure, S., Vasudevan, S., & Pezzullo, L. (2021). Disease burden and economic impact of diagnosed non-alcoholic steatohepatitis (NASH) in the United Kingdom (UK) in 2018. *The European Journal of Health Economics*, *22*(4), 505–518. https://doi.org/10.1007/s10198-020-01256-y
182. Alexander, M., Loomis, A. K., Fairburn-Beech, J., van der Lei, J., Duarte-Salles, T., Prieto-Alhambra, D., Ansell, D., Pasqua, A., Lapi, F., Rijnbeek, P., Mosseveld, M., Avillach, P., Egger, P., Kendrick, S., Waterworth, D. M., Sattar, N., & Alazawi, W. (2018). Real-world data reveal a diagnostic gap in non-alcoholic fatty liver disease. *BMC Medicine*, *16*(1), 130. https://doi.org/10.1186/s12916-018-1103-x
183. Younossi, Z., Anstee, Q. M., Marietti, M., Hardy, T., Henry, L., Eslam, M., George, J., & Bugianesi, E. (2018). Global burden of NAFLD and NASH: trends, predictions, risk factors and prevention. *Nature Reviews Gastroenterology & Hepatology*, *15*(1), 11–20. https://doi.org/10.1038/nrgastro.2017.109
184. García-Pagán, J.-C., Gracia-Sancho, J., & Bosch, J. (2012). Functional aspects on the pathophysiology of portal hypertension in cirrhosis. *Journal of Hepatology*, *57*(2), 458–461. https://doi.org/10.1016/j.jhep.2012.03.007
185. Iwakiri, Y. (2007). The Molecules: mechanisms of arterial vasodilatation observed in the splanchnic and systemic circulation in portal hypertension. *Journal of Clinical Gastroenterology*, *41*(Supplement 3), S288–S294. https://doi.org/10.1097/MCG.0b013e3181468b4c
186. McConnell, M., & Iwakiri, Y. (2018). Biology of portal hypertension. *Hepatology International*, *12*(S1), 11–23. https://doi.org/10.1007/s12072-017-9826-x
187. May, D., Djonov, V., Zamir, G., Bala, M., Safadi, R., Sklair-Levy, M., & Keshet, E. (2011). A Transgenic Model for Conditional Induction and Rescue of Portal

Hypertension Reveals a Role of VEGF-Mediated Regulation of Sinusoidal Fenestrations. *PLoS ONE*, *6*(7), e21478. https://doi.org/10.1371/journal.pone.0021478

188. Maeso-Díaz, R., Ortega-Ribera, M., Fernández-Iglesias, A., Hide, D., Muñoz, L., Hessheimer, A. J., Vila, S., Francés, R., Fondevila, C., Albillos, A., Peralta, C., Bosch, J., Tacke, F., Cogger, V. C., & Gracia-Sancho, J. (2018). Effects of aging on liver microcirculatory function and sinusoidal phenotype. *Aging Cell*, *17*(6). https://doi.org/10.1111/acel.12829
189. Poisson, J., Lemoinne, S., Boulanger, C., Durand, F., Moreau, R., Valla, D., & Rautou, P.-E. (2017). Liver sinusoidal endothelial cells: Physiology and role in liver diseases. *Journal of Hepatology*, *66*(1), 212–227. https://doi.org/10.1016/j.jhep.2016.07.009
190. Engström-Laurent, A., Lööf, L., Nyberg, A., & Schröder, T. (1985). Increased serum levels of hyaluronate in liver disease. *Hepatology*, *5*(4), 638–642. https://doi.org/10.1002/hep.1840050420
191. Géraud, C., Mogler, C., Runge, A., Evdokimov, K., Lu, S., Schledzewski, K., Arnold, B., Hämmerling, G., Koch, P. S., Breuhahn, K., Longerich, T., Marx, A., Weiss, C., Damm, F., Schmieder, A., Schirmacher, P., Augustin, H. G., & Goerdt, S. (2013). Endothelial transdifferentiation in hepatocellular carcinoma: loss of Stabilin-2 expression in peri-tumourous liver correlates with increased survival. *Liver International*, *33*(9), 1428–1440. https://doi.org/10.1111/liv.12262
192. Wu, A. H., Parker, O. S., & Ford, L. (1984). Hyperviscosity caused by hyaluronic acid in serum in a case of Wilms' tumor. *Clinical Chemistry*, *30*(6), 914–916.
193. Domenicali, M., Caraceni, P., Giannone, F., Baldassarre, M., Lucchetti, G., Quarta, C., Patti, C., Catani, L., Nanni, C., Lemoli, R. M., & Bernardi, M. (2009). A novel model of CCl4-induced cirrhosis with ascites in the mouse. *Journal of Hepatology*, *51*(6), 991–999. https://doi.org/10.1016/j.jhep.2009.09.008
194. Su, T., Yang, Y., Lai, S., Jeong, J., Jung, Y., McConnell, M., Utsumi, T., & Iwakiri, Y. (2021). Single-Cell Transcriptomics Reveals Zone-Specific Alterations of Liver Sinusoidal Endothelial Cells in Cirrhosis. *Cellular and Molecular Gastroenterology and Hepatology*, *11*(4), 1139–1161. https://doi.org/10.1016/j.jcmgh.2020.12.007
195. Muro, H., Shirasawa, H., Kosugi, I., & Ito, I. (1990). Defect of sinusoidal Fc receptors and immune complex uptake in CCl4-induced liver cirrhosis in rats. *Gastroenterology*, *99*(1), 200–210. https://doi.org/10.1016/0016-5085(90)91249-6
196. Muro, H., Shirasawa, H., Kosugi, I., & Nakamura, S. (1993). Defect of Fc receptors and phenotypical changes in sinusoidal endothelial cells in human liver cirrhosis. *The American Journal of Pathology*, *143*(1), 105–120.
197. Muro, H., Shirasawa, H., Kosugi, I., & Ito, I. (1990). Defect of sinusoidal Fc receptors and immune complex uptake in CCl4-induced liver cirrhosis in rats.

Gastroenterology, *99*(1), 200–210. https://doi.org/10.1016/0016-5085(90)91249-6

198. Arteta, B., Lasuen, N., Lopategi, A., Sveinbjörnsson, B., Smedsrød, B., & Vidal-Vanaclocha, F. (2010). Colon carcinoma cell interaction with liver sinusoidal endothelium inhibits organ-specific antitumor immunity through interleukin-1-induced mannose receptor in mice. *Hepatology (Baltimore, Md.)*, *51*(6), 2172–2182. https://doi.org/10.1002/hep.23590
199. Knolle, P. A., Uhrig, A., Hegenbarth, S., Löser, E., Schmitt, E., Gerken, G., & Lohse, A. W. (1998). IL-10 down-regulates T cell activation by antigen-presenting liver sinusoidal endothelial cells through decreased antigen uptake via the mannose receptor and lowered surface expression of accessory molecules. *Clinical and Experimental Immunology*, *114*(3), 427–433. https://doi.org/10.1046/j.1365-2249.1998.00713.x
200. van der Zande, H. J. P., Nitsche, D., Schlautmann, L., Guigas, B., & Burgdorf, S. (2021). The Mannose Receptor: From Endocytic Receptor and Biomarker to Regulator of (Meta)Inflammation. *Frontiers in Immunology*, *12*. https://doi.org/10.3389/fimmu.2021.765034
201. Sandahl, T. D., Støy, S. H., Laursen, T. L., Rødgaard-Hansen, S., Møller, H. J., Møller, S., Vilstrup, H., & Grønbæk, H. (2017). The soluble mannose receptor (sMR) is elevated in alcoholic liver disease and associated with disease severity, portal hypertension, and mortality in cirrhosis patients. *PLOS ONE*, *12*(12), e0189345. https://doi.org/10.1371/journal.pone.0189345
202. Andersen, E. S., Rødgaard-Hansen, S., Moessner, B., Christensen, P. B., Møller, H. J., & Weis, N. (2014). Macrophage-related serum biomarkers soluble CD163 (sCD163) and soluble mannose receptor (sMR) to differentiate mild liver fibrosis from cirrhosis in patients with chronic hepatitis C: a pilot study. *European Journal of Clinical Microbiology & Infectious Diseases : Official Publication of the European Society of Clinical Microbiology*, *33*(1), 117–122. https://doi.org/10.1007/s10096-013-1936-3
203. Saha, B., Tornai, D., Kodys, K., Adejumo, A., Lowe, P., McClain, C., Mitchell, M., McCullough, A., Dasarathy, S., Kroll-Desrosiers, A., Barton, B., Radaeva, S., & Szabo, G. (2019). Biomarkers of Macrophage Activation and Immune Danger Signals Predict Clinical Outcomes in Alcoholic Hepatitis. *Hepatology*, *70*(4), 1134–1149. https://doi.org/10.1002/hep.30617
204. Kong, X. Y., Nesset, C. K., Damme, M., Løberg, E.-M., Lübke, T., Mæhlen, J., Andersson, K. B., Lorenzo, P. I., Roos, N., Thoresen, G. H., Rustan, A. C., Kase, E. T., & Eskild, W. (2014). Loss of lysosomal membrane protein NCU-G1 in mice results in spontaneous liver fibrosis with accumulation of lipofuscin and iron in Kupffer cells. *Disease Models & Mechanisms*, *7*(3), 351–362. https://doi.org/10.1242/dmm.014050

205. Antwi, M. B., Dumitriu, G., Simón-Santamaria, J., Romano, J. S., Li, R., Smedsrød, B., Vik, A., Eskild, W., & Sørensen, K. K. (2023). Liver sinusoidal endothelial cells show reduced scavenger function and downregulation of Fc gamma receptor IIb, yet maintain a preserved fenestration in the Glmpgt/gt mouse model of slowly progressing liver fibrosis. *PloS One*, *18*(11), e0293526. https://doi.org/10.1371/journal.pone.0293526
206. Daemen, S., Gainullina, A., Kalugotla, G., He, L., Chan, M. M., Beals, J. W., Liss, K. H., Klein, S., Feldstein, A. E., Finck, B. N., Artyomov, M. N., & Schilling, J. D. (2021). Dynamic Shifts in the Composition of Resident and Recruited Macrophages Influence Tissue Remodeling in NASH. *Cell Reports*, *34*(2), 108626. https://doi.org/10.1016/j.celrep.2020.108626
207. Tran, S., Baba, I., Poupel, L., Dussaud, S., Moreau, M., Gélineau, A., Marcelin, G., Magréau-Davy, E., Ouhachi, M., Lesnik, P., Boissonnas, A., le Goff, W., Clausen, B. E., Yvan-Charvet, L., Sennlaub, F., Huby, T., & Gautier, E. L. (2020). Impaired Kupffer Cell Self-Renewal Alters the Liver Response to Lipid Overload during Non-alcoholic Steatohepatitis. *Immunity*, *53*(3), 627-640.e5. https://doi.org/10.1016/j.immuni.2020.06.003
208. Lawrence, T., & Natoli, G. (2011). Transcriptional regulation of macrophage polarization: enabling diversity with identity. *Nature Reviews Immunology*, *11*(11), 750–761. https://doi.org/10.1038/nri3088
209. Olsavszky, V., Sticht, C., Schmid, C. D., Winkler, M., Wohlfeil, S. A., Olsavszky, A., Schledzewski, K., Géraud, C., Goerdt, S., Leibing, T., & Koch, P.-S. (2021). Exploring the transcriptomic network of multi-ligand scavenger receptor Stabilin-1- and Stabilin-2-deficient liver sinusoidal endothelial cells. *Gene*, *768*, 145284. https://doi.org/10.1016/j.gene.2020.145284
210. Mahamid, M., Mader, R., & Safadi, R. (2011). Hepatotoxicity of tocilizumab and anakinra in rheumatoid arthritis: management decisions. *Clinical Pharmacology : Advances and Applications*, *3*, 39–43. https://doi.org/10.2147/CPAA.S24004
211. James, B. H., Papakyriacou, P., Gardener, M. J., Gliddon, L., Weston, C. J., & Lalor, P. F. (2022). The Contribution of Liver Sinusoidal Endothelial Cells to Clearance of Therapeutic Antibody. *Frontiers in Physiology*, *12*. https://doi.org/10.3389/fphys.2021.753833
212. Joplin, R., Strain, A. J., & Neuberger, J. M. (1989). Immuno-isolation and culture of biliary epithelial cells from normal human liver. *In Vitro Cellular & Developmental Biology*, *25*(12), 1189–1192. https://doi.org/10.1007/BF02621273
213. Baxter, E. W., Graham, A. E., Re, N. A., Carr, I. M., Robinson, J. I., Mackie, S. L., & Morgan, A. W. (2020). Standardized protocols for differentiation of THP-1 cells to macrophages with distinct M(IFNγ+LPS), M(IL-4) and M(IL-10) phenotypes. *Journal of Immunological Methods*, *478*, 112721. https://doi.org/10.1016/j.jim.2019.112721

214. Ruifrok, A. C., & Johnston, D. A. (2001). Quantification of histochemical staining by color deconvolution. *Analytical and Quantitative Cytology and Histology*, *23*(4), 291–299.
215. Bradbury, A. and Pluckthun, A. (2015) Reproducibility: Standardize antibodies used in research. *Nature.* 518, 27-29. https://doi.org/10.1038/518027a
216. Segaliny, A.I., Jayaraman, J., Chen, X., Chong, J., Luxon, R., Fung, A., Fu, Q., Jiang, X., Rivera, R., Ma, X., Ren, C., Zimak, J., Hedde, Y.S., Wu, G and Zhao, W. (2023) A high throughout bispecific antibody discovery pipeline. *Commun Biol,* 6, 380.
217. Bates, A. and Power, C.A. (2019) David vs Goliath: The structure, function, and clinical prospects of antibody fragments. *Antibodies*. 8(2) 28/ doi: 10.3390/antib8020028.
218. Nisanoff, A. and Rivers, MM. (1961) Recombinant of a mixture of univalent antibody fragments of different specificity. *Arch Biophys.* 93:460-462
219. Lafoz, E., Ruart, M., Anton, A., Oncins, A. and Hernandez-Gea, V. (2020) The endothelium as a driver of liver fibrosis and regeneration. *Cells* 9(4) 929 doi:10.3390/cells9040929
220. Rockey, D.C. and Chung, J.J. (1998) Reduced nitric oxide production by endothelial cells in cirrhotic rat liver: Endothelial dysfunction in portal hypertension. *Gastroenterology*. 114:344-351. Doi: 10.1016/S0016-5085(98)70487-1
221. Garcia-Sancho, J., Lavina, B., Rodriguez-Vilarrupla, A., Garcia-Caldero, H., Bosch, J. and Garcia-Pagan, J.C. (2007) Enhanced Vascoconstrictor prostanoid production by sinusoidal endothelial cells increases portal perfusion pressue in cirrhotic rat livers. *J. Hepatol.* 47:220-227. Doi: 10.1016/j.jhep.2007.03.014.
222. US Market Reports (Published 2023) Global monoclonal antibodies market by source type. https://market.us/report/monoclonal-antibodies-market/ (accessed 29/02/2024
223. Poisson, J., Lemoinne, S., Boulanger, C., Durand, F., Moreau, R., Valla, D. and Rautou, P-E. (2017) Liver sinusoidal endothelial cells: Physiology and role in liver disease. *J. Hepatol.* 66(1) 212-227 doi:10.1016/j.jhep.2016.07.009
224. Ortega-Ribera, M., Igelais-Fernandez, A., Illa, X.,Moya, A., Molina, V., Maeso-Dias, R., Fondevila, C., Peralta, C., Bosch, J., Villa, R. and Garcia-Sancho, J. (2018) Resemblance of human liver sinusoid in a fluidic device with biomedical and pharmaceutical application. *Biotech and Bioeng.* 115(10) 2585-2594.
225. Sanders, L. A., Feldman, R. G., Voorhorst-Ogink, M. M., de Haas, M., Rijkers, G. T., Capel, P. J., Zegers, B. J., & van de Winkel, J. G. (1995). Human immunoglobulin G (IgG) Fc receptor IIA (CD32) polymorphism and IgG2-mediated bacterial phagocytosis by neutrophils. *Infection and Immunity*, *63*(1), 73–81. https://doi.org/10.1128/iai.63.1.73-81.1995
226. Clark, M. R., Clarkson, S. B., Ory, P. A., Stollman, N., & Goldstein, I. M. (1989). Molecular basis for a polymorphism involving Fc receptor II on human monocytes.

The Journal of Immunology, *143*(5), 1731–1734. https://doi.org/10.4049/jimmunol.143.5.1731

227. Junker, F., Gordon, J., & Qureshi, O. (2020). Fc Gamma Receptors and Their Role in Antigen Uptake, Presentation, and T Cell Activation. *Frontiers in Immunology*, *11*, 1393. https://doi.org/10.3389/fimmu.2020.01393
228. Sondermann, P., Huber, R., Oosthuizen, V., & Jacob, U. (2000). The 3.2-Å crystal structure of the human IgG1 Fc fragment–FcγRIII complex. *Nature*, *406*(6793), 267–273. https://doi.org/10.1038/35018508
229. Duncan, A. R., Woof, J. M., Partridge, L. J., Burton, D. R., & Winter, G. (1988). Localization of the binding site for the human high-affinity Fc receptor on IgG. *Nature*, *332*(6164), 563–564. https://doi.org/10.1038/332563a0
230. Gessner, J. E., Heiken, H., Tamm, A., & Schmidt, R. E. (1998). The IgG Fc receptor family. *Annals of Hematology*, *76*(6), 231–248. https://doi.org/10.1007/s002770050396
231. Kinet, J. P. (1992). The gamma-zeta dimers of Fc receptors as connectors to signal transduction. *Current Opinion in Immunology*, *4*(1), 43–48. https://doi.org/10.1016/0952-7915(92)90122-u
232. Shields, R. L., Namenuk, A. K., Hong, K., Meng, Y. G., Rae, J., Briggs, J., Xie, D., Lai, J., Stadlen, A., Li, B., Fox, J. A., & Presta, L. G. (2001). High Resolution Mapping of the Binding Site on Human IgG1 for FcγRI, FcγRII, FcγRIII, and FcRn and Design of IgG1 Variants with Improved Binding to the FcγR. *Journal of Biological Chemistry*, *276*(9), 6591–6604. https://doi.org/10.1074/jbc.M009483200
233. Gessner, J. E., Heiken, H., Tamm, A., & Schmidt, R. E. (1998). The IgG Fc receptor family. *Annals of Hematology*, *76*(6), 231–248. https://doi.org/10.1007/s002770050396
234. Mkaddem, S. ben, Murua, A., Flament, H., Titeca-Beauport, D., Bounaix, C., Danelli, L., Launay, P., Benhamou, M., Blank, U., Daugas, E., Charles, N., & Monteiro, R. C. (2017). Lyn and Fyn function as molecular switches that control immunoreceptors to direct homeostasis or inflammation. *Nature Communications*, *8*(1), 246. https://doi.org/10.1038/s41467-017-00294-0
235. Patel, J. C., Hall, A., & Caron, E. (2002). Vav Regulates Activation of Rac but Not Cdc42 during FcγR-mediated Phagocytosis. *Molecular Biology of the Cell*, *13*(4), 1215–1226. https://doi.org/10.1091/mbc.02-01-0002
236. Zhu, L., Jones, C., & Zhang, G. (2018). The Role of Phospholipase C Signaling in Macrophage-Mediated Inflammatory Response. *Journal of Immunology Research*, *2018*, 1–9. https://doi.org/10.1155/2018/5201759
237. Vanhaesebroeck, B., Ali, K., Bilancio, A., Geering, B., & Foukas, L. C. (2005). Signalling by PI3K isoforms: insights from gene-targeted mice. *Trends in Biochemical Sciences*, *30*(4), 194–204. https://doi.org/10.1016/j.tibs.2005.02.008

238. ben Mkaddem, S., Benhamou, M., & Monteiro, R. C. (2019). Understanding Fc Receptor Involvement in Inflammatory Diseases: From Mechanisms to New Therapeutic Tools. *Frontiers in Immunology*, *10*. https://doi.org/10.3389/fimmu.2019.00811
239. Getahun, A., & Cambier, J. C. (2015). Of ITIMs, ITAMs, and ITAMis: revisiting immunoglobulin Fc receptor signaling. *Immunological Reviews*, *268*(1), 66–73. https://doi.org/10.1111/imr.12336
240. Muta, T., Kurosaki, T., Misulovin, Z., Sanchez, M., Nussenzweig, M. C., & Ravetch, J. v. (1994). A 13-amino-acid motif in the cytoplasmic domain of FcγRIIB modulates B-cell receptor signalling. *Nature*, *368*(6466), 70–73. https://doi.org/10.1038/368070a0
241. Vivier, E., & Daëron, M. (1997). Immunoreceptor tyrosine-based inhibition motifs. *Immunology Today*, *18*(6), 286–291. https://doi.org/10.1016/S0167-5699(97)80025-4
242. Huang, Z.-Y., Hunter, S., Kim, M.-K., Indik, Z. K., & Schreiber, A. D. (2003). The effect of phosphatases SHP-1 and SHIP-1 on signaling by the ITIM- and ITAM-containing Fcγ receptors FcγRIIB and FcγRIIA. *Journal of Leukocyte Biology*, *73*(6), 823–829. https://doi.org/10.1189/jlb.0902454
243. Kant, A. M., De, P., Peng, X., Yi, T., Rawlings, D. J., Kim, J. S., & Durden, D. L. (2002). SHP-1 regulates Fcgamma receptor-mediated phagocytosis and the activation of RAC. *Blood*, *100*(5), 1852–1859.
244. Hunter, S., Indik, Z. K., Kim, M. K., Cauley, M. D., Park, J. G., & Schreiber, A. D. (1998). Inhibition of Fcgamma receptor-mediated phagocytosis by a nonphagocytic Fcgamma receptor. *Blood*, *91*(5), 1762–1768.
245. Lenz, G., Dreyling, M., Hoster, E., Wörmann, B., Dührsen, U., Metzner, B., Eimermacher, H., Neubauer, A., Wandt, H., Steinhauer, H., Martin, S., Heidemann, E., Aldaoud, A., Parwaresch, R., Hasford, J., Unterhalt, M., & Hiddemann, W. (2005). Immunochemotherapy With Rituximab and Cyclophosphamide, Doxorubicin, Vincristine, and Prednisone Significantly Improves Response and Time to Treatment Failure, But Not Long-Term Outcome in Patients With Previously Untreated Mantle Cell Lymphoma: Results of a Prospective Randomized Trial of the German Low Grade Lymphoma Study Group (GLSG). *Journal of Clinical Oncology*, *23*(9), 1984–1992. https://doi.org/10.1200/JCO.2005.08.133
246. Lee, C. S., Ashton-Key, M., Cogliatti, S., Rondeau, S., Schmitz, S. H., Ghielmini, M., Cragg, M. S., & Johnson, P. (2015). Expression of the inhibitory Fc gamma receptor IIB (FCGR2B, CD32B) on follicular lymphoma cells lowers the response rate to rituximab monotherapy (SAKK 35/98). *British Journal of Haematology*, *168*(1), 145–148. https://doi.org/10.1111/bjh.13071

247. Lee, L., Crump, M., Khor, S., Hoch, J. S., Luo, J., Bremner, K., Krahn, M., & Hodgson, D. C. (2012). Impact of rituximab on treatment outcomes of patients with diffuse large b-cell lymphoma: a population-based analysis. *British Journal of Haematology*, *158*(4), 481–488. https://doi.org/10.1111/j.1365-2141.2012.09177.x
248. Nowicka, M., Hilton, L. K., Ashton-Key, M., Hargreaves, C. E., Lee, C., Foxall, R., Carter, M. J., Beers, S. A., Potter, K. N., Bolen, C. R., Klein, C., Knapp, A., Mir, F., Rose-Zerilli, M., Burton, C., Klapper, W., Scott, D. W., Sehn, L. H., Vitolo, U., … Cragg, M. S. (2021). Prognostic significance of FCGR2B expression for the response of DLBCL patients to rituximab or obinutuzumab treatment. *Blood Advances*, *5*(15), 2945–2957. https://doi.org/10.1182/bloodadvances.2021004770
249. Hallek, M., Fischer, K., Fingerle-Rowson, G., Fink, A., Busch, R., Mayer, J., Hensel, M., Hopfinger, G., Hess, G., von Grünhagen, U., Bergmann, M., Catalano, J., Zinzani, P., Caligaris-Cappio, F., Seymour, J., Berrebi, A., Jäger, U., Cazin, B., Trneny, M., … Stilgenbauer, S. (2010). Addition of rituximab to fludarabine and cyclophosphamide in patients with chronic lymphocytic leukaemia: a randomised, open-label, phase 3 trial. *The Lancet*, *376*(9747), 1164–1174. https://doi.org/10.1016/S0140-6736(10)61381-5
250. Lim, S. H., Vaughan, A. T., Ashton-Key, M., Williams, E. L., Dixon, S. v., Chan, H. T. C., Beers, S. A., French, R. R., Cox, K. L., Davies, A. J., Potter, K. N., Mockridge, C. I., Oscier, D. G., Johnson, P. W. M., Cragg, M. S., & Glennie, M. J. (2011). Fc gamma receptor IIb on target B cells promotes rituximab internalization and reduces clinical efficacy. *Blood*, *118*(9), 2530–2540. https://doi.org/10.1182/blood-2011-01-330357
251. Vaughan, A. T., Iriyama, C., Beers, S. A., Chan, C. H. T., Lim, S. H., Williams, E. L., Shah, V., Roghanian, A., Frendéus, B., Glennie, M. J., & Cragg, M. S. (2014). Inhibitory FcγRIIb (CD32b) becomes activated by therapeutic mAb in both cis and trans and drives internalization according to antibody specificity. *Blood*, *123*(5), 669–677. https://doi.org/10.1182/blood-2013-04-490821
252. Mousavi, S. A., Sporstøl, M., Fladeby, C., Kjeken, R., Barois, N., & Berg, T. (2007). Receptor-mediated endocytosis of immune complexes in rat liver sinusoidal endothelial cells is mediated by FcγRIIb2. *Hepatology*, *46*(3), 871–884. https://doi.org/10.1002/hep.21748
253. Wu, X., Zhao, X., Baylor, L., Kaushal, S., Eisenberg, E., & Greene, L. E. (2001). Clathrin exchange during clathrin-mediated endocytosis. *The Journal of Cell Biology*, *155*(2), 291–300. https://doi.org/10.1083/jcb.200104085
254. Boucrot, E., Saffarian, S., Massol, R., Kirchhausen, T., & Ehrlich, M. (2006). Role of lipids and actin in the formation of clathrin-coated pits. *Experimental Cell Research*, *312*(20), 4036–4048. https://doi.org/10.1016/j.yexcr.2006.09.025

255. QEHB pathology reference ranges https://qehbpathology.uk/component/search/?searchword=liver&searchphrase=all&Itemid=113 (accessed 07/11/23)
256. UK Gov. (2022). *Guidance Adult Obesity: All our health*. https://www.gov.uk/government/publications/adult-obesity-applying-all-our-health/adult-obesity-applying-all-our-health (accessed 07/11/23)
257. Giannini, E. G., Testam R and Savarino, V. (2005). Liver enzyme alteration: a guide for clinicians. *Canadian Medical Association Journal*, *172*(3), 367–379. https://doi.org/10.1503/cmaj.1040752
258. Rej, R. (1989). Aminotransferases in disease. *Clinics in Laboratory Medicine*, *9*(4), 667–687.
259. Vanderlinde, R. E. (1986). Review of pyridoxal phosphate and the transaminases in liver disease. *Annals of Clinical and Laboratory Science*, *16*(2), 79–93.
260. Dufour, D. R., Lott, J. A., Nolte, F. S., Gretch, D. R., Koff, R. S., & Seeff, L. B. (2000). Diagnosis and monitoring of hepatic injury. I. Performance characteristics of laboratory tests. *Clinical Chemistry*, *46*(12), 2027–2049.
261. Kamimoto, Y., Horiuchi, S., Tanase, S., & Morino, Y. (1985). Plasma clearance of intravenously injected aspartate aminotransferase isozymes: Evidence for preferential uptake by sinusoidal liver cells. *Hepatology*, *5*(3), 367–375. https://doi.org/10.1002/hep.1840050305
262. Duan, J., Ruan, B., Yan, X., Liang, L., Song, P., Yang, Z., Liu, Y., Dou, K., Han, H., & Wang, L. (2018). Endothelial Notch activation reshapes the angiocrine of sinusoidal endothelia to aggravate liver fibrosis and blunt regeneration in mice. *Hepatology*, *68*(2), 677–690. https://doi.org/10.1002/hep.29834
263. Schlaeger, R., Haux, P., & Kattermann, R. (1982). Studies on the Mechanism of the Increase in Serum Alkaline Phosphatase Activity in Cholestasis: Significance of the Hepatic Bile Acid Concentration for the Leakage of Alkaline Phosphatase from Rat Liver. *Enzyme*, *28*(1), 3–13. https://doi.org/10.1159/000459078
264. Fevery, J., & Blanckaert, N. (1986). What can we learn from analysis of serum bilirubin? *Journal of Hepatology*, *2*(1), 113–121. https://doi.org/10.1016/S0168-8278(86)80014-9
265. Green, R. M., & Flamm, S. (2002). AGA technical review on the evaluation of liver chemistry tests. *Gastroenterology*, *123*(4), 1367–1384. https://doi.org/10.1053/gast.2002.36061
266. Peck-Radosavljevic, M. (2017). Thrombocytopenia in chronic liver disease. *Liver International*, *37*(6), 778–793. https://doi.org/10.1111/liv.13317
267. Nomura, S., Ogami, K., Kawamura, K., Tsukamoto, I., Kudo, Y., Kanakura, Y., Kitamura, Y., Miyazaki, H., & Kato, T. (1997). Cellular localization of thrombopoietin mRNA in the liver by in situ hybridization. *Experimental Hematology*, *25*(7), 565–572.

268. Malinchoc, M., Kamath, P. S., Gordon, F. D., Peine, C. J., Rank, J., & ter Borg, P. C. J. (2000). A model to predict poor survival in patients undergoing transjugular intrahepatic portosystemic shunts. *Hepatology*, *31*(4), 864–871. https://doi.org/10.1053/he.2000.5852
269. Mofrad, P., Contos, M. J., Haque, M., Sargeant, C., Fisher, R. A., Luketic, V. A., Sterling, R. K., Shiffman, M. L., Stravitz, R. T., & Sanyal, A. J. (2003). Clinical and histologic spectrum of nonalcoholic fatty liver disease associated with normal ALT values. *Hepatology (Baltimore, Md.)*, *37*(6), 1286–1292. https://doi.org/10.1053/jhep.2003.50229
270. Ali Samjo, S., Abbas, Z., Asim, M., & Tahir, K. (2020). The Pattern of Alcohol Consumption and the Severity of Alcohol-related Liver Disease in Patients Visiting the Liver Clinic. *Cureus*. https://doi.org/10.7759/cureus.7251
271. Schuppan, D., & Afdhal, N. H. (2008). Liver cirrhosis. *The Lancet*, *371*(9615), 838–851. https://doi.org/10.1016/S0140-6736(08)60383-9
272. Schuppan, D., Ruehl, M., Somasundaram, R., & Hahn, E. G. (2001). Matrix as a Modulator of Hepatic Fibrogenesis. *Seminars in Liver Disease*, *21*(03), 351–372. https://doi.org/10.1055/s-2001-17556
273. Benyon, R. C., & Arthur, M. J. P. (2001). Extracellular Matrix Degradation and the Role of Hepatic Stellate Cells. *Seminars in Liver Disease*, *21*(03), 373–384. https://doi.org/10.1055/s-2001-17552
274. Ruan, B., Duan, J.-L., Xu, H., Tao, K.-S., Han, H., Dou, G.-R., & Wang, L. (2021). Capillarized Liver Sinusoidal Endothelial Cells Undergo Partial Endothelial-Mesenchymal Transition to Actively Deposit Sinusoidal ECM in Liver Fibrosis. *Frontiers in Cell and Developmental Biology*, *9*. https://doi.org/10.3389/fcell.2021.671081
275. Sakhuja, P. (2014). Pathology of alcoholic liver disease, can it be differentiated from nonalcoholic steatohepatitis? *World Journal of Gastroenterology*, *20*(44), 16474. https://doi.org/10.3748/wjg.v20.i44.16474
276. Suk, K. T. and Kim, D.J. (2015). Staging of liver fibrosis or cirrhosis: The role of hepatic venous pressure gradient measurement. *World Journal of Hepatology*, *7*(3), 607. https://doi.org/10.4254/wjh.v7.i3.607
277. Marrero, I., Maricic, I., Morgan, T. R., Stolz, A. A., Schnabl, B., Liu, Z., Tsukamoto, H., & Kumar, V. (2020). Differential Activation of Unconventional T Cells, Including iNKT Cells, in Alcohol-Related Liver Disease. *Alcoholism: Clinical and Experimental Research*, *44*(5), 1061–1074. https://doi.org/10.1111/acer.14323
278. Brempelis, K. J., & Crispe, I. N. (2016). Infiltrating monocytes in liver injury and repair. *Clinical & Translational Immunology*, *5*(11). https://doi.org/10.1038/cti.2016.62
279. Crawford, J. M. (2012). Histologic Findings in Alcoholic Liver Disease. *Clinics in Liver Disease*, *16*(4), 699–716. https://doi.org/10.1016/j.cld.2012.08.004

280. Theise, N. D. (2013). Histopathology of alcoholic liver disease. *Clinical Liver Disease*, *2*(2), 64–67. https://doi.org/10.1002/cld.172
281. Harrison, S. A., Kadakia, S., Lang, K. A., & Schenker, S. (2002). Nonalcoholic steatohepatitis: what we know in the new millennium. *The American Journal of Gastroenterology*, *97*(11), 2714–2724. https://doi.org/10.1111/j.1572-0241.2002.07069.x
282. Steinman, J. B., Salomao, M. A., & Pajvani, U. B. (2021). Zonation in NASH – A key paradigm for understanding pathophysiology and clinical outcomes. *Liver International*, *41*(11), 2534–2546. https://doi.org/10.1111/liv.15025
283. Gadd, V. L., Skoien, R., Powell, E. E., Fagan, K. J., Winterford, C., Horsfall, L., Irvine, K., & Clouston, A. D. (2014). The portal inflammatory infiltrate and ductular reaction in human nonalcoholic fatty liver disease. *Hepatology*, *59*(4), 1393–1405. https://doi.org/10.1002/hep.26937
284. Remmerie, A., Martens, L., Thoné, T., Castoldi, A., Seurinck, R., Pavie, B., Roels, J., Vanneste, B., de Prijck, S., Vanhockerhout, M., Binte Abdul Latib, M., Devisscher, L., Hoorens, A., Bonnardel, J., Vandamme, N., Kremer, A., Borghgraef, P., van Vlierberghe, H., Lippens, S., … Scott, C. L. (2020). Osteopontin Expression Identifies a Subset of Recruited Macrophages Distinct from Kupffer Cells in the Fatty Liver. *Immunity*, *53*(3), 641-657.e14. https://doi.org/10.1016/j.immuni.2020.08.004
285. Steinman, J. B., Salomao, M. A., & Pajvani, U. B. (2021). Zonation in NASH – A key paradigm for understanding pathophysiology and clinical outcomes. *Liver International*, *41*(11), 2534–2546. https://doi.org/10.1111/liv.15025
286. Ehrlich, P. Ueber Immunität durch Vererbung und Säugung. *Zeitschr. f. Hygiene.* 12, 183–203 (1892). https://doi.org/10.1007/BF02284236
287. BRAMBELL FW, HEMMINGS WA, HENDERSON M, KEKWICK RA. Electrophoretic studies of serum proteins of foetal rabbits. Proc R Soc Lond B Biol Sci. 1953 Jul 15;141(904):300-14. doi: 10.1098/rspb.1953.0044.
288. BRAMBELL FW, HEMMINGS WA, OAKLEY CL, PORTER RR. The relative transmission of the fractions of papain hydrolyzed homologous gamma-globulin from the uterine cavity to the foetal circulation in the rabbit. Proc R Soc Lond B Biol Sci. 1960 Mar 1;151:478-82. doi: 10.1098/rspb.1960.0011
289. BRAMBELL FW, HEMMINGS WA, MORRIS IG. A THEORETICAL MODEL OF GAMMA-GLOBULIN CATABOLISM. Nature. 1964 Sep 26;203:1352-4. doi: 10.1038/2031352a0.
290. BRAMBELL, F. W., HEMMINGS, W. A., & MORRIS, I. G. (1964). A THEORETICAL MODEL OF GAMMA-GLOBULIN CATABOLISM. *Nature*, *203*, 1352–1354. https://doi.org/10.1038/2031352a0
291. Rodewald, R. (1976). pH-dependent binding of immunoglobulins to intestinal cells of the neonatal rat. *The Journal of Cell Biology*, *71*(2), 666–669. https://doi.org/10.1083/jcb.71.2.666

292. Simister, N. E., & Mostov, K. E. (1989). An Fc receptor structurally related to MHC class I antigens. *Nature*, *337*(6203), 184–187. https://doi.org/10.1038/337184a0
293. Burmeister, W. P., Gastinel, L. N., Simister, N. E., Blum, M. L., & Bjorkman, P. J. (1994). Crystal structure at 2.2 Å resolution of the MHC-related neonatal Fc receptor. *Nature*, *372*(6504), 336–343. https://doi.org/10.1038/372336a0
294. Passot, C., Azzopardi, N., Renault, S., Baroukh, N., Arnoult, C., Ohresser, M., Boisdron-Celle, M., Gamelin, E., Watier, H., Paintaud, G., & Gouilleux-Gruart, V. (2013). Influence of *FCGRT* gene polymorphisms on pharmacokinetics of therapeutic antibodies. *MAbs*, *5*(4), 614–619. https://doi.org/10.4161/mabs.24815
295. Story, C. M., Mikulska, J. E., & Simister, N. E. (1994). A major histocompatibility complex class I-like Fc receptor cloned from human placenta: possible role in transfer of immunoglobulin G from mother to fetus. *The Journal of Experimental Medicine*, *180*(6), 2377–2381. https://doi.org/10.1084/jem.180.6.2377
296. Vaughn, D. E., & Bjorkman, P. J. (1998). Structural basis of pH-dependent antibody binding by the neonatal Fc receptor. *Structure*, *6*(1), 63–73. https://doi.org/10.1016/S0969-2126(98)00008-2
297. Ghetie, V., Hubbard, J. G., Kim, J., Tsen, M., Lee, Y., & Ward, E. S. (1996). Abnormally short serum half-lives of IgG in β2-microglobulin-deficient mice. *European Journal of Immunology*, *26*(3), 690–696. https://doi.org/10.1002/eji.1830260327
298. Israel, E. J., Patel, V. K., Taylor, S. F., Marshak-Rothstein, A., & Simister, N. E. (1995). Requirement for a beta 2-microglobulin-associated Fc receptor for acquisition of maternal IgG by fetal and neonatal mice. *Journal of Immunology (Baltimore, Md. : 1950)*, *154*(12), 6246–6251.
299. Praetor, A., & Hunziker, W. (2002). β2-microglobulin is important for cell surface expression and pH-dependent IgG binding of human FcRn. *Journal of Cell Science*, *115*(11), 2389–2397. https://doi.org/10.1242/jcs.115.11.2389
300. Qiu, X., & Wang, M. Z. (2020). Quantification of Neonatal Fc Receptor and Beta-2 Microglobulin in Human Liver Tissues by Ultraperformance Liquid Chromatography–Multiple Reaction Monitoring–based Targeted Quantitative Proteomics for Applications in Biotherapeutic Physiologically-based Pharmacokinetic Models. *Drug Metabolism and Disposition*, *48*(10), 925–933. https://doi.org/10.1124/dmd.120.000075
301. Wani, M. A., Haynes, L. D., Kim, J., Bronson, C. L., Chaudhury, C., Mohanty, S., Waldmann, T. A., Robinson, J. M., & Anderson, C. L. (2006). Familial hypercatabolic hypoproteinemia caused by deficiency of the neonatal Fc receptor, FcRn, due to a mutant β_2-microglobulin gene. *Proceedings of the National Academy of Sciences*, *103*(13), 5084–5089. https://doi.org/10.1073/pnas.0600548103

302. Raghavan, M., & Bjorkman, P. J. (1996). Fc RECEPTORS AND THEIR INTERACTIONS WITH IMMUNOGLOBULINS. *Annual Review of Cell and Developmental Biology*, *12*(1), 181–220. https://doi.org/10.1146/annurev.cellbio.12.1.181
303. Martin, W. L., West, A. P., Gan, L., & Bjorkman, P. J. (2001). Crystal Structure at 2.8 Å of an FcRn/Heterodimeric Fc Complex. *Molecular Cell*, *7*(4), 867–877. https://doi.org/10.1016/S1097-2765(01)00230-1
304. Vaughn, D. E., Milburn, C. M., Penny, D. M., Martin, W. L., Johnson, J. L., & Bjorkman, P. J. (1997). Identification of critical IgG binding epitopes on the neonatal Fc receptor. *Journal of Molecular Biology*, *274*(4), 597–607. https://doi.org/10.1006/jmbi.1997.1388
305. Spiekermann, G. M., Finn, P. W., Ward, E. S., Dumont, J., Dickinson, B. L., Blumberg, R. S., & Lencer, W. I. (2002). Receptor-mediated Immunoglobulin G Transport Across Mucosal Barriers in Adult Life. *The Journal of Experimental Medicine*, *196*(3), 303–310. https://doi.org/10.1084/jem.20020400
306. Bitonti AJ, Dumont JA, Low SC, Peters RT, Kropp KE, Palombella VJ, et al. Pulmonary delivery of an erythropoietin Fc fusion protein in non-human primates through an immunoglobulin transport pathway. *Proc Natl Acad Sci USA*. (2004) 101:9763–8. doi: 10.1073/pnas.0403235101
307. Pyzik, M., Sand, K. M. K., Hubbard, J. J., Andersen, J. T., Sandlie, I., & Blumberg, R. S. (2019). The Neonatal Fc Receptor (FcRn): A Misnomer? *Frontiers in Immunology*, *10*. https://doi.org/10.3389/fimmu.2019.01540
308. Kim, J. K., Firan, M., Radu, C. G., Kim, C. H., Ghetie, V., & Ward, E. S. (1999). Mapping the site on human IgG for binding of the MHC class I-related receptor, FcRn. *European Journal of Immunology*, *29*(9), 2819–2825. https://doi.org/10.1002/(SICI)1521-4141(199909)29:09<2819::AID-IMMU2819>3.0.CO;2-6
309. Wang, W., Lu, P., Fang, Y., Hamuro, L., Pittman, T., Carr, B., Hochman, J., & Prueksaritanont, T. (2011). Monoclonal Antibodies with Identical Fc Sequences Can Bind to FcRn Differentially with Pharmacokinetic Consequences. *Drug Metabolism and Disposition*, *39*(9), 1469–1477. https://doi.org/10.1124/dmd.111.039453
310. Popov, S., Hubbard, J. G., Kim, J.-K., Ober, B., Ghetie, V., & Ward, E. S. (1996). The stoichiometry and affinity of the interaction of murine Fc fragments with the MHC class I-related receptor, FcRn. *Molecular Immunology*, *33*(6), 521–530. https://doi.org/10.1016/0161-5890(96)00004-1
311. Chaudhury, C., Mehnaz, S., Robinson, J. M., Hayton, W. L., Pearl, D. K., Roopenian, D. C., & Anderson, C. L. (2003). The Major Histocompatibility Complex–related Fc Receptor for IgG (FcRn) Binds Albumin and Prolongs Its Lifespan. *The Journal of Experimental Medicine*, *197*(3), 315–322. https://doi.org/10.1084/jem.20021829

312. Chaudhury, C., Brooks, C. L., Carter, D. C., Robinson, J. M., & Anderson, C. L. (2006). Albumin Binding to FcRn: Distinct from the FcRn−IgG Interaction. *Biochemistry*, *45*(15), 4983–4990. https://doi.org/10.1021/bi052628y
313. Kim, J., Hayton, W. L., Robinson, J. M., & Anderson, C. L. (2007). Kinetics of FcRn-mediated recycling of IgG and albumin in human: Pathophysiology and therapeutic implications using a simplified mechanism-based model. *Clinical Immunology*, *122*(2), 146–155. https://doi.org/10.1016/j.clim.2006.09.001
314. Blumberg, R. S., Koss, T., Story, C. M., Barisani, D., Polischuk, J., Lipin, A., Pablo, L., Green, R., & Simister, N. E. (1995). A major histocompatibility complex class I-related Fc receptor for IgG on rat hepatocytes. *Journal of Clinical Investigation*, *95*(5), 2397–2402. https://doi.org/10.1172/JCI117934
315. D'Hooghe, L., Chalmers, A. D., Heywood, S., & Whitley, P. (2017). Cell surface dynamics and cellular distribution of endogenous FcRn. *PLOS ONE*, *12*(8), e0182695. https://doi.org/10.1371/journal.pone.0182695
316. van der Flier, A., Liu, Z., Tan, S., Chen, K., Drager, D., Liu, T., Patarroyo-White, S., Jiang, H., & Light, D. R. (2015). FcRn Rescues Recombinant Factor VIII Fc Fusion Protein from a VWF Independent FVIII Clearance Pathway in Mouse Hepatocytes. *PLOS ONE*, *10*(4), e0124930. https://doi.org/10.1371/journal.pone.0124930
317. Pyzik, M., Rath, T., Kuo, T. T., Win, S., Baker, K., Hubbard, J. J., Grenha, R., Gandhi, A., Krämer, T. D., Mezo, A. R., Taylor, Z. S., McDonnell, K., Nienaber, V., Andersen, J. T., Mizoguchi, A., Blumberg, L., Purohit, S., Jones, S. D., Christianson, G., … Blumberg, R. S. (2017). Hepatic FcRn regulates albumin homeostasis and susceptibility to liver injury. *Proceedings of the National Academy of Sciences*, *114*(14). https://doi.org/10.1073/pnas.1618291114
318. Fan YY, Avery LB, Wang M, O'Hara DM, Leung S, Neubert H. Tissue expression profile of human neonatal Fc receptor (FcRn) in Tg32 transgenic mice. *mAbs.* (2016) 8:848–53. doi: 10.1080/19420862.2016.1178436
319. Borvak J, Richardson J, Medesan C, Antohe F, Radu C, Simionescu M, et al. Functional expression of the MHC class I-related receptor, FcRn, in endothelial cells of mice. *Int Immunol.* (1998) 10:1289–98. doi: 10.1093/intimm/10.9.1289
320. Latvala S, Jacobsen B, Otteneder MB, Herrmann A, Kronenberg S. Distribution of FcRn across species and tissues. *J Histochem Cytochem.* (2017) 65:321–33. doi: 10.1369/0022155417705095
321. Yip, V., Palma, E., Tesar, D. B., Mundo, E. E., Bumbaca, D., Torres, E. K., Reyes, N. A., Shen, B. Q., Fielder, P. J., Prabhu, S., Khawli, L. A., & Boswell, C. A. (2014). Quantitative cumulative biodistribution of antibodies in mice. *MAbs*, *6*(3), 689–696. https://doi.org/10.4161/mabs.28254
322. Chen, N., Wang, W., Fauty, S., Fang, Y., Hamuro, L., Hussain, A., & Prueksaritanont, T. (2014). The effect of the neonatal Fc receptor on human IgG biodistribution in mice. *MAbs*, *6*(2), 502–508. https://doi.org/10.4161/mabs.27765

323. Stahl, P., Six, H., Rodman, J. S., Schlesinger, P., Tulsiani, D. R., & Touster, O. (1976). Evidence for specific recognition sites mediating clearance of lysosomal enzymes in vivo. *Proceedings of the National Academy of Sciences*, *73*(11), 4045–4049. https://doi.org/10.1073/pnas.73.11.4045
324. van der Zande, H. J. P., Nitsche, D., Schlautmann, L., Guigas, B., & Burgdorf, S. (2021). The Mannose Receptor: From Endocytic Receptor and Biomarker to Regulator of (Meta)Inflammation. *Frontiers in Immunology*, *12*. https://doi.org/10.3389/fimmu.2021.765034
325. Lee, S. J., Evers, S., Roeder, D., Parlow, A. F., Risteli, J., Risteli, L., Lee, Y. C., Feizi, T., Langen, H., & Nussenzweig, M. C. (2002). Mannose Receptor-Mediated Regulation of Serum Glycoprotein Homeostasis. *Science*, *295*(5561), 1898–1901. https://doi.org/10.1126/science.1069540
326. Shepherd, V. L., & Hoidal, J. R. (1990). Clearance of Neutrophil-derived Myeloperoxidase by the Macrophage Mannose Receptor. *American Journal of Respiratory Cell and Molecular Biology*, *2*(4), 335–340. https://doi.org/10.1165/ajrcmb/2.4.335
327. Prigozy, T. I., Sieling, P. A., Clemens, D., Stewart, P. L., Behar, S. M., Porcelli, S. A., Brenner, M. B., Modlin, R. L., & Kronenberg, M. (1997). The Mannose Receptor Delivers Lipoglycan Antigens to Endosomes for Presentation to T Cells by CD1b Molecules. *Immunity*, *6*(2), 187–197. https://doi.org/10.1016/S1074-7613(00)80425-2
328. Mastrotto, F., Pirazzini, M., Negro, S., Salama, A., Martinez-Pomares, L., & Mantovani, G. (2022). Sulfation at Glycopolymer Side Chains Switches Activity at the Macrophage Mannose Receptor (CD206) In Vitro and In Vivo. *Journal of the American Chemical Society*, *144*(50), 23134–23147. https://doi.org/10.1021/jacs.2c10757
329. Fiete, D. J., Beranek, M. C., & Baenziger, J. U. (1998). A cysteine-rich domain of the "mannose" receptor mediates GalNAc-4-SO $_4$ binding. *Proceedings of the National Academy of Sciences*, *95*(5), 2089–2093. https://doi.org/10.1073/pnas.95.5.2089
330. Napper, C. E., Drickamer, K., & Taylor, M. E. (2006). Collagen binding by the mannose receptor mediated through the fibronectin type II domain. *Biochemical Journal*, *395*(3), 579–586. https://doi.org/10.1042/BJ20052027
331. Taylor ME, Bezouska K, Drickamer K. Contribution to Ligand Binding by Multiple Carbohydrate-Recognition Domains in the Macrophage Mannose Receptor. *J Biol Chem* (1992) 267:1719–26. doi: 10.1016/S0021-9258(18)46005-X
332. TAYLOR, P., GORDON, S., & MARTINEZPOMARES, L. (2005). The mannose receptor: linking homeostasis and immunity through sugar recognition. *Trends in Immunology*, *26*(2), 104–110. https://doi.org/10.1016/j.it.2004.12.001

333. Gazi, U., & Martinez-Pomares, L. (2009). Influence of the mannose receptor in host immune responses. *Immunobiology*, *214*(7), 554–561. https://doi.org/10.1016/j.imbio.2008.11.004
334. Feinberg, H., Jégouzo, S. A. F., Lasanajak, Y., Smith, D. F., Drickamer, K., Weis, W. I., & Taylor, M. E. (2021). Structural analysis of carbohydrate binding by the macrophage mannose receptor CD206. *Journal of Biological Chemistry*, *296*, 100368. https://doi.org/10.1016/j.jbc.2021.100368
335. Schweizer, A., Stahl, P. D., & Rohrer, J. (2000). A Di-aromatic Motif in the Cytosolic Tail of the Mannose Receptor Mediates Endosomal Sorting. *Journal of Biological Chemistry*, *275*(38), 29694–29700. https://doi.org/10.1074/jbc.M000571200
336. Dong, X., Storkus, W. J., & Salter, R. D. (1999). Binding and Uptake of Agalactosyl IgG by Mannose Receptor on Macrophages and Dendritic Cells. *The Journal of Immunology*, *163*(10), 5427–5434. https://doi.org/10.4049/jimmunol.163.10.5427
337. Mastrotto, F., Pirazzini, M., Negro, S., Salama, A., Martinez-Pomares, L., & Mantovani, G. (2022). Sulfation at Glycopolymer Side Chains Switches Activity at the Macrophage Mannose Receptor (CD206) In Vitro and In Vivo. *Journal of the American Chemical Society*, *144*(50), 23134–23147. https://doi.org/10.1021/jacs.2c10757
338. Feinberg, H., Park-Snyder, S., Kolatkar, A. R., Heise, C. T., Taylor, M. E., & Weis, W. I. (2000). Structure of a C-type Carbohydrate Recognition Domain from the Macrophage Mannose Receptor. *Journal of Biological Chemistry*, *275*(28), 21539–21548. https://doi.org/10.1074/jbc.M002366200
339. Linehan, S.A. The mannose receptor is expressed by subsets of APC in non-lymphoid organs. *BMC Immunol* 6, 4 (2005). https://doi.org/10.1186/1471-2172-6-4
340. de Haan W., Øie C., Benkheil M., Dheedene W., Vinckier S., Coppiello G., et al. (2020). Unraveling the transcriptional determinants of liver sinusoidal endothelial cell specialization.*Am. J. Physiol. Gastrointest. Liver Physiol.* 318G803–G815. 10.1152/ajpgi.00215.2019
341. MacParland S. A., Liu J. C., Ma X. Z., Innes B. T., Bartczak A. M., Gage B. K., et al. (2018). Single cell RNA sequencing of human liver reveals distinct intrahepatic macrophage populations. *Nat. Commun.* 9:4383. 10.1038/s41467-018-06318-7
342. Limmer A., Ohl J., Kurts C., Ljunggren H. G., Reiss Y., Groettrup M., et al. (2000). Efficient presentation of exogenous antigen by liver endothelial cells to CD8+ T cells results in antigen-specific T-cell tolerance. *Nat. Med.* 6 1348–1354. 10.1038/82161
343. Schurich A., Bottcher J. P., Burgdorf S., Penzler P., Hegenbarth S., Kern M., et al. (2009). Distinct kinetics and dynamics of cross-presentation in liver sinusoidal

endothelial cells compared to dendritic cells. *Hepatology* 50 909–919. 10.1002/hep.23075

344. Asumendi, A., Alvarez, A., Martinez, I., Smedsrod, B., and Vidal-Vanaclocha, F. (1996). Hepatic sinusoidal endothelium heterogeneity with respect to mannose receptor activity is interleukin-1 dependent. *Hepatology* 23, 1521–1529. doi: 10.1053/jhep.1996.v23.pm0008675173
345. Arteta, B., Lasuen, N., Lopategi, A., Sveinbjörnsson, B., Smedsrød, B., & Vidal-Vanaclocha, F. (2010). Colon carcinoma cell interaction with liver sinusoidal endothelium inhibits organ-specific antitumor immunity through interleukin-1-induced mannose receptor in mice. *Hepatology*, *51*(6), 2172–2182. https://doi.org/10.1002/hep.23590
346. Liu Y., Gardner C. R., Laskin J. D., Laskin D. L. (2013). Classical and alternative activation of rat hepatic sinusoidal endothelial cells by inflammatory stimuli. *Exp. Mol. Pathol.* 94 160–167. 10.1016/j.yexmp.2012.10.015
347. Knolle, P. A., Uhrig, A., Hegenbarth, S., Löser, E., Schmitt, E., Gerken, G., & Lohse, A. W. (2001). IL-10 down-regulates T cell activation by antigen-presenting liver sinusoidal endothelial cells through decreased antigen uptake via the mannose receptor and lowered surface expression of accessory molecules. *Clinical and Experimental Immunology*, *114*(3), 427–433. https://doi.org/10.1046/j.1365-2249.1998.00713.x
348. Jordens R, Thompson A, Amons R, Koning F. Human Dendritic Cells Shed a Functional, Soluble Form of the Mannose Receptor. *Int Immunol* (1999) 11:1775–80. doi: 10.1093/intimm/11.11.1775
349. Martínez-Pomares L, Mahoney JA, Káposzta R, Linehan SA, Stahl PD, Gordon S. A Functional Soluble Form of the Murine Mannose Receptor Is Produced by Macrophages *In Vitro* Is Present Mouse Serum. *J Biol Chem* (1998) 273:23376–80. doi: 10.1074/jbc.273.36.23376
350. Sandahl T. D., Stoy S. H., Laursen T. L., Rodgaard-Hansen S., Moller H. J., Moller S., et al. (2017). The soluble mannose receptor (sMR) is elevated in alcoholic liver disease and associated with disease severity, portal hypertension, and mortality in cirrhosis patients. *PLoS One* 12:e0189345. 10.1371/journal.pone.0189345
351. Pöhlmann, S., Soilleux, E. J., Baribaud, F., Leslie, G. J., Morris, L. S., Trowsdale, J., Lee, B., Coleman, N., & Doms, R. W. (2001). DC-SIGNR, a DC-SIGN homologue expressed in endothelial cells, binds to human and simian immunodeficiency viruses and activates infection in trans. *Proceedings of the National Academy of Sciences*, *98*(5), 2670–2675. https://doi.org/10.1073/pnas.051631398
352. Soilleux, E. J., Barten, R., & Trowsdale, J. (2000). Cutting Edge: DC-SIGN; a Related Gene, DC-SIGNR; and CD23 Form a Cluster on 19p13 . *The Journal of Immunology*, *165*(6), 2937–2942. https://doi.org/10.4049/jimmunol.165.6.2937

353. Grimwood J., Gordon L. A., Olsen A., Terry A., Schmutz J., Lamerdin J., et al. (2004). The DNA sequence and biology of human chromosome 19. *Nature* 428 529–535. 10.1038/nature02399
354. Swystun, L. L., Notley, C., Georgescu, I., Lai, J. D., Nesbitt, K., James, P. D., & Lillicrap, D. (2019). The endothelial lectin clearance receptor CLEC4M binds and internalizes factor VIII in a VWF-dependent and independent manner. *Journal of Thrombosis and Haemostasis*, *17*(4), 681–694. https://doi.org/10.1111/jth.14404
355. Rydz, N., Swystun, L. L., Notley, C., Paterson, A. D., Riches, J. J., Sponagle, K., Boonyawat, B., Montgomery, R. R., James, P. D., & Lillicrap, D. (2013). The C-type lectin receptor CLEC4M binds, internalizes, and clears von Willebrand factor and contributes to the variation in plasma von Willebrand factor levels. *Blood*, *121*(26), 5228–5237. https://doi.org/10.1182/blood-2012-10-457507
356. Lai, W. K., Sun, P. J., Zhang, J., Jennings, A., Lalor, P. F., Hubscher, S., McKeating, J. A., & Adams, D. H. (2006). Expression of DC-SIGN and DC-SIGNR on Human Sinusoidal Endothelium. *The American Journal of Pathology*, *169*(1), 200–208. https://doi.org/10.2353/ajpath.2006.051191
357. Uhlén, M., Fagerberg, L., Hallström, B. M., Lindskog, C., Oksvold, P., Mardinoglu, A., Sivertsson, Å., Kampf, C., Sjöstedt, E., Asplund, A., Olsson, I., Edlund, K., Lundberg, E., Navani, S., Szigyarto, C. A.-K., Odeberg, J., Djureinovic, D., Takanen, J. O., Hober, S., … Pontén, F. (2015). Tissue-based map of the human proteome. *Science*, *347*(6220). https://doi.org/10.1126/science.1260419
358. Uhlen, M., Karlsson, M. J., Zhong, W., Tebani, A., Pou, C., Mikes, J., Lakshmikanth, T., Forsström, B., Edfors, F., Odeberg, J., Mardinoglu, A., Zhang, C., von Feilitzen, K., Mulder, J., Sjöstedt, E., Hober, A., Oksvold, P., Zwahlen, M., Ponten, F., … Brodin, P. (2019). A genome-wide transcriptomic analysis of protein-coding genes in human blood cells. *Science*, *366*(6472). https://doi.org/10.1126/science.aax9198
359. Human Protein Atlas (2003) https://www.proteinatlas.org/ENSG00000104938-CLEC4M/single+cell+type/liver
360. MacParland, S. A., Liu, J. C., Ma, X.-Z., Innes, B. T., Bartczak, A. M., Gage, B. K., Manuel, J., Khuu, N., Echeverri, J., Linares, I., Gupta, R., Cheng, M. L., Liu, L. Y., Camat, D., Chung, S. W., Seliga, R. K., Shao, Z., Lee, E., Ogawa, S., … McGilvray, I. D. (2018). Single cell RNA sequencing of human liver reveals distinct intrahepatic macrophage populations. *Nature Communications*, *9*(1), 4383. https://doi.org/10.1038/s41467-018-06318-7
361. Ramachandran, P., Dobie, R., Wilson-Kanamori, J. R., Dora, E. F., Henderson, B. E. P., Luu, N. T., Portman, J. R., Matchett, K. P., Brice, M., Marwick, J. A., Taylor, R. S., Efremova, M., Vento-Tormo, R., Carragher, N. O., Kendall, T. J., Fallowfield, J. A., Harrison, E. M., Mole, D. J., Wigmore, S. J., … Henderson, N. C. (2019). Resolving

the fibrotic niche of human liver cirrhosis at single-cell level. *Nature*, *575*(7783), 512–518. https://doi.org/10.1038/s41586-019-1631-3

362. Mouriaux, F., Zaniolo, K., Bergeron, M.-A., Weidmann, C., de La Fouchardière, A., Fournier, F., Droit, A., Morcos, M. W., Landreville, S., & Guérin, S. L. (2016). Effects of Long-term Serial Passaging on the Characteristics and Properties of Cell Lines Derived From Uveal Melanoma Primary Tumors. *Investigative Opthalmology & Visual Science*, *57*(13), 5288. https://doi.org/10.1167/iovs.16-19317
363. Koehler, K. R., Tropel, P., Theile, J. W., Kondo, T., Cummins, T. R., Viville, S., & Hashino, E. (2011). Extended passaging increases the efficiency of neural differentiation from induced pluripotent stem cells. *BMC Neuroscience*, *12*(1), 82. https://doi.org/10.1186/1471-2202-12-82
364. Murray, J. K., Balan, C., Allgeier, A. M., Kasparian, A., Viswanadhan, V., Wilde, C., Allen, J. R., Yoder, S. C., Biddlecome, G., Hungate, R. W., & Miranda, L. P. (2010). Dipeptidyl-Quinolone Derivatives Inhibit Hypoxia Inducible Factor-1α Prolyl Hydroxylases-1, -2, and -3 with Altered Selectivity. *Journal of Combinatorial Chemistry*, *12*(5), 676–686. https://doi.org/10.1021/cc100073a
365. le Couteur, D. (2001). Pseudocapillarization and associated energy limitation in the aged rat liver. *Hepatology*, *33*(3), 537–543. https://doi.org/10.1053/jhep.2001.22754
366. McLean, A. J., Cogger, V. C., Chong, G. C., Warren, A., Markus, A. M., Dahlstrom, J. E., & le Couteur, D. G. (2003). Age-related pseudocapillarization of the human liver. *The Journal of Pathology*, *200*(1), 112–117. https://doi.org/10.1002/path.1328
367. Cogger, V. C., Warren, A., Fraser, R., Ngu, M., McLean, A. J., & le Couteur, D. G. (2003). Hepatic sinusoidal pseudocapillarization with aging in the non-human primate. *Experimental Gerontology*, *38*(10), 1101–1107. https://doi.org/10.1016/j.exger.2003.07.002
368. Cotreau, M. M., von Moltke, L. L., & Greenblatt, D. J. (2005). The Influence of Age and Sex on the Clearance of Cytochrome P450 3A Substrates. *Clinical Pharmacokinetics*, *44*(1), 33–60. https://doi.org/10.2165/00003088-200544010-00002
369. le Couteur, D. G., & McLean, A. J. (1998). The Aging Liver. *Clinical Pharmacokinetics*, *34*(5), 359–373. https://doi.org/10.2165/00003088-199834050-00003
370. Qiu, X., & Wang, M. Z. (2020). Quantification of Neonatal Fc Receptor and Beta-2 Microglobulin in Human Liver Tissues by Ultraperformance Liquid Chromatography–Multiple Reaction Monitoring–based Targeted Quantitative Proteomics for Applications in Biotherapeutic Physiologically-based Pharmacokinetic Models. *Drug Metabolism and Disposition*, *48*(10), 925–933. https://doi.org/10.1124/dmd.120.000075

371. Fan, Y.-Y., Farrokhi, V., Caiazzo, T., Wang, M., O'Hara, D. M., & Neubert, H. (2019). Human FcRn Tissue Expression Profile and Half-Life in PBMCs. *Biomolecules*, *9*(8), 373. https://doi.org/10.3390/biom9080373
372. Sachs, U. J. H., Socher, I., Braeunlich, C. G., Kroll, H., Bein, G., & Santoso, S. (2006). A variable number of tandem repeats polymorphism influences the transcriptional activity of the neonatal Fc receptor α-chain promoter. *Immunology*, *119*(1), 83–89. https://doi.org/10.1111/j.1365-2567.2006.02408.x
373. Gouilleux-Gruart, V., Chapel, H., Chevret, S., Lucas, M., Malphettes, M., Fieschi, C., Patel, S., Boutboul, D., Marson, M.-N., Gérard, L., Lee, M., Watier, H., & Oksenhendler, E. (2013). Efficiency of immunoglobulin G replacement therapy in common variable immunodeficiency: correlations with clinical phenotype and polymorphism of the neonatal Fc receptor. *Clinical and Experimental Immunology*, *171*(2), 186–194. https://doi.org/10.1111/cei.12002
374. Passot, C., Azzopardi, N., Renault, S., Baroukh, N., Arnoult, C., Ohresser, M., Boisdron-Celle, M., Gamelin, E., Watier, H., Paintaud, G., & Gouilleux-Gruart, V. (2013). Influence of *FCGRT* gene polymorphisms on pharmacokinetics of therapeutic antibodies. *MAbs*, *5*(4), 614–619. https://doi.org/10.4161/mabs.24815
375. Luzio, J. P., Parkinson, M. D. J., Gray, S. R., & Bright, N. A. (2009). The delivery of endocytosed cargo to lysosomes. *Biochemical Society Transactions*, *37*(5), 1019–1021. https://doi.org/10.1042/BST0371019
376. Gage, B. K., Liu, J. C., Innes, B. T., MacParland, S. A., McGilvray, I. D., Bader, G. D., & Keller, G. M. (2020). Generation of Functional Liver Sinusoidal Endothelial Cells from Human Pluripotent Stem-Cell-Derived Venous Angioblasts. *Cell Stem Cell*, *27*(2), 254-269.e9. https://doi.org/10.1016/j.stem.2020.06.007
377. Roberts, G. M., Davies, E. V., Pettit, E. J., & Hallett, M. B. (1997). The Timing and Magnitude of Ca2+Signaling by CD32 Depends on Its Redistribution on the Cell Surface. *Experimental Cell Research*, *230*(2), 303–309. https://doi.org/10.1006/excr.1996.3416
378. Ionele, C. M., Subtirelu, M. S., Ungureanu, B. S., Serbanescu, M.-S., & Rogoveanu, I. (2022). Calcium and Phosphorus Deficiencies in Patients with Liver Cirrhosis. *Current Health Sciences Journal*, *48*(3), 311–316. https://doi.org/10.12865/CHSJ.48.03.09
379. Ganesan L. P., Mohanty S., Kim J., Clark K. R., Robinson J. M., Anderson C. L. (2011). Rapid and efficient clearance of blood-borne virus by liver sinusoidal endothelium. *PLoS Pathog.*7:e1002281. 10.1371/journal.ppat.1002281
380. Simon-Santamaria J., Rinaldo C. H., Kardas P., Li R., Malovic I., Elvevold K., et al. (2014). Efficient uptake of blood-borne BK and JC polyomavirus-like particles in endothelial cells of liver sinusoids and renal vasa recta. *PLoS One* 9:e111762. 10.1371/journal.pone.0111762

381. Zdanowicz, K., Kowalczuk-Kryston, M., Olanski, W., Werpachowska, I., Mielech, W., & Lebensztejn, D. M. (2022). Increase in Serum MMP-9 and TIMP-1 Concentrations during Alcohol Intoxication in Adolescents—A Preliminary Study. *Biomolecules*, *12*(5), 710. https://doi.org/10.3390/biom12050710
382. Vigerust, D. J., Vick, S., & Shepherd, V. L. (2012). Characterization of functional mannose receptor in a continuous hybridoma cell line. *BMC Immunology*, *13*(1), 51. https://doi.org/10.1186/1471-2172-13-51
383. Cambi, A., Beeren, I., Joosten, B., Fransen, J. A., & Figdor, C. G. (2009). The C-type lectin DC-SIGN internalizes soluble antigens and HIV-1 virions *via* a clathrin-dependent mechanism. *European Journal of Immunology*, *39*(7), 1923–1928. https://doi.org/10.1002/eji.200939351
384. Gracia-Sancho, J., Caparrós, E., Fernández-Iglesias, A., & Francés, R. (2021). Role of liver sinusoidal endothelial cells in liver diseases. *Nature Reviews Gastroenterology & Hepatology*, *18*(6), 411–431. https://doi.org/10.1038/s41575-020-00411-3
385. DeLeve, L., & Maretti-Mira, A. (2017). Liver Sinusoidal Endothelial Cell: An Update. *Seminars in Liver Disease*, *37*(04), 377–387. https://doi.org/10.1055/s-0037-1617455
386. Kingeter, L. M., & Lin, X. (2012). C-type lectin receptor-induced NF-κB activation in innate immune and inflammatory responses. *Cellular & Molecular Immunology*, *9*(2), 105–112. https://doi.org/10.1038/cmi.2011.58
387. Murai, M. Aramaki, Y. and Tsuchiya, S. (1995) Contribution of mannose receptor to signal transduction in Fc gamma receptor-mediated phagocytosis of mouse peritoneal macrophages induced by liposomes. *J Leukoc Biol.* 57(4) 687-691. doi: 10.1002/jib.57.4.687.
388. Chavele, K.-M., Martinez-Pomares, L., Domin, J., Pemberton, S., Haslam, S. M., Dell, A., Cook, H. T., Pusey, C. D., Gordon, S., & Salama, A. D. (2010). Mannose receptor interacts with Fc receptors and is critical for the development of crescentic glomerulonephritis in mice. *Journal of Clinical Investigation*, *120*(5), 1469–1478. https://doi.org/10.1172/JCI41560
389. Gasmi, B., & Kleiner, D. E. (2020). Liver Histology. *Clinics in Liver Disease*, *24*(1), 61–74. https://doi.org/10.1016/j.cld.2019.09.004
390. Grinshpun, B., Thorsteinson, N., Pereira, J. N., Rippmann, F., Nannemann, D., Sood, V. D., & Fomekong Nanfack, Y. (2021). Identifying biophysical assays and in silico properties that enrich for slow clearance in clinical-stage therapeutic antibodies. MAbs, 13(1). https://doi.org/10.1080/19420862.2021.1932230
391. Prot pi (2014) *Prot pi: protein tool: https://www.protpi.ch/Calculator/ProteinTool [Accessed December 2023].*

392. Platchek, M., Lu, Q., Tran, H., & Xie, W. (2020). Comparative Analysis of Multiple Immunoassays for Cytokine Profiling in Drug Discovery. *SLAS Discovery*, *25*(10), 1197–1213. https://doi.org/10.1177/2472555220954389
393. Anderson, A., Rowles, W., Poole, S., Balan, A., Bevan, C., Brandstadter, R., Ciplea, A. I., Cooper, J., Fabian, M., Hale, T. W., Jacobs, D., Kakara, M., Krysko, K. M., Longbrake, E. E., Marcus, J., Repovic, P., Riley, C. S., Romeo, A. R., Rutatangwa, A., … Bove, R. (2023). <scp>Anti-CD20</scp> monoclonal antibody therapy in postpartum women with neurological conditions. *Annals of Clinical and Translational Neurology*, *10*(11), 2053–2064. https://doi.org/10.1002/acn3.51893
394. Ramachandran, P., Xu, G., Huang, H. H., Rice, R., Zhou, B., Lindpaintner, K., & Serie, D. (2022). Serum Glycoprotein Markers in Nonalcoholic Steatohepatitis and Hepatocellular Carcinoma. *Journal of Proteome Research*, *21*(4), 1083–1094. https://doi.org/10.1021/acs.jproteome.1c00965
395. Vanderschaeghe, D., Laroy, W., Sablon, E., Halfon, P., van Hecke, A., Delanghe, J., & Callewaert, N. (2009). GlycoFibroTest Is a Highly Performant Liver Fibrosis Biomarker Derived from DNA Sequencer-based Serum Protein Glycomics. *Molecular & Cellular Proteomics*, *8*(5), 986–994. https://doi.org/10.1074/mcp.M800470-MCP200
396. Callewaert, N., Vlierberghe, H. van, Hecke, A. van, Laroy, W., Delanghe, J., & Contreras, R. (2004). Noninvasive diagnosis of liver cirrhosis using DNA sequencer–based total serum protein glycomics. *Nature Medicine*, *10*(4), 429–434. https://doi.org/10.1038/nm1006
397. Gligorijević, N., Minić, S., & Nedić, O. (2022). Structural changes of proteins in liver cirrhosis and consequential changes in their function. *World Journal of Gastroenterology*, *28*(29), 3780–3792. https://doi.org/10.3748/wjg.v28.i29.3780
398. Ehret, J., Zimmermann, M., Eichhorn, T., & Zimmer, A. (2019). Impact of cell culture media additives on IgG glycosylation produced in Chinese hamster ovary cells. *Biotechnology and Bioengineering*, *116*(4), 816–830. https://doi.org/10.1002/bit.26904
399. SKLAR, L., CARTER, M., & EDWARDS, B. (2007). Flow cytometry for drug discovery, receptor pharmacology and high-throughput screening. *Current Opinion in Pharmacology*, *7*(5), 527–534. https://doi.org/10.1016/j.coph.2007.06.006
400. Noguchi, Y., Ozeki, K., Takesue, H., & Akita, H. (2021). A cell based assay for evaluating binding and uptake of an antibody using hepatic nonparenchymal cells. *Scientific Reports*, *11*(1), 8383. https://doi.org/10.1038/s41598-021-87912-6
401. Falkowska-Hansen, B., Falkowski, M., Metharom, P., Krunic, D., & Goerdt, S. (2007). Clathrin-coated vesicles form a unique net-like structure in liver sinusoidal endothelial cells by assembling along undisrupted microtubules. Experimental Cell Research, 313(9), 1745–1757. https://doi.org/10.1016/j.yexcr.2007.02.026

402. Chakravarti, A. (2015). Perspectives on Human Variation through the Lens of Diversity and Race: Figure 1. Cold Spring Harbor Perspectives in Biology, 7(9), a023358. https://doi.org/10.1101/cshperspect.a023358
403. Doppalapudi, V. R., Huang, J., Liu, D., Jin, P., Liu, B., Li, L., Desharnais, J., Hagen, C., Levin, N. J., Shields, M. J., Parish, M., Murphy, R. E., del Rosario, J., Oates, B. D., Lai, J.-Y., Matin, M. J., Ainekulu, Z., Bhat, A., Bradshaw, C. W., … Lappe, R. W. (2010). Chemical generation of bispecific antibodies. Proceedings of the National Academy of Sciences, 107(52), 22611–22616. https://doi.org/10.1073/pnas.1016478108
404. Marckel, J. A., Wetzel, H. N., Bell-Horwath, T. R., Turner, M. E., Webster, R. P., Kirley, T. L., Crutchfield, C. A., & Norman, A. B. (2020). The pharmacokinetics of the Fab fragment of a humanized anti-cocaine monoclonal antibody and its effects on cocaine's distribution in mice. The FASEB Journal, 34(S1), 1–1. https://doi.org/10.1096/fasebj.2020.34.s1.06272
405. Hellevik, T., Martinez, I., Olsen, R., Toh, B.-H., Webster, P., & Smedsrød, B. (1998). Transport of residual endocytosed products into terminal lysosomes occurs slowly in rat liver endothelial cells. Hepatology, 28(5), 1378–1389. https://doi.org/10.1002/hep.510280529
406. Motley, A., Bright, N. A., Seaman, M. N. J., & Robinson, M. S. (2003). Clathrin-mediated endocytosis in AP-2–depleted cells. The Journal of Cell Biology, 162(5), 909–918. https://doi.org/10.1083/jcb.200305145
407. Blouin, A., Bolender, R. P., & Weibel, E. R. (1977). Distribution of organelles and membranes between hepatocytes and nonhepatocytes in the rat liver parenchyma. A stereological study. The Journal of Cell Biology, 72(2), 441–455. https://doi.org/10.1083/jcb.72.2.441
408. Eskelinen, E.L. (2006) Role of LAMP1 and LAMP2 in lysosome biogenesis and autophagy. *Mol Asp of Med,* 27(5-6) 495-502. doi: 10.1016j.mam.2006.08.005
409. New-Aaron, M., Thomes, P.G., Ganesan, M., Dagur, R.S., Donohue Jr, T.M., Kusum, K.K., Poluektova., L.Y. and Osna, N.A. (2021) Alcohol-induced lysosomal damage and suppression of lysosome biogenesis contribute to hepatotoxicity in HIV-exposed Liver Cells. *Biomolecules,* 11(10) 1907. doi: 10.3390/biom11101497
410. Cook, N. R., Row, P. E., & Davidson, H. W. (2004). Lysosome Associated Membrane Protein 1 (Lamp1) Traffics Directly from the TGN to Early Endosomes. Traffic, 5(9), 685–699. https://doi.org/10.1111/j.1600-0854.2004.00212.x
411. Ihrke, G., Kyttala, A., Russel, M.R., Rous, B.A. and Luzio, J.P. (2004) Differential use of two AP-3 mediated pathways by lysosomal membrane proteins. *Traffic.* 5(12) 946-962. doi: 10.1111/j.1600-0854.2004.00236.x.
412. Tai, Y.T., Horton, H.M., Kong, S-Y., Pong, E., Chen, H., Cemerski, S., Bernett, M.J., Nguyen, D-H.T., Karki, S., Chu, S.Y., Lazar, G.A., Munshi, N., Desjarlais, J.R., Anderson, K.C. and Muchhal, U.S. (2012) Potent in vitro and in vivo activity of an

Fc-engineered humanised anti-HM1.24 antibody against multiple myeloma via augmented effector function. *Blood.* 119(9) 2074-2082

413. Ghitescu, L., & Fixman, A. (1984). Surface charge distribution on the endothelial cell of liver sinusoids. The Journal of Cell Biology, 99(2), 639–647. https://doi.org/10.1083/jcb.99.2.639
414. Salinas-Jazmín, N., Hisaki-Itaya, E., & Velasco-Velázquez, M. A. (2014). *A Flow Cytometry-Based Assay for the Evaluation of Antibody-Dependent Cell-Mediated Cytotoxicity (ADCC) in Cancer Cells* (pp. 241–252). https://doi.org/10.1007/978-1-4939-0856-1_16
415. Kozakov, D., Hall, D. R., Xia, B., Porter, K. A., Padhorny, D., Yueh, C., Beglov, D., & Vajda, S. (2017). The ClusPro web server for protein–protein docking. Nature Protocols, 12(2), 255–278. https://doi.org/10.1038/nprot.2016.169
416. Brenke R, Hall DR, Chuang G-Y, Comeau SR, Bohnuud T, Beglov D, Schueler-Furman O, Vajda S, Kozakov D. Application of asymmetric statistical potentials to antibody-protein docking. *Bioinformatics*. 2012 Oct; 28(20):2608-2614;
417. Sotudian, S., Desta, I. T., Hashemi, N., Zarbafian, S., Kozakov, D., Vakili, P., Vajda, S., & Paschalidis, I. Ch. (2021). Improved cluster ranking in protein–protein docking using a regression approach. Computational and Structural Biotechnology Journal, 19, 2269–2278. https://doi.org/10.1016/j.csbj.2021.04.028
418. Laskowski, R. A., Jabłońska, J., Pravda, L., Vařeková, R. S., & Thornton, J. M. (2018). PDBsum: Structural summaries of PDB entries. Protein Science, 27(1), 129–134. https://doi.org/10.1002/pro.3289
419. García-García, E., & Rosales, C. (2002). Signal transduction during Fc receptor-mediated phagocytosis. Journal of Leukocyte Biology, 72(6), 1092–1108. https://doi.org/10.1189/jlb.72.6.1092
420. Zhao, J., Nussinov, R., & Ma, B. (2019). Antigen binding allosterically promotes Fc receptor recognition. MAbs, 11(1), 58–74. https://doi.org/10.1080/19420862.2018.1522178
421. Beers, S.A., French, R. R., Chan, H. T. C., Lim, S. H., Jarrett, T. C., Vidal, R. M., Wijayaweera, S. S., Dixon, S. v., Kim, H., Cox, K. L., Kerr, J. P., Johnston, D. A., Johnson, P. W. M., Verbeek, J. S., Glennie, M. J., & Cragg, M. S. (2010). Antigenic modulation limits the efficacy of anti-CD20 antibodies: implications for antibody selection. Blood, 115(25), 5191–5201. https://doi.org/10.1182/blood-2010-01-263533
422. Meikle, P. J., Brooks, D. A., Ravenscroft, E. M., Yan, M., Williams, R. E., Jaunzems, A. E., Chataway, T. K., Karageorgos, L. E., Davey, R. C., Boulter, C. D., Carlsson, S. R., & Hopwood, J. J. (1997). Diagnosis of lysosomal storage disorders: evaluation of lysosome-associated membrane protein LAMP-1 as a diagnostic marker. Clinical Chemistry, 43(8), 1325–1335. https://doi.org/10.1093/clinchem/43.8.1325

423. Kumari, S., MG, S., & Mayor, S. (2010). Endocytosis unplugged: multiple ways to enter the cell. Cell Research, 20(3), 256–275. https://doi.org/10.1038/cr.2010.19
424. Stopforth, R. J., Oldham, R. J., Tutt, A. L., Duriez, P., Chan, H. T. C., Binkowski, B. F., Zimprich, C., Li, D., Hargreaves, P. G., Cong, M., Reddy, V., Leandro, M. J., Cambridge, G., Lux, A., Nimmerjahn, F., & Cragg, M. S. (2018). Detection of Experimental and Clinical Immune Complexes by Measuring SHIP-1 Recruitment to the Inhibitory FcγRIIB. The Journal of Immunology, 200(5), 1937–1950. https://doi.org/10.4049/jimmunol.1700832
425. Temming, A. R., Dekkers, G., van de Bovenkamp, F. S., Plomp, H. R., Bentlage, A. E. H., Szittner, Z., Derksen, N. I. L., Wuhrer, M., Rispens, T., & Vidarsson, G. (2019). Human DC-SIGN and CD23 do not interact with human IgG. Scientific Reports, 9(1), 9995. https://doi.org/10.1038/s41598-019-46484-2
426. Iborra, S., Martínez-López, M., Cueto, F. J., Conde-Garrosa, R., Del Fresno, C., Izquierdo, H. M., Abram, C. L., Mori, D., Campos-Martín, Y., Reguera, R. M., Kemp, B., Yamasaki, S., Robinson, M. J., Soto, M., Lowell, C. A., & Sancho, D. (2016). Leishmania Uses Mincle to Target an Inhibitory ITAM Signaling Pathway in Dendritic Cells that Dampens Adaptive Immunity to Infection. Immunity, 45(4), 788–801. https://doi.org/10.1016/j.immuni.2016.09.012
427. Caron, E., & Hall, A. (1998). Identification of Two Distinct Mechanisms of Phagocytosis Controlled by Different Rho GTPases. Science, 282(5394), 1717–1721. https://doi.org/10.1126/science.282.5394.1717
428. Allen, L. A., & Aderem, A. (1996). Molecular definition of distinct cytoskeletal structures involved in complement- and Fc receptor-mediated phagocytosis in macrophages. The Journal of Experimental Medicine, 184(2), 627–637. https://doi.org/10.1084/jem.184.2.627
429. Lodeiro, M., Alén, B. O., Mosteiro, C. S., Beiroa, D., Nogueiras, R., Theodoropoulou, M., Pardo, M., Gallego, R., Pazos, Y., Casanueva, F. F., & Camiña, J. P. (2011). The SHP-1 protein tyrosine phosphatase negatively modulates Akt signaling in the ghrelin/GHSR1a system. Molecular Biology of the Cell, 22(21), 4182–4191. https://doi.org/10.1091/mbc.E11-04-0373
430. , P., Zhang, Y., Mohan, S., Levinsohn, E., Gaeta, I., Hoppe, A. D., & Swanson, J. A. (2010). A Cdc42 Activation Cycle Coordinated by PI 3-Kinase during Fc Receptor-mediated Phagocytosis. Molecular Biology of the Cell, 21(3), 470–480. https://doi.org/10.1091/mbc.e08-05-0494
431. Mkaddem, S., Benhamou, M., & Monteiro, R. C. (2019). Understanding Fc Receptor Involvement in Inflammatory Diseases: From Mechanisms to New Therapeutic Tools. Frontiers in Immunology, 10. https://doi.org/10.3389/fimmu.2019.00811
432. Scott, C. C., Dobson, W., Botelho, R. J., Coady-Osberg, N., Chavrier, P., Knecht, D. A., Heath, C., Stahl, P., & Grinstein, S. (2005). Phosphatidylinositol-4,5- bis

phosphate hydrolysis directs actin remodeling during phagocytosis. The Journal of Cell Biology, 169(1), 139–149. https://doi.org/10.1083/jcb.200412162

433. Groves, E., Dart, A. E., Covarelli, V., & Caron, E. (2008). Molecular mechanisms of phagocytic uptake in mammalian cells. Cellular and Molecular Life Sciences, 65(13), 1957–1976. https://doi.org/10.1007/s00018-008-7578-4
434. Smith, S. M., Baker, M., Halebian, M., & Smith, C. J. (2017). Weak Molecular Interactions in Clathrin-Mediated Endocytosis. Frontiers in Molecular Biosciences, 4. https://doi.org/10.3389/fmolb.2017.00072
435. Boucrot, E., Saffarian, S., Zhang, R., & Kirchhausen, T. (2010). Roles of AP-2 in Clathrin-Mediated Endocytosis. PLoS ONE, 5(5), e10597. https://doi.org/10.1371/journal.pone.0010597
436. Jansen, R. W., Molema, G., Ching, T. L., Oosting, R., Harms, G., Moolenaar, F., Hardonk, M. J., & Meijer, D. K. (1991). Hepatic endocytosis of various types of mannose-terminated albumins. What is important, sugar recognition, net charge, or the combination of these features. The Journal of Biological Chemistry, 266(5), 3343–3348.
437. Oka, J. A., & Weigel, P. H. (1989). The pathways for fluid phase and receptor mediated endocytosis in rat hepatocytes are different but thermodynamically equivalent. Biochemical and Biophysical Research Communications, 159(2), 488–494. https://doi.org/10.1016/0006-291X(89)90019-3
438. Drácz, B., Müller, V., Takács, I., Hagymási, K., Dinya, E., Miheller, P., Szijártó, A., & Werling, K. (2023). Hypocalcemia on Admission Is a Predictor of Disease Progression in COVID-19 Patients with Cirrhosis: A Multicenter Study in Hungary. Biomedicines, 11(6), 1541. https://doi.org/10.3390/biomedicines11061541
439. Martínez-Esparza, M., Ruiz-Alcaraz, A. J., Carmona-Martínez, V., Fernández-Fernández, M. D., Antón, G., Muñoz-Tornero, M., Lencina, M., Pagán, I., de la Peña, J., & García-Peñarrubia, P. (2019). Expression of LAIR-1 (CD305) on Human Blood Monocytes as a Marker of Hepatic Cirrhosis Progression. Journal of Immunology Research, 2019, 1–12. https://doi.org/10.1155/2019/2974753
440. Wu, X., Zhang, L., Zhou, J., Liu, L., Fu, Q., Fu, A., Feng, X., Xin, R., Liu, H., Gao, Y., & Xue, J. (2019). Clinicopathologic significance of LAIR-1 expression in hepatocellular carcinoma. Current Problems in Cancer, 43(1), 18–26. https://doi.org/10.1016/j.currproblcancer.2018.04.005
441. Jansen, R. W., Molema, G., Ching, T. L., Oosting, R., Harms, G., Moolenaar, F., Hardonk, M. J., & Meijer, D. K. (1991). Hepatic endocytosis of various types of mannose-terminated albumins. What is important, sugar recognition, net charge, or the combination of these features. The Journal of Biological Chemistry, 266(5), 3343–3348.
442. Yamazaki, H., Oda, M., Takahashi, Y., Iguchi, H., Yoshimura, K., Okada, N., & Yokomori, H. (2013). Relation between Ultrastructural Localization, Changes in

Caveolin-1, and Capillarization of Liver Sinusoidal Endothelial Cells in Human Hepatitis C–Related Cirrhotic Liver. Journal of Histochemistry & Cytochemistry, 61(2), 169–176. https://doi.org/10.1369/0022155412468590

443. Baschong, W., & Stierhof, Y.-D. (1998). Preparation, use, and enlargement of ultrasmall gold particles in immunoelectron microscopy. Microscopy Research and Technique, 42(1), 66–79. https://doi.org/10.1002/(SICI)1097-0029(19980701)42:1<66::AID-JEMT8>3.0.CO;2-P
444. Synnes, M., Prydz, K., Løvdal, T., Brech, A., & Berg, T. (1999). Fluid phase endocytosis and galactosyl receptor-mediated endocytosis employ different early endosomes. Biochimica et Biophysica Acta (BBA) - Biomembranes, 1421(2), 317–328. https://doi.org/10.1016/S0005-2736(99)00134-0
445. Jaradat, D. M. M., Mebs, S., Chęcińska, L., & Luger, P. (2007). Experimental charge density of sucrose at 20K: bond topological, atomic, and intermolecular quantitative properties. Carbohydrate Research, 342(11), 1480–1489. https://doi.org/10.1016/j.carres.2007.04.004
446. Alieva IB, Vorob'ev IA. Izuchenie usloviĭ obratimosti metafaznogo bloka i induktsii mnogopoliusnykh mitozov pri deĭstvii nokodazola [Conditions of the reversibility of metaphase arrest and induction of multi-polar mitoses after treatment with nocodazole]. Tsitologiia. 1987 May;29(5):560-8. PMID: 3617221
447. Surviladze Z, Waller A, Strouse JJ, et al. A Potent and Selective Inhibitor of Cdc42 GTPase. 2010 Feb 27 [Updated 2010 Dec 16]. In: Probe Reports from the NIH Molecular Libraries Program [Internet]. Bethesda (MD): National Center for Biotechnology Information (US); 2010-. Available from: https://www.ncbi.nlm.nih.gov/books/NBK51965/
448. Haddad, G., Dylewski, J., Evans, R., Lewis, L., & Blaine, J. (2023). Knockout of the neonatal Fc receptor alters immune complex trafficking and lysosomal function in cultured podocytes. PLOS ONE, 18(4), e0284636. https://doi.org/10.1371/journal.pone.0284636
449. Gan, Z., Ram, S., Vaccaro, C., Ober, R. J., & Ward, E. S. (2009). Analyses of the Recycling Receptor, FcRn, in Live Cells Reveal Novel Pathways for Lysosomal Delivery. Traffic, 10(5), 600–614. https://doi.org/10.1111/j.1600-0854.2009.00887.x
450. Xie, F., Wang, J. and Zhang, B (2023) RefFinder: a web-based tool for comprehensively analysing reference genes. *Funct Integr Genomics.* 23(2) 125. doi: 10.1007/s10142-023-0195507
451. Vandesompele, J., Preter, K., Pattyn, F., Poppe, B., Van Roy, N., De Paepe, A. and Speleman, F. (2002) Accurate normalization of real-time quantitative RT-PCR data by geometric averaging of multiple internal control genes. *Genome Biology*. Doi: 10.1196/gb-2002-3-7-research0034

452. Anderson, C.L., Jensen, J.L. and Orntoft, T.F. (2004) Normalisation of real-time quantitative reverse transcription-PCR data: a model-based variance estimation approach to identify genes suits for normalisation, applied to bladder and colon cancer data sets. *Cancer Res.* 64(15) 5245-5250
453. Pfaffl, M.W., Tichopod, Ales, Prgomet, C. and Neuvians, T.P. (2004) Determination of stable housekeeping genes, differentially regulated targets genes and samples integrity: Bestkeeper—Excel-based tool using pair-wise correlations. *Biotechnol lett.* 26(6) 509-515
454. Silver, N., Best, S., Jiang, J. and Thein, S.L. (2006) Selection of housekeeping genes for gene expression studies in human reticulocytes using real-time PCR. *BMC Molecular Biology.* 7(33)
455. Grevys, A., Nilsen, J., Sand, K.M.K., Daba, M.B., Oynebraten, I., Bern, M., McAdam, M.B., Foss, S., Schlothaur, T., Michaelsen, T.E., Christianson, G.J., Roopenian, D.C., Blumberg, R.S., Sandlie, I. and Anderson, J.T. (2018) A human endothelial cell-based recycling assay for screening of FcRn targeted molecules. *Nat Commun* 9(1) 621.
456. Bolte, S. and Cordelieres, F.P. (2006) A guided tour into subcellular colocalisation analysis in light microscopy. *J Microsc. 224(3)* 213-231. doi: 10.1111/j.1365-2818.2006.01706.x
457. Guerra, R., Armando, R., Crespo, J., López M., Rosa M., Iruzubieta, P., Casals M., Gregori, L.G., Marta, L., Bernardo,. and Morales Ruiz, M. (2021) "Measurement and clinical usefulness of bilirubin in liver disease" *Advances in Laboratory Medicine / Avances en Medicina de Laboratorio*, vol. 2, no. 3, 2021, pp. 352-361. https://doi.org/10.1515/almed-2021-0047
458. Flores Molina M, Abdelnabi MN, Mazouz S, Villafranca-Baughman D, Trinh VQ, Muhammad S, Bédard N, Osorio Laverde D, Hassan GS, Di Polo A, Shoukry NH. Distinct spatial distribution and roles of Kupffer cells and monocyte-derived macrophages in mouse acute liver injury. Front Immunol. 2022 Sep 30;13:994480. doi: 10.3389/fimmu.2022.994480.

Supplementary Methods and Figures

Cell Culture and maintenance of HepG2

HepG2 are an immortalised human cell line derived from a liver hepatocellular carcinoma from a 15-year-old Caucasian male. Cells were sourced from the European Collection of Authenticated Cell Cultures (ECACC catalogue no. 85011430); and cultured in complete media comprising Dulbecco's Modified Eagle Medium (DMEM; ThermoFisher, USA) with 10% (v/v) heat-inactivated fetal bovine serum (FBS, Fisher Scientific, UK) and 1% (v/v) PSG (ThermoFisher, USA). The culture and passage protocol is similar to that described for LSEC, however using uncoated 75cm^2 Corning flasks. Media was renewed twice weekly, with a sub-cultivation ratio of 1:4.

Cell Culture and maintenance of THP-1s

THP-1 cells are an immortal human monocytic cell line derived from an acute monocytic leukaemia patient. Cells were sourced from the European Collection of Authenticated Cell Cultures (ECACC catalogue no. 88081201); and cultured in complete media comprised of Roswell Park Memorial Institute 1640 Medium (RPMI; Gibco, USA) supplemented with 10% (v/v) heat-inactivated FBS, 1% (v/v) PSG and a final working concentration of 0.05mM 2-mercaptoethanol (BME) to reduce oxidative stress and premature differentiation. Cells were grown in suspension; therefore, floating cells were classified viable. The monitoring of cells was conducted twice weekly, and it was endeavoured to keep the cells at a density of between 1x10^5- 1x10^6/mL. Here cultures were maintained by the addition of fresh media or complete replacement whereby cells were pelleted at 870xg for 5 minutes and resuspended in 20mL of fresh media. Flasks were kept in an upright position in the incubator.

Polarisation of THP-1 cells into pro- and anti-inflammatory phenotypes

Macrophages within the liver exist as heterogenous populations ranging from tissue resident Kupffer cells (KCs) to recruited macrophages classed as M(LPS+IFNy, formerly M1, pro-inflammatory) and M(IL-4, formerly M2; anti-inflammatory) phenotypes. Baxter

et al.,[213] published a detailed protocol for cell differentiation that recreated the full spectrum of macrophage polarization and their downstream receptor expression effects. This formed the foundation for my differentiation protocol. THP-1 were seeded at $3x10^5$ in 2mL/ well in a 6 well plate (Corning Inc, USA). THP-1 were primed with 10ng/mL Phorbol-12-myristate-13-acetate (PMA, Peprotech, UK) for 24 hours to induce differentiation into macrophages. The medium was removed, and cells were left to rest in complete THP-1 media for 72 hours. To induce polarisation into the desired phenotype, cells were treated with either 30ng/mL of IL-4 (Peprotech, UK) or 20ng/mL of IFN-γ (Peprotech, USA) and 250ng/mL of lipopolysaccharide (LPS) (Sigma, USA) for a further 48 hours. Post this incubation, cells were utilised in experimentation.

Coculture of HepG2 and LSEC

To recapitulate some of the complex cell to cell interactions seen within the liver, a co-culture of HepG2 and LSEC was established on transwells (12-well), with a pore size of 0.3μm (Greiner, Germany). Each insert was pre-incubated with 30% RTC for 2 hours at 37°C before collagen was removed and the inserts left to dry. LSEC were then seeded at a density of $4x10^4$ in 900μl of LSEC media per insert; in a separate 12 well plate (Corning Inc, USA) HepG2 cells were seeded at $6x10^4$ in 1mL/well, in their complete media. Both plates were then incubated at 5% CO_2 and 37°C for 2 hours to allow cells to settle. Following this, media was removed from each plate and the LSEC coated transwells were placed in the HepG2 companion plate (as shown in the schematic below Figure S.2). The HepG2 media in the bottom reservoir was topped up to 2.5mL and 1.5 mL LSEC media was replaced in the upper inserts. This co-culture was left for 48 hours before being used in experimentation.

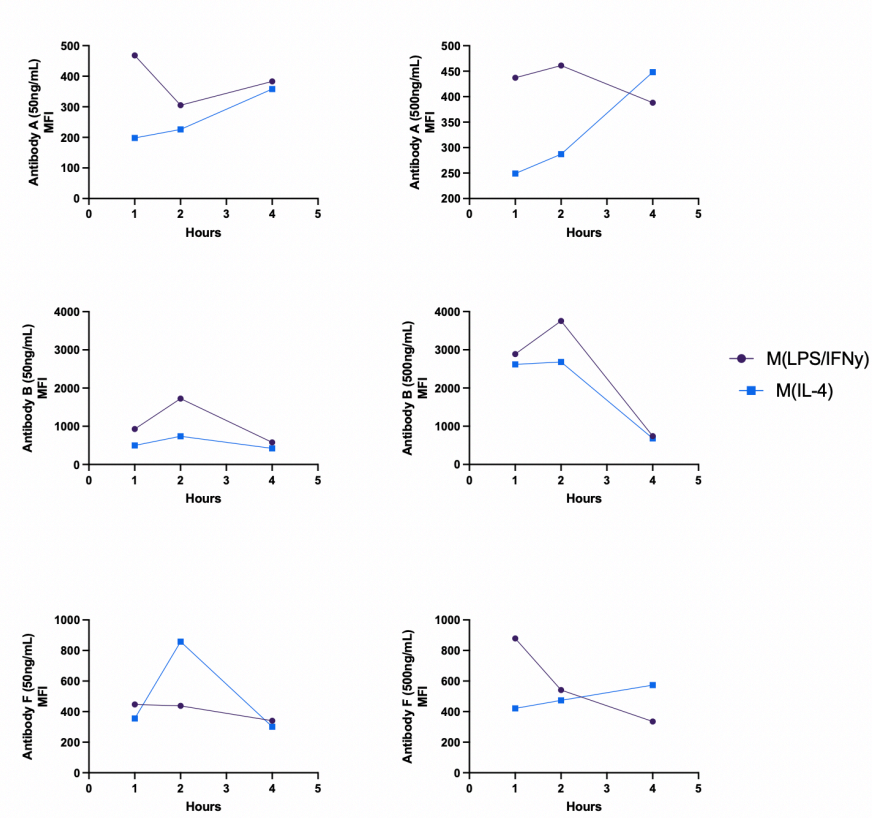


Figure S. 1: THP-1 antibody uptake. THP-1 were pushed towards either pro- (via LPS/IFNy) or anti-(via IL-4) inflammatory phenotypes. They were then incubated with 500ng/mL of antibody A (chimeric), B (humanised) and F (Human) for 1-, 2- and 4-hours prior to being taken for flow cytometry analysis. MFI was recorded and plotted in Prism. Please note Antibody B reads higher as it targets a monocytic marker.

Table S. 1: CT values for liver lysates. This table outlines an example of 11 whole liver lysates used to obtain the qPCR data seen throughout chapter 3. Here it reports the CT value for each gene; the cut off used was 35.

	SRSF4	CD32b	MRC1	FCRN	B2M	CD209
Healthy 1	32	34	35	29	24	0
Healthy 2	27	32	31	26	21	34
Healthy 3	31	35	35	34	25	0
NASH 1	30	33	34	33	23	35
NASH 2	28	32	33	30	22	34
NASH 3	30	33	35	30	23	35
NASH 4	30	35	31	30	26	35
ALD 1	27	34	31	25	20	33
ALD 2	26	32	30	26	20	31
ALD 3	27	30	31	29	20	33
ALD 4	29	33	33	31	22	35

Table S. 2: Target/Ref values for liver lysates. This table outlines an example of 11 whole liver lysates used to obtain the qPCR data seen throughout chapter 3. Here it reports the target/reference values used to plot, here the housekeeper used was SRSF4.

	CD32b	MRC1	FCRN	B2M	CD209
Healthy 1	0.2565	0.2217	17.85	532.6	0
Healthy 2	0.0201	0.051	1.355	41.68	0.00622
Healthy 3	0.0668	0.0668	0.1731	78.44	0
NASH 1	0.148	0.0705	0.1092	117.7	0.0295
NASH 2	0.0416	0.0366	0.1852	54.07	0.00843
NASH 3	0.1297	0.0854	1.036	111.2	0.0425
NASH 4	0.0335	0.0335	0.9185	20.97	0.0335
ALD 1	0.0322	0.0532	3.442	122.7	0.0195
ALD 2	0.02	0.0728	0.9824	74.46	0.031
ALD 3	0.0981	0.0498	0.3402	109	0.0156
ALD 4	0.905	0.0641	0.354	146.6	0.0176

	1	2	3	4	5	6	
A	sc 1000		sc 0		uptake lysate 3.2		
	3.782	3.396	0.085	0.089	0.301	0.213	405
	0.041	0.04	0.041	0.041	0.041	0.042	650
	3.741	3.356	0.044	0.048	0.26	0.171	Delta
B	sc 316		uptake well 1: 0ng		uptake lysate 200		
	3.021	2.585	1.056	0.965	0.208	0.239	405
	0.044	0.042	0.04	0.04	0.04	0.041	650
	2.977	2.543	1.016	0.925	0.168	0.198	Delta
C	sc 100		uptake well 1: 3.2ng		Recycle 0		
	2.015	1.58	0.993	1.01	0.163	0.208	405
	0.041	0.042	0.041	0.04	0.04	0.042	650
	1.974	1.538	0.952	0.97	0.123	0.166	Delta
D	sc 32		uptake well 1: 200ng		recycle 3.2		
	0.807	0.667	1.039	1.04	0.156	0.162	405
	0.041	0.053	0.041	0.04	0.041	0.04	650
	0.766	0.614	0.998	1	0.115	0.122	Delta
E	sc 10		uptake well 2: 0		recycle 200		
	0.308	0.257	0.605	0.647	0.157	0.187	405
	0.038	0.041	0.041	0.041	0.039	0.086	650
	0.27	0.216	0.564	0.606	0.118	0.101	Delta
F	sc 3.2		uptake well 2: 3.2		lysate 0		
	0.152	0.143	0.568	0.649	0.447	0.375	405
	0.039	0.041	0.04	0.04	0.04	0.041	650
	0.113	0.102	0.528	0.609	0.407	0.334	Delta
G	sc 1		uptake well 2: 200		lysate 3.2		
	0.114	0.111	0.906	0.949	0.42	0.492	405
	0.041	0.04	0.04	0.042	0.037	0.038	650
	0.073	0.071	0.866	0.907	0.383	0.454	Delta
H	sc 0.32		uptake lysate: 0		lysate 200		
	0.094	0.102	0.303	0.277	0.666	0.343	405
	0.04	0.041	0.038	0.041	0.041	0.039	650
	0.054	0.061	0.265	0.236	0.625	0.304	Delta

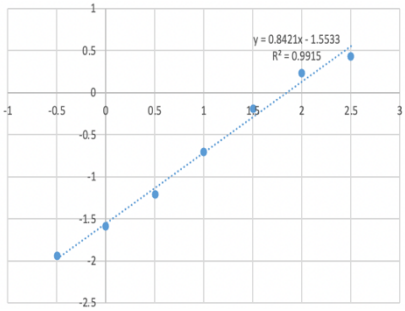


Figure S. 2: Raw HERA data: This figure shows an example of raw anti-CD20 ELISA data with the coinciding standards plotted (right). Cells and supernatants were taken from the HERA assay as described in the main text (Figure 2.3). Absorbance measurements were taken at 405 and 650 and subtracted to report the delta values. Calculations of the concentrations were then performed using the linear equation obtained from the standards.

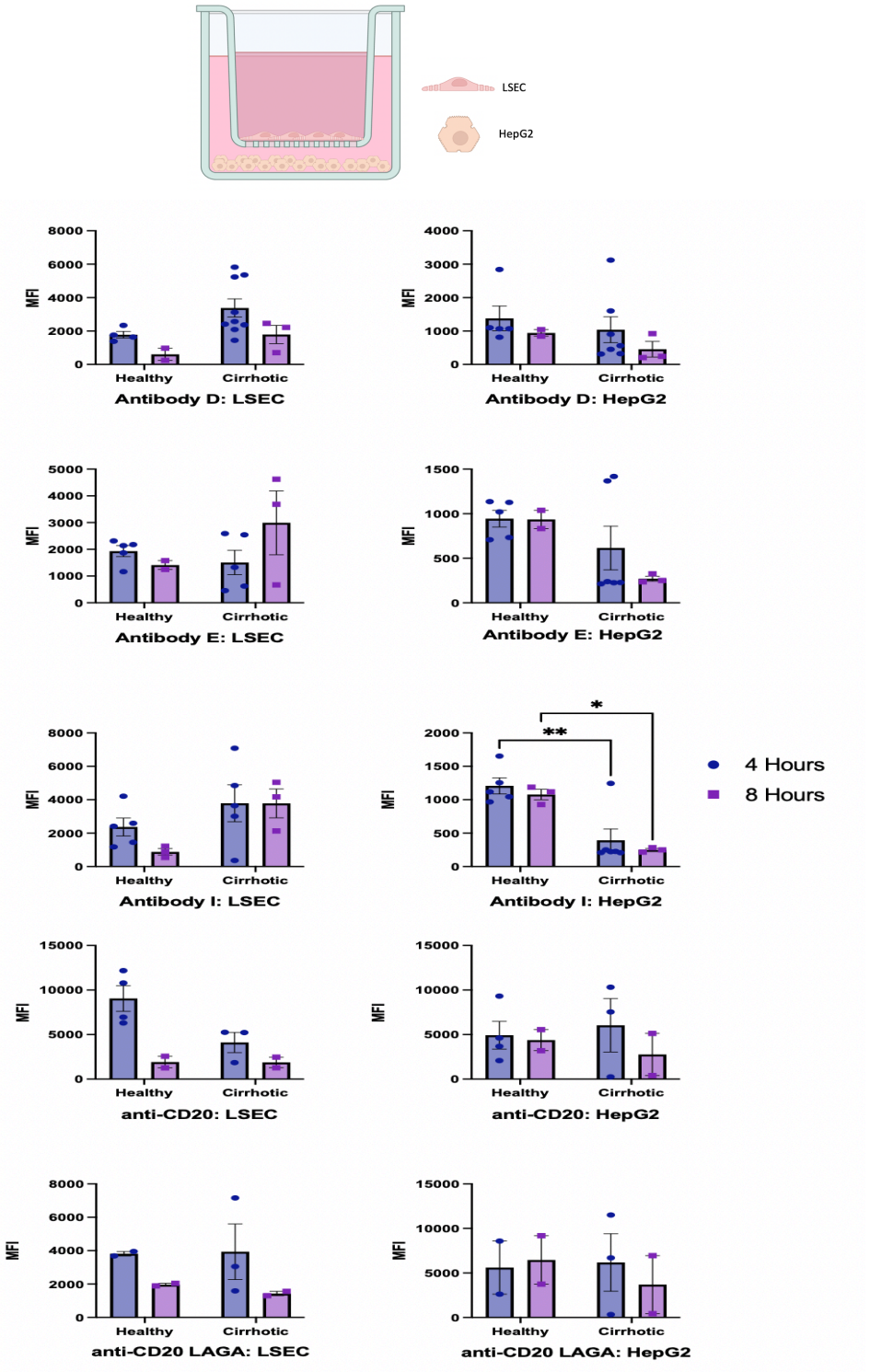


Figure S. 3: Coculture treated with therapeutic antibodies. A co-culture of LSEC and HepG2s were cultured for 48-hours on *0.3µm* inserts (top panel schematic) prior to being treated with antibodies D (humanised), E (human), I (bsAb), anti-CD20 and anti-CD20 LAGA for 4- and 8-hours. Cells were taken for flow cytometry and MFI was recorded. D,E, and I were all conjugated to Alexafluor647 whereas anti-CD20 and anti-CD20 LAGA was detected using an anti-mouse IgG Alexafluor 647 secondary. Left hand side shows results for LSEC, right hand side shows the results for HepG2. Each point represents an individual liver.

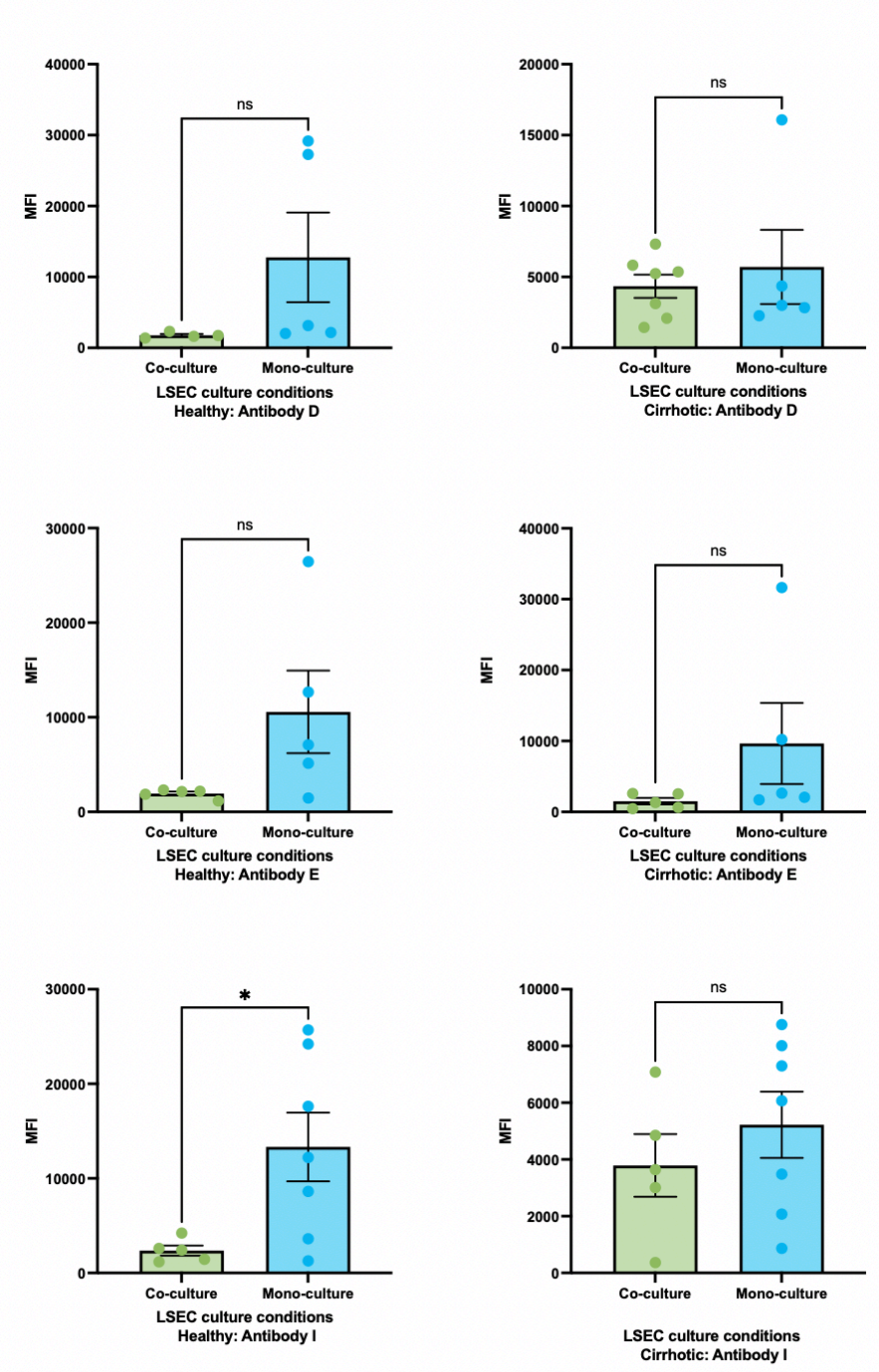


Figure S. 4: Comparison of mono- vs co-cultures in LSEC uptake of antibody. These figures show the comparison of LSEC internalisation of AF647 conjugated antibodies: D (humanised), E (human) and I (bsAb) taken at 4-hours in mono- and co-cultured (with HepG2 cells) LSEC. Significance was calculated with unpaired T-tests *<0.05 . Error bars show SEM.

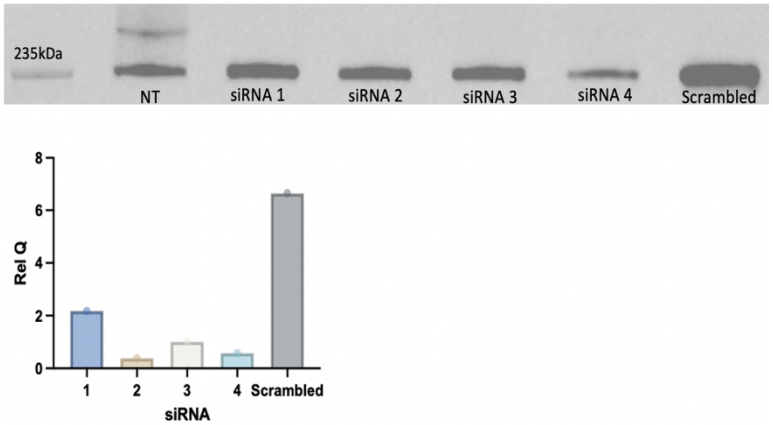


Figure S.5: Validation of *MRC1* Knockdown. Top panel shows the western blot for LSEC knockdown with varying *MRC1* siRNA (1-4). It also contains a non-treated (NT) and scrambled siRNA control. This is from one liver but pooled from two wells. To note, no housekeeping control is present as this was performed on a stain free gel so compensation was performed on total loaded protein. Below shows the mRNA expression of 1 liver for siRNA knockdown of *MRC1* siRNA like above. From these results we chose siRNA 4 to utilise in our functional experiments.

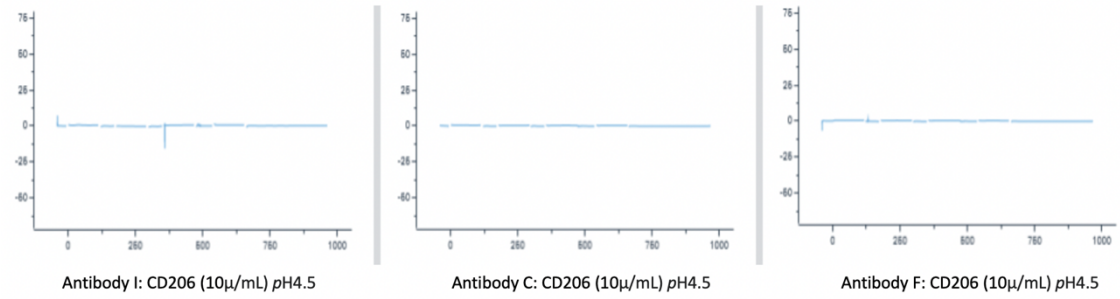


Figure S. 6: SPR sensograms for CD206 binding kinetics with antibodies. Here shows the failed SPR experiment attempting to establish binding kinetics between CD206 and antibodies I, C and F.

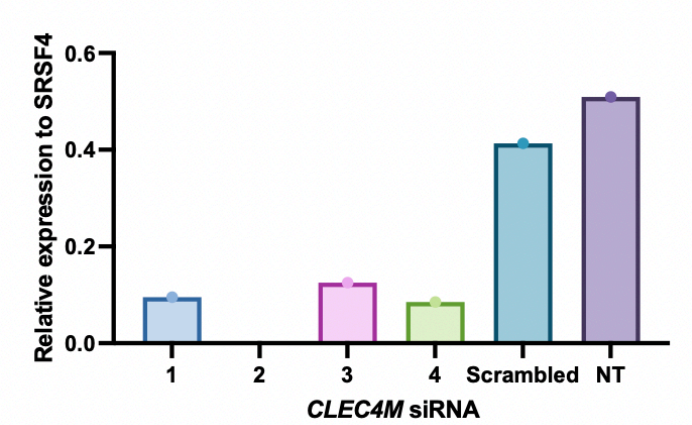


Figure S. 7: mRNA expression validation of *CLEC4M* knockdown. This figure shows the mRNA expression of 1 liver for siRNA knockdown of *CLEC4M* siRNA like above. From these results we chose siRNA 4 to utilise in our functional experiments. 2 was not chosen as it was unclear with this was a cytotoxic loss or a very efficient knock down.

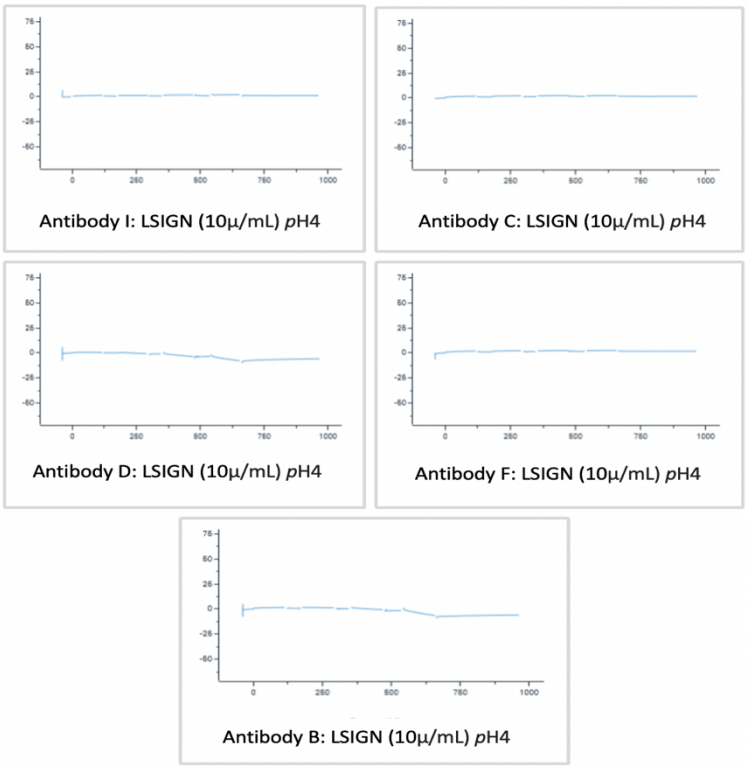


Figure S. 8: SPR sensograms for LSIGN binding kinetics with antibodies. Here shows the failed SPR experiment attempting to establish binding kinetics between LSIGN and antibodies I (bsAb), C (humanised), D (humanised),F (human) and B (humanised).

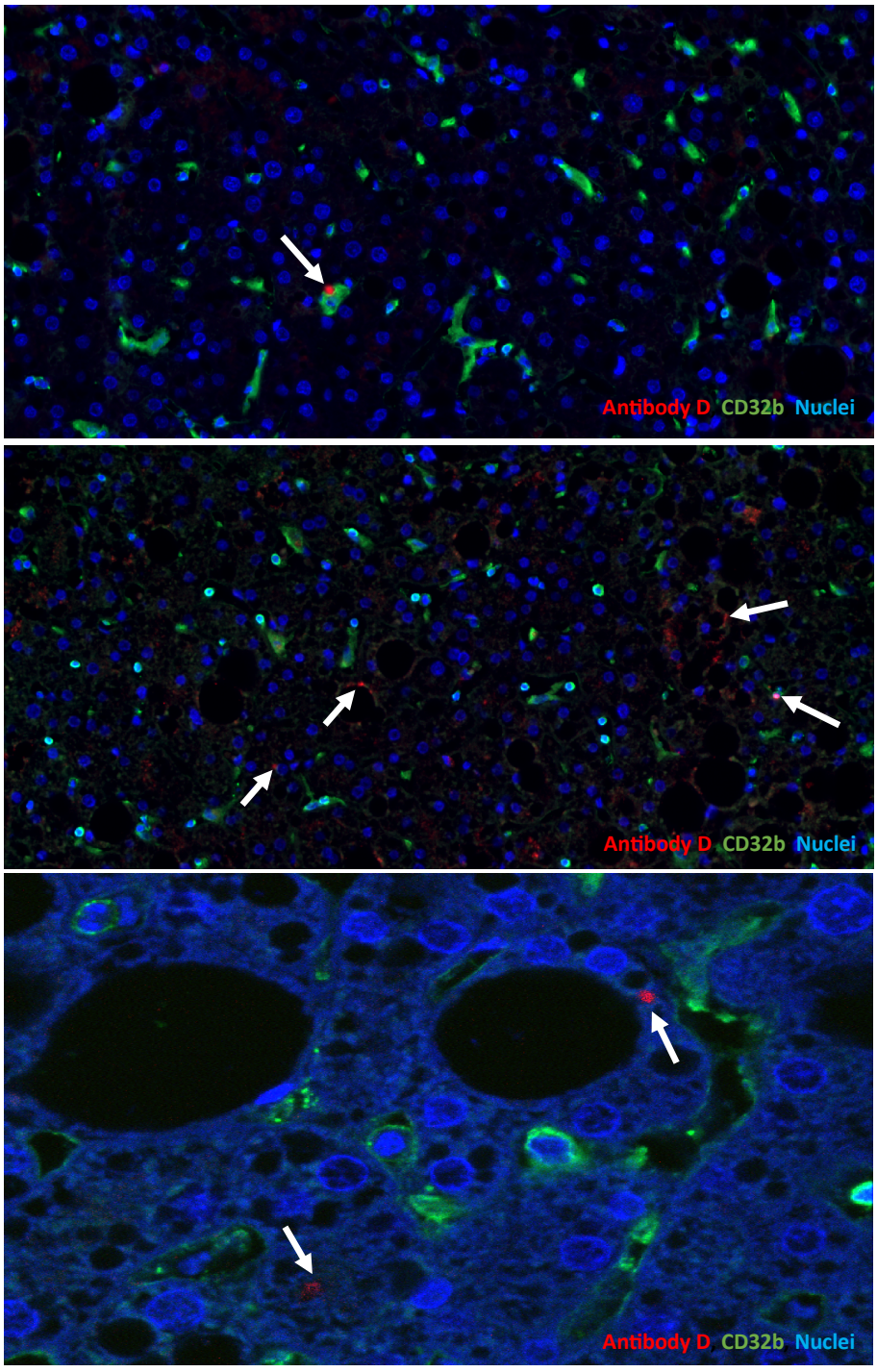


Figure S.9: Liver tissue injections of Antibody D. Small blocks of resected liver tissue was injected with a blunt ended needle containing 3ug/mL of AF647 conjugated antibody D (humanised). This was then left to incubate in media on a rocker at 37-degrees for 2-hours. Blocks where then fixed with 4% PFA before being embedded in paraffin and sectioned via a microtome. Slides were then stained for CD32b and DAPI and imaged on the Axio slide scanner Z.1 at 20x. These are representative images, antibody D (red), CD32b (green) and Nuclei (blue)